DP-1374

663014

SAVANNAH RIVER LABORATORY
ENVIRONMENTAL TRANSPORT AND EFFECTS RESEARCH
ANNUAL REPORT - 1974

E. I. du Pont de Nemours & Co.
Savannah River Laboratory
Aiken, S. C. 29801

PREPARED FOR THE U. S. ENERGY RESEARCH AND DEVELOPMENT ADMINISTRATION UNDER CONTRACT AT(07-2)-1

Printed in the United States of America

Available from
National Technical Information Service
U. S. Department of Commerce
5285 Port Royal Road
Springfield, Virginia 22161

Price: Printed Copy $7.60; Microfiche $2.25

663014

DP-1374
Distribution Category UC-11

SAVANNAH RIVER LABORATORY ENVIRONMENTAL TRANSPORT AND EFFECTS RESEARCH ANNUAL REPORT - 1974

by

T. V. Crawford, Compiler

Contributing Authors:

Savannah River Laboratory

Analytical Chemistry Division
K. W. MacMurdo

Computer Applications Division
M. R. Buckner, K. R. Routt

Environmental Effects Division
R. C. Milham

Environmental Transport Division
J. C. Corey, T. V. Crawford, B. Gottlieb, R. S. Harvey, D. W. Hayes, G. B. Johnson, C. D. Kern, I. W. Marine, M. M. Pendergast, P. J. Schneider, J. F. Schubert, L. J. Tilly, J. R. Watts

Savannah River Plant
Works Technical Department - Health Physics Division

J. W. McMahan

Approved by
T. V. Crawford, Research Manager
Environmental Transport Division
Savannah River Laboratory

Publication Date: June 1975

E. I. du Pont de Nemours & Co.
Savannah River Laboratory
Aiken, S. C. 29801

PREPARED FOR THE U. S. ENERGY RESEARCH AND DEVELOPMENT ADMINISTRATION UNDER CONTRACT AT(07-2)-1

ABSTRACT

Research on the transport of pollutants through environmental systems and their effects on ecosystems conducted at the Savannah River Laboratory in fiscal year 1974 is presented. A series of articles, within a wide variety of disciplines, describes, through computer modeling and field experiments:

- The transport and dispersion of pollutants through the atmosphere of the southeastern United States (Papers 1-11).
- Transport and dispersion of pollutants in the surface and ground water systems in the vicinity of the Savannah River Plant (Papers 12-14).
- Movement of radioactivity in soil and plant systems (Papers 15-17).
- The effect of carbon-14 production by the nuclear industry (Paper 18).
- Thermal stress on aquatic organisms (Papers 19-25).
- The effects of earthquakes upon ground displacement velocity and acceleration in the southeastern United States (Paper 26).

FOREWORD

Environmental research at the Savannah River Laboratory, particularly that done within the Environmental Transport Division, is aimed at developing and testing improved models for predicting the transport and dispersion of pollutants through a number of environmental systems. Logically, this is followed by development of improved methods of assessing the effects of pollutants on biotic systems. This approach provides a basis for evaluating the total environmental consequences of releases of pollutants and for planning future activities in such a way as to minimize adverse environmental effects. This research is being conducted primarily at the Savannah River Plant site near Aiken, South Carolina, but includes the entire southeastern United States.

The preparation of this report was a teamwork effort of the members of the Environmental Transport Division of the Savannah River Laboratory with contributions from other research divisions. The report includes the major research activities of the Environmental Transport Division during FY-1974; in addition, many applied short range jobs were completed. Other environmental efforts performed by Du Pont at the site, such as the large effort of the SRP Health Physics Section in environmental monitoring, are reported elsewhere.

Todd V. Crawford
Research Manager
Environmental Transport Division

CONTENTS

INTRODUCTION

I. ATMOSPHERIC TRANSPORT AND DISPERSION

1. Actual Standard Deviations of Vertical and Horizontal Wind Direction Compared to Estimates from Other Measurements 1-1

2. Aerodynamic Flying of Bivane Wind Direction Indicators 2-1

3. Evaluation of Different Methods of Estimating Vertical Eddy Diffusivities from TV Tower Data 3-1

4. A Climatology of the Mixed Layer Using Acoustic Methods 4-1

5. Verification of SRL Buoyant Plume Calculational Procedures Through Use of Measured SO_2 Concentrations 5-1

6. A Technique for Field Measurements of Atmospheric Tritiated Hydrogen and Tritiated Water Vapor 6-1

7. A Simple Model Used to Determine Downwind Concentrations Resulting from Either Continuous or Instantaneous Releases Using Meteorological Observations from a Single Tower 7-1

8. A Computer Program for Objective Analysis and Display of Meteorological Fields 8-1

9. Preliminary Mesoscale Calculations for the Southeastern United States Using the Two and One-Half Dimensional Lavoie Model 9-1

10. A Trajectory and Dispersion Computer Program Which Uses Objectively Analyzed, Observed or Forecast Meteorological Fields 10-1

11. Real Time Prediction and Verification of Argon-41 Concentrations - A Joint Effort with the Lawrence Livermore Laboratory 11-1

II. SURFACE AND GROUND WATER TRANSPORT AND DISPERSION

12. Computer Modeling of Stream and River Systems 12-1

13. A Universal Environmental Water Sampler 13-1

14. A Ground Water Model of the Tuscaloosa Aquifer at the Savannah River Plant 14-1

III. BIOTIC TRANSPORT AND EFFECTS

15. Tritium Behavior in Pine Trees 15-1

16. Strontium, Cesium, and Plutonium in Various Soils and Plants at the Savannah River Plant 16-1

17. Contaminated Solvent Degradation 17-1

18. Carbon-14 Production by the Nuclear Industry and its Potential Effects 18-1

19. The Differing Temperature Responses of Two Species of Ramshorn Snails 19-1

20. The Critical Thermal Maxima of Snails Raised in Warm and in Cold Water 20-1

21. The Effect of Distance from Thermal Effluent and of Species on Reproduction in Helisoma Snails 21-1

22. Plankton Productivity as a Function of Nutrient Concentration Changes over a Decade of Time in a Reactor Cooling Pond 22-1

23. Periphyton Colonization and Productivity as a Function of Reactor Effluent Temperatures 23-1

24. Baseline Studies of the Biotic and Abiotic Factors of Upper Three Runs Creek and Six Experimental Streams in the Thermal Effects Laboratory 24-1

25. Temperature Effects on Growth and Respiration Rates of *Dolania Americana* (Ephemeroptera) 25-1

IV. SEISMIC EFFECTS

26. The Application of Recent Seismic Research to the Evaluation of Seismic Risk in the South-Eastern United States 26-1

SAVANNAH RIVER LABORATORY
ENVIRONMENTAL TRANSPORT AND EFFECTS RESEARCH
ANNUAL REPORT - 1974

INTRODUCTION

The Savannah River Laboratory (SRL) is operated by the Atomic Energy Division of the E. I. du Pont de Nemours & Company under contract with the U. S. Energy Research and Development Administration (ERDA). The laboratory consists of about 900 employees. The Du Pont Company also operates the Savannah River Plant (SRP), which is physically located at the same site. SRP employs about 5,000 people engaged in operating a nuclear fuel manufacturing facility, three large production reactors, two large chemical reprocessing plants, a heavy water production plant, and various waste management facilities. These facilities, as well as the laboratory, are located on a 300-square-mile site south of Aiken, South Carolina.

On the same site is the Savannah River Ecology Laboratory (SREL) operated by the University of Georgia, and a United States Forest Service group. Overall program management and site co-ordination are done by the Savannah River Operations Office of the U. S. Energy Research and Development Administration (ERDA-SR) also located onsite.

Research in environmental transport at SRL was funded by two divisions of the U. S. Atomic Energy Commission. Applied research in support of the operation of SRP was funded by the Division of Production and Materials Management, and research of general applicability to the power industry was funded by the Division of Biomedical and Environmental Research. In FY-1974, the Environmental Transport Division of SRL was about equally funded by both of these divisions. In January, 1975, the Atomic Energy Commission was abolished, and its operations were transferred to the newly formed ERDA.

A principal objective of environmental transport research at SRL is to develop, apply, adapt, use, test, and verify models that predict the directions and magnitude of ecosystem processes. Since an ecosystem is understood to be a complex ecological unit composed of physical, chemical, and biotic components interacting in the cycling and transport of matter and the flow of energy, the understanding of ecosystem processes demands integrated study by scientists of differing disciplines. The immediate goal of such integrated studies is to produce methods and knowledge which

are useful to the operation of SRP, to the power industry of the southeastern United States, and to the nuclear industry. Cooperative efforts are also being conducted with SREL, the U. S. Forest Service group at Savannah River, and the following offsite organizations: the Lawrence Livermore Laboratory at Livermore, California (LLL); the Atmospheric Turbulence and Diffusion Laboratory of the National Oceanic and Atmospheric Administration (NOAA) at Oak Ridge, Tennessee; the Oak Ridge National Laboratory (ORNL); and the Air Resources Laboratories of NOAA at Silver Spring, Maryland.

This Annual Report summarizes the research results accomplished in FY-1974. This is the first such Annual Report in what is planned to be a continuing series. A somewhat similar report was prepared for the FY-1973 Dose-To-Man Program.[1] In the earlier report, atmospheric research facilities and research results were emphasized. Some of the atmospheric sciences articles in this Annual Report are extensions of the work reported earlier. The reader is referred to the earlier report for a detailed discussion of atmospheric research facilities at SRL.

---

1. T. V. Crawford. *Progress Report Dose-To-Man Program FY-1973.* USAEC Report DP-1341, E. I. du Pont de Nemours and Company, Inc., Savannah River Laboratory, Aiken, South Carolina (1974).

I. ATMOSPHERIC TRANSPORT AND DISPERSION

The objective of the atmospheric transport and dispersion studies is to develop and test models for predicting meteorological fields and for calculating transport and dispersion of pollutants in meteorological fields. The planetary boundary layer of the atmosphere, covering the regional environment surrounding the Savannah River Plant site and the southeastern United States is being studied. Efforts have focused on improving the data and interpretations relative to diffusion in the planetary boundary layer, development of a mesoscale prediction model, development of trajectory and dispersion calculational models, and testing these calculational methods against measurement of atmospheric pollutants.

1. ACTUAL STANDARD DEVIATIONS OF VERTICAL AND HORIZONTAL WIND DIRECTION COMPARED TO ESTIMATES FROM OTHER MEASUREMENTS †

INTRODUCTION

Meteorological data were collected at the WJBF-TV tower located near the Savannah River Plant in Aiken County, South Carolina. These data have been used to assess the applicability of several techniques to determine σ_θ and σ_ϕ, the standard deviations for horizontal and vertical wind directions, respectively. The magnitudes of σ_θ and σ_ϕ are used for determining coefficients for the calculation of downwind concentrations of airborne contaminants.

Although the 367-m-high tower has been instrumented to collect meteorological data since 1966, recent improvements in the data acquisition system and bivane instrumentation have produced data of sufficient resolution to permit direct calculation of σ_θ and σ_ϕ at 7 levels between 10 and 304 m. This paper presents results of analyses of data collected during two periods. Period 1 was May 18-30, 1973, during which data were collected at a sample interval, s, of 0.2 sec. Period 2 was June-November 1973, with data collected at s = 5.0 sec.

VARIATION OF σ_θ AND σ_ϕ WITH SAMPLING INTERVAL

Data from Period 1 were used to examine the effects of different sample intervals on resulting wind statistics. The true statistics were assumed to be given by data collected at a sample interval of 0.2 sec, which for a 1-hr period consisted of 18,000 data points. These statistics were compared with those obtained by using every other point, every third point, etc., corresponding to sample intervals of 0.4, 0.6, 0.8, ... 360.0 sec (41 in all).

Figure 1a depicts the mean value (from 93 different 1-hr periods) of the ratio $\sigma_\theta/\sigma_\theta$ as a function of sampling interval.

---

† Work done by M. M. Pendergast and T. V. Crawford. Presented at the *Symposium on Atmospheric Diffusion and Air Pollution* held at Santa Barbara, California, on September 9-13, 1974.

σ_θ and σ_{θ_o} are the standard deviations of horizontal wind direction for 1-hr periods of sampling intervals s and 0.2 sec, respectively, where s ranges between 0.4 and 360.0 sec. The values of $\sigma_\theta/\sigma_{\theta_o}$ fluctuate around a value of 1.0 even though the scatter of points increases with increasing s. Figure 1b shows the data from Figure 1a expressed in terms of the absolute value of the departure from unity, $\left|1.0 - \left(\sigma_\theta/\sigma_{\theta_o}\right)\right|$, which will be referred to as the probable error in σ_θ. These data, which include all stability categories, clearly show an increase in the probable error (PE) with increasing s. A PE of 0.2 in σ_θ implies that the value of σ_θ is 80 to 120% of the true value, σ_{θ_o}.

The curve shown in Figure 1b can be used to estimate PE in σ_θ as a function of s (in sec) and is represented by an equation of the form

$$\text{PE in } \sigma_\theta \equiv \left|1.0 - \left(\sigma_\theta/\sigma_{\theta_o}\right)\right| = 1-\exp(-\alpha_\theta s) \qquad (1)$$

where α_θ is a coefficient determined by the method of least squares. Table 1 presents a summary of α_θ evaluated from data collected at 7 levels and grouped according to 6 different Pasquill stability categories. These stability categories were determined from $\partial T/\partial z$ evaluated between 3 and 91 m. The variation of α_θ with

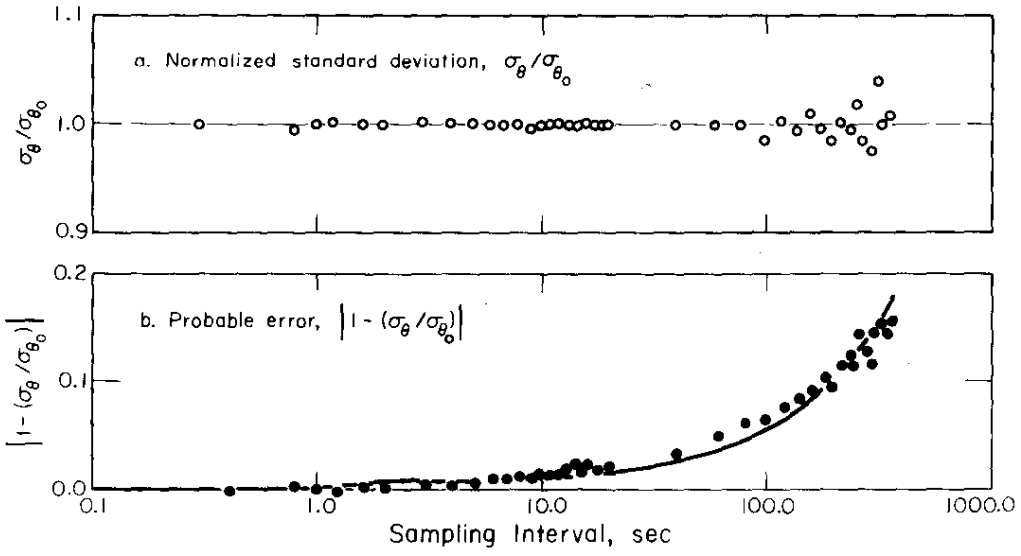

FIGURE 1. Standard Deviation of Horizontal Wind Direction at 18-m (WJBF-TV Tower)

height and stability is thus a measure of the variability of the PE in σ_θ for different sampling intervals as a function of height and stability condition. An identical procedure was used to examine the PE in σ_ϕ. Individual values of α_ϕ are also presented in Table 1.

TABLE 1

α_θ and α_ϕ as Functions of Height and Pasquill Stability Category

α_θ, 10^{-4} sec^{-1}

Pasquill Stability Category	Height Above Ground Level, m						No. of Cases	Average of All Heights
	10	18	91	137	243	304		
A	5.2	6.7	5.2	4.8	5.2	6.7	5	5.6
B	6.7	5.8	6.8	3.1	6.9	5.6	1	5.8
C	6.6	8.1	6.8	5.2	3.8	5.7	2	6.0
D	5.9	6.4	6.4	7.1	8.8	5.8	19	6.7
E	6.2	5.6	5.5	5.9	6.2	5.1	37	5.8
F	4.2	4.4	3.7	5.9	2.8	3.6	14	4.1
All	5.4	5.3	5.1	5.8	5.5	5.0	93	5.4

α_ϕ, 10^{-4} sec^{-1}

Pasquill Stability Category	Height Above Ground Level, m						No. of Cases	Average of All Heights
	10	18	91	137	243	304		
A	9.8	9.7	7.3	8.8	6.9	7.7	5	8.4
B	9.2	9.0	13.4	14.5	10.8	12.6	1	11.6
C	6.3	8.0	6.6	6.8	6.4	7.4	2	6.9
D	7.0	8.5	8.2	7.5	7.4	7.1	19	7.6
E	7.6	8.2	8.7	8.3	8.7	8.4	37	8.3
F	8.5	8.9	11.1	8.4	7.6	8.9	14	8.9
All	7.8	8.6	8.9	8.0	8.0	9.5	93	8.4

Probable error in σ_θ and σ_ϕ from using average values of α_θ and α_ϕ

	Sampling Interval, sec						
	5	10	20	30	60	180	300
PE in σ_θ, %	0.3	0.5	1.1	1.6	3.2	9.3	14.8
PE in σ_ϕ, %	0.4	0.8	1.7	2.5	4.9	14.0	22.4

The data in Table 1 do not indicate that a simple relationship exists between α_θ (or α_ϕ) and height. The values of α_θ and, hence, PE of σ_θ decreased by about 30% between categories D and F. No corresponding decrease in the value of α_ϕ is indicated although the data indicate larger probable errors in σ_ϕ than in σ_θ at any particular value of s. Note that the data in Table 1 are mostly for stable conditions.

The magnitude of the probable errors due to sampling interval is shown at the bottom of Table 1. The probable error of σ_θ and α_ϕ is less than 5% for sampling intervals of less than 60 sec when the sampling period is at least one hour long.

A similar method is used to examine the ratios $\theta_{pp}/\sigma_\theta$ and ϕ_{pp}/σ_ϕ. The major difference is that the value of the ratios rather than the probable error is given by an equation of the form:

$$\theta_{pp}/\sigma_\theta = \left[\theta_{pp_o}/\sigma_{\theta_o}\right] e^{-\beta\sqrt{s}} \qquad (2)$$

where θ_{pp} and θ_{pp_o} are the maximum ranges of azimuth observed over a 1-hr period for sampling intervals s and 0.4 sec, respectively, and β is a coefficient determined by the method of least squares.

Table 2 shows values of β as a function of height and stability. The data indicate that β_θ and β_ϕ do not vary appreciably with height, although β_θ decreases with increasing stability, and β_ϕ increases with increasing stability.

At the bottom of Table 2, representative values of $\theta_{pp}/\sigma_\theta$ and ϕ_{pp}/σ_ϕ are presented for several different sampling intervals. These values were obtained by use of mean values of β over all heights and stabilities, and average values of $\theta_{pp_o}/\sigma_{\theta_o}$ and $\phi_{pp_o}/\sigma_{\phi_o}$ of 7.0 and 10.7, respectively, for Period 1. Note that a commonly used assumption that $\theta_{pp}/\sigma_\theta = 6$ is seen to be most appropriate when a sampling interval near 15 sec is utilized and note that $\phi_{pp}/\sigma_\phi > \theta_{pp}/\sigma_\theta$.

TABLE 2

β_θ and β_ϕ as Functions of Height and Pasquill Stability Category

β_θ, 10^{-2} sec^{-1}

Pasquill Stability Category	Height Above Ground Level, m						No. of Cases	Average of All Heights
	10	18	91	137	243	304		
A	4.5	4.3	3.8	4.4	3.9	4.3	5	4.2
B	8.4	7.1	7.4	6.3	4.4	5.9	1	6.6
C	5.6	5.8	5.0	5.2	4.9	4.1	2	5.1
D	4.7	5.0	4.6	4.3	3.7	4.3	19	4.4
E	4.8	4.6	4.8	4.6	4.4	4.5	37	4.6
F	4.4	3.4	3.1	2.7	2.5	2.9	14	3.2
All	4.4	4.2	4.1	4.0	3.7	3.9	93	4.0

β_ϕ, 10^{-2} sec^{-1}

Pasquill Stability Category	Height Above Ground Level, m						No. of Cases	Average of All Heights
	10	18	91	137	243	304		
A	5.3	4.8	4.5	4.0	4.4	4.3	5	4.6
B	6.6	5.4	6.0	5.8	9.5	1.1	1	5.7
C	5.8	5.7	4.6	5.6	5.7	5.8	2	5.5
D	6.2	6.1	6.2	6.1	5.9	5.7	19	6.0
E	6.6	6.8	7.1	6.7	6.9	6.9	37	6.9
F	7.1	7.4	8.0	6.6	6.1	6.0	14	6.9
All	6.7	6.7	6.9	6.5	6.3	6.5	93	6.6

The ratios $\theta_{pp}/\alpha_\theta$ and ϕ_{pp}/α_ϕ obtained from using $\bar{\beta}_\theta$ and $\bar{\beta}_\phi$, and the average values for $\theta_{pp_o}/\sigma_{\theta_o}$ and $\phi_{pp_o}/\sigma_{\phi_o}$ of 7.0 and 10.7, respectively.

	Sampling Interval, sec						
	5	10	15	30	60	180	300
$\theta_{pp}/\sigma_\theta$	6.4	6.2	6.0	5.6	5.1	4.1	3.5
ϕ_{pp}/σ_ϕ	9.2	8.7	8.3	7.4	6.4	4.4	3.4

σ_θ AND VERTICAL TEMPERATURE GRADIENTS

For purposes of calculation, atmospheric stability is usually grouped into a finite number of categories. Each category defines separate equations to quantify the rate of atmospheric diffusion. Stability categories[1] are usually selected by means of σ_θ (limiting values are shown in column headings in Table 3). When σ_θ values are not available, stability categories are frequently defined by estimates of the vertical temperature gradient, $\partial T/\partial z$. Large variations in estimates of the value of $\partial T/\partial z$ obtained from temperature measurements at two heights are caused by the selection of these heights. For this reason, the use of $\partial T/\partial z$ to define stability categories is often used only as a last resort. Reference 2 defines stability categories to be used in assessment of releases made from nuclear facilities by the use of $\partial T/\partial z$ without specifying the measurement height. The defining values of $\partial T/\partial z$ used in Reference 2 are listed in Table 3.

The relationship between σ_θ and $\partial T/\partial z$ was examined when $\partial T/\partial z$ was estimated from temperature measurements over several different layers. The frequency of occurrence of each stability category as defined by σ_θ for Period 2 was compared with the frequency of stability categories obtained from estimates of $\partial T/\partial z$ for Period 2. Because different frequencies of stability categories would lead to different concentration estimates, the usefulness of $\partial T/\partial z$ to estimate σ_θ is evaluated best by using this method of comparison.

Table 3 presents frequencies of stability categories for Period 2 defined with σ_θ and $\partial T/\partial z$ by using limits outlined in Reference 2. The frequency distributions defined by σ_θ for the seven levels show a marked dependency on height and exhibit three distinct patterns: LOW, at 10 and 36 m; MID, at 91 and 137 m; and HIGH at 182, 243, and 304 m.

The frequency distribution of stability categories defined with $\partial T/\partial z$, however, show large departures from the above three basic patterns. The distributions given for the 10 to 91-m layer and the 10 to 137-m layer appear to be most representative of the HIGH pattern; the distribution given by the 36 to 137-m layer is best representative of MID, and the distribution given by the 91 to 137-m layer is best representative of LOW.

TABLE 3

Frequency Distribution of Pasquill Stability Categories[a]

Height, m	Stability Categories based on σ_θ							
	A σ_θ >23	B 18 ≤σ_θ <23	C 13 ≤σ_θ <18	D 8 ≤σ_θ <13	E 4 ≤σ_θ <8	F 2 ≤σ_θ <4	G σ_θ <2	
10	22.6	13.9	21.8	28.9	8.9	0.4	3.5	LOW
36	19.3	11.8	19.4	32.4	15.9	0.7	0.5	
91	9.6	6.7	13.5	21.7	29.6	16.4	2.5	MID
137	9.3	5.8	11.7	20.8	28.5	18.4	5.5	
182	7.0	2.9	6.8	17.1	25.9	25.6	14.7	
243	7.7	4.3	9.4	17.7	27.6	22.9	10.4	HIGH
304	7.2	3.7	8.0	17.2	28.7	23.9	11.3	

Layer	Stability Categories determined from $\partial T/\partial z$, °C/100 m						
	A γ ≤-1.9	B -1.9 ≤γ <-1.7	C -1.7 ≤γ <-1.5	D -1.5 ≤γ <-0.5	E -0.5 ≤γ <1.5	F 1.5 ≤γ <4.0	G γ >4.0
2- 10 m	49.8	0.4	0.8	4.8	8.1	6.7	29.4
2- 36	24.8	1.4	1.3	8.4	16.1	16.2	31.8
2- 91	19.1	3.7	4.0	13.4	23.0	23.0	13.8
2-137	16.5	6.1	5.3	18.7	27.7	21.1	4.6
2-243	0.0	1.1	5.9	30.7	47.5	13.8	1.0
2-335	0.0	0.2	5.9	33.5	54.7	5.5	0.2
10- 36 m	8.0	2.2	2.0	10.3	10.3	31.2	36.0
10- 91	2.9	4.0	5.9	22.3	14.8	38.8	11.3
10-137	3.2	5.6	7.7	27.0	16.4	37.6	2.5
10-243	0.0	0.0	0.0	33.7	28.9	37.3	0.1
10-335	0.1	0.0	0.0	38.2	36.4	25.3	0.0
36- 91	4.4	4.2	8.7	32.3	34.5	12.7	3.2
36-137	3.8	8.2	14.9	30.5	34.5	8.0	0.1
36-243	0.0	0.0	0.0	43.3	51.6	5.1	0.0
36-335	0.0	0.0	0.1	47.9	51.2	0.8	0.0
91-137	16.0	11.7	12.6	32.8	23.2	3.6	0.1
91-243	0.0	0.0	0.0	44.6	51.8	3.6	0.0
91-335	0.0	0.0	0.0	55.5	44.1	0.4	0.0

Stability Categories determined from Ri evaluated for the 10-91-m layer						
A Ri<-3.5	B -3.5≤Ri<-0.75	C -0.75≤Ri<-0.1	D -0.1≤Ri<0.15	E 0.15≤Ri<0.75	F[b] 0.75≤Ri<+3.5	G[b] Ri>3.5
3.0	6.1	28.0	10.0	31.4	19.5	1.8

a. During the period June 22, 1973, to November 23, 1973, for the Savannah River Plant, as determined from temperature gradients, standard deviation of horizontal wind speed, and Richardson numbers. The sampling period for all data was one hour. The total number of cases equalled 3600.

b. Golder's[3] stability category F was split into two, F and G, at Ri = 3.5.

Figure 2 presents frequency distributions of σ_θ for Period 2. The solid lines represent the observed distributions of σ_θ for LOW (10 to 36 m), MID (91, 137, and 182 m), and HIGH (243 to 304 m). The symbols indicate the frequency distribution obtained from use of $\partial T/\partial z$ evaluated over different layers to estimate σ_θ from the correlation in Reference 2 and presented in Table 3. The plotting code is located at the top of the figure. For the most part, temperature measurements for assessing atmospheric dispersion at a proposed site are obtained below a level of 100 m. For this reason, only temperature measurements at 2, 10, 36, and 91 m are used in this comparison. This presentation points out the inadequacy of $\partial T/\partial z$ to represent σ_θ, especially for a value of σ_θ <4 deg for which the frequencies are greatly overestimated. The value of σ_θ obtained from $\partial T/\partial z$ evaluated over the 36 to 91-m layer show the best fit with the observed distributions at small values of σ_θ (Figure 2).

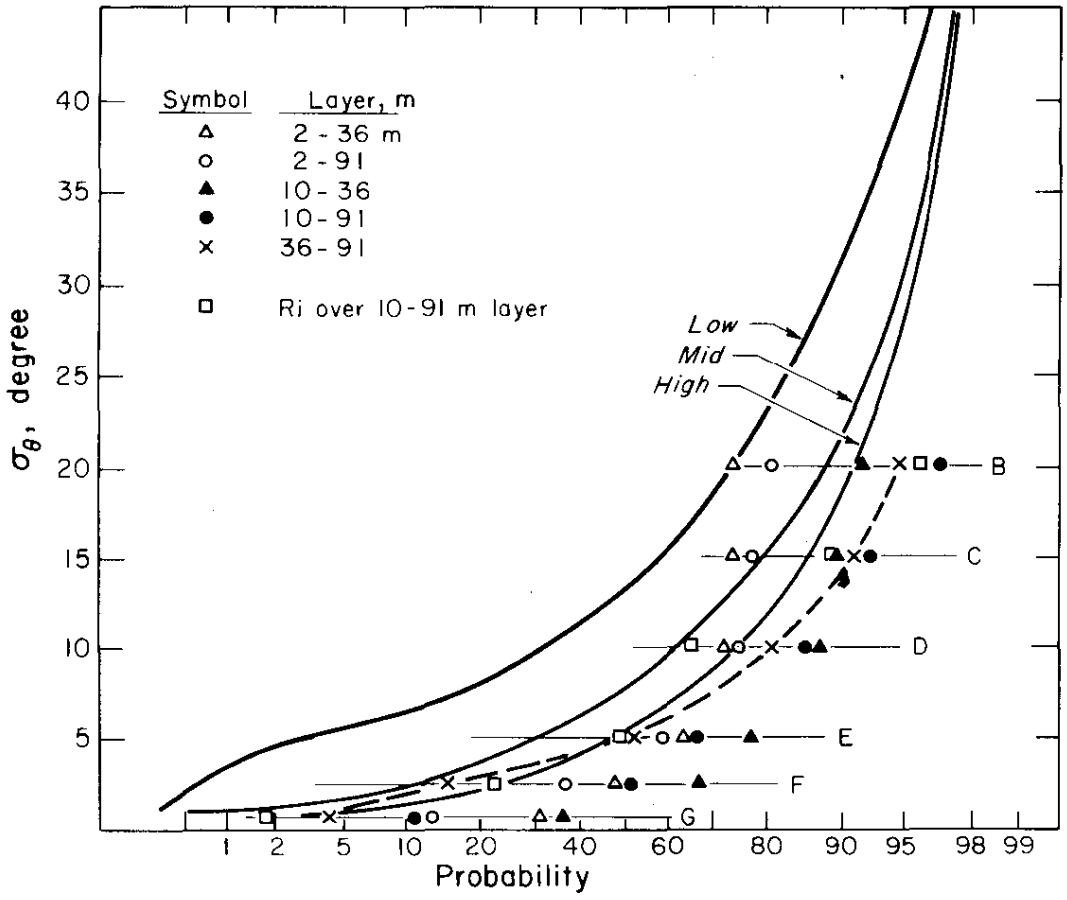

FIGURE 2. Frequency Distribution of σ_θ for Period 2

STABILITY CATEGORIES AND RICHARDSON NUMBER

A parameter that is a better indicator of stability than $\partial T/\partial z$ is the Richardson number, Ri, given by

$$Ri = \frac{g/\overline{\theta} \cdot \partial\theta/\partial z}{(\partial V/\partial z)^2} \qquad (3)$$

where g is acceleration due to gravity, $\overline{\theta}$ is the mean potential temperature, $\partial\theta/\partial z$ is the vertical gradient of potential temperature, and $\partial V/\partial z$ is the vertical wind shear within the layer.

The relationship between Ri, stability category, and surface roughness used in this study is given in Reference 3. At the bottom of Table 3 is presented a frequency distribution of stability categories defined through use of Ri calculated from data at the 10- and 91-m levels. The limiting values were extracted from Reference 3 and assumed to apply at a height of 50 m and to a surface roughness of 50 cm. Note that the frequency distribution is similar to MID except for D and C stability categories.

ESTIMATES OF σ_θ AND σ_ϕ BASED ON θ_{pp} AND ϕ_{pp}

The ratios $\theta_{pp}/\sigma_\theta$ and ϕ_{pp}/σ_ϕ were obtained for each hour of Period 2. Table 4 presents average values of the ratios tabulated as a function of height and Pasquill stability category (evaluated from $\partial T/\partial z$ over the 10 to 91-m layer). The data indicate a different magnitude of the ratio for the stable cases (Pasquill categories E-G) than for the unstable cases (Pasquill categories A-D). Furthermore, the ratios appear to be uniform within the three layers (LOW, MID, and HIGH) as defined above. The data at the bottom of Table 4 present mean values of the ratios expressed in terms of these broad stability and height categories.

The largest value of the ratio $\theta_{pp}/\sigma_\theta$ occurs for unstable/HIGH and the smallest value for stable/HIGH. Note for unstable cases, the ratio increases with height; and for stable cases, the ratio decreases with height. The use of the approximation $\sigma_\theta = \theta_{pp}/6$ would provide estimates only 0.3% too high for unstable/LOW, but 10% too low for unstable/HIGH, and 34% too high for stable/HIGH.

For the ratio ϕ_{pp}/σ_ϕ, the largest value occurs for stable/LOW, and the smallest value occurs for unstable/HIGH. Note for both stable and unstable cases, the ratio decreases with increasing height. The use of the approximation $\sigma_\phi = \phi_{pp}/6$ would produce

TABLE 4

Average Values of $\theta_{pp}/\sigma_\theta$ and σ_{pp}/σ_ϕ as Functions of Height and Pasquill Stability Categories for Period 2

$\theta_{pp}/\sigma_\theta$

Stability[a]	Height, m 10	36	91	137	182	243	304	No. of Cases[b]
A	5.9	6.1	6.3	6.4	6.3	7.0	5.9	71
B	6.1	5.9	6.4	6.6	6.7	6.9	6.8	98
C	6.1	5.8	6.4	6.7	6.4	6.8	6.7	145
D	6.1	5.9	6.4	6.6	6.2	6.5	6.7	548
E	6.0	5.8	5.8	5.9	5.0	5.0	5.1	363
F	5.4	4.9	4.8	4.8	4.2	4.3	4.2	941
G	5.2	5.8	4.8	4.6	4.5	4.0	4.0	278

ϕ_{pp}/σ_ϕ

A	7.4	6.9	6.4	6.7	6.3	6.1	5.7	71
B	7.6	7.4	6.7	6.7	6.4	6.2	6.2	98
C	7.6	7.4	6.6	6.6	6.4	6.5	6.1	145
D	7.6	7.3	6.7	6.9	6.8	6.9	6.8	548
E	7.5	8.0	8.0	8.3	8.1	7.4	7.5	363
F	7.9	8.6	8.4	7.3	7.4	6.6	7.9	941
G	8.1	7.8	7.0	7.1	7.7	5.8	7.5	278

	LOW		MID		HIGH	
	$\theta_{pp}/\sigma_\theta$	ϕ_{pp}/σ_ϕ	$\theta_{pp}/\sigma_\theta$	ϕ_{pp}/σ_ϕ	$\theta_{pp}/\sigma_\theta$	ϕ_{pp}/σ_ϕ
Unstable	5.98	7.40	6.47	6.66	6.58	6.37
Stable	5.52	7.98	5.12	7.68	4.48	7.32

a. The Pasquill Stability Category was based upon $\partial T/\partial z$ evaluated over the 10-91 m layer.

b. The total number of cases was 2444, and the sample interval was 5.0 sec.

estimates of σ_ϕ that would be in error by an amount ranging between 6% too low for unstable/HIGH and 25% too low for stable/LOW.

Since pollutant concentration is inversely related to σ_θ and σ_ϕ, the estimates of σ_ϕ would overestimate concentrations for all stability cases, while estimates of σ_θ would tend to underestimate concentrations for stable cases and overestimate for unstable cases. The combination of the two would produce overestimates during unstable conditions and slight underestimates for stable conditions.

The use of the average ratios in Table 4 (in place of the constant 6) may prove to be the most appropriate means of estimating σ_θ or σ_ϕ from θ_{pp} and ϕ_{pp}, respectively.

COMPARISON OF METHODS FOR CALCULATING DILUTION FACTORS

Different methods to estimate the value of the dispersion coefficients σ_y and σ_z are used with diffusion models, such as the continuous point source model shown in Equation 4.

$$\chi = \frac{Q}{2\pi} \frac{1}{u\sigma_y\sigma_z} e^{-(h^2/2\sigma_z^2 + y^2/2\sigma_y^2)} \qquad (4)$$

A number of the formulations for σ_y and σ_z are listed in Table 5. The frequency distribution of the dilution factor, $u\sigma_y\sigma_z$, was obtained with these various methods using data collected during Period 2. This frequency distribution allows the effects of several methods for estimating atmospheric dispersion to be compared. This comparison was done for a downwind distance of 5 km and is shown in Figure 3.

CONCLUSIONS

This comparison of the frequency distributions of the dilution factor (Figure 3) leads to the following conclusions:

1. Curve 1, based on direct measurements of σ_θ and σ_ϕ, is assumed to provide the best estimate.

2. Frequency distributions calculated by the different methods vary greatly. The variations are particularly evident at high cumulative probabilities but also occur at low probabilities, i.e., for a similar value of the dilution factor, the probability of occurrence ranges between 1 and 15%.

3. The discontinuity in Curve 2 is caused by a step function in stability categories.

4. Large variations occur as a result of the choice of layers over which vertical temperature measurements are obtained. In fact, the comparison between Curves 3 and 6 indicates much bigger effects of the height of measurement than from the method used to calculate σ_y and σ_z as a function of distance.

The errors caused by the use of $\partial T/\partial z$ are greater than those involved in calculating σ_θ and σ_ϕ directly from measurements of θ and ϕ with sampling times as long as a few minutes (Table 1), or even from those obtained by examining the peak-to-peak values of θ and ϕ (Table 2).

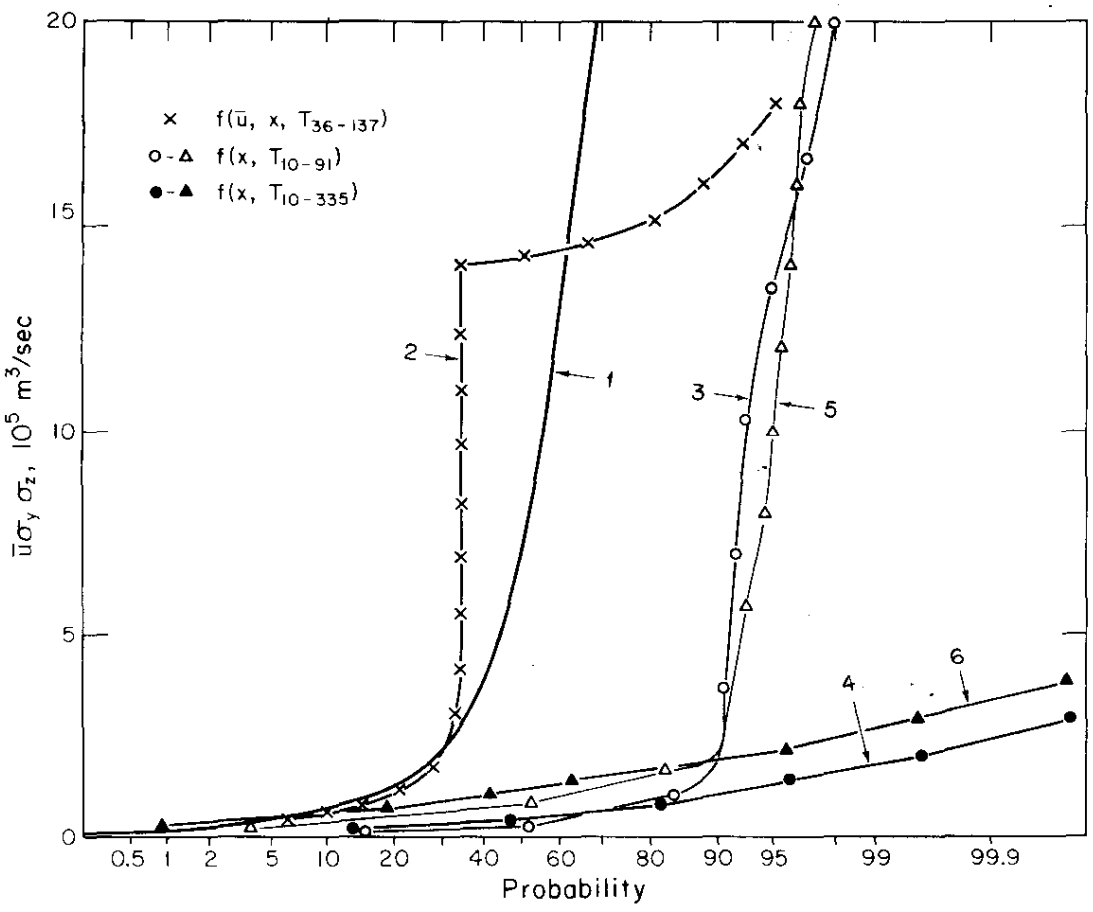

FIGURE 3. Frequency Distribution of the Dilution Factor, $\sigma_y\sigma_z\bar{u}$, Downwind Distance of 5 km during June to November 1973. Statistics Obtained for Observation Made at a Height of 91 m (WJBF-TV Tower)

TABLE 5

Commonly Used Methods for Obtaining Estimates of Dispersion Coefficients

A. Relationship of the form $\sigma_y = \alpha\sigma_\theta x^B$, $\sigma_z = \alpha\sigma_\phi x^C$

Stability	α	σ_θ	σ_ϕ	B	C	Curve No.	Reference
Stable $T_{137} - T_{36} > 0$	0.15	Observed	Observed	0.71	0.71	1	4
Unstable $T_{137} - T_{36} \leq 0$	0.045	Observed	Observed	0.86	0.86	1	4
Stable $T_{137} - T_{36} > 0$	0.15	3.0R + 2.0	(0.5R + 0.2) σ_θ	0.71	0.71	2	5
Unstable $T_{137} - T_{36} < 0$	0.045	23/$\bar{u}$ + 4.75	0.7 σ_θ	0.86	0.86	2	5
Very Unstable $\partial T/\partial z < -1.9$°C/100 m	1	0.40	0.40	0.91	0.91	3,4	6
Unstable $-1.9 \leq \partial T/\partial z < -1.5$	1	0.36	0.33	0.86	0.86	3,4	6
Neutral $-1.5 \leq \partial T/\partial z < -0.5$	1	0.32	0.22	0.78	0.71	3,4	6
Stable $\partial T/\partial z > -0.5$	1	0.31	0.06	0.71	0.71	3,4	6

B. Simple formulation with Stability Category obtained from estimates of $\partial T/\partial z$

Temperature Change with Height, °C/100 m	σ_y	σ_z	Curve No.	Reference
$\partial T/\partial z < -1.9$	$0.22x(1 + 10^{-4}x)^{-\frac{1}{2}}$	$0.20x$	5,6	*c*
$-1.9 \leq \partial T/\partial z < -1.7$	$0.16x(1 + 10^{-4}x)^{-\frac{1}{2}}$	$0.12x$	5,6	*c*
$-1.7 \leq \partial T/\partial z < -1.5$	$0.11x(1 + 10^{-4}x)^{-\frac{1}{2}}$	$0.08x(1 + 2\cdot10^{-4}x)^{-\frac{1}{2}}$	5,6	*c*
$-1.5 \leq \partial T/\partial z < -0.5$	$0.08x(1 + 10^{-4}x)^{-\frac{1}{2}}$	$0.06x(1 + 1.5\cdot10^{-3}x)^{-\frac{1}{2}}$	5,6	*c*
$-0.5 \leq \partial T/\partial z < 1.5$	$0.06x(1 + 10^{-4}x)^{-\frac{1}{2}}$	$0.03x(1 + 3\cdot10^{-4}x)$	5,6	*c*
$\partial T/\partial z \geq 1.5$	$0.04x(1 + 10^{-4}x)^{-\frac{1}{2}}$	$0.02x(1 + 3\cdot10^{-4}x)$	5,6	*c*

a. R is a random number generated independently and uniformly between 0.0 and 1.0.

b. Curve 3 and 5 $\partial T/\partial z$ evaluated over 10-91 m layer; Curve 4 and 6 $\partial T/\partial z$ evaluated over 10-335 m layer.

c. G. A. Briggs, Oak Ridge National Laboratory, Oak Ridge, Tenn. Personal communication (1974).

REFERENCES

1. F. Pasquill. "The Estimation of the Dispersion of Windborne Material." *Meteorol. Mag. 90*, 1063 (1961).

2. United States Atomic Energy Commission. "Safety Guides for Water Cooled Nuclear Power Plants." *Safety Guide Number 23: Onsite Meteorological Programs*, pp 23.1 - 23.13. USAEC, Division of Reactor Standards, Washington, DC. (1972).

3. D. Golder. "Relations Among Stability Parameters in the Surface Layer." *Boundary-Layer Meteorol. 3*, 47-58.

4. I. A. Singer, J. A. Frizzola, and M. A. Smith. "A Simplified Method of Estimating Atmospheric Diffusion Parameters." *J. Air Pollution Control Assoc. 16* (11), 594-596 (1966).

5. T. V. Crawford. *Progress Report Dose-To-Man Program — FY 1973.* USAEC Report DP-1341, E. I. du Pont de Nemours and Co., Savannah River Laboratory, Aiken, S. C. (1974).

6. M. E. Smith, ed. *Recommended Guide for the Prediction of the Dispersion of Airborne Effluents.* The American Society of Mechanical Engineers Press, New York, N. Y. (1968).

2. AERODYNAMIC FLYING OF BIVANE WIND DIRECTION INDICATORS †

INTRODUCTION

In October 1965, the 427-meter WJBF-TV tower near Beech Island, South Carolina, was instrumented to obtain meteorological data for reactor safety studies at the Savannah River Plant. Data were continuously collected from the tower between 1966 and 1968 and then intermittently until May 1972 when a fire at the TV station suspended data collection. In May 1973, the bivane wind systems and platinum resistance thermometers were improved, and a *Datacom* magnetic recording acquisition system was installed.

Measurements of temperature, azimuth (θ), elevation angle (ϕ), and wind speed (V) at seven levels between 2 and 335 m on the TV tower are currently monitored at a sampling interval of five seconds. The primary objectives of the data acquisition program is to compile statistics relevant to atmospheric diffusion models (e.g., σ_θ, σ_ϕ, $\bar{\theta}$).

Current programs at the Savannah River Laboratory involve modeling the transport and diffusion of radioactive effluents over large travel distances. In this research effort, empirical relationships must be developed to provide estimates of vertical fluxes within the planetary boundary layer by measuring vertical gradients of temperature and wind speed. To obtain relevant data to meet this objective, accurate measurements of vertical elevation angle, ϕ, must be obtained.

As a result of an analysis of mean values of ϕ obtained during the 1966-1968 study, the validity of ϕ has been questioned, and the source of errors has been examined. Several factors could have led to errors in the measurement of ϕ: improper leveling of the direction transmitter, faulty potentiometers, improper conversion of output signal, and poor aerodynamic characteristics of bivane tail. Error due to improper leveling has been reduced through use of electrostatic levelers built into the direction transmitters. Potentiometer problems have been minimized by routine replacement at 3-month intervals. In this paper, the order of magnitude of the error that results when the tail assembly acts as an airfoil has been determined.

---

† Work done by M. M. Pendergast and J. F. Schubert. Accepted for publication in the *Journal of Applied Meteorology*.

EXPERIMENTAL PROCEDURE

Aerodynamic flying of new bivane tails was examined by comparing elevation angles associated with different tail orientations. The tail assembly was placed in a wind tunnel, and the orientation of the tail with respect to the wind direction was carefully noted. The output from the elevation angle potentiometer was recorded on a strip-chart recorder. The tail was rotated, and a recording was made of the output at the new tail orientation after a sufficient time had been allowed for the wind tunnel flow to stabilize. The procedure was repeated until the tail was returned to its original position. This procedure required that the flow be steady so that the range of ϕ was not due to oscillations of flow in the wind tunnel.

Figure 1a shows the results of the wind tunnel test of Tail 2. The five strip chart segments, labeled A through E, represent ϕ at the different tail orientations. The symbol $\dot{X}$ represents the tail orientation; the dot over the X indicates a reference point, at the top for segment A and rotated 90 deg in a counterclockwise direction about the longitudinal axis for other segments. Note that segments A and E have the same tail orientation and similar values of ϕ. Segment C corresponding to a rotation of 180 deg from the original position shows a departure of 3.5 deg from the original. Figure 1b shows the results of a similar test for Tail 3. The values of ϕ for this tail deviate less than 1 deg as the tail is rotated through the full 360 deg. This range of ϕ as the tail is rotated through 360 deg is assumed to be a measure of the error attributed to aerodynamic flying of the tail.

The range of ϕ determined for eight Climet* and 22 MRI** bivane tails are summarized in Table 1. The Climet tails were taken directly out of the shipping boxes and tested at the Southern Forest Fire Laboratory wind tunnel at Macon, Georgia. The results of these tests are shown in Table 1a and labeled "before". After the tails had been in operation on the TV tower for five months they were tested again. These tests were accomplished through the use of the new wind tunnel test facility at the Savannah River Plant and are labeled "after" in Table 1a.

Table 1b presents results of tests of the aerodynamic characteristics of the MRI bivane tails conducted at the SRP wind tunnel. The mean values of the range of ϕ for the MRI tails are slightly smaller than the Climet tails although the standard deviations of the range of ϕ are about equal.

---

* Climet Instrument Company, Sunnyvale, California
**Meteorology Research Inc., Altadena, California

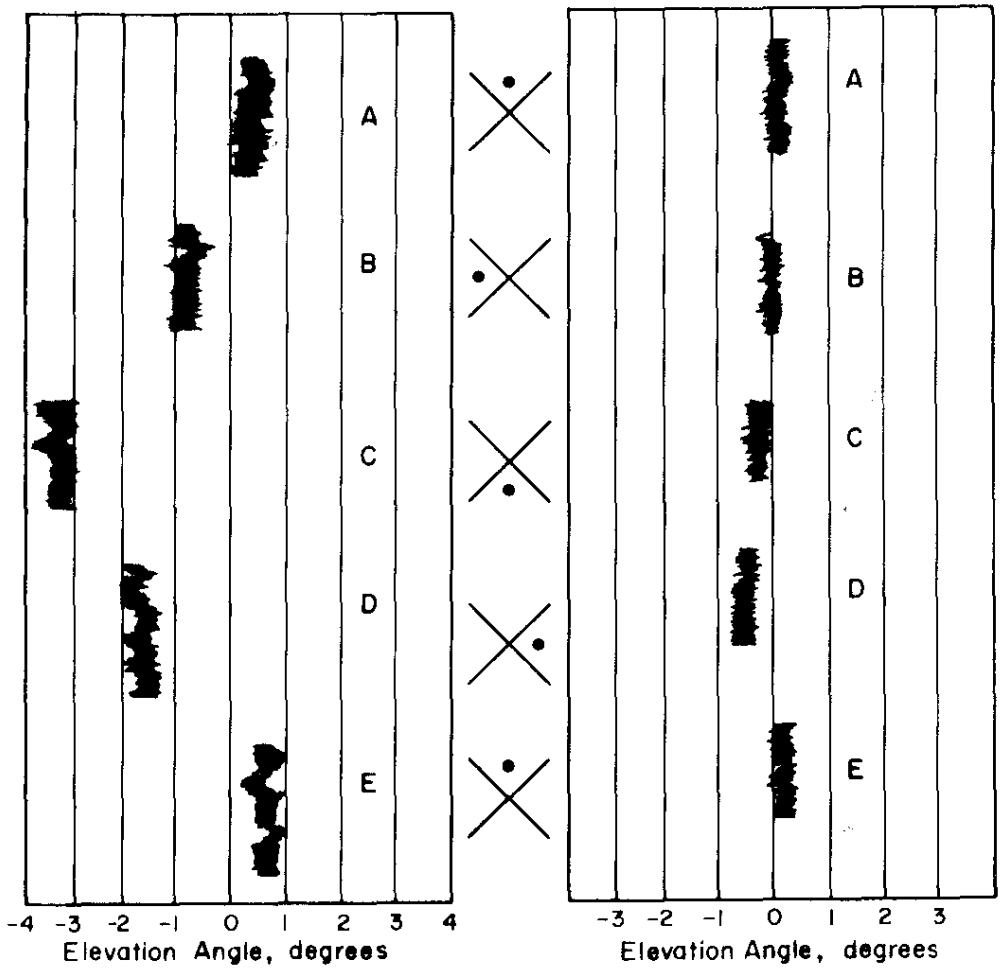

FIGURE 1. Results of the Wind Tunnel Tests of Bivane Tails

(the Symbol, X, at the center of the figure represents a view of the tail looking upwind, and the dot indicates a reference point).

TABLE 1. Range of Elevation Angle, ϕ, as Result of Rotation of Tails through 360 Degrees.

Climet Tails

Tail	Range of Elevation Angle, degrees		Instrument Height Above Ground, meters
	Before Service	After Service	
1	0.5	4.0	18
2	3.5	3.0	10
3	1.0	1.5	137
4	2.5	3.0	91
5	4.0	6.5	243
6	1.5	6.0	183
7	4.5	-	-
8	1.5	7.0	305
Avg	2.4	4.4	
Std Dev	1.5	2.1	

MRI Tails

No. of Tails Tested	Mean Range of Elevation Angle, degrees	Standard Deviation of Elevation Angle, degrees
22	1.5	1.3

DISCUSSION

The wind tunnel experiments indicate that the advertised accuracy of the Climet bivane system of ±1 deg for ϕ does not take into account the variability due to aerodynamic lift as the result of tail orientation. Even after the direction translator is mounted in a vertical position, flying of the tail could cause an offset of as much as 3 deg in the value of ϕ. By analogy, one can assume that the horizontal direction could be offset by a similar amount.

After the Climet tails had been in operation for five months, a significant amount of the tail had deteriorated. The primary effect of the deterioration was to alter the balance of the tail assembly. The largest increase of the error due to flying was found to occur to tails installed at the three highest levels of the tower (183, 243, and 305 m above ground).

SUMMARY

An appreciable error in ϕ can be introduced by the orientation of the bivane tail as it is mounted on the wind sensor. For most tails, no visible damage is apparent. As the tail becomes weathered and starts to deteriorate, the changed dynamic characteristics can cause additional errors.

3. EVALUATION OF DIFFERENT METHODS OF ESTIMATING VERTICAL EDDY DIFFUSIVITIES FROM TV TOWER DATA†

INTRODUCTION

The simple diffusion process is one in which the rate of transfer of an entity across a reference level is expressed by the product of a diffusion coefficient and the spatial gradient of the entity at that level. The flux of parameter χ, F_χ, in the z direction is given by

$$F_\chi = -K_z \frac{\partial \chi}{\partial z} \tag{1}$$

which is the defining equation for K_z.

The conduction equation, shown below, makes use of this approximation to describe diffusion of atmospheric constituents in the vertical direction.

$$\frac{\partial \chi}{\partial t} = \frac{\partial}{\partial z}\left(K_z \frac{\partial \chi}{\partial z}\right) \tag{2}$$

Successful application of this relationship is dependent on selection of values of the coefficient K_z, called the vertical eddy transfer coefficient. The simplest solution of the conduction equation occurs when K_z is constant (i. e., independent of x, y, and z) which is referred to as Fickian diffusion.

K_z can be determined by evaluating the flux and the vertical gradient of χ over a prescribed time interval, τ. Generally, the value of K_z determined in this way is assumed to be valid at the center of a time interval, τ, and at the height at which the flux and gradients are evaluated. This relationship is useful because a value of K_z determined through observations of one constituent can often be applied to other constituents, and also it makes many of the applied diffusion problems numerically tractable.

This paper is concerned with the determination of K_z as a function of height and time, utilizing meteorological data collected at the WJBF-TV tower, located near the Savannah River Plant.

---

† Work done by M. M. Pendergast and B. Gottlieb (Faculty Research Participant), to be published.

PROCEDURE

The data collected at the WJBF-TV tower consists of the three-dimensional wind velocity and temperature at seven levels between 2 and 335 m. The data acquisition program at the WJBF-TV tower was initiated by the Savannah River Laboratory in 1966 in order to collect meteorological statistics relevant to SRP safety studies. In 1972, the data acquisition system was refined so that statistics relevant to SRP and AEC studies (i.e., σ_a, σ_e, and dT/dz...) could be computed directly. The fast response of the wind instruments (0.5 sec) also permits the direct calculation of momentum flux, which, when combined with the vertical gradients of wind speed can be used to determine the vertical exchange coefficient for momentun, K_m, using the defining relationship[1]

$$K_m = \left(\frac{\overline{u'w'}^2 + \overline{v'w'}^2}{\left(\frac{\partial \bar{u}}{\partial z}\right)^2 + \left(\frac{\partial \bar{v}}{\partial z}\right)^2} \right)^{\frac{1}{2}} \qquad (3)$$

where $\bar{u}$, $\bar{v}$, and $\bar{w}$ are the mean east-west, north-south, and vertical wind, respectively, and primed values are fluctuations about the mean value. Analogously, the vertical exchange coefficient for heat, K_h, is defined by

$$K_h = \frac{\overline{\theta'w'}}{\frac{\partial \bar{\theta}}{\partial z}} \qquad (4)$$

where θ is the potential temperature.[1] Factors other than vertical eddy transport influence the air temperature distribution, namely, horizontal advection and radiation. Thus, calculation of K_h from its definition is not quite as satisfying as is the applications of this approach for K_m. In 1972, the principal measuring sensors were platinum resistance thermometers with time constants of about 40 sec. Thus, it was not possible to calculate $\overline{\theta'w'}$ with much meaning because much of the flux is caused by eddies with characteristic time scales less than 40 sec.

Another approach for determining K_h makes use of the diurnal change of temperature at several levels above the ground. This approach is practical because a fast response thermometer is not required. The basis for this approach is the assumption that the eddy transport is the major mechanism of altering the air temperature. The ground is heated and then turbulent transport causes the temperature wave to propagate upward. A finite time is needed to alter the phase and the amplitude of the diurnal temperature wave with height. The rate at which the amplitude and phase relationships change with height can be related to the eddy transport coefficient for heat. Sutton[1] has shown that the temperature wave can be given by

$$T(z,t) = T_o + \sum_{n=1}^{N} T_n \exp\left(-z\sqrt{\frac{n\omega}{2K_h}}\right)\cos\left[n\omega t - \left(\varepsilon_n + z\sqrt{\frac{n\omega}{2K_h}}\right)\right] \quad (5)$$

under the assumption of Fickian diffusion (K_h constant with time and space) where $T(z,t)$ is temperature at height z and time t; T_n is the amplitude of the n^{th} Fourier harmonic; ε_n is the phase lag in radians; and ω is the angular velocity of earth's rotation. This relationship has been used to express K_h as a function of the phase and amplitude relationships for the first two harmonics (n=1 and n=2). The resulting equations shown below provide estimates of K_h based on Equation 5.

$$\omega\delta_1 = (z_2 - z_1)\sqrt{\frac{\omega}{2K_h}} \quad (6)$$

$$\alpha_1 = \exp\left[\sqrt{\frac{\omega}{2K_h}}\ (z_2 - z_1)\right] \quad (7)$$

$$2\omega\delta_2 = (z_2 - z_1)\sqrt{\frac{\omega}{K_h}} \quad (8)$$

$$\alpha_2 = \exp\left[\sqrt{\frac{\omega}{K_h}}\ (z_2 - z_1)\right] \quad (9)$$

The coefficients α_1 and α_2 are the ratios of amplitudes of the wave at level z_1 and z_2 for the first and second harmonic, respectively; δ_1 and δ_2 are the phase lags in seconds between levels z_1 and z_2 for the first and second harmonic, respectively. After a number of diurnal temperature waves were compared with a plot of the first and second harmonic, the first harmonic was found to be a reasonable first approximation to the observed temperature wave; however, inclusion of the second harmonic is necessary.

A previous study of the vertical variation of K_h was reported in Reference 2. In these calculations, the phase lag and amplitude change with height of mean observed temperature waves were used. The procedure involved the visual determination of the temperature maxima and minima as well as the time of maxima and the time of minima as shown in Figure 1. Note that the time of maxima would be determined by the three points surrounding the maximum temperature, and the time of minima would also be determined by the three points near the time of minima. By breaking the wave down into the Fourier components, all points are utilized to determine the maxima and minima rather than just relying on the two or three points near the maxima or minima.

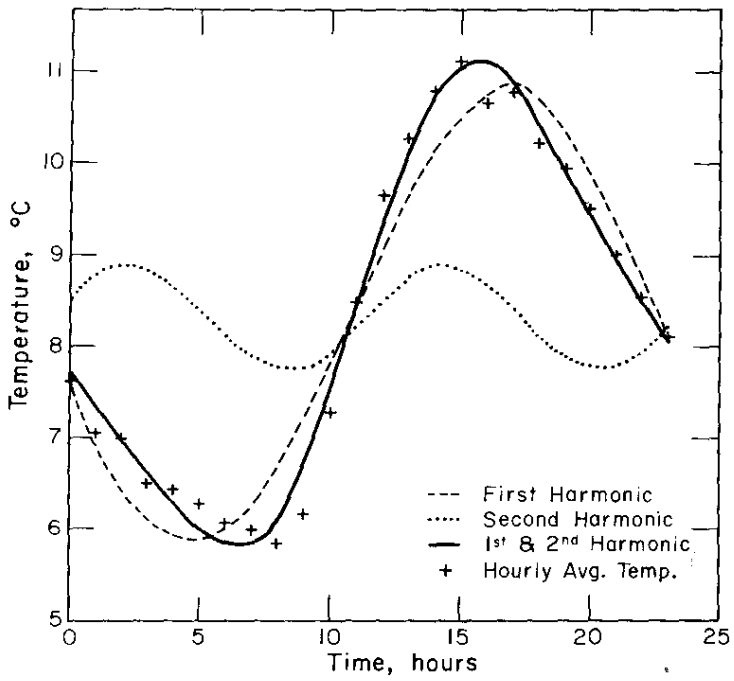

FIGURE 1. Hourly Average Temperature for the 10-m Level of the WJBF-TV Tower

DATA FILTERING

The determination of the various terms in Equations 3 and 5 are not as straightforward as it might appear. Erroneous values of meteorological parameters can occur due to instrument and recorder malfunction. These errors must be removed from the data base as they greatly affect the results.

Errors in the raw data are minimized by checking the data and filtering out erroneous points or ignoring a portion of the time series completely. The filtered data are used to calculate vertical gradients either analytically, from use of profiles fitted by curves using a method of least squares, or directly, using finite difference approximation. Specific methods are discussed in a later section.

The filtering portion of the computer code uses current estimates of the mean and the standard deviation of each parameter. Initially, these are given values based on a subjective assessment of the data. Because the calculations are done on a continuous time series and because mean values and standard deviations are calculated for finite time periods ranging from 20 min to 1 hr, the values of the mean and the standard deviation determined in the first time period are used as an estimate for the second. The filtering procedure is as follows:

1. Calculate the mean and standard deviation for the time series for various sample periods.

2. Compare the calculated value of the mean with the expected value (from the preceding time period). If the difference is greater than twice the expected value, then disregard the data from this sensor.

3. Compare the calculated standard deviation with the expected one, and reject data if the difference between the two is greater than twice the expected value.

4. When both the mean and the standard deviation have passed the tests, scrutinize each data point and assure that the individual values do not deviate from the mean values by more than 4 standard deviations. When more than a prescribed number of data points fail this test, delete this time period in the time series. If only a few records show erroneous "spikes" replace the individual points with the mean value and recalculate means and standard deviations.

CALCULATION OF K_m

The calculation of K_m at several different heights is obtained by use of Equation 3 and data collected between May and November 1973. The term in the numerator is estimated from measurements at each of the 7 levels. The denominator, $\sqrt{(\partial\bar{u}/\partial z)^2 + (\partial\bar{v}/\partial z)^2}$ is evaluated by obtaining an analytical expression for the variation of each wind component with height. The form of this expression is assumed to be a polynomial of the form

$$\bar{u} = az^2 + bz + c \qquad (10)$$

where a, b, and c are coefficients determined by least squares and $\bar{u}$ is the average east-west component of the wind at height z. A similar expression was used for the north-south component of the wind.

The resulting expression is differentiated and used to determine K_m at the level for which the numerator was evaluated. This provides a profile of K_m representative of the time period over which the data were taken.

When the filtering portion of the procedure rejects data for a level, this level is eliminated from the calculation. When more than 2 levels are rejected, the entire period is ignored because the analytical expression used to fit the components is assumed to be unsatisfactory.

RESULTS

Figures 2 and 3 show results of calculation of K_m at several levels during October 1973. The dotted line on Figure 3 represents diurnal change in K_m using a 30-min averaging time, and the solid line represents values using 60-min averaging time. Although considerable scatter is encountered in the preliminary calculations, a few generalized conclusions can be drawn:

1. Most values of K_m are within the ranges 1×10^4 to 1×10^6 cm^2/sec, which are in agreement with previous investigators.[1,2,3]
2. Profiles show a general increase with height up to 200 m during late morning and early afternoon.
3. Several profiles of K_m during early morning decrease slowly with height and show values generally less than 3×10^5 cm^2/sec. Several of the values of K_m calculated at 10 m during stable periods are very large ($>3 \times 10^5$ cm^2/sec) which may be the result of a poor fit of the wind profiles at the bottom of the profile giving unusually small values for the wind gradient.
4. Scatter of points is greatest during the hours 1000-1600, coinciding with the largest expected value of K_m.
5. Using a sample period of 1 hr produces different values of K_m than those calculated from using a sample period of 1/2 hr. For the cases examined, the values of K_m for stable periods were within a factor of 3; for unstable periods, differences of as large as an order of magnitude were observed.

CALCULATION OF K_h

The value of K_h is evaluated using Equation 5 and an analytical expression relating the phase and amplitude of the Fourier components of the diurnal temperature wave with height. These expressions are obtained from use of the filtered data fitted to an equation of the form

$$\delta = az^2 + bz + c + \frac{d}{z} + \frac{e}{z^2} \qquad (11)$$

through method of least squares. Note the fourth and fifth terms on the right side are most important in the lower levels and cause the curve to be nearly exponential near the ground which agrees with observed data. At higher levels the other terms predominate which causes the curve to approach a constant. This feature also agrees with observations. This curve fitting scheme appears to eliminate an improper change in phase and amplitude with height at the higher levels where phase and amplitudes change slowly with height.

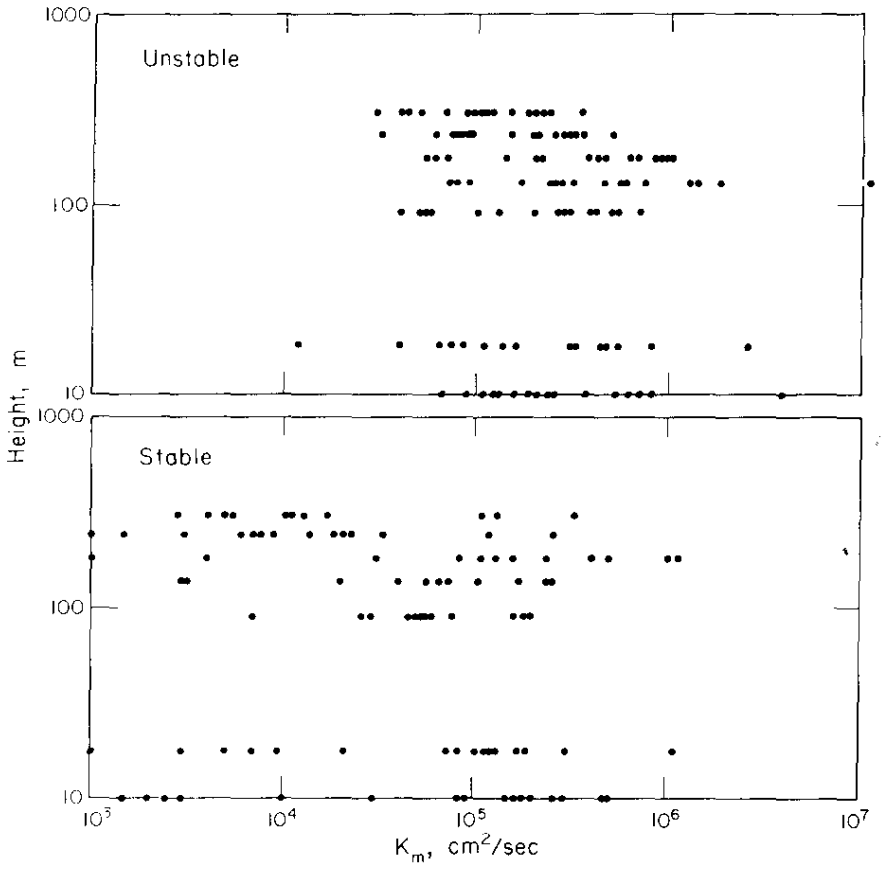

FIGURE 2. Representative Values of K_m as a Function of Height during October 1973

a. 1000-1500 EST

b. 0000-0959 EST

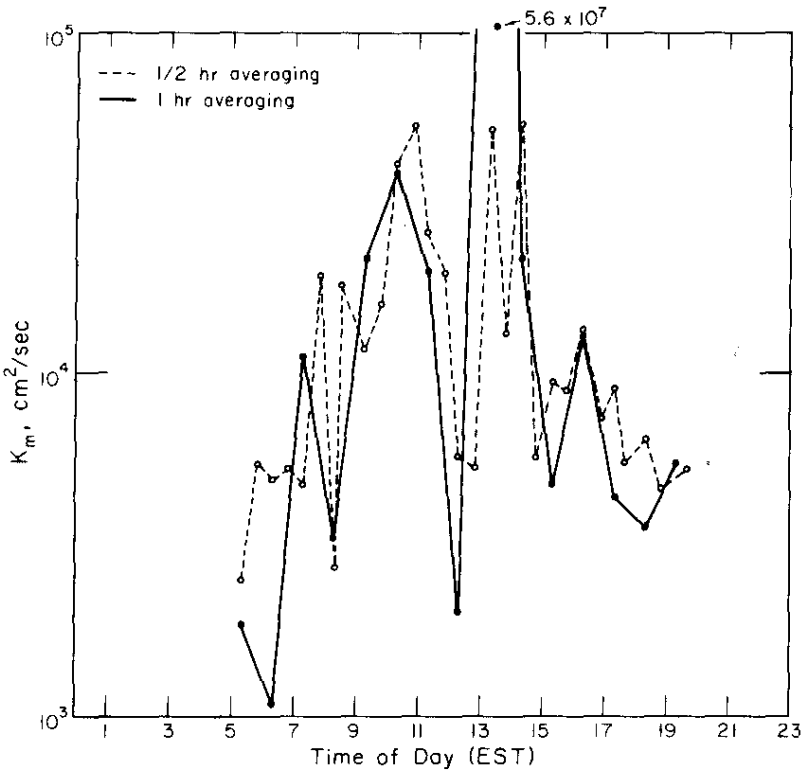

FIGURE 3. Diurnal Change of K_m at a Height of 91-m for October 2, 1973 using average times of 1/2 hr and 1 hr

PRELIMINARY RESULTS, K_h

The following represent results obtained using temperature data collected during the period 1966 to 1968. The resulting vertical profiles of K_h for several seasons have been compared to those made in a previous study[2] which involved plotting the mean temperature waves and picking off the amplitude and phase relationship subjectively. These data were then plotted on log-log paper, and a straight-line fit was made. Thus, the comparison not only checks the calculation procedure, but provides a means to determine the effect caused by using an objective analysis of the data. Figure 4 shows proviles of K_h for April 1966 determined objectively (indicated with closed symbols) and subjectively (indicated with open symbols) for Spring.[2] Profiles of K_h determined from phase relationships are shown with dashed lines, and profiles determined from amplitude relationships are shown with solid lines. Note the objective profile determined from the amplitude of the first harmonic is intermediate between profiles corresponding to the total amplitude and from the maximum temperature as determined by Crawford and Pendergast.[2] The subjective profiles seem more smooth and are in general agreement with profiles obtained by other investigators.[1] It is concluded that the calculational procedure fitting the amplitude of the first harmonic can be utilized with reasonable success to determine the profiles of K_h for various time periods.

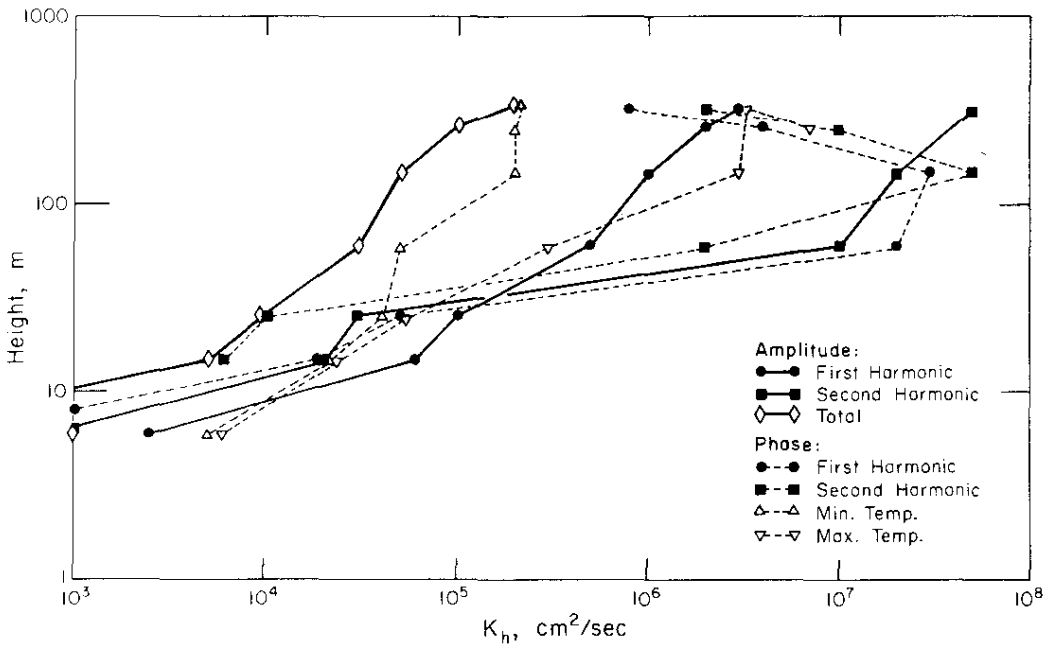

FIGURE 4. Profiles of K_h for April, 1966

REFERENCES

1. O. G. Sutton. *Micrometeorology.* McGraw-Hill, New York (1953).

2. T. V. Crawford and M. M. Pendergast. "Eddy Diffusivity as a Function of Height from TV Tower Temperature Data" in *Progress Report, Dose-To-Man Program, FY-1973.* USAEC Report DP-1341, E. I. du Pont de Nemours and Co., Savannah River Laboratory, Aiken, S. C. (1973).

3. D. H. Slade. *Meteorology and Atomic Energy.* USAEC Division of Technical Information, Oak Ridge, Tenn. (1968).

4. A CLIMATOLOGY OF THE MIXED LAYER USING ACOUSTIC METHODS †

INTRODUCTION

One of the major environmental concerns of today is the transport and dispersion of atmospheric pollutants. To improve predictive capabilities in this area, the fine-scale structure of the atmospheric mixed layer must be known. The need for more economical methods of obtaining data has resulted in a growing effort to study the structure of the atmospheric boundary layer through the use of remote sensing techniques. One of the methods proven successful for detecting small-scale fluctuations of the refractive index associated with changes in temperature, wind, and humidity in clear air is the use of acoustic echo sounding.

Acoustic waves propagating through the atmosphere are attenuated, scattered, and refracted by the fluctuations of the refractive index of air. If the interactions of acoustic waves are expressed in terms of the sonic refractive index where one N unit is one part in 10^6, the interaction of acoustic waves can be compared with those of radio and optical waves for a given change in atmospheric temperature, velocity, or absolute humidity. This is shown in Table 1 which is taken from the work of Little.[1]

The interaction of acoustic energy with the atmosphere is strong, because the atmosphere is the transmitting vehicle for the longitudinal pressure vibrations which travel with the velocity of sound. The speed of sound is given by

$$C = 331\sqrt{\frac{T}{273}}, \text{ m/sec} \qquad (1)$$

for dry air where T is air temperature in °K.

† Work done by J. F. Schubert. Presented at the *Third Symposium on Meteorological Observations and Instrumentations*, Washington, D. C., February 10-13, 1975.

TABLE 1

Comparison of Refractive Index Change for Acoustic, Radio, and Optical Waves for Small Changes in Atmospheric Parameters

Magnitude of Parameter Change	Change in Refractive Index, N Units[a]		
	Acoustic	Radio	Optical
1°K fluctuation in temperature	1700	1	1
1 m/sec variation in wind speed	3000	2×10^{-6}	2×10^{-6}
1 mb change in water vapor pressure	140	4	0.04

a. One N unit equals one part in 10^6.

ACOUSTIC SOUNDER

The system used at the Savannah River Laboratory (SRL) was developed by the University of Melbourne at Melbourne, Australia. When used in the monostatic mode, this system has a height range of 6,000 ft, frequency 1 to 2 KH_Z (variable), band width 5 H_Z, pulse length 0.1 to 1.0 sec (variable), transducer input 100 watts (max), and a sensitivity 0.9°C/100 ft.

SOUNDER DATA FROM THE SAVANNAH RIVER LABORATORY

To identify the various phenomena of climatological interest, a system of categorization proposed by G. H. Clark[2] and modified for use at SRL (Table 2) has been used.

The sounder was operated during various periods from September 1973, to June 1974, at SRL for a total of 916 hr (September, 12 hr; February, 167 hr; March, 408 hr; April, 98 hr; May, 231 hr). The data were tabulated by the maximum height of the mixed layer for each hourly period and frequency of occurrence (Table 3) and category and frequency of occurrence (Table 4). The height and category were tabulated for each hour during the period the sounder was operating. Table 3 shows that the mixed layer height was between 1,000 and 2,700 ft for 72.8% of the time for the periods sampled. When the data were compared to the calculated mean maximum mixed height (Pack and Hosler,[3] and Holzworth[4]), the calculated mean annual afternoon mixed height[4] was 4,600 ft, and the sounder maximum mean for the 916 hr sampled

was 2,600 ft. During this same period, most of the sounder records showed returns from a mixed layer, which was interpreted to be caused by surface heating (see Category Distribution in Table 4).

TABLE 2

Acoustic Sounder Data Categories

	99 - no data -- just plain wind noise
Category	1 - 0 to 500 ft thermospikes up to 1000 ft
Category	2 - back scattered layer
Category	3 - back scattered layer with waves
Category	4 - plumes over 1000 ft; very, very complex; many waves in the bottom layer
Category	5 - two layers in the bottom
Category	6 - two layers; separate, one over the other; large separation from the top to the bottom layer
Category	7 - multiple weak layers
Category	8 - strong multiple layers
Category	9 - ascending layer from the surface
Category	10 - ascending layer but not starting at the surface
Category	11 - descending layer but not merging with the surface
Category	12 - descending layer merging with the surface layer
Category	13 - just plain thermal plumes
Category	14 - stable multiple layer

By identifying the data in this manner, a statistical climatology may be constructed.

TABLE 3

Hourly Height Data at SRL

Height, ft	Frequency	Percent
500	2	0.218
700	1	0.109
800	1	0.109
900	1	0.109
1000	17	1.856
1100	13	1.419
1200	32	3.493
1300	37	4.039
1400	64	6.987
1500	93	10.153
1600	29	3.166
1700	41	4.476
1800	45	4.913
1900	5	0.546
2000	90	9.825
2100	23	2.511
2200	24	2.620
2300	20	2.183
2400	36	3.930
2500	62	6.769
2600	21	2.293
2700	15	1.638
2800	6	0.655
2900	1	0.109
3000	20	2.183
3100	2	0.218
3200	3	0.328
3300	2	0.218
3400	1	0.109
3500	9	0.983
3600	1	0.109
3700	2	0.218
4000	10	1.092
4500	17	1.856
9999	2	0.218
99999	168	18.341
TOTALS	916	100.000

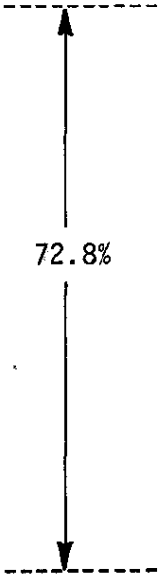

TABLE 4

Hourly Category Data at SRL

Category	Frequency	Percent
1	10	1.092
2	404	44.105
3	20	2.183
4	4	0.437
5	23	2.511
7	4	0.437
8	5	0.546
9	25	2.729
10	9	0.983
11	5	0.546
12	4	0.437
13	124	13.537
14	108	11.790
99	171	18.668
TOTALS	916	100.000

Table 4 shows that Category 2 was present for 44% of the time. Category 2 is usually a well-mixed convective layer with a well-defined upper boundary (Figure 1). In Category 13, there are well-developed thermal plumes (Figure 2). In Category 14, there are very stable multiple layers of temperature-turbulence stratification (Figure 3). Figures 4 and 5 depict the formation and dissipation of an inversion layer with a large separation between the inversion and the mixed layer near the ground surface (Category 6). In Category 99, the data are obscured by noise (wind, rain, etc.), or the data are missing because of equipment malfunction.

A typical diurnal pattern for March at SRL would show a stable multiple layer (Category 14) forming after sundown and persisting until a little after sunrise, and an ascending layer from the surface (Category 9) until about noon. About noon, the record shows a pattern of well-developed thermal plumes caused by surface heating. These thermal plumes continue until sundown,and the cycle is repeated.

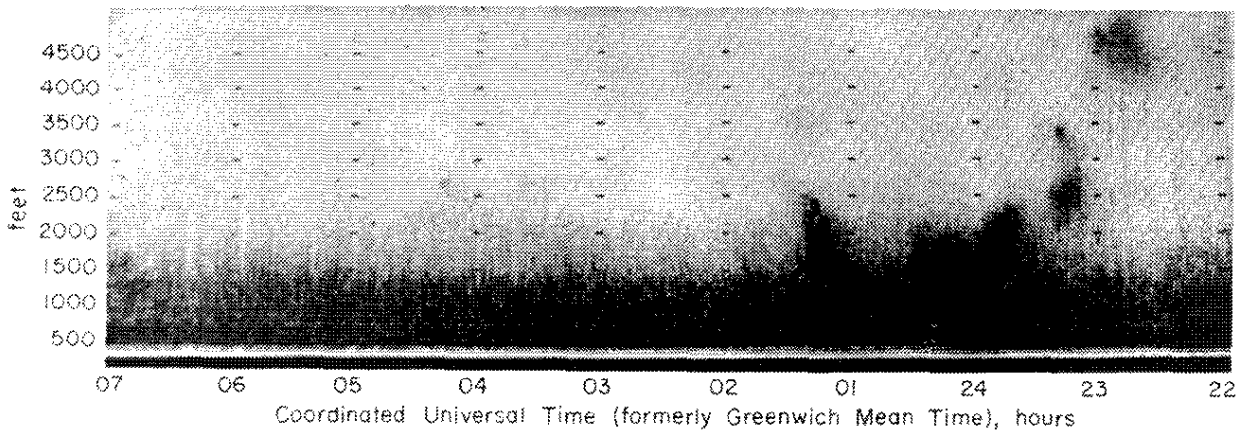

FIGURE 1. Category 2, Back Scattered Layer

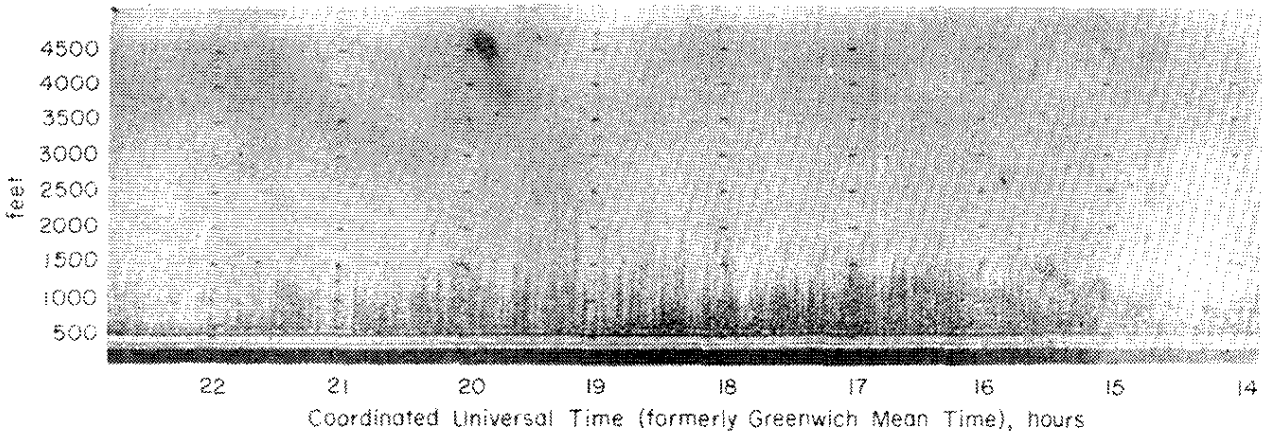

FIGURE 2a. Category 13, Thermal Plumes

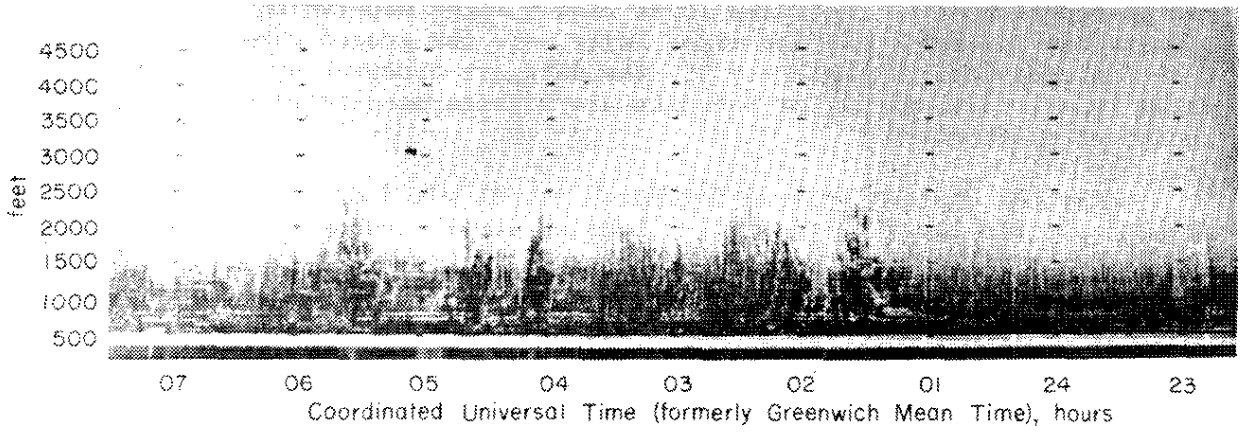

FIGURE 2b. Category 13, Thermal Plumes

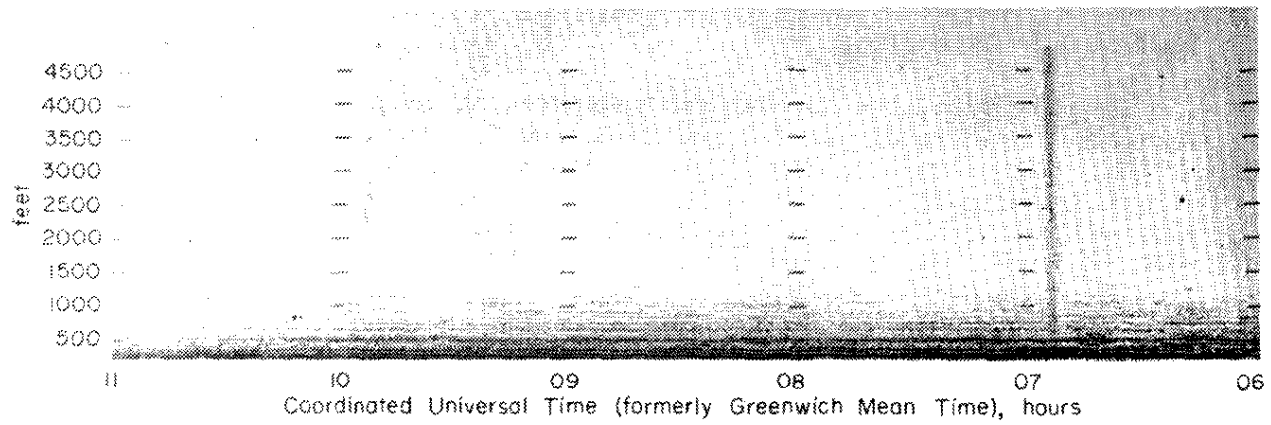

FIGURE 3. Category 14, Stable Multiple Layers Near the Surface

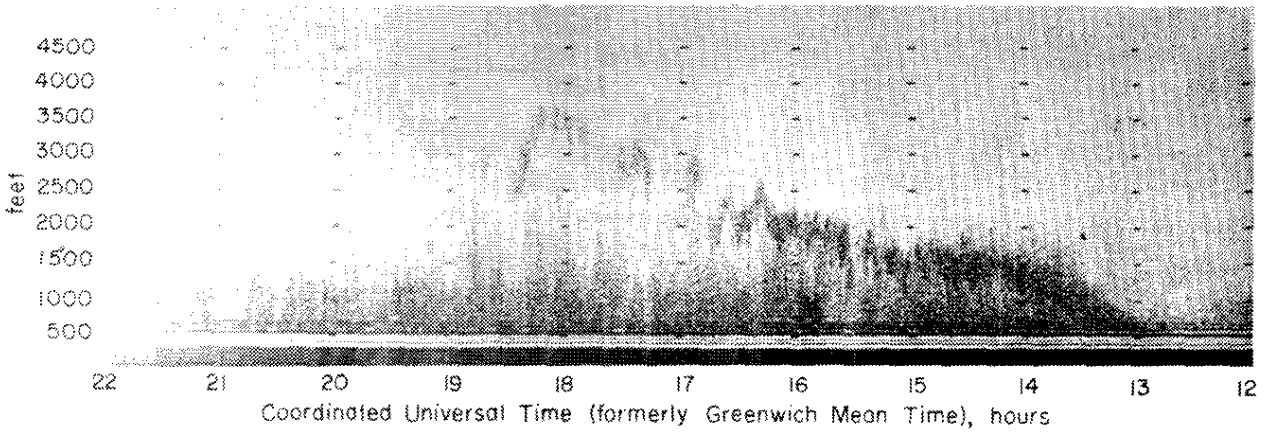

FIGURE 4. Category 9, Ascending Layer Starting Near the Ground Surface

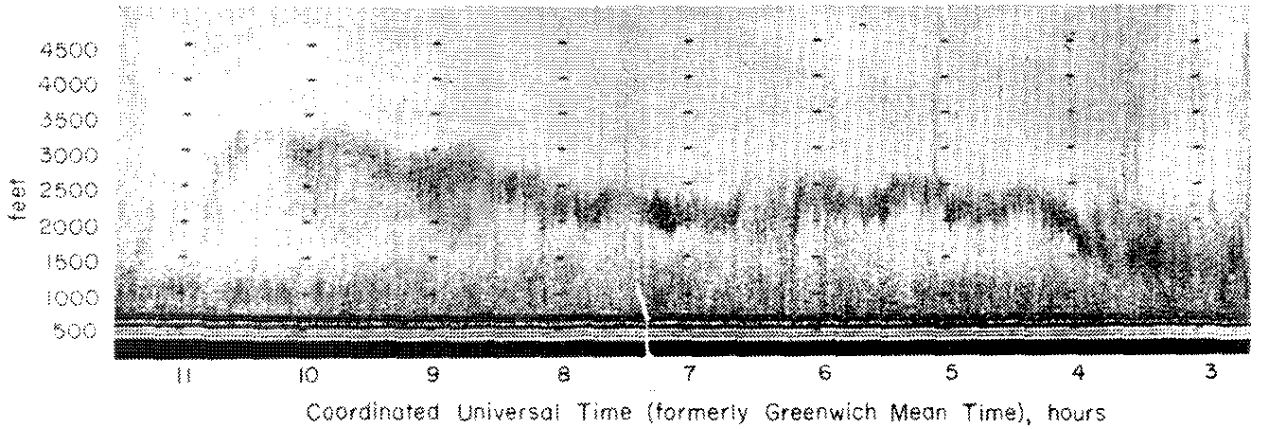

FIGURE 5. Category 10, Ascending Layer but not Starting Near the Ground Surface and Transforming into a Category 6, Two Layers with a Large Separation Between the Top and Bottom Layer

SOUNDER DATA FROM ETTEX

In July 1974, the sounder was relocated at Oak Ridge, Tennessee, as part of the Eastern Tennessee Trajectory Experiment (ETTEX). The sounder data for the period of June 25 to July 9 (Table 5) indicate that the height of the mixed layer was between 2300 and 2600 ft for 82% of the time, and between 2000 and 2700 ft for 90% of the time.

TABLE 5

Hourly Height Data From ETTEX

Height, ft	Frequency	Percent
1600	2	0.662
1700	1	0.331
1800	3	0.993
2000	6	1.987
2200	7	2.318
2300	33	10.927
2400	110	36.424
2500	70	23.179
2600	35	11.589
2700	11	3.642
2800	1	0.331
3000	1	0.331
99999	22	7.285
TOTALS	302	100.000

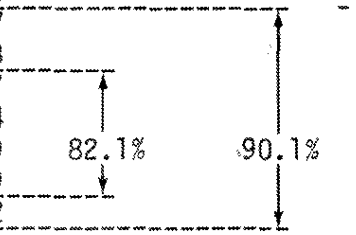

Maximum mixed depth data from the sounder was compared with calculated daily maximum mixed depth for Nashville, Tennessee (Table 6).

TABLE 6

Comparison of the Oak Ridge Tennessee, Sounder Mixed Depth and Nashville, Tennessee, Calculated Maximum Mixed Depth

Date	Oak Ridge Acoustic Sounder, ft	Nashville Calculated, ft
6-27	2,500	8,530
7-1	2,700	6,167
7-2	2,700	5,446
7-4	3,000	6,600
7-7	2,700	4,265
7-8	2,700	4,527
7-9	2,600	3,969

These data show that the calculated height was much higher than the height as recorded by the acoustic sounder. Holzworth[4] reported the mean summer mixing depth for the Oak Ridge, Tennessee, area as 5,900 ft. This value is not inconsistent with that in the table for the calculated height considering the small sample size; the mean maximum sounder data were much lower.

The sounder data for this period show returns from a well-mixed back-scattered layer 56% of the time and thermal plume activity for another 13% of the time (Table 7). Thus, a well-mixed layer exists during 60% of the sampling period.

TABLE 7

Category Data From ETTEX

Category	Frequency	Percent
2	170	56.291
3	3	0.993
4	41	13.576
6	28	9.272
7	2	0.662
13	6	1.987
14	30	9.934
99	22	7.285
TOTALS	302	100.000

CONCLUSIONS

Although long-term testing of the acoustic sounder as a real time monitor of the atmospheric mixed layer remains to be completed, the experiments at two different sites clearly indicate this method has potential for remote sensing of the mixed layer, and a statistical climatology of the atmospheric boundary layer can be built. The results to date also indicate the calculated maximum mixed heights are much higher than those depicted by the sounder. One cause for this discrepancy is the lack of sensitivity of the system for identifying the height of the tops of the thermal plumes when there is no capping inversion (Category 13, 2% of the time at Oak Ridge). This difference between calculated and measured heights could cause significant discrepancies between actual and predicted concentrations of air pollutants.

REFERENCES

1. C. G. Little. "Acoustic Methods for the Remote Probing of the Lower Atmosphere." *Proc. IEEE 57*,(4) (1969).

2. G. H. Clark. "The Acoustic Sounding Research Program of the Australian Atomic Energy Commission." *1973 Workshop in Atmospheric Acoustics*, Univ. of Oklahoma, Norman, Okla. (1973).

3. D. Pack and C. Hosler. "A Meteorological Study of Potential Atmospheric Contamination from Multiple Nuclear Reactor Sites." *Proc. of the 2nd United Nations International Conference of the Peaceful Uses of Atomic Energy, Geneva*, Vol. 18, pp. 265-271, United Nations, N. Y. (1958).

4. G. Holzworth. *Mixing Heights, Wind Speeds, and Potential for Urban Air Pollution Through the Contiguous United States.* NOAA Air Programs Publication, No. AP-101 (1972).

5. VERIFICATION OF SRL BUOYANT PLUME CALCULATIONAL PROCEDURES THROUGH USE OF MEASURED SO_2 †

INTRODUCTION

This paper presents results of an SO_2 survey initiated in 1973, and described in the 1973 Dose-To-Man Annual Report.[1] The objective of the survey was to make a comparison of calculated and observed concentrations of SO_2 for six sites surrounding the 400-D power plant (Figure 1). This paper presents these comparisons using calculational procedures currently in use at SRL for the assessment of off-site effluent concentrations from a buoyant plume.[1,2]

The meteorological variables needed for the calculations are the wind velocity and atmospheric stability. Wind velocity measurements are frequently not made at the point of release but at some distance away and assumed to apply at the source. Atmospheric stability estimates are normally obtained from the vertical lapse rate of temperature measured in the lowest several hundred meters or through use of measurements of the variability of the horizontal or vertical wind direction, see for example Reference 3. Because wind velocity measurements were obtained at several different sites during this survey, the error caused by using wind measurements not at the point of release will be assessed. In addition, several different approaches used to determine atmospheric stability will also be used to assess their effect on the resulting concentrations. Therefore, this paper presents a comparison of different methods used to calculate the concentration of SO_2 at downwind positions to actual measurements. The primary difference between the methods is the input data; all methods use the same basic predictive equations.

SOURCE OF DATA

The data utilized for verification consist of one hour averaged SO_2 concentrations at six sites during the period May 1973, through February 1974. (For a discussion of the SO_2 sampling procedures, see Reference 1.) Meteorological data used in the calculations were from three locations. Wind velocity measurements were obtained at the bubble tower in D Area (Building 412-D) from a height of 38 m (see BUB in Figure 1). The

† Work done by M. M. Pendergast.

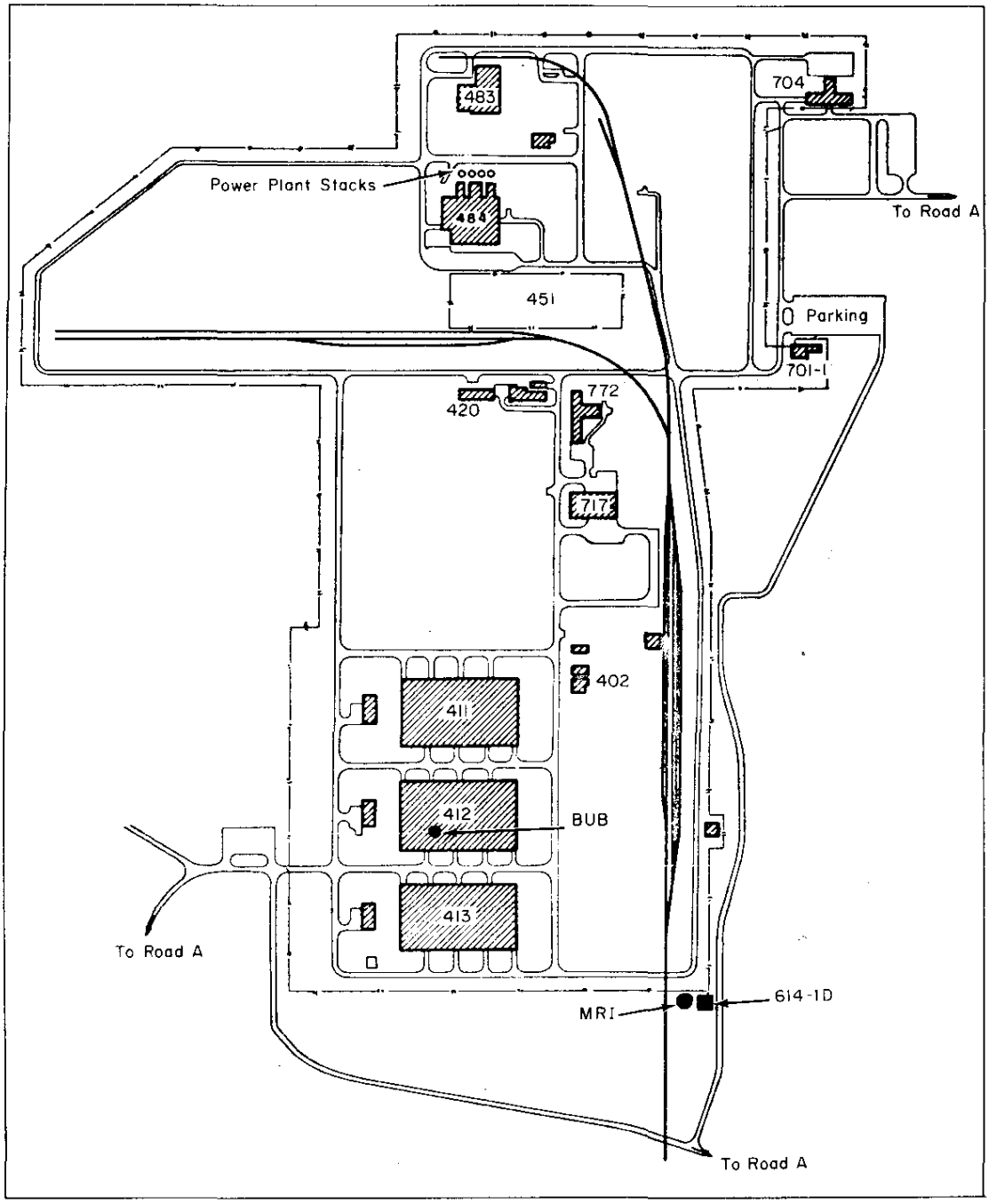

FIGURE 1. Map of D Area Showing the Power Plant, Stacks, and Location of Bubble Tower (BUB)

bubble tower is approximately 0.8 km from the D-Area power plant. Wind velocity and temperature data were obtained from the Vogtle meteorological tower operated by the Georgia Power Company located 8 km to the SSW. These data consist of hourly averaged wind speed and direction at 11 m and 46 m, the range of horizontal and vertical elevation angle at 27 m, and temperature data at 12, 30, and 46 m.

Meteorological data were also obtained from the WJBF-TV tower, located approximately 16 km to the northwest. These data consist of wind speed and direction, vertical elevation angle and temperatures at seven levels between 2 m and 335 m. Note the meteorological data from the bubble tower and the Vogtle meteorological tower are available only as hourly averaged values, whereas the data from the WJBF-TV tower were available at 5-sec intervals. The locations of these meteorological data sources, the SO_2 sampling stations, and the coal burning power plant are indicated in Figure 2.

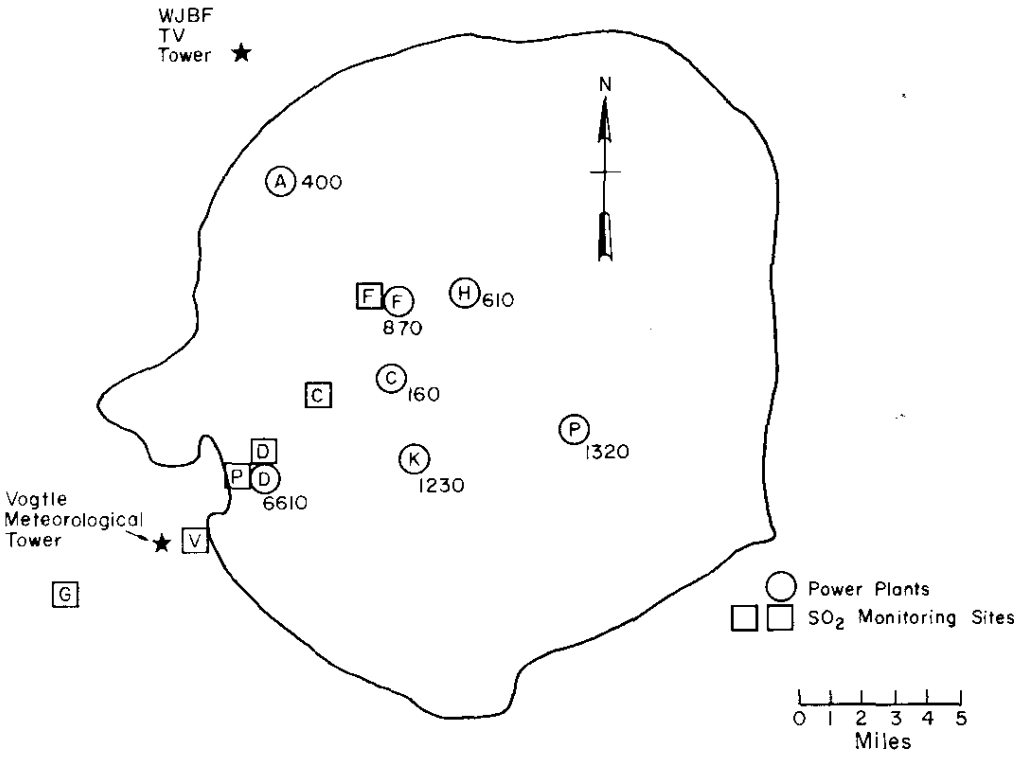

FIGURE 2. Coal-fired Power Plants at SRP and the Average Annual Emissions of Sulfur Dioxide (in tons). Also shown are the sulfur dioxide monitoring sites for the onsite and offsite survey

The emission rate of SO_2 and the heat output of the stack were tabulated for each hour utilizing continuous records of the boiler steam output. The power plant produces steam from coal to provide process steam for the heavy water plant in D Area and to generate electricity when it is not economical to purchase electricity from the South Carolina Electric and Gas Company. The steam plant has a nominal rating of about 464 MW thermal input. Thus, the fluctuations of the SO_2 output over several hours can be quite significant. The emission rate of SO_2 in lb/hr is given by

$$Q' = \frac{4.142 \times 10^5 + 22.58\ a}{b}\ s \qquad (1)$$

where a is the total boiler output in pounds per hour, b is the heating value of coal as received in BTU's per pound,* and s is the sulphur content of the coal, expressed as a percent. 95% of the sulphur released during the combustion process is assumed to go to the stacks. For the calculation of effective plume height, the heat output in BTU/hour is given by

$$Q_H = [2.18 \times 10^7 + 1.188 \times 10^3\ a]\ d \qquad (2)$$

where a represents the total boiler output in lb/hr, and d is the percentage of the heat that is released through the stack. In this case, d is assumed to equal 15%.**

CALCULATION PROCEDURES

The predictive model used is broken down into two principal equations. The first equation,

$$\chi = \frac{Q'}{\sigma_y \sigma_z u \pi}\ \exp\left[-\frac{1}{2}\frac{h_e^2}{\sigma_z^2} + \frac{1}{2}\frac{y^2}{\sigma_y^2}\right] \qquad (3)$$

is the Gaussian plume equation which gives downwind concentration, χ, as a function of an effective height of the plume, h_e, a mean transport wind, u, and atmospheric dispersion coefficients, σ_y and σ_z.

---

* Nominal value is 12,000 BTU/lb.

** The above equations were provided by A. H. Kaiser of Savannah River Plant Power Department.

The second equation,

$$h_e = h + \Delta h, \tag{4}$$

gives the effective height of the plume centerline, where h is the physical height of the stack and Δh is the smallest of Δh_1 and Δh_2 where

$$\Delta h_1 = 1.6\ [3.8^{-5} \times 10\ Q_H]^{1/3}\ x/u$$

and,

$$\Delta h_2 = \frac{2.9\ [3.8 \times 10^{-5}\ Q_H]^{1/3}}{uS}$$

for stable cases, and

$$\Delta h_2 = \frac{1.6\ [3.8 \times 10^{-5}\ Q_H]^{1/3}\ [10\ h]^{2/3}}{u}$$

for unstable cases, where Q_H is the heat output in cal/sec and S is a stability parameter given by

$$S = \frac{g}{\theta}\frac{\partial \theta}{\partial z}$$

where g is acceleration due to gravity, and θ is the potential temperature in °K.

The preceding expressions can be used to account for the effect of buoyancy and follow the expressions given in Reference 4. Note the effective source height is a function of the actual stack height, the heat output, the ambient temperature, and the average wind speed, u.

Equation 3 does not take into account variations due to topography, chemical reactions of the SO_2, uptake of SO_2 by plants, or scavenging by precipitation. These effects are assumed to be much less significant than are the wind direction, wind speed, and the dispersion conditions. Table 1 lists methods used to calculate the downwind concentrations. (For explanation of terms and references see Reference 5.) As mentioned above, these methods all utilize Equations 3 and 4 to make the determinations. The variation is caused by the different approximations used for the input variables to Equation 3.

TABLE 1

Methods of Determining Meteorological Parameters Utilized in the Predictive Equation

Method	Source of Wind	Stability	σ_y	σ_z
1	Vogtle	Stable	$0.15\ \sigma_a\ x^{.71}$	$0.15\ \sigma_e\ x^{.71}$
	46 m	$T_{41} - T_{11} > 0$	$[\sigma_a = \frac{\theta_{pp}}{5.52}]^{\alpha}$	$[\sigma_e = \frac{\phi_{pp}}{7.98}]^{\alpha}$
		Unstable	$0.045\ \sigma_a\ x^{.86}$	$0.045\ \sigma_e\ x^{.86}$
		$T_{41} - T_{11} \leq 0$	$[\sigma_a = \frac{\theta_{pp}}{5.98}]$	$[\sigma_e = \frac{\phi_{pp}}{7.40}]$
2	Wind direction from bubble tower ϕ_{pp} and θ_{pp} from Vogtle 40 m	Same as Method 1		
3	Bubble 40 m	$\partial T/\partial z$ evaluated between 11 and 46 m on Vogtle tower		
		$\partial T/\partial z < -1.9$ °C/100 m	$.40\ x^{.91}$	$.40\ x^{.91}$
		$-1.9 < \partial T/\partial z < -1.5$	$.36\ x^{.86}$	$.33\ x^{.86}$
		$-1.5 < \partial T/\partial z < -0.5$	$.32\ x^{.78}$	$.22\ x^{.71}$
		$-0.5 < \partial T/\partial z$	$.31\ x^{.71}$	$.06\ x^{.71}$
4	WJBF	Stable $T_{91} - T_{10} > 0$	$0.15\ \sigma_a\ x^{.71}$	$0.15\ \sigma_e\ x^{.71}$
	36-91 m	Unstable $T_{91} - T_{10} \leq 0$	$0.045\ \sigma_a\ x^{.86}$	$0.045\ \sigma_e\ x^{.86}$

a. θ_{pp} is range of azimuth and ϕ_{pp} is range of elevation achieved at 27 m level of Vogtle tower over a 1-hr period.

RESULTS

Frequency Distribution of SO_2 Concentration

Figure 3 presents plots of the cumulative frequency distribution of observed and calculated hourly averaged SO_2 concentrations for the 6 locations. The most outstanding feature of the plots for observed concentrations is the high frequency of occurrence of zero concentrations with values ranging between 85 and 96%. This result agrees with a conclusion drawn from an examination of annual wind rose statistics; these statistics indicate a uniform distribution of wind direction over 16 sectors. The frequency of occurrence of the low concentrations seems to be independent of distance from the source indicating the expected dependence on wind direction. The maximum observed concentration ranges between 30 and 285 ppb and does show an inverse dependence upon travel distance.

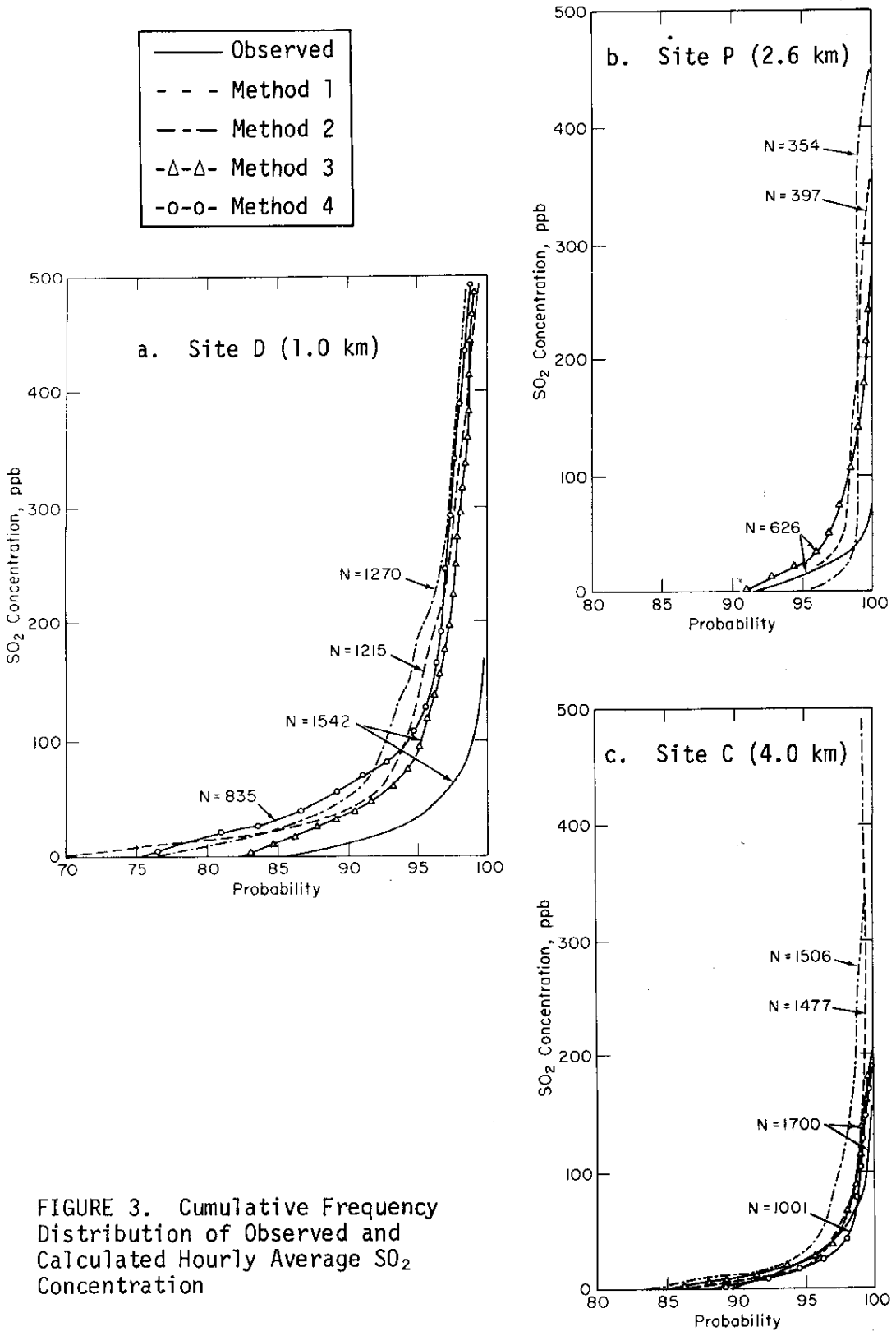

FIGURE 3. Cumulative Frequency Distribution of Observed and Calculated Hourly Average SO_2 Concentration

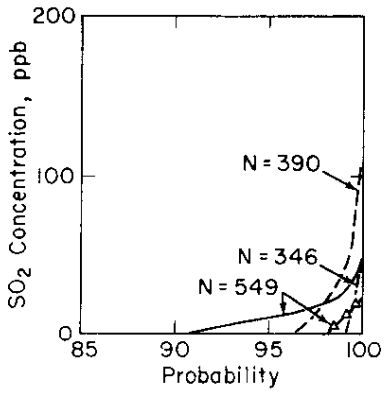

d. Site V (7.8 km)

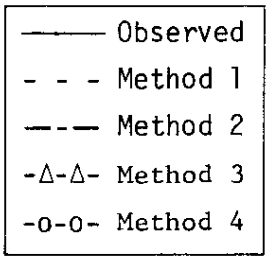

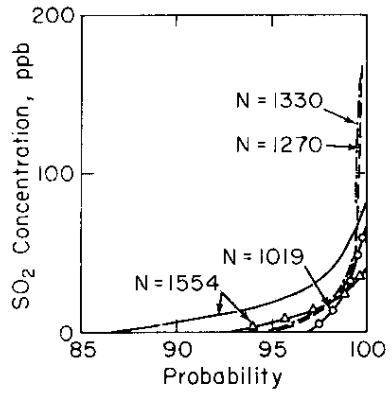

e. Site F (10.6 km)

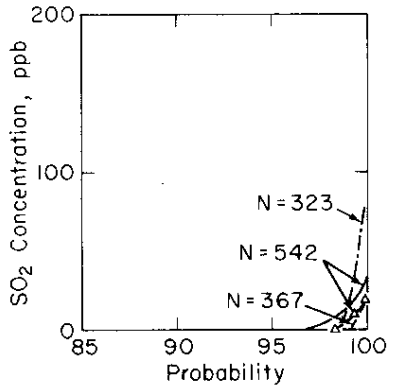

f. Site G (16.1 km)

FIGURE 3. Continued

The frequency distribution obtained from calculated values show, in general, only slight variation depending on the method used. The largest difference between calculated and observed occurs for Site D. For Site D (1.0 km), the calculated values tend to be very conservative; i.e., overestimating frequency of occurrence and magnitudes of concentration which could be attributed to improper handling of the buoyancy of the plume. For Site P (2.6 km) and Site C (4.0 km), the calculations are in good agreement with observations although slightly conservative. At Sites V, F, and G, the calculations tend to overestimate the peak concentration and underestimate the frequency of occurrence of low concentrations

Comparison of Observed and Calculated Hourly Average SO_2 Concentration

Table 2 shows the results of a comparison of calculated and observed hourly average SO_2 concentration for 6 locations ranging from 1.0 to 16.1 km from the D-Area power plant. The percentage of time that the calculated value was within a factor of 2 of the observed value is shown. This value is considered a good result, and a value within a factor of 10 is considered a fair result for several calculational methods. Also shown are the number of cases for each site and method. Table 2a was constructed using all comparisons when the observed concentration exceeded instrument sensitivity (5 ppb); Table 2b includes comparisons when both calculated and observed concentrations were less than 5 ppb; Table 2c includes comparisons when the calculated concentration exceeded 1 ppb.

Table 2a shows a higher percentage of good and fair results at the closest sites than at the more distant sites. Generally, about 10 to 15% of cases are good and 30 to 40% are fair within 4 km of the source. At increased distance (7.8 to 16.1 km), about 5% of cases are good and about 10% are fair. The different methods give slightly different results with the greatest difference occuring within 4 km. Note M1 gives much better results for Site D than is given by M2. This result is unexpected because M1 is based on wind data observed at Site V (7.8 km distant), and M2 is based on wind data 0.8 km from the source. No explanation is given for the observation except that the Vogtle tower is located in a clearing surrounded by a pine forest and the anemometer in D Area is located on the top of chemical processing columns. High SO_2 concentrations observed at ground level imply that the plume is mixing to the ground, a condition during which effects from buildings on the anemometer at top of the bubble tower is more likely.

TABLE 2

Percentage of Time that Calculated Concentrations were within a Factor of 10 and within a Factor of 2 of the Observed Hourly Concentrations of SO_2 for Several Different Methods

a. For periods when observed SO_2 concentrations exceeded 5 ppb

Site	D	P	C	V	F	G
Distance from Source	1.0 km	2.6	4.0	7.8	10.6	16.1
Method 1	15/51[a] (253)	8/23 (39)	9/33 (261)	3/7 (73)	5/11 (283)	0/0 (48)
2	8/28 (284)	19/30 (37)	15/36 (289)	6/9 (66)	4/14 (320)	9/13 (32)
3	7/20 (361)	16/31 (76)	13/30 (311)	7/18 (88)	4/11 (351)	8/21 (71)
4	17/37 (176)	-- --	7/18 (183)	-- --	1/5 (189)	-- --

b. All periods. [When both observed and calculated less than 5 ppb considered good forecast]

Site	D	P	C	V	F	G
Distance from Source	1.0 km	2.6	4.0	7.8	10.6	16.1
Method 1	75/86 (840)	91/92 (372)	80/85 (1165)	81/81 (373)	76/79 (1130)	87/87 (360)
2	73/79 (963)	91/93 (346)	79/84 (1162)	82/83 (341)	72/75 (1103)	91/91 (321)
3	-- --	89/91 (577)	-- --	85/86 (533)	--- --	88/89 (529)
4	78/83 (653)	-- --	80/83 (853)	-- --	80/81 (917)	-- --

c. For periods when calculated SO_2 concentrations exceeded 1 ppb

Site	D	P	C	V	F	G
Distance from Source	1.0 km	2.6	4.0	7.8	10.6	16.1
Method 1	17/54 (689)	11/43 (44)	20/69 (614)	23/49 (31)	31/68 (342)	46/91 (11)
2	14/44 (520)	25/46 (24)	18/64 (614)	41/70 (17)	30/79 (422)	46/73 (11)
3	15/43 (478)	18/50 (95)	20/65 (565)	22/74 (54)	26/76 (429)	31/86 (37)
4	19/51 (325)	-- --	20/71 (245)	-- --	33/79 (200)	-- --

---

a. (15/51) means 15% of cases were within a factor of 2
51% of cases were within a factor of 10

The results presented in Table 2c are significantly better than those shown in Table 2a. The largest improvements are for the more distant sites where the number of good and fair forecasts was increased by 5 times or more. This method of comparison tends to minimize the possibility of interference from sources other than the D-Area power plant. For example, at C Area (Figure 2) when the wind is from the north, any observed SO_2 would probably be due to F- or H-Area power plants. The statistics presented in Table 2a incorrectly include the comparison of this observed value with the calculated value (contribution from D-Area stacks) which would be zero for a northerly wind. The comparisons shown in 2c were determined for those cases for which the calculated concentration exceeded 0.1 ppb which would occur when the wind is from the D-Area source. This tends to eliminate the effects from the other (smaller) sources.

The fact that the statistics presented in Tables 2a and 2c are different suggests that observed concentrations are not dependent solely on the effluent from D Area.

The results shown in Table 2a are disappointing especially at distances in excess of 4 km. By including in the calculation the number of cases when no SO_2 was observed (2b) much more favorable statistics are obtained with good and fair results occurring 75 and 85% of the time, respectively. The results in 2c show a vast improvement over 2a which is due primarily to reducing the interference from other sources. These results are, however, still disappointing.

CONCLUSIONS

Tentatively, the SO_2 survey conducted at SRP tends to substantiate the expectation that the Gaussian plume equation can produce reasonable results with respect to frequency distribution of pollutant concentrations. Little difference between different methods is apparent from examination of concentration frequency distributions. These data have shown that the Gaussian plume models show best agreement for distance between 2 and 10 km from the source.

These simple models were quite ineffective in calculating concentrations at a particular point in time. A major difficulty occurs because of the dependence on wind direction so that much of the error is caused by improper selection of plume orientation. Data indicate that interference from other sources of SO_2, especially at sites C and F, are significant. The equations utilized in these models and/or the selection of diffusion coefficients and transport winds have been shown to produce, for real time assessment, concentrations which should be assumed to be accurate in order of magnitude only.

REFERENCES

1. M. M. Pendergast and E. L. Wilhite. "Meteorology and Sulfur Dioxide Concentrations at SRP." *Progress Report, Dose-To-Man Program, FY-1973.* USAEC Report DP-1341, E. I. du Pont de Nemours and Co., Savannah River Laboratory, Aiken, S. C. (1974).

2. R. E. Cooper and B. C. Rusche. *The SRL Meteorological Program and Off-Site Dose Calculations.* USAEC Report DP-1163, E. I. du Pont de Nemours and Co., Savannah River Laboratory, Aiken, S. C. (1968).

3. *Safety Guides for Water Cooled Nuclear Power Plants.* USAEC Division of Reactor Standards, Safety Guide 23 (1972).

4. G. Briggs. *Plume Rise.* A Critical Survey. Report TID 25075, ERDA-TIC, Oak Ridge, Tenn. (1969).

5. M. M. Pendergast and T. V. Crawford. "Actual Standard Deviations of Vertical and Horizontal Wind Direction Compared to Estimates from other Measurements." Paper No. 1 of this report.

6. A TECHNIQUE FOR FIELD MEASUREMENTS OF ATMOSPHERIC TRITIATED HYDROGEN AND TRITIATED WATER VAPOR †

INTRODUCTION

A sampler to collect the tritiated hydrogen (HT*) and tritiated water vapor (HTO) components separately from air for later analysis was needed for stack and environmental monitoring. The sampler had to be capable of collecting a 1500-ℓ sample over time periods ranging from 1/2 day (2 ℓ/min) to 1 month (35 cc/min). The 1500-ℓ sample was required to meet a sensitivity goal of 0.002 pCi/ℓ air for HT using a liquid scintillation counter. This section describes the development of a HT-HTO sampler that will separate HTO from HT and then concentrate the HT present at environmental levels (1 ppm) of H_2 into a form that is amenable to analysis.

PROCESS

The process requires the separation of HTO from HT. Separation of HTO from air is simple and is normally done with silica gel or molecular sieves; the resulting air stream then contains HT minus HTO. HTO is removed from the water-sorbing material by heating and vacuum distillation for analysis.

Possible methods of concentrating the HT from the resulting air stream include collecting the water from oxidation in a furnace, oxidation using a catalyst, and combustion of the H_2-containing neon fraction from liquid air plants. The liquid air plant technique is not readily amenable to a simple field sampling technique.

The HT in the air stream can be oxidized directly in a furnace, but low yields are obtained due to the exceedingly small amounts of water produced from 1 ppm of H_2. To assure good recovery in the oxidation method, H_2 (from 0.3 to 2%) carrier is normally added to the air stream before HTO removal.[1]

---

† Work done by D. W. Hayes and R. C. Milham.

*HT is taken to mean all of the tritium forms, i.e., HT, DT, and T_2.

H_2 can be oxidized to water at room temperature in the presence of platium or palladium catalysts. This is better than the power-consuming, cumbersome furnace. Palladium powder was found effective for combustion, but it is difficult to contain unless filters that restrict air flow are used. Palladium on alumina sorbs too much water.

A convenient method of combining combustion and water collection is used by Dr. Ostlund[2] and was used in the final sampler design. The palladium catalyst is placed directly on molecular sieve material. The palladium molecular sieve catalyst is made by adding a HCl - $PdCl_2$ solution directly to the molecular sieve and reducing the $PdCl_2$ to palladium by adding a basic solution of formaldehyde or by passing H_2 gas through it. The latter method is preferred because the addition of extra water from the formaldehyde solution to the sieve material replaces some structural ions with protons. These additional hydrogen ions increase the memory for HTO of the sieve material. HTO is recovered from the HT column by heating and vacuum distillation of the palladium coated molecular sieve. The palladium control molecular sieve is regenerated by treatment with H_2.

SAMPLER

Figure 1 outlines the basic HT-HTO sampler. An electrolysis cell is used as a simple source of controlled carrier H_2 for the entire air flow range of 35 cc/min to 2 ℓ/min. A cell with a capacity for 60 cc of water - NaOH electrolyte was constructed from stainless steel tubing. A constant current power supply was designed with a range of 0.01 to 1 amp. A simple vibration pump was used for a vacuum supply to pull air through the columns. If carrier H_2 is not added, widely varying recoveries for HT were observed (20 to 80%). H_2 added at 4 parts per thousand and greater* assured a recovery of >90%. A small flow of methane was added to test for CH_4 oxidation with and without H_2 carrier, and no conversion was observed at room temperature.

REFERENCES

1. P. Patigny. "Detection et Mesure de la Contamination des Gaz et Vapeurs." Seminaire Sur La Protection Contre Les Dangers Du Tritium, Le Vesinet, April 16-18, 1964. CONF-640413, ERDA-TIC Oak Ridge, Tenn. (1964).

2. H. G. Ostlund and A. S. Mason. "Atmospheric HT and HTO, I. Experimental Procedures and Troposheric Data 1968-72." *Tellus XXVI*, 91 (1974).

*Caution: The lower explosive limit for H_2 is 41 parts per thousand.

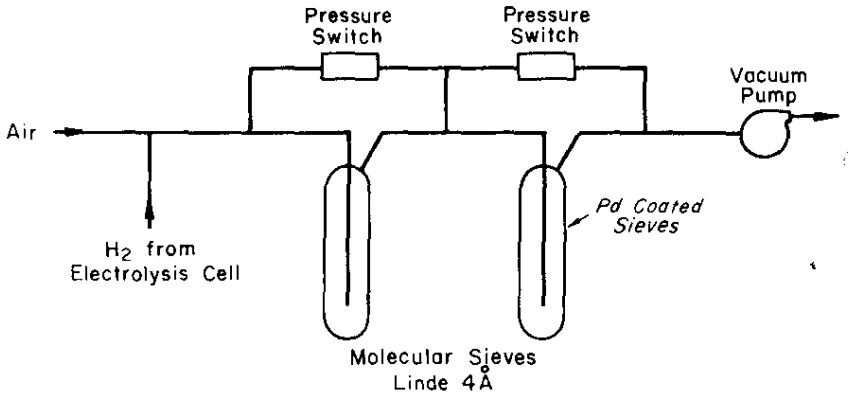

FIGURE 1. Schematic of HT-HTO Sampler

7. A SIMPLE MODEL USED TO DETERMINE DOWNWIND CONCENTRATIONS RESULTING FROM EITHER CONTINUOUS OR INSTANTANEOUS RELEASES USING METEOROLOGICAL OBSERVATIONS FROM A SINGLE TOWER †

INTRODUCTION

In most site surveys utilized to make decisions concerning the environmental effects of a nuclear reactor site, a meteorological tower is instrumented and data are collected over a prescribed period of time, usually one or two years. Calculations based on data from this single tower are frequently used to estimate concentrations of effluent emanating from the proposed site. These results are often the basis for policy decisions. In most cases, the calculations are based on simple wind rose models which use the frequency of occurrence of wind direction and stability category to provide a gross estimate of expected concentration distributions.

The code presented in this report makes use of tower data to calculate concentrations from accidental or short-term releases in real-time. A code of this kind, with small storage requirements and requiring minimal computer time, will be adapted for a PDP 11/40 computer to provide a means for obtaining a first estimate of expected concentrations. Refined estimates such as obtained from the ADPIC code in the ARAC concept could follow later.[1]

DESCRIPTION OF THE CODE

A computer code (PUF/PLM) was written to provide the capability of determining the concentration resulting from an accidental release of either a short duration, so that the cloud can be considered to be a puff, or a continuous release, for which the cloud is assumed to resemble a continuous plume. The equations utilized are.

$$\chi = \frac{Q'}{2\pi\sigma_y\sigma_z\bar{u}} \exp - \left[\frac{y^2}{2\sigma_y^2}\right] \left\{\exp\left[-\frac{(z-h)^2}{2\sigma_z^2}\right] + \exp\left[-\frac{(z+h)^2}{2\sigma_z^2}\right]\right\} \quad (1)$$

† Work done by M. M. Pendergast.

for a continuous plume, and

$$\chi = \frac{Q'}{\sqrt{2}\pi^{3/2}\sigma_{yI}\sigma_{xI}\sigma_{zI}} \exp -\left\{\left[\frac{(x-\bar{u}t)^2}{2\sigma_{xI}^2} + \frac{y^2}{2\sigma_{yI}^2} + \frac{h^2}{2\sigma_{zI}^2}\right]\right\} \qquad (2)$$

for an instantaneous point source. Equation 1 is used to provide an estimate of the concentration, χ, at any position (x, y, z) resulting from a continuous point source at height, h, emitting at a rate, Q'. The distance, x, is measured along the axis of the plume, y, measured perpendicular to the plume, and z, measured above ground level.

The parameters in Equation 1 that are functions of meteorological variables are determined from data from towers located near the operating areas. The instruments are at a height of 62 m above the ground, which is the height of most stacks at SRP. The wind speed, u, is an arithmetic mean over a particular averaging time, τ. For the purpose of this paper, τ will be assumed to be equal to one hour. The cloud dimensions,* σ_y and σ_z are estimated from the observed standard deviations of azimuth, σ_a, and elevation, σ_e, respectively, using the relationships developed by Smith[2]

$$\begin{aligned} \sigma_y &= a\,\sigma_a\,x^b \\ \sigma_z &= a\,\sigma_e\,x^b \end{aligned} \qquad (3)$$

where the respective coefficients a and b are 0.15 and 0.71 for stable conditions and 0.045 and 0.86 for unstable conditions.

The coefficients used in Equation 2 for instantaneous point sources are similar to those used in Equation 1, except that the source term, Q, is the total release, and the dispersion coefficients, (σ_{xI}, σ_{yI}, and σ_{zI}) are evaluated using a relationship of the form

$$\sigma_{rI}^2 = 2K_r\,t \qquad (4)$$

*The dimension of the cloud is assumed to be the width between positions at which concentration falls to 0.1 the centerline concentration. Furthermore, the concentrations are assumed to be Gaussian, so the width of the plume is 4.3 σ_y and, analogously, the depth is given by 4.3 σ_z.

where r is measured along the x, y, and z direction, σ_{rI}^2, is the variance of concentration for a puff along the r direction, K_r is the eddy diffusivity in the r direction, and t is elapsed time.[3]

For Fickian diffusion, the eddy diffusivity is invarient with time and space. For most instances, vertical profiles of the eddy diffusivities can be used to estimate appropriate values for the three dispersion coefficients. At the present time, profiles of eddy diffusivity are being examined at Savannah River and are described more fully in another section of this report.[4] Unfortunately, most atmospheric diffusion processes are not Fickian. Numerous comparisons of the above expressions with experimental data on diffusion in the atmosphere have shown that K varies systematically with time of travel, position, and scale of the diffusion process.[5] As a means of including this time and scale dependence of K in the simple calculation for puff diffusion, the relationship developed by Walton[6] for a time and scale dependent eddy diffusivity is used. This is given by

$$K(t) = c_1 \varepsilon^{1/3} (\sigma_o^{2/3} + 2/3\ c_2 \varepsilon^{1/3} t)^2 \qquad (5)$$

where c_1 and c_2 are constants of order unity, ε is the turbulent dissipation rate, and σ_o is related to the initial size of the release in the r direction. In order to put restraints on the maximum value that the eddy diffusivities can obtain, Walton uses the following expression

$$K(t)' = \frac{K(t)\ K_{max}}{K(t) + K_{max}} \qquad (6)$$

where $K(t)'$ is the adjusted eddy diffusivity, K_{max} is the maximum expected eddy diffusivity, and K(t) is the eddy diffusivity given by Equation 5.

The above relationships show that the dispersion coefficients and the eddy diffusivities can be expressed as a function of the single variable, ε, which can be calculated from meteorological data obtained at each tower using the expression

$$\varepsilon = \frac{u_*^3\ k}{z} \qquad (7)$$

where k is the Von Karman constant (0.4), z is the height above ground level, and u_* is the friction velocity defined by

$$u_* = (\overline{u'w'})^{1/2} \tag{8}$$

An alternate expression based on empirical results by Crawford[7] gives ε as a function of wind speed, u, and height above ground given by

$$\varepsilon = \frac{300}{z} \times \left(\frac{u}{5}\right)^3 \tag{9}$$

where ε is in ergs/(g-sec), z is height above ground in m, and u is wind speed at height z in m/sec.

DISCUSSION

At present, the PUF/PLM computer code is very simple with only the basic equations utilized to determine the downwind concentration. There are several refinements that could be applied to this simple model. They are: 1) inclusion of topography, 2) inclusion of a deposition velocity, 3) inclusion of rainout or precipitation scavenging, 4) a radioactive decay function, and 5) allowance for a curved trajectory.

Because changes of direction can be significant over a several hour period (especially during light wind conditions), the approximation of the curved trajectories utilizing the winds at the source of the release is assumed to be beneficial. Thus, travel time and downwind distance are computed along the curved path obtained by the vector addition of one hour segments.

COMPARISONS WITH OTHER METHODS

In order to evaluate the effectiveness of the PUF/PLM code to calculate downwind concentrations, the code is compared with other frequently used methods of estimating concentrations, either through use of nomograms or simplifying equations. For the continuous point source release, the methods for determining stability categories developed by Smith[2] are used; a comparison of several different methods of obtaining relative concentration is included in Section 1 and 11 of this report.[1,8] The rationale for determining dispersion coefficients developed by Smith are comparable with those developed by other authors; however, particularly in the 10 to 100 km range, additional data are needed as a basis for evaluating these different methods. As a means of verifying the instantaneous point source calculations, the relationship developed by Högström and reported by Slade[9] shows variation of σ_{yI} with distance expressed as a power function. Table 1 shows a comparison

of the values of σ_{yI} and σ_{zI} obtained using different values of ε of 0.1, 1.0, and 10 cm^2/sec^3 are assumed to represent stable, neutral, and unstable, respectively. Note that the values for σ_{yI} and σ_{zI} are within 30% of Högström's values out to 4 km which was the intended limit of Högström's relationships.

TABLE 1

Comparison of Calculated and Experimental Values of σ_{yI} and σ_{zI} as Functions of Distance and Stability

Calculated from Equations 4-6 using σ_{y_o} = 1.0 m, σ_{z_o} = 1.0 m

	σ_{yI}, m			σ_{zI}, m			ε	$K_{y\ max}$,	$K_{z\ max}$,
Distance, km →	1.3	2.7	4.0	1.3	2.7	4.0	cm^2/sec^3	cm^2/sec	cm^2/sec
Stable	15	25	31	3	4	5	0.1	5×10^3	1×10^2
Neutral	47	78	100	25	37	46	1.0	5×10^4	1×10^4
Unstable	138	242	313	78	117	145	10.0	5×10^5	1×10^5

Experimental Results of Högström

	σ_{yI}, m			σ_{zI}, m		
Distance, km →	1.3	2.7	4.0	1.3	2.7	4.0
Stable	12	22	32	4	6	8
Neutral	45	85	124	23	38	50
Unstable	105	199	288	101	168	226

USE OF THE MODEL

The model is fast, easy to use, and requires less than 3,000 bytes of computer storage. Operationally this model will be stored on disk in compiled form so that it will be quickly accessible for running on the PDP 11/40 minicomputer to be located at the Weather Center-Analysis Laboratory of the Environmental Transport Division. The major function of this minicomputer is to process meteorological data collected at SRP. The data processing includes checking data quality, archiving data on magnetic tape, and continually updating a buffer containing up-to-the-minute observations from the 8 towers. During an emergency, the data in this data buffer would provide the input to the PUF/PLM code.

REFERENCES

1. C. D. Kern. "Real Time Prediction and Verification of Argon-41 Concentrations - A Joint Effort with the Lawrence Livermore Laboratory." Paper No. 11 of this report.

2. M. E. Smith (ed). *Recommended Guide for the Prediction of Airborne Effluents.* The American Society of Mechanical Engineers Press, New York, N. Y. (1968).

3. O. G. Sutton. *Micrometeorology.* McGraw-Hill, New York, N. Y. (1953).

4. M. M. Pendergast and B. Gottlieb. "Evaluation of Different Methods of Estimating Vertical Eddy Diffusivities from TV Tower Data." Paper No. 3 of this report.

5. F. Pasquill. *Atmospheric Diffusion.* D. Von Nostrand Ltd., London, England (1962).

6. J. J. Walton. "Scale Dependent Diffusion." *J. Appl. Meteorol. 12,* 547 (1973).

7. T. V. Crawford. *A Computer Program for Calculating the Atmospheric Dispersion of Large Clouds.* USAEC Report UCRL-50179, Lawrence Livermore Laboratory, Livermore, Calif. (1966).

8. M. M. Pendergast and T. V. Crawford. "Actual Standard Deviations of Vertical and Horizontal Wind Direction Compared to Estimates from Other Measurements." Paper No. 1 of this report.

9. D. Slade. *Meteorology and Atomic Energy.* USAEC Division of Technical Information, Oak Ridge, Tennessee (1968). Available from NTIS Springfield, Va., TID-24190.

8. A COMPUTER PROGRAM FOR OBJECTIVE ANALYSIS AND DISPLAY OF METEOROLOGICAL FIELDS †

INTRODUCTION

Meteorological data are available from a nearby instrumented TV-tower, from seven 62-meter meteorological towers on the SRP site,[1] from National Weather Service (NWS) surface observing stations, from NWS upper air reporting stations, and from National Meteorological Center (NMC) forecasts for station locations and particular grid points. These data define meteorological parameters over sections of the southeastern United States of interest to SRP.

For input to trajectory/diffusion models, dynamic models, and display programs, a computer program was developed to analyze these observations objectively at fixed locations to obtain detailed analysis of meteorological variables over selected regions of the southeastern United States. Three overlying grid networks, composed of 1,089 grid points (a 33 x 33 array) in a single horizontal (or terrain following) slice, are approximately centered on SRP and are subsets of the NMC polar sterographic square grids. The nets have grid spacings of 40 km (1/8 NMC grid), 10 km (1/32 NMC grid) and 2.5 km (1/128 NMC grid). The area covered by these grids can be seen in Figures 1, 2, and 3.

The analysis procedure is basically a method of successive corrections to a first guess field. This analysis scheme differs from the conventional macroscale analysis programs in that a variable scan radius is used rather than a fixed scan radius. The more dense the data coverage, the smaller scan radius. The program is currently a two-dimensional one, in that values are only analyzed along horizontal or terrain-following surfaces without vertical links. Future programs will be three-dimensional and will permit stability checks between pressure surfaces to prevent the introduction of unstable lapse rates and unrealistic shears.

†Work done by C. D. Kern.

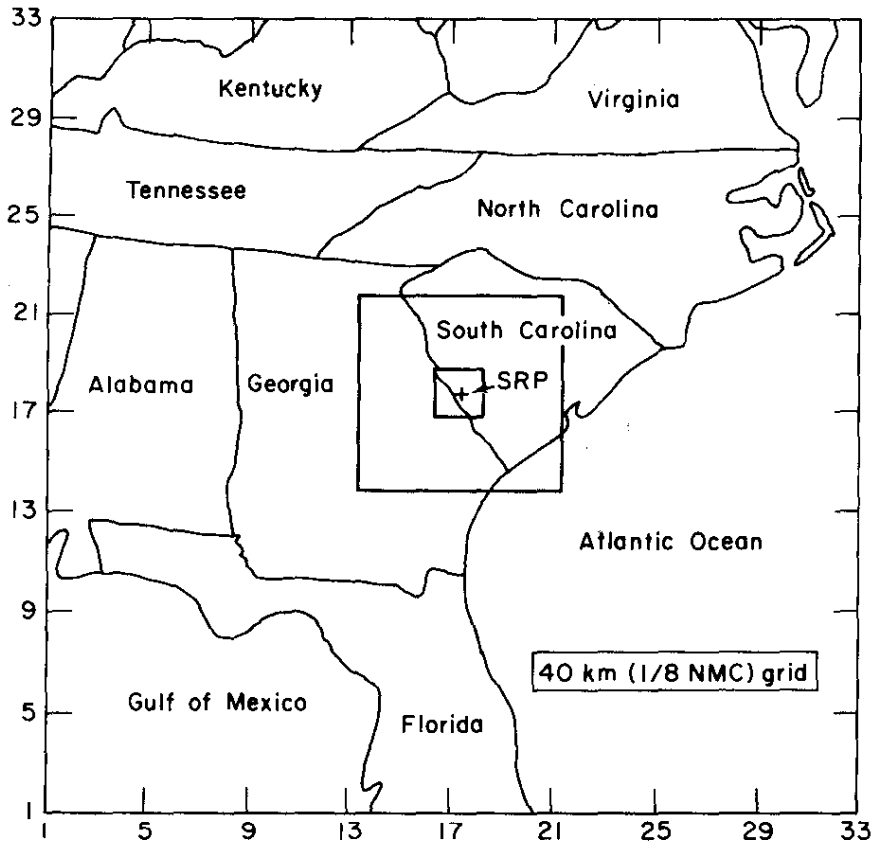

FIGURE 1. The Largest Grid Analysis Net. The two internal squares show the area covered by the medium and smallest nets

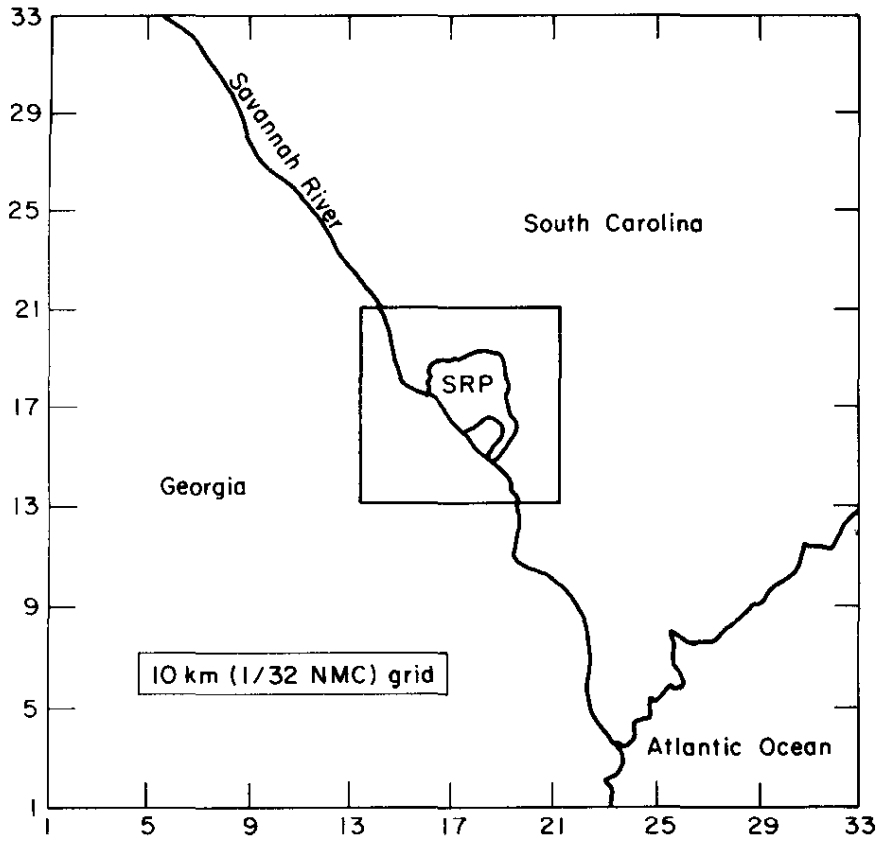

FIGURE 2. The Medium Grid Analysis Net. The internal square shows the area encompassed by the smallest net

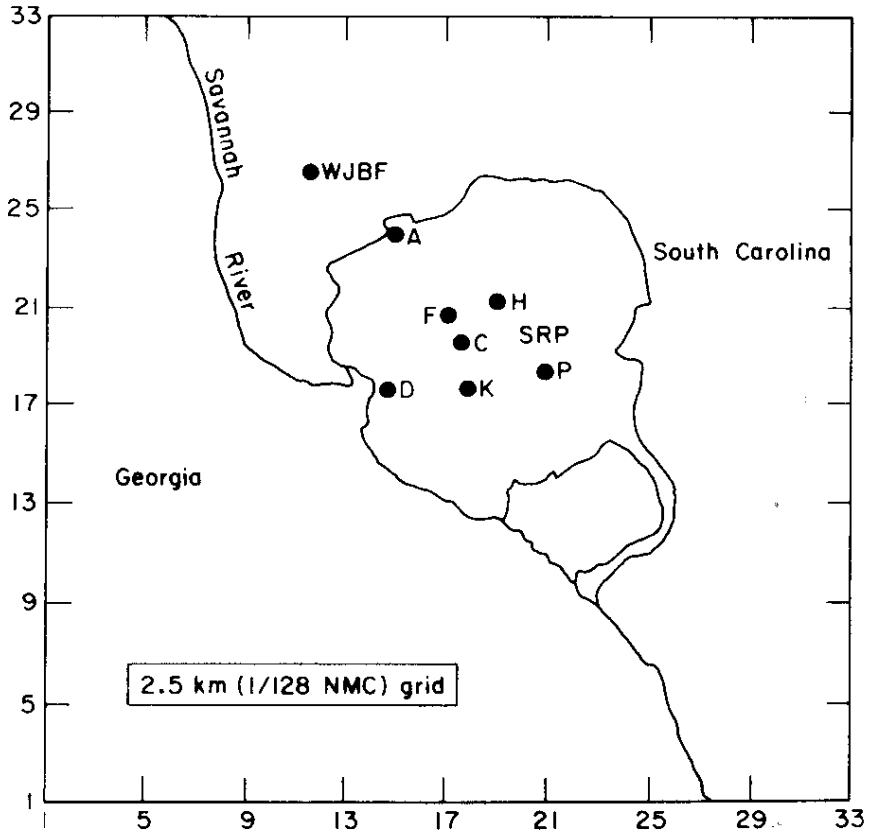

FIGURE 3. The Smallest Grid Analysis Net

MODEL

First Guess

This objective analysis technique requires first-guess fields which represent approximations to the final analysis fields.

For pressure, temperature, and thickness of the inversion, a single value is normally assigned to the entire grid for the medium and smaller grid nets. For example, the temperature value over land is set equal to the climatological average for shelter-height temperature for that region and time of day; for values over the ocean, the temperature is set equal to the ocean surface temperature for that month. Direct climatological values or values obtained by "hand analysis" of most recent weather maps are used for pressure or inversion thickness. Two procedures are used for winds: (1) a program that gives a quick analysis for the medium and smaller grid nets using a first guess with a uniform wind over the entire grid, and (2), a longer version for which first-guess grid-point values of pressure are assigned for the larger net at every fourth grid point, or a 9 x 9 array. The pressure values at the 81 grid points of the large net are then used to calculate the first guess of geostrophic wind at the center of each of these large grid squares. These 64 wind values are then smoothed over the 1089 grid points of the entire large grid network. The analysis is performed over the large net first; then the completed analysis of the large net provides a first-guess value at every fourth grid intersection for the next smaller grid, whose values are then smoothed over those 1089 points, and so on down to the smallest grid net; i. e., a large net analysis is performed first, then a medium grid net analysis, and finally, a small grid net analysis. However, all use the same initial data points that fall within the particular grid area.

Analysis Techniques

The objective analysis scheme is one adapted from Fleming,[2] which is a modification of the technique of Barnes.[3] Observations are compared with the first-guess values at the grid points and the differences are used to "correct" the first-guess values. The analysis program makes a number of scans through the observations for the level and parameter being analyzed. Currently, all data are entered by punched card or are input at a time-sharing type console. There is no validation at this time of upper air reports, nor are there throwout criteria to see if the data deviate excessively from the first-guess fields. Since surface

winds, for example, can be so erratic, a throwout criteria has not been adopted. The human analyst extracting the data performs a certain degree of quality control. Bogus data can also be entered for data sparse regions or other desired areas. The grid location and the value of the particular parameter are given, and this information is treated by the program as actual observed data.

Scan Procedure

This objective analysis technique differs from the normal technique in that a variable scan radius is used. This scan radius is dependent upon the distribution of data. The scan radius (radius of influence each observation exerts on the gridded field) is of fundamental importance in maximizing detail and minimizing "noise" in the analysis. The scan radius is selected to be large enough to avoid irregularities in sparse data regions, yet small enough to ensure maximum detail in data-dense regions.

The scan radius (R) is derived for each observation, according to the following technique:

An array ($M^n_{i,j}$), corresponding to the grid, is initially set to zero prior to starting the analysis. Then, for each observation, an $M_{i,j}$ for all grid points within a radius of four fine-mesh grid intervals about the observation is calculated according to the formula:

$$M^n_{i,j} = M^o_{i,j} + (4 - dd)$$

where: dd is the distance in fine mesh grid units between the observation points and the grid point (i,j); $M^n_{i,j}$ is the new value at that grid point; and $M^o_{i,j}$ is the old value that resulted from other observations within four grid intervals of that grid point. After all of the observations have been considered, the scan radius for each observation is determined by:

$$R = 30/M^n_{i,j}$$

where the grid point (i,j) is the nearest grid point to the observation point. Finally, upper and lower limits for the scan radii are imposed according to the following criteria:

$$R > 7, \text{ then set } R = 7$$

$$R < 2, \text{ then set } R = 2.$$

A scan is made of the grid points in a circular area surrounding the observation point. For each grid point within the circular scan area, the difference between the reported observation and the grid point value times the weighting factor (W_n) is computed and stored. The weighting factor (W_n) is a function of the distance between the grid point being influenced and the observation. After all the reports have been considered, the corrections are summed according to the following equation:

$$C_{i,j} = a(d_{i,j}) \left[\frac{\sum_{n=1}^{N} c_n}{\sum_{n=1}^{N} w_n} \right]$$

where:

$C_{i,j}$ = total correction applied to grid point (i,j)

c_n = individual correction (difference between interpolated grid point value and observed value) multiplied by w_n

w_n = weighting factor given by

$$w_n = \exp(-4\, r^2/R^2)$$

r = distance from grid point to observation point

R = scan radius (variable)

$a(d_{i,j})$ = 1, or the maximum value of w_n, depending on the value of $d_{i,j}$

$d_{i,j}$ = number of data points within the area bounded by scan radius R

$a(d_{i,j}) = \max w_n$ if, $d_{i,j} < 3$

$a(d_{i,j}) = 1$ if, $d_{i,j} > 3$

The total corrections for all grid points are then added to the grid point values to yield a revised first-guess field one step closer to the final analysis field. Three scans are made through the reports to produce the final analysis field.

Smoothing Procedure

A light nine-point smoothing operation is applied to all fields after they have been analyzed. This smoothing operation effectively removes irregularities from observational errors and inherent "noise" in the data. Meteorologically significant waves are not destroyed, because the grid point spacing for each net is much less than the average distance between data points.

For interior points, a given field A(i,j) is smoothed by the following equation:

$$A(i,j) = 0.75 \cdot A(i,j) + \frac{0.25}{9} [A(i-1, j-1) + A(i,j-1) + A(i + 1, j-1) + A(i-1,j) + A(i,j) + A(i + 1,j) + A(i-1, j + 1) + A(i,j + 1) + A(i + 1, j + 1)]$$

A somewhat comparable smoothing operation is used for corner and edge points of the grid.

EXAMPLES AND DISPLAY

Figure 4 shows a plot of vectors of wind observations on the largest grid net. The length of the vector is proportional to the speed of the wind; where the display program sets the minimum wind equal to a point, and a maximum wind equal to the length of two grid units. The data displayed in Figure 4 provided the analysis shown in Figure 5. The same convention is used throughout for the vector length display. Figures 6 and 7 show comparable data for the medium grid nets and Figures 8 and 9 show comparable data for the smallest grid networks. The first guess for the largest net was a constant wind field over the whole grid. The first guess for the medium net came from the analyzed data for the large net, i.e., every fourth grid point was smoothed over the entire grid of the medium net. Likewise, the smaller net used the medium net analysis as its first guess.

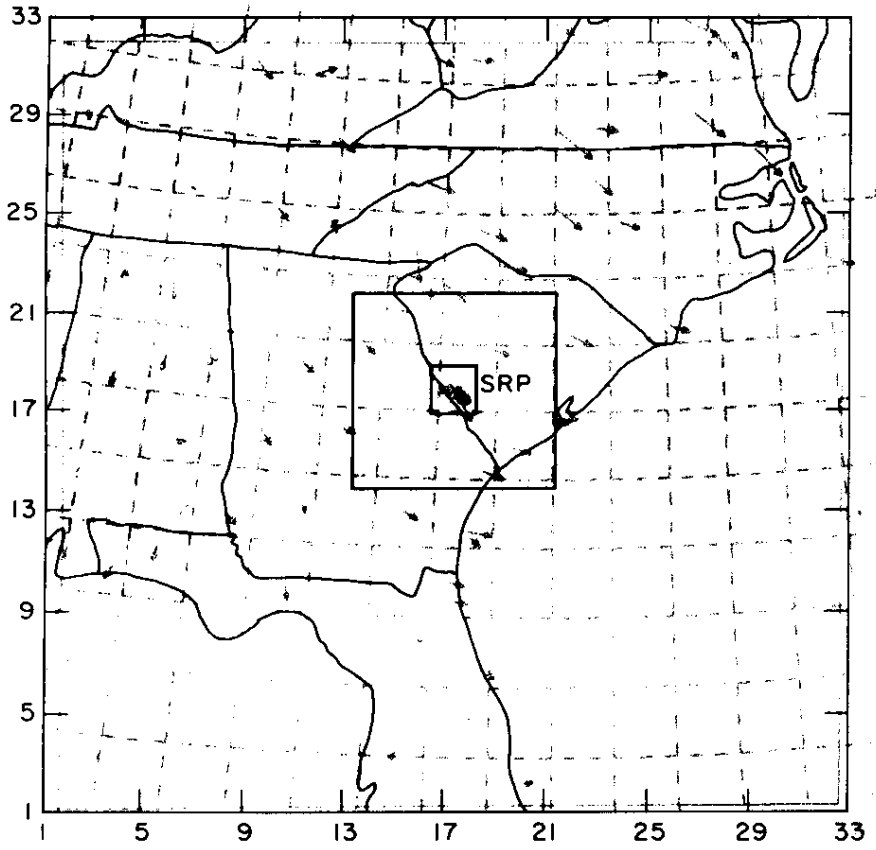

FIGURE 4. Data Input for the Largest Analysis Grid. The vectors are adjusted such that the strongest wind is two grid units in length and the lightest wind is just a dot

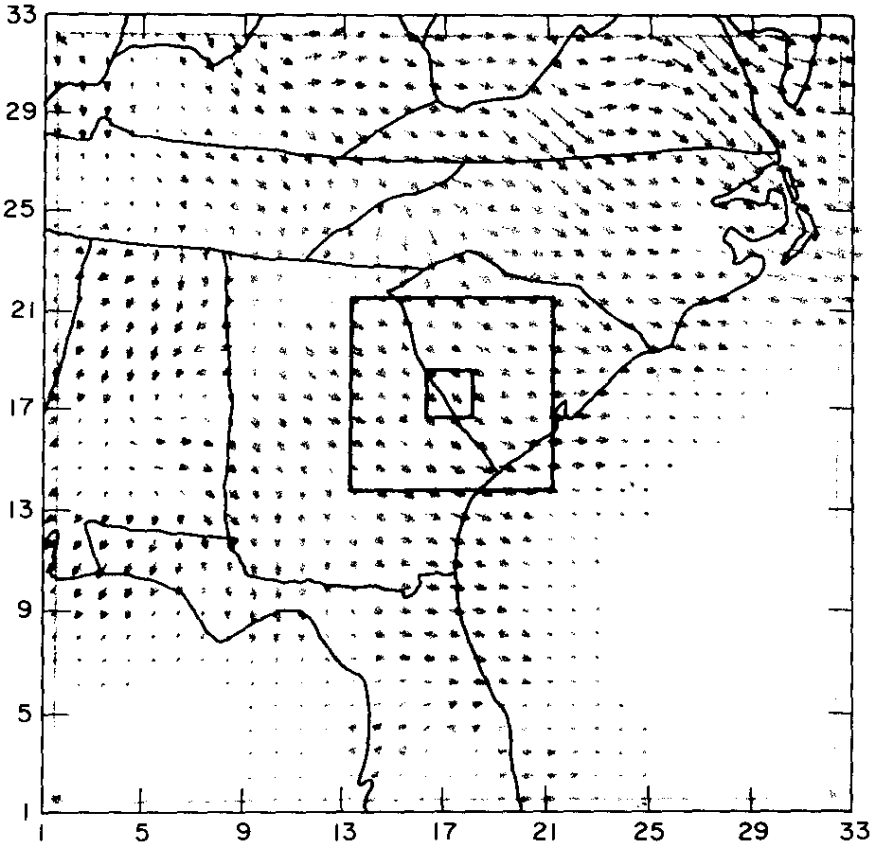

FIGURE 5. The Analysis Resulting From the Data Shown in Figure 4. There were no data in the ocean areas and the first-guess field was calm over the entire wind field. That is why no data are shown in the lower right and lower left hand corners

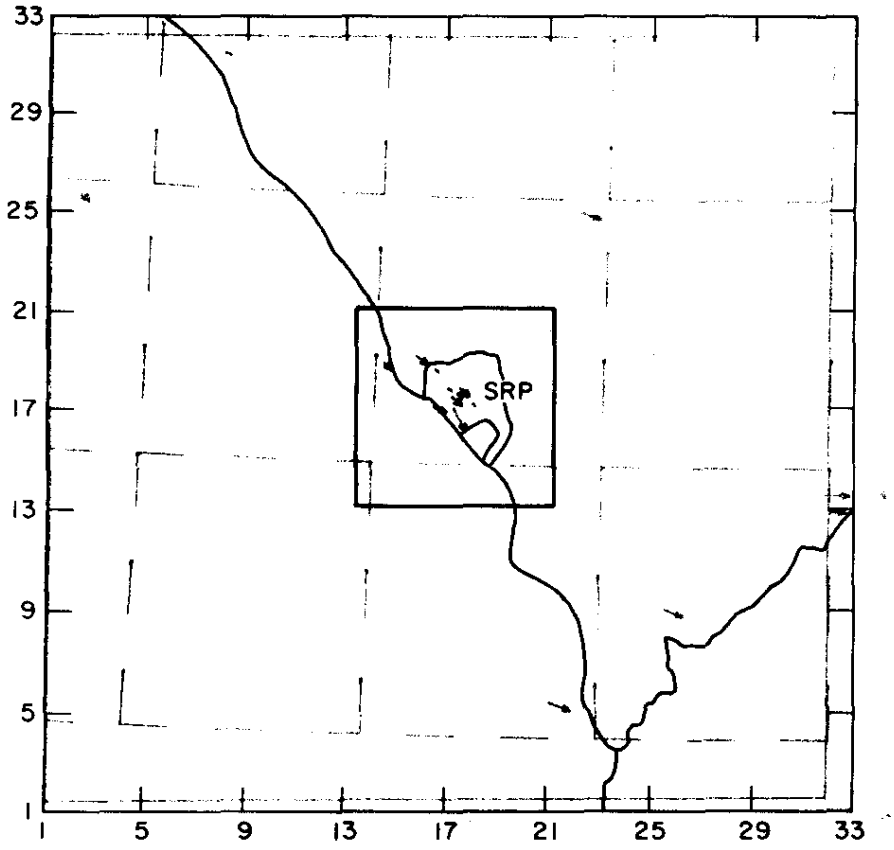

FIGURE 6. Wind Data for Medium Grid Analysis

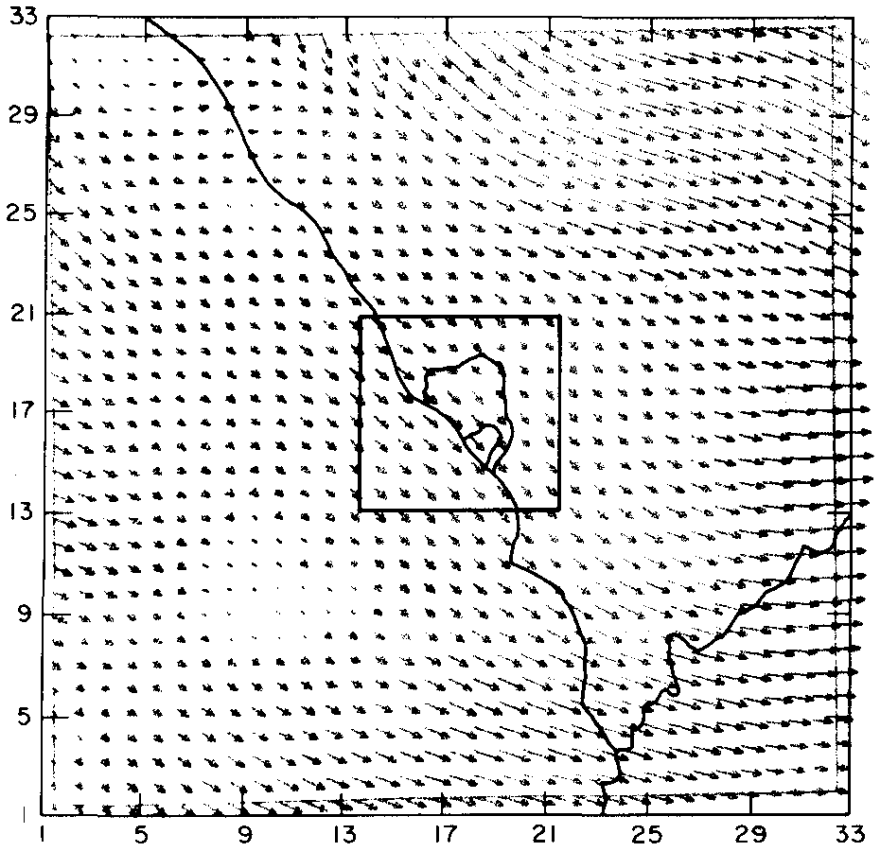

FIGURE 7. The Resulting Wind Grid Analysis From the Data in Figure 6. The first guess came from the analyzed fields in Figure 5

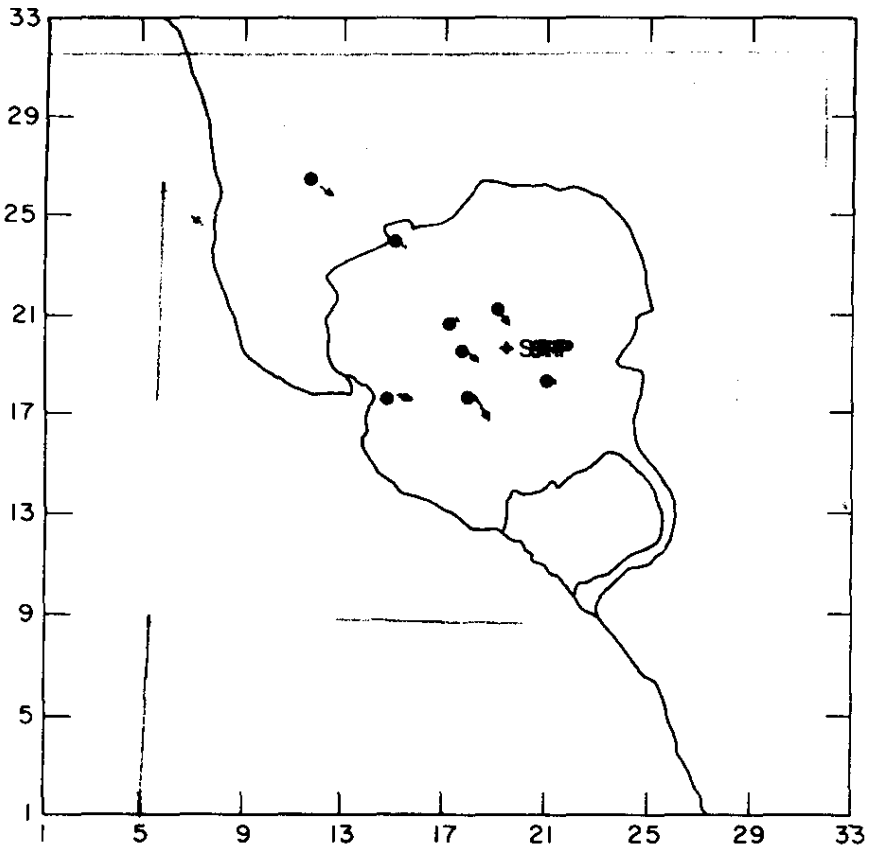

FIGURE 8. Wind Data for Smallest Grid Analysis

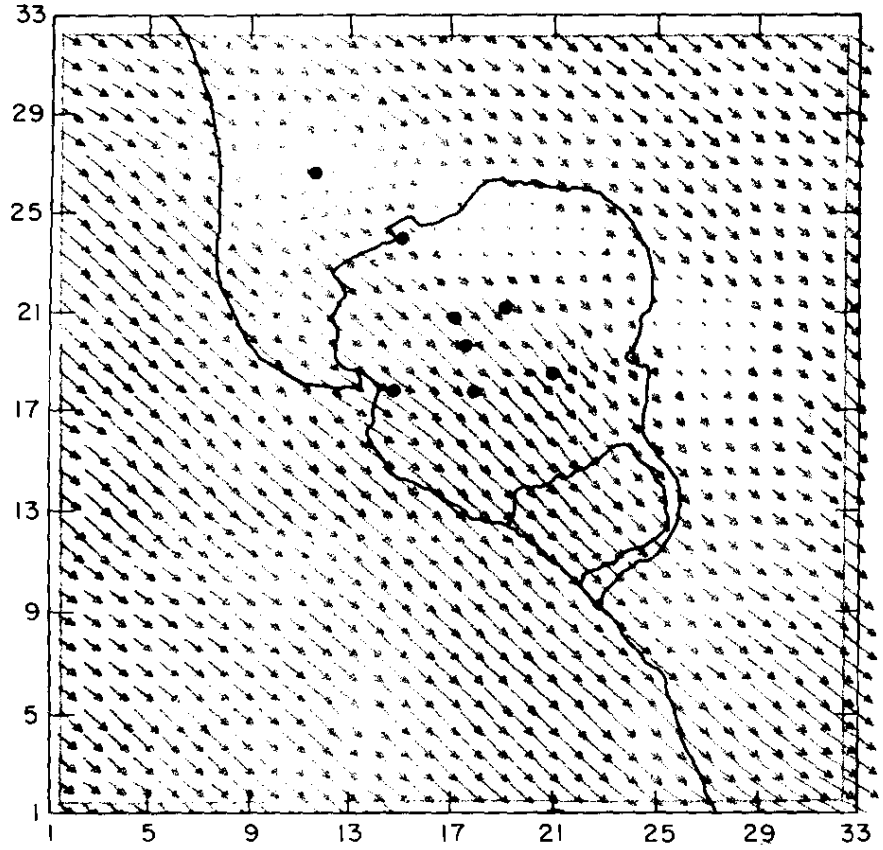

FIGURE 9. The Resulting Analysis From the Data Listed in Figure 8. The first guess came from the analyzed fields in Figure 7

SUMMARY

The analysis scheme described here provides input data for trajectory programs, diffusion programs, and prognostic models which are determined at the Savannah River Laboratory. The analysis is very rapid, taking just a few seconds on the IBM S/360-195 computer. The analysis will be expanded to three-dimensions, and eventually, improved analysis techniques will provide mass-consistent wind fields. The mass-consistent wind fields avoid the inherent strong local divergencies and convergencies in the present analysis scheme.

REFERENCES

1. T. V. Crawford, "Facilities for Atmospheric Science Research," in *Progress Report Dose-To-Man Program, FY-1973*, pp 13-20. USAEC Report DP-1341, E. I. du Pont de Nemours and Company, Savannah River Laboratory, Aiken, S. C. (1974).

2. R. J. Fleming. *AFGWC Fine-Mesh Upper Air Analysis Model.* AFGWC Report TM 69-2(December, 1969). Available through Federal Clearing House under AD 710203.

3. S. L. Barnes. "A Technique for Maximizing Details in Numerical Weather Map Analysis." *J. Appl. Meteorol., 3,* 396-409(1964).

9. PRELIMINARY MESOSCALE CALCULATIONS FOR THE SOUTH-EASTERN UNITED STATES USING THE TWO AND ONE-HALF DIMENSIONAL LAVOIE MODEL

INTRODUCTION

A three-layer mesoscale model was developed [1-3] for analyzing lake-effect storms over the eastern half of Lake Erie and its drainage basin. This model included surface influences of friction, heating, and topography. The model has been modified to provide forecasts of horizontal wind components (u,v), the potential temperature of a well-mixed layer, and the thickness of a well-mixed layer. This prognostic model was developed to provide the meteorological parameters necessary to calculate the location, time, and concentration of pollutants accidentally released to the atmosphere. This model is a first, though quite small, step in the direction of developing other, more definitive models. Another argument for developing complex dynamic prediction models is to use them in those cases where the observations required for mesoscale prediction are so infrequent that a dynamic model must be used to generate mesoscale flow patterns from uneven topography, uneven roughnesses, uneven heating, etc. Scanty mesoscale data can be used to generate such models. After the mesoscale model operates for a period of time, mesoscale motions are then spread over the entire grid of interest.

MODEL

The dry Lavoie model (DLM), developed in the course of this work, includes the surface influences of friction, heating, and topography. The three layers in the model (Figure 1) are a constant flux layer at the surface (I), a well-mixed, homogeneous layer (II), and a deep stable upper layer (III).

The dry thermal structure of the Lavoie model at initial time is shown in Figure 2, where θ represents the potential temperature, and Z is the altitude above some datum plane (usually

---

† Work done by C. D. Kern, presented at the *Symposium on Atmospheric Diffusion and Air Pollution*, held at Santa Barbara, California, September 9-13, 1974.

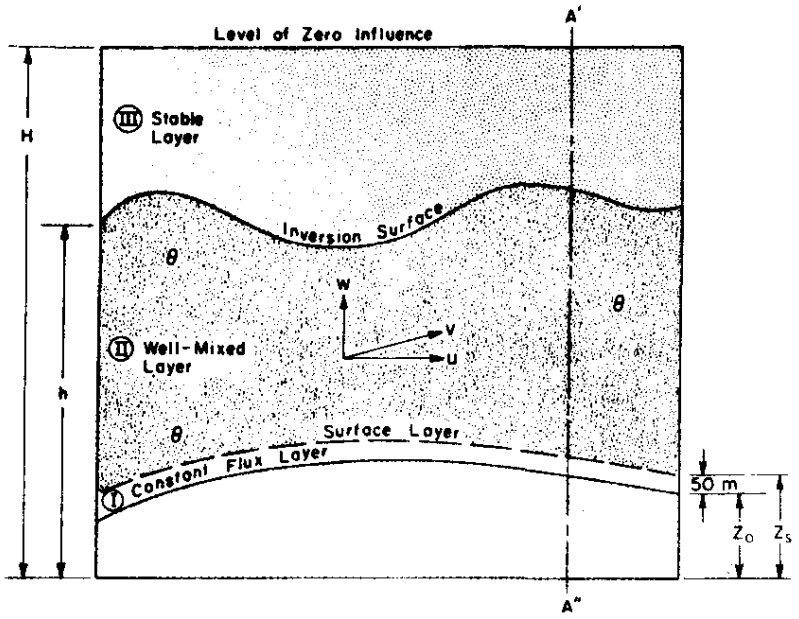

FIGURE 1 Vertical Profile of Lavoie's Three-Layer Model

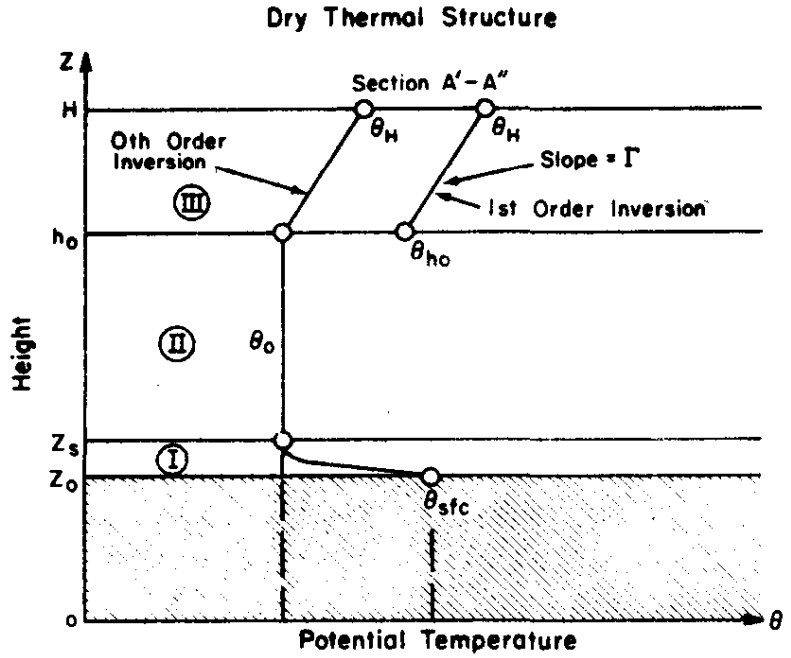

FIGURE 2. The Dry Thermal Structure of Lavoie's Model: Section A'-A" of Figure 1

mean sea level). During daytime insolation, Layer I is characterized by a superadiabatic lapse rate with an upward transfer of heat and a downward transfer of momentum; this layer is assumed to be 50 m thick. Layer II exhibits a dry adiabatic lapse rate, as this layer is assumed to be well-mixed by strong winds and surface heating. Finally, Layer III, a deep stratum, possesses a constant, stable lapse rate.

It is possible, without violating the derivation of the governing equations, to modify Layer I if Layers II and III retain their basic character. That is, Layer I could be either neutral or stable, and its depth could be any specified quantity. Hence, the applicability of the Lavoie model can be broader than originally intended if one is sufficiently cautious.

The initial set of equations for the DLM contains equations for the horizontal motions of the wind field vectors (u and v), the hydrostatic pressure equation, the thermodynamic energy equation for the potential temperature (Θ), the equation of state for dry air, and the equation for conservation of mass. These equations are only applied in Layer II. As Layer II is homogeneous in the vertical direction, the above equations are integrated vertically from the top of the surface friction layer (Layer I) to the top of the well-mixed layer (Layer II). The altitude of the top of Layer II is denoted by h. Hence, the final set consists of equations governing the behavior of the well-mixed layer as a whole. The dependent variables are the wind field vectors (u and v), potential temperature (Θ), and the height of the well-mixed layer (h). These variables are functions of the horizontal coordinates (x,y) and time t. The average vertical velocity in Layer II is given by the continuity equation. For a given set of boundary and initial conditions, this system is very similar to the shallow water equations of oceanography.

The influence of Layer I is represented in the above system by the parameters in the momentum and energy equations. That is, the transfer of momentum and heat from Layer I to Layer II is defined by the bulk aerodynamic formulation.[4,5] The influence of Layer III on Layer II is determined by the horizontal pressure gradient terms in the momentum equations.

In our research at SRL, we found a thermal structure which closely approximates that of the DLM under inversion conditions. The diurnal mixing height in this area varies from near the top of the forest canopy in the morning to about 800 meters in the afternoon.[6]

The DLM assumes the disturbances in Layer III are produced by the more-active Layer II and decrease with height, becoming negligible at some arbitrary height Z = H (Figures 1 and 2).

However, Lavoie found that the resulting disturbances were much too weak whenever Layer III possessed significant gravitational stability. Therefore, in the DLM the "highest level of influence" is related to the maximum height (h_m) of the disturbed inversion surface. That is, H is replaced by $(h_m + h_o)/2$, where h_o is the initial height of the inversion surface. This factor enters into the derivations of the following conservation equations.

The averaged conservation of momentum in Layer II is given by:

$$\frac{Du}{Dt} = -\frac{C_D|\underset{\sim}{V}|u}{h - z_s} + fv + \frac{g}{2\theta}(h - z_s)\frac{\partial\theta}{\partial x}$$

$$+ \frac{g}{\theta}\left[\theta - \theta_h - \frac{\Gamma}{4}(h_m - h_o)\right]\frac{\partial h}{\partial x}$$

$$+ \left[h_o - h + \frac{h_m - h_o}{2}\right] f\psi_y - \left(\frac{1}{\rho}\cdot\frac{\partial\rho}{\partial x}\right)_{h_o} \qquad (1)$$

and

$$\frac{Dv}{Dt} = -\frac{C_D|\underset{\sim}{V}|v}{h - z_s} - fu + \frac{g}{2\theta}(h - z_s)\frac{\partial\theta}{\partial y}$$

$$+ \frac{g}{\theta}\left[\theta - \theta_h - \frac{\Gamma}{4}(h_m - h_o)\right]\frac{\partial h}{\partial y}$$

$$- \left[h_o - h + \frac{h_m - h_o}{2}\right] f\psi_x - \left(\frac{1}{\rho}\cdot\frac{\partial\rho}{\partial}\right)_{h_o} \qquad (2)$$

where:

$$\frac{D}{Dt} = \frac{\partial}{\partial t} + u\frac{\partial}{\partial x} + v\frac{\partial}{\partial y} = \frac{\partial}{\partial t} + \left(\underset{\sim}{v}_h \cdot \nabla_h\right)$$

t is time); (x,y), the horizontal Cartesian coordinates; u and v, the horizontal wind vectors in Layer II; h and z_s, heights (defined in Figure 1); C_D, the drag coefficient for momentum; f, the Coriolus parameter; g, the gravitational acceleration; θ, the potential temperature in Layer II; Γ, the constant lapse rate

in Layer III; ψ_x and ψ_y, the vertical shear of the geostrophic wind in Layer III, ρ, the air density; and P, the air pressure.

The first terms on the right-hand sides of Equations 1 and 2 describe the momentum loss from Layer II caused by surface friction (Layer I). The second terms on the right are the contributions of Coriolis forces. All the other terms on the right are the various contributions to the horizontal pressure gradient forces in Layer II from changes in Layer II and interactions between Layers II and III.

The velocity vector at elevation z_s is assumed to be parallel to the topography with horizontal components equal to u and v. Hence, the vertical component (w_s) at $z = z_s$ is equal to

$$w_s = \underset{\sim}{v}_h \cdot \nabla_h \cdot z_o$$

In Equation 3, the quantity z_o is equal to $z_o(x,y)$ and describes the given topography of the area in question.

The quantity $[(1/\rho) \cdot (D\rho/Dt)]$ represents the rate of change of density of a parcel of air. In Layer II, the most important contribution to this term is the pressure change due to vertical motion. Considering this fact, and then averaging $[(1/\rho) \cdot (D\rho/Dt)]$ through the layer from z_s to z, the resulting mean value is

$$\frac{1}{\rho} \cdot \frac{D\rho}{Dt} = - \frac{g}{c^2} \cdot \frac{w_z + w_s}{2}$$

$$c^2 = \frac{C_p R}{C_v} \theta \sim 402.2\ \theta$$

where; c is in m/s; θ, °K; C_p, specific heat at constant pressure; R, the gas constant for dry air; and C_v, the specific heat for constant volume.

If the continuity equation for a compressible gas is averaged over Layer II for the interval z_s to z, where $z_s < z < h$, then the resulting equation for w_z can be written as

$$w_z = \left[\frac{2c^2 + g(z - z_s)}{2c^2 - g(z - z_s)}\right] \cdot w_s - \left[\frac{2c^2(z - z_s)}{2c^2 - g(z - z_s)}\right] \cdot \nabla_h \cdot \underset{\sim}{v}_h \qquad (6)$$

where Equations 3 and 4 have been used in its derivation. When $2c^2 >> g(z-z_s)$, then Equation 6 reduces to the incompressible case, namely,

$$w_z + w_s - (z - z_s)\nabla_h \cdot \underset{\sim}{v}_h \qquad (7)$$

The governing equation for h is obtained when the inversion surface is assumed to be a material surface, that is,

$$w_h = \left(\frac{Dh}{Dt}\right) \qquad (8)$$

where w_h is the vertical velocity at z = h. Combining Equations 6 and 8 gives the defining equation for h, except for a correction term:

$$\frac{Dh}{Dt} = \frac{2c^2}{2c^2 - g(h - z_s)} \left\{\left[\frac{2c^2 + g(h - z_s)}{2c^2} \cdot w_s\right] - \left[(h - z_s)(\nabla_h \cdot \underset{\sim}{v}_h)\right]\right\}$$

$$+ (1/\Gamma) \cdot (\partial\theta/\partial t) \qquad (9)$$

where the last term on the right is a correction term which preserves the first order inversion (Figure 2). This correction term is zero if $\theta < \theta_h$, and $[(1/\Gamma) \cdot (\partial\theta/\partial t)]$ when $\theta > \theta_h$. The perturbations this correction induces in the conservation equations are neglected.

The final conservation equation in the DLM system is the thermal energy equation, namely

$$\frac{D\theta}{Dt} = \frac{C_H \left|\underset{\sim}{v}\right| (\theta_s - \theta)}{h - z_s} \qquad (10)$$

where C_H is the drag coefficient for heat, and θ_s is the surface potential temperature. The term on the right is the heat added by the surface to the air.

The differencing scheme used for the flow field is referred to as "forward-upstream" differencing.[1,2] This scheme uses a forward extrapolation in time together with a one-sided, upstream difference to approximate the spatial derivatives in the advection terms. All other spatial derivatives are replaced by centered differences. The uncentered, upstream differencing is acceptable if the gradients are always being evaluated in the fluid region being advected over the grid point during the forecast time interval. However, if the upstream convection is violated, the scheme is unstable.

In summary, the forward-upstream difference formulation offers advantages in seeking steady-state solutions of this initial value problem. The advantages are due to the strong damping of transient motions, the restraining influences on boundary difficulties, and the control of non-linear instability. The major disadvantage is that instability may occur if the initial flow field is reversed at some grid points as the computation proceeds.

The above development of the DLM has been adapted directly from Drake, *et al.*,[7] in their studies of pollution transport in the Four Corners area of the United States.

OUTPUT

For research studies and operational use, a network of three nested grids was established for the southeastern United States.[8] Figures 3 through 7 show a vector display of the wind fields calculated from the DLM over the largest grid over a twenty-four hour forecast period at timed interals of 600 seconds each. The depth of the well-mixed layer was a constant 500 m above smoothed terrain. Sea surface temperature was held constant and equal to October's climatological value (298-300°K). Land surface temperature was also held constant (300°K). The initial well-mixed layer potential temperature was 295°K, and initial winds in the well-mixed layer maintained a constant speed of 5 m/sec from the southwest. Drag coefficient (C_D) was taken as a function of surface elevation, with the lowest value at sea surface (1.5×10^{-3}) and increasing to the largest value (7.0×10^{-3}) for surface elevations above 100 m. Figure 3 shows the initial wind field. Figure 4 shows the wind field after 6 hours. On this display, the smallest value of the wind is a small arrowhead, and the largest value is set equal to a vector of two grid units in length. On this figure, the magnitudes varied from a minimum value of 4.4 m/sec to a maximum of 7.9 m/sec.) Figure 5 shows the field after 12 hours

(minimum speed of 4.0 m/sec, maximum speed of 8.1 m/sec). Figure 6 shows the field after 18 hours (minimum speed 3.3 m/sec, maximum speed 8.2 m/sec), and Figure 7 shows the field after 24 hours (minimum speed of 0.3 m/sec, maximum speed of 8.5 m/sec). The effect of elevation and surface drag can be seen clearly. The effect of the boundary (evident in Figure 7) has been corrected by applying a four-grid smoothing operation along the boundary in subsequent versions of the model. All three nested grids with real data have been analyzed with the DLM.

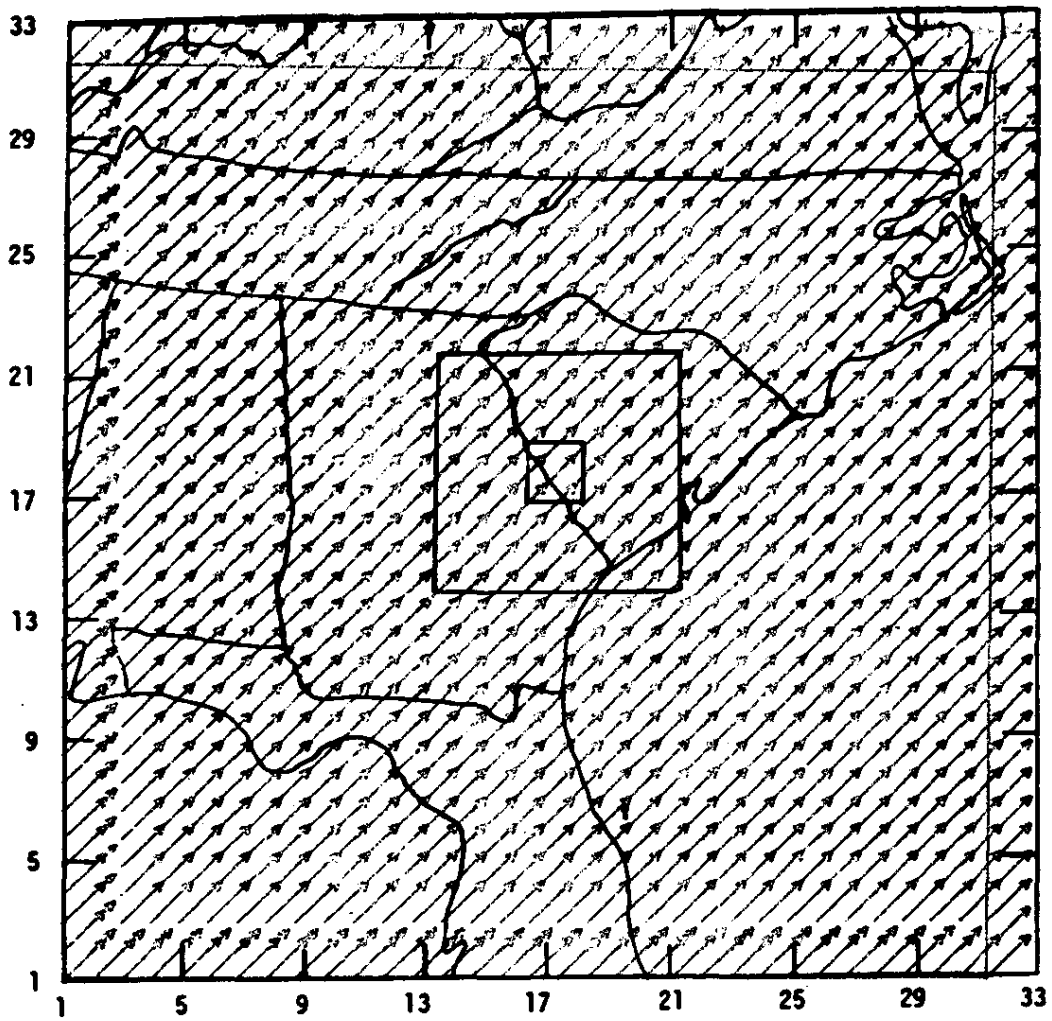

FIGURE 3. Initial Wind Field, Wind from Southwest at 5 m/sec

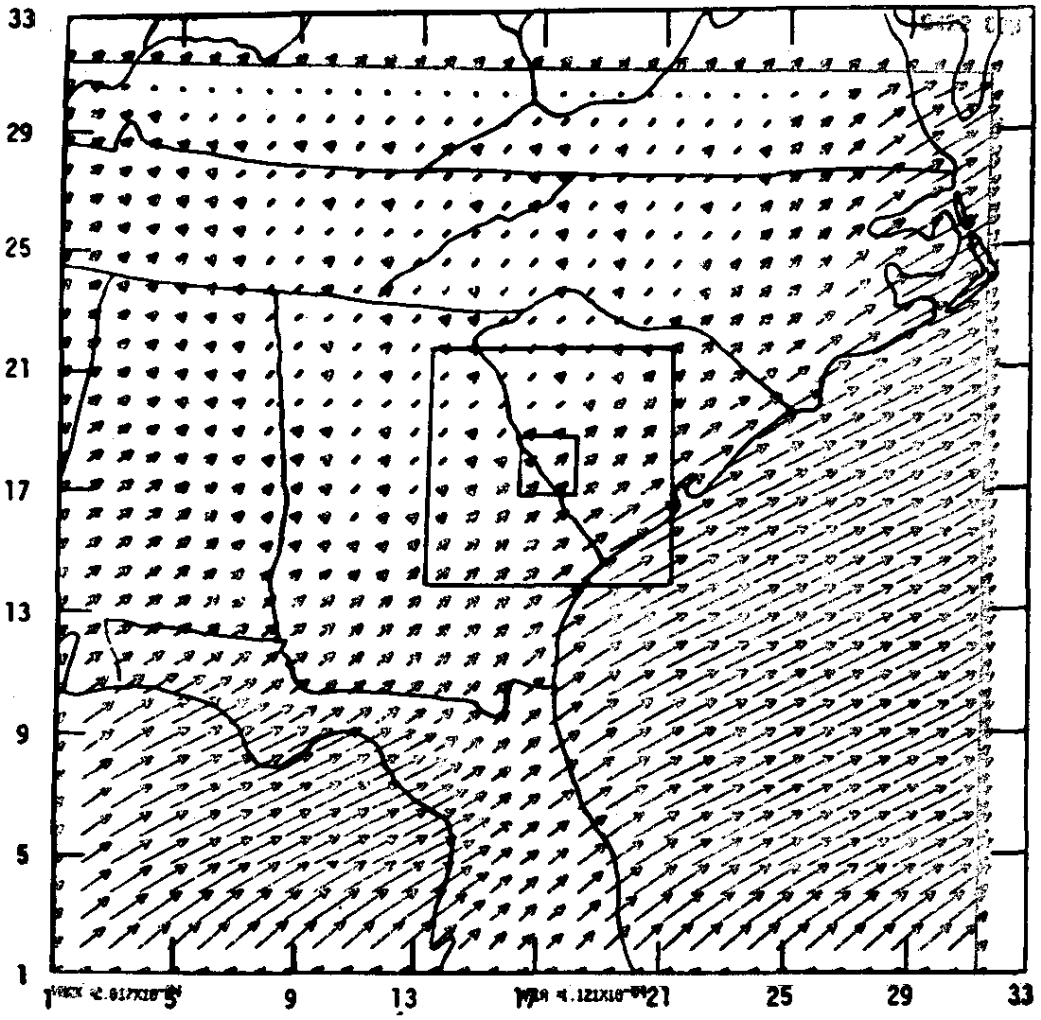

FIGURE 4. Wind Field after 6 Hours, Wind from Southwest

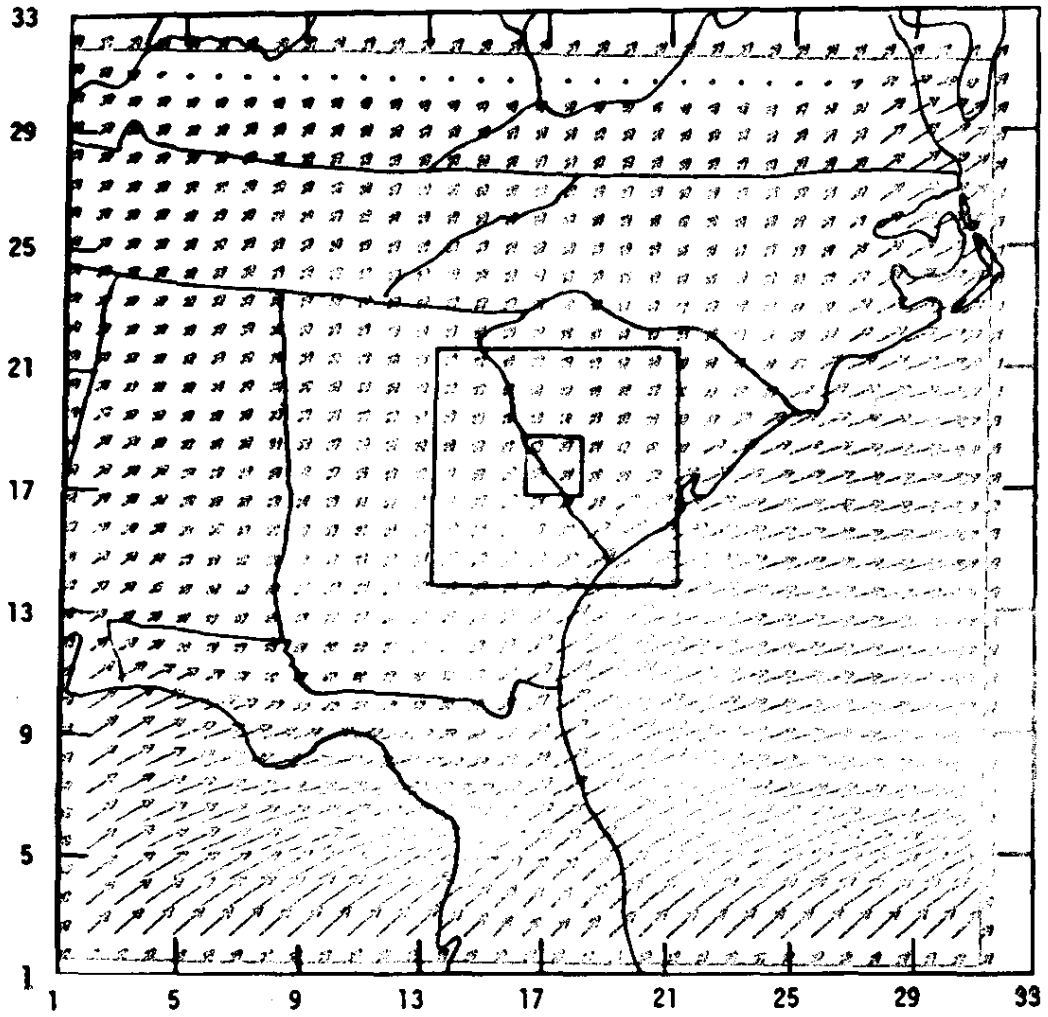

FIGURE 5. Wind Field after 12 Hours, Wind from Southwest

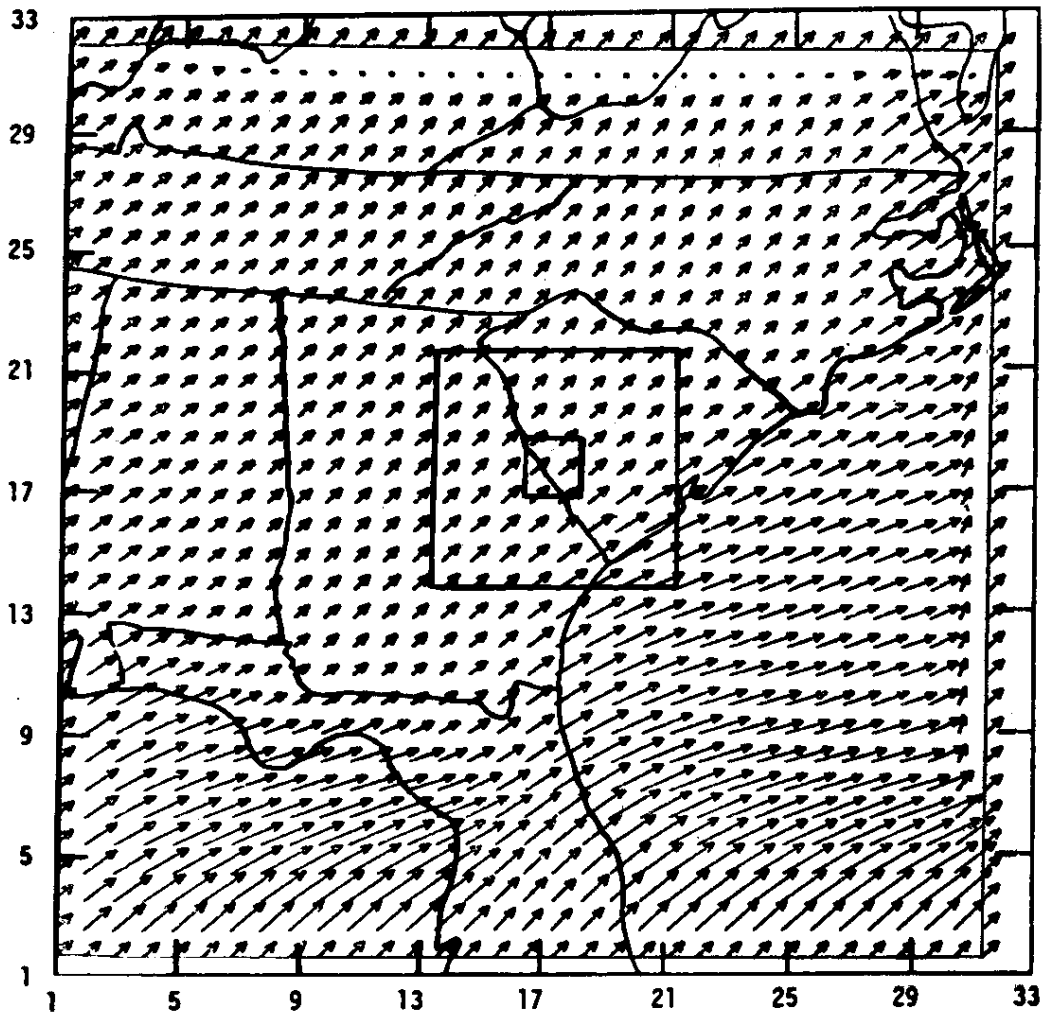

FIGURE 6. Wind Field after 18 Hours, Wind from Southwest

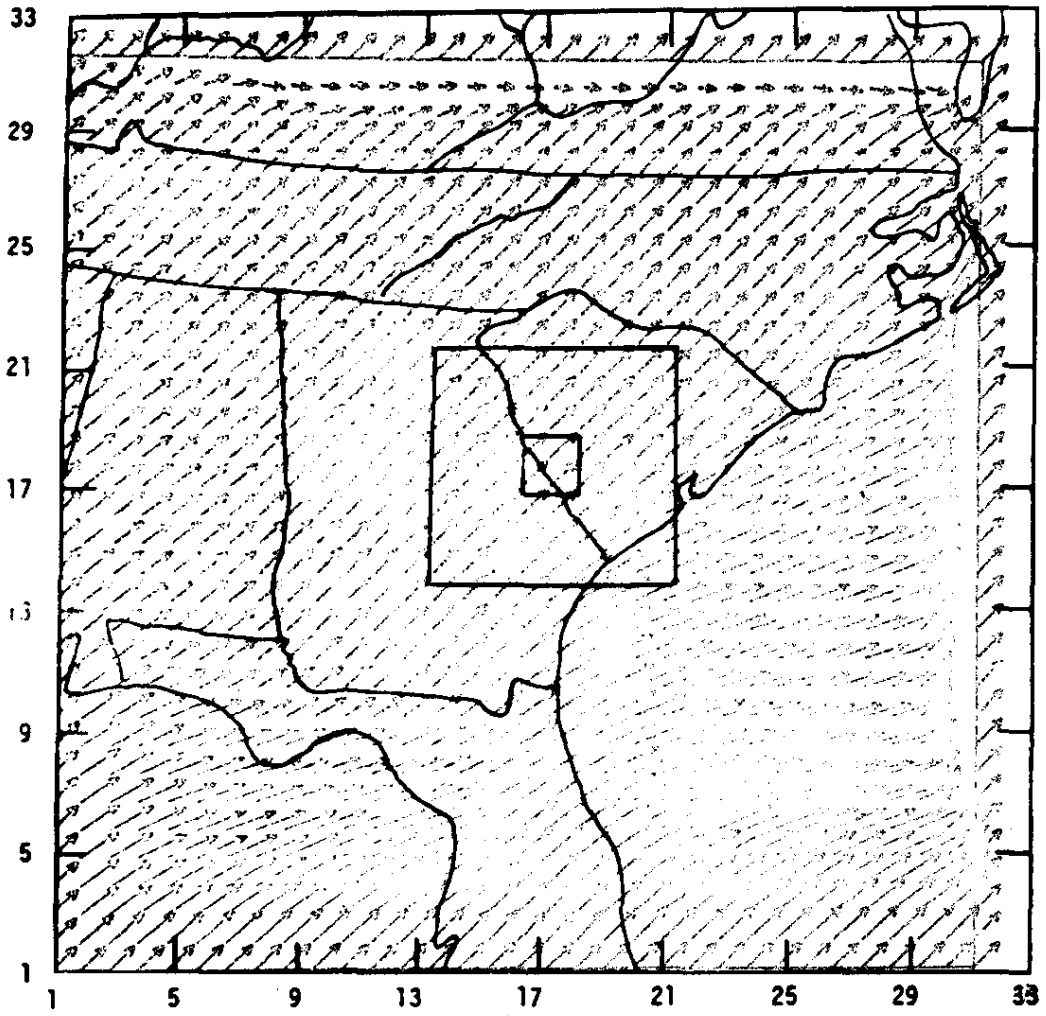

FIGURE 7. Wind Field after 24 Hours, Wind from Southwest

CONCLUSIONS

The DLM is but a small step in the development of a model which will forecast the meteorological parameters necessary for pollution transport modeling.

REFERENCES

1. R. L. Lavoie. *A Mesoscale Numerical Model and Lake-Effect Storms.* Ph.D. Dissertation, The Pennsylvania State University, College Park, Pa., 102 pp (1968).

2. R. L. Lavoie. "A Mesoscale Numerical Model of Lake-Effect Storms." *J. Atmos. Sci. 29,* 1025-1040 (1972).

3. L. G. Davis, R. L. Lavoie, J. I. Kelley, and C. L. Hosler. *Lake Effect Studies.* Final Report for ESSA Contr. No. E22-80-67 (N). The Pennsylvania State University, College Park, Pa., 108 pp. (1968).

4. C. H. B. Priestley. *Turbulent Transfer in the Lower Atmosphere.* Univ. of Chicago Press, Chicago, Ill., 130 pp (1969).

5. H. V. Roll. *Physics of the Marine Atmosphere.* Academis Press, New York, N. Y., 426 pp (1965).

6. J. F. Schubert. "A Climatology of the Mixed Layer Using Acoustic Methods." Paper No. 4 of this report.

7. R. L. Drake, Celeste P. Peterson, and D. L. Anderson. *The Feasibility of Using the Lavoie Lake Storm Model in Air Pollution Studies: The Four Corners Area.* Paper presented at the American Geophysical Union meeting in San Francisco, California, December 6-9 (1971). To be published.

8. C. D. Kern. "A Computer Program for Objective Analysis and Display of Meteorological Fields." Paper No. 8 of this report.

10. A TRAJECTORY AND DISPERSION COMPUTER PROGRAM WHICH USES OBJECTIVELY ANALYZED, OBSERVED OR FORECAST METEOROLOGICAL FIELDS †

INTRODUCTION

From the gridded analyses and gridded forecasts of winds described in the previous two sections,[1,2] the dispersion of pollutants released to the atmosphere can be calculated by direct solution of the diffusion equation. However, these solutions of the diffusion equation tend to be very time-consuming in a computational sense or tend to have numerical errors, which produce artificial dispersions greater than the actual dispersions occurring in the atmosphere. To overcome these problems and to generate relatively quickly estimates of dispersion from multiple elevated point sources, a computer program was developed which generates two-dimensional horizontal or terrain-following trajectories. The standard plume equation is solved along the centerline of these trajectories. Appropriate dispersion parameters are necessary to calculate the concentration along the centerline of such plumes. These dispersion parameters are derived by two methods; one of which is adapted from Slade,[3] and the other is the SRP modification to the Brookhaven National Laboratory (BNL) method.[4]

THE TRAJECTORY MODEL

Parcel displacements are calculated along trajectories computed from wind analysis fields, linear interpolation in time between sequential analysis fields, or from forecast gridded fields. Parcel displacements start at the location of the elevated stack and move forward in space and time. The two horizontal components of the wind are available at analysis time(s), or at some forecast time which allows linear interpolations forward in time or between analysis times. Considering first the persistent wind field, i.e., a single gridded analyzed wind field, the procedure is to step forward in small time increments until the trajectory is carried to the edge of the grid.

---

†Work done by C. D. Kern.

Considering one grid point in one dimension, a first approximation of the displacement for one time step is obtained by

$$\Delta x_1 = \left(u_i^t\right) \Delta t \tag{1}$$

where Δx = the displacement (in grid units)

u = the east-west grid component (in grid units/sec)

Δt = the time step, sec

i = the initial point

1 = the iteration number

The subsequent iterations can be performed by

$$\Delta x_n = \left[\frac{u_i^t - \left(u_{n-1}^{t-\Delta t}\right)}{2}\right] \Delta t \tag{2}$$

where $\left(u_{n-1}^{t-\Delta t}\right)$ is the wind component from the previous time step interpolated at the point x_{n-1} given by

$$x_{n-1} = x_i - \Delta x_{n-1} \tag{3}$$

When $\Delta x_n - \Delta x_{n-1} \leq e$, a new initial point is determined and the process is repeated until the edge of the grid is reached. The value, e, is taken to be equal to 0.01 grid units. The Δt tends to be so small (normally 600 seconds) that one iteration of Equation 1 is sufficient, and no further iterations are normally needed. This procedure can be used for any of the three grid nets described in the previous two sections.[1,2]

When interpolating in time, Equation 1 is used; however, the value for u_I^t is determined by interpolating both in space and time.

Figure 1 shows a typical trajectory from one of the reactor areas at SRP.

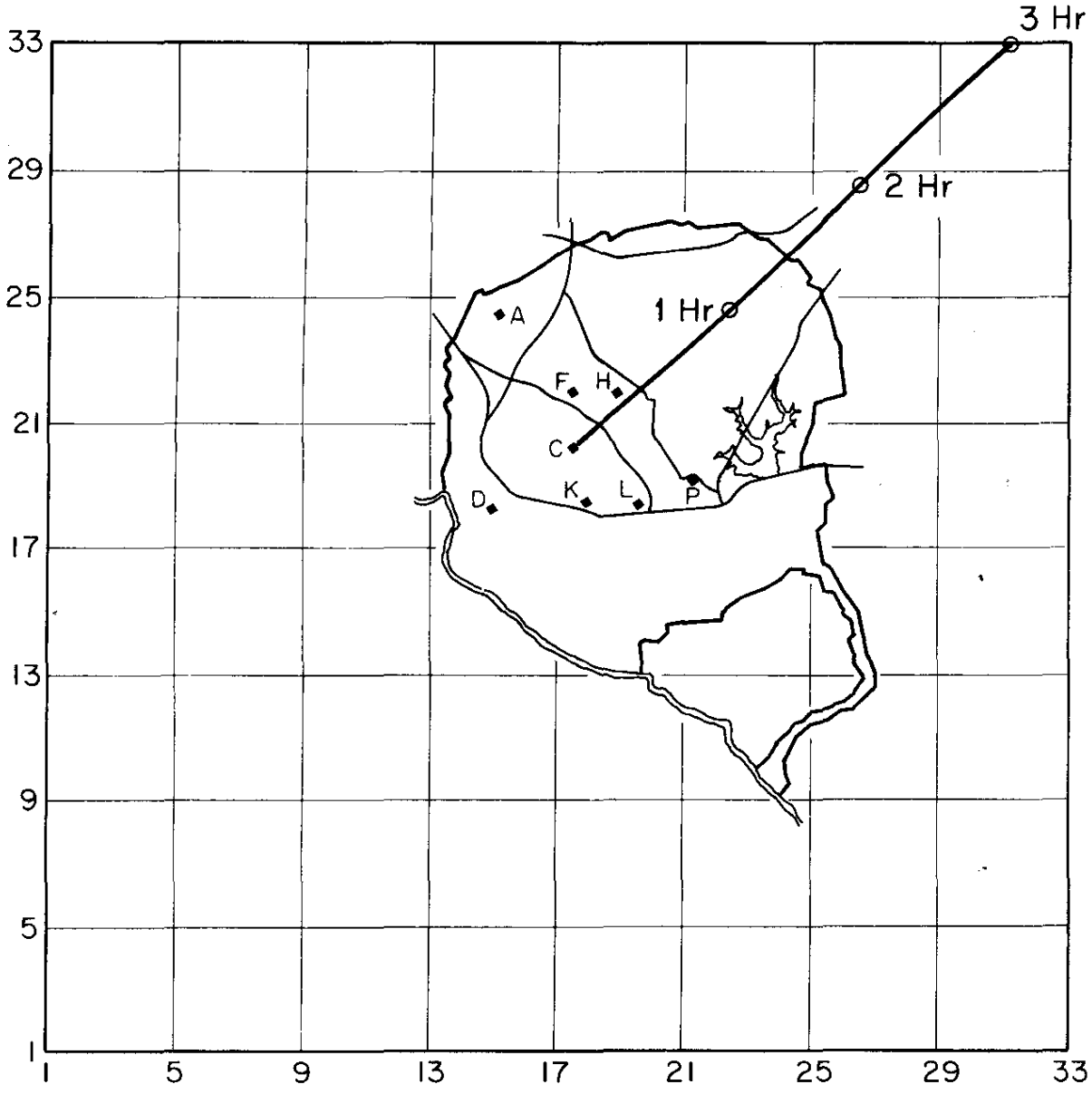

FIGURE 1. A Straight Line Trajectory from C-Reactor

CONCENTRATION CALCULATIONS

Estimates of downwind concentrations (along centerline of trajectory) are made by the Gaussian Plume Model which is expressed by:

$$\chi = \left(\frac{S}{\pi \bar{u} \sigma_y \sigma_z}\right) \exp \cdot \left(\frac{-\lambda x}{\bar{u}}\right) \exp - \left[1/2 \left(\frac{(z-h)^2}{\sigma_z^2} + \frac{y^2}{\sigma_y^2}\right)\right] \qquad (4)$$

where χ = downwind concentration, pCi/m^3

S = source term, pCi/sec

λ = radioactive decay constant, sec^{-1}

$\bar{u}$ = average wind speed, m/sec

x = downwind distance, m

h = release height, m

y = distance from plume centerline, m

z = height above ground level, m

σ_y = horizontal Gaussian dispersion coefficient, m

σ_z = vertical Gaussian dispersion coefficient, m

Given the source term, half life (isotope), wind field, and the location where the downwind concentration is needed, and with an estimate of the horizontal and the vertical Gaussian dispersion coefficients, the concentration at that location can be calculated. Two methods are used to calculate the horizontal and vertical Gaussian dispersion coefficient. One method is based on procedures developed by BNL[5] and modified by Cooper and Rusche.[4] The other method is an adaptation of the curves displayed by Slade.[3]

A. BNL Method

For stable atmospheric condition, the horizontal and vertical Gaussian dispersion coefficients are given by

$$\sigma_y = 0.15\sigma_a \cdot x^{0.71} \qquad (5)$$

$$\sigma_z = 0.15\sigma_e \cdot x^{0.71} \qquad (6)$$

where σ_a = standard deviation of the horizontal wind direction, in degrees

σ_e = standard deviation of wind direction, in degrees.

For unstable atmospheric conditions, the Gaussian dispersion coefficients are determined by:

$$\sigma_y = 0.045\sigma_a \cdot x^{0.86} \quad (7)$$

$$\sigma_z = 0.045\sigma_e \cdot x^{0.86} \quad (8)$$

B. Slade Method

The Slade method for calculating the horizontal and vertical dispersion coefficients are taken from his Figures 3.10 and 3.11 in Reference 3. These are shown in Figures 2 and 3. An analytical approximation to these curves for the vertical dispersion function is made with the empirical power law in the form of:

$$\sigma_z = ax^b \quad (9)$$

The parameters a and b for various stabilities and ranges of distance, x, are given in Table 1.

TABLE 1

Parametric Values for σ_z (meters)

Stability Class (σ_e)	Distance, meters: 100 to 500		500 to 5000		5000 to 50,000	
	a	b	a	b	a	b
A (25°)	0.0383	1.2812	0.002539	2.0886	0.002539	2.0886
B (20°)	0.1393	0.9467	0.04936	1.1137	0.04936	1.1137
C (15°)	0.1120	0.9100	0.1014	0.9260	0.1154	0.9109
D (10°)	0.0856	0.8650	0.2591	0.6869	0.7368	0.5642
E (5°)	0.0818	0.8155	0.2527	0.6341	1.2969	0.4421
F (2.5°)	0.0545	0.8124	0.2017	0.6020	1.5763	0.3606

The stability classes A through F are for the Pasquill stability categories and are listed as follows:

Pasquill Stability Categories	σ_a or σ_e
A, extremely unstable	25.0°
B, moderately unstable	20.0°
C, slightly unstable	15.0°
D, neutral	10.0°
E, slightly stable	5.0°
F, moderately stable	2.5°

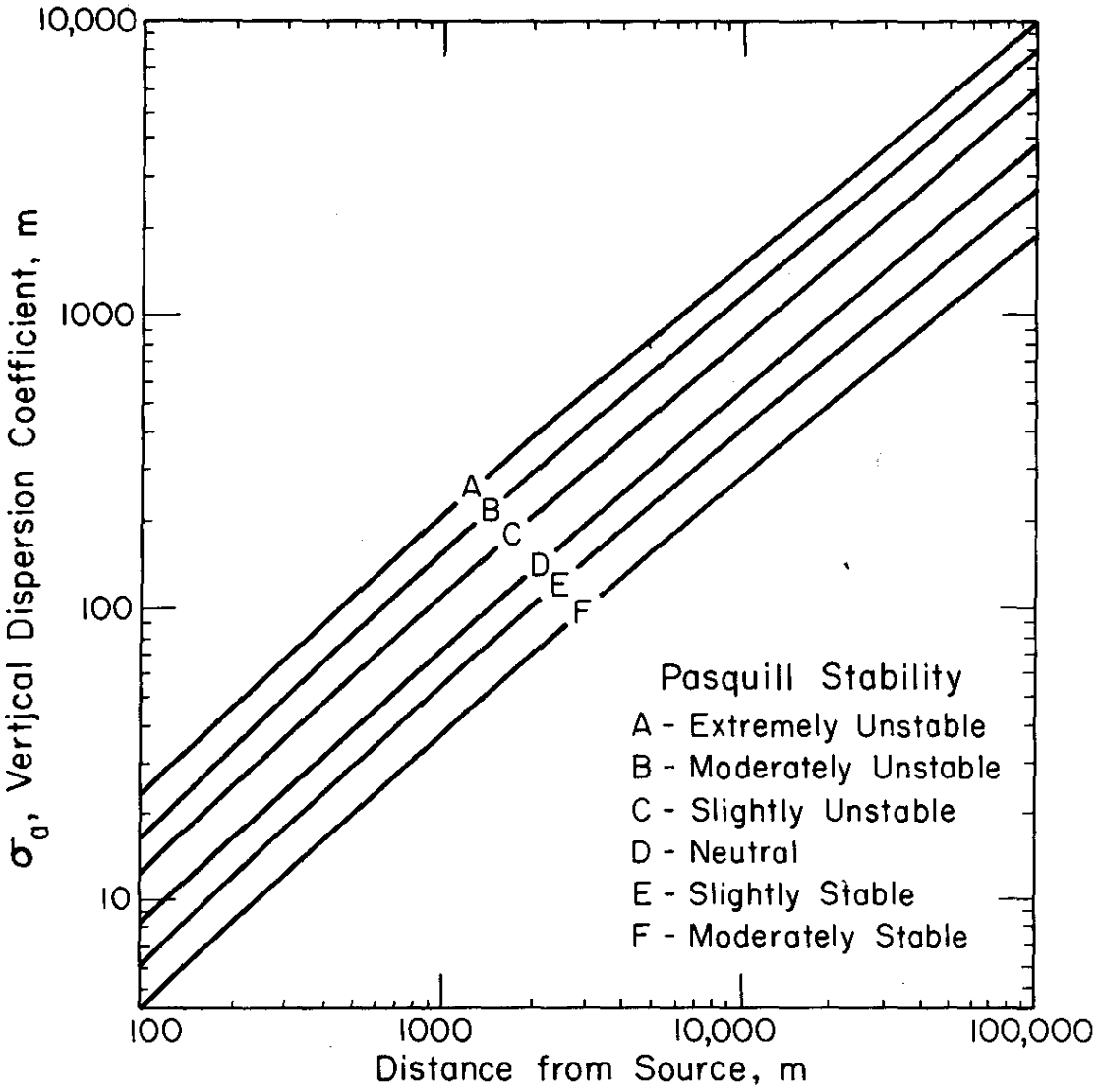

FIGURE 2. Lateral Diffusion (σ_y) vs Downwind Distance from Source

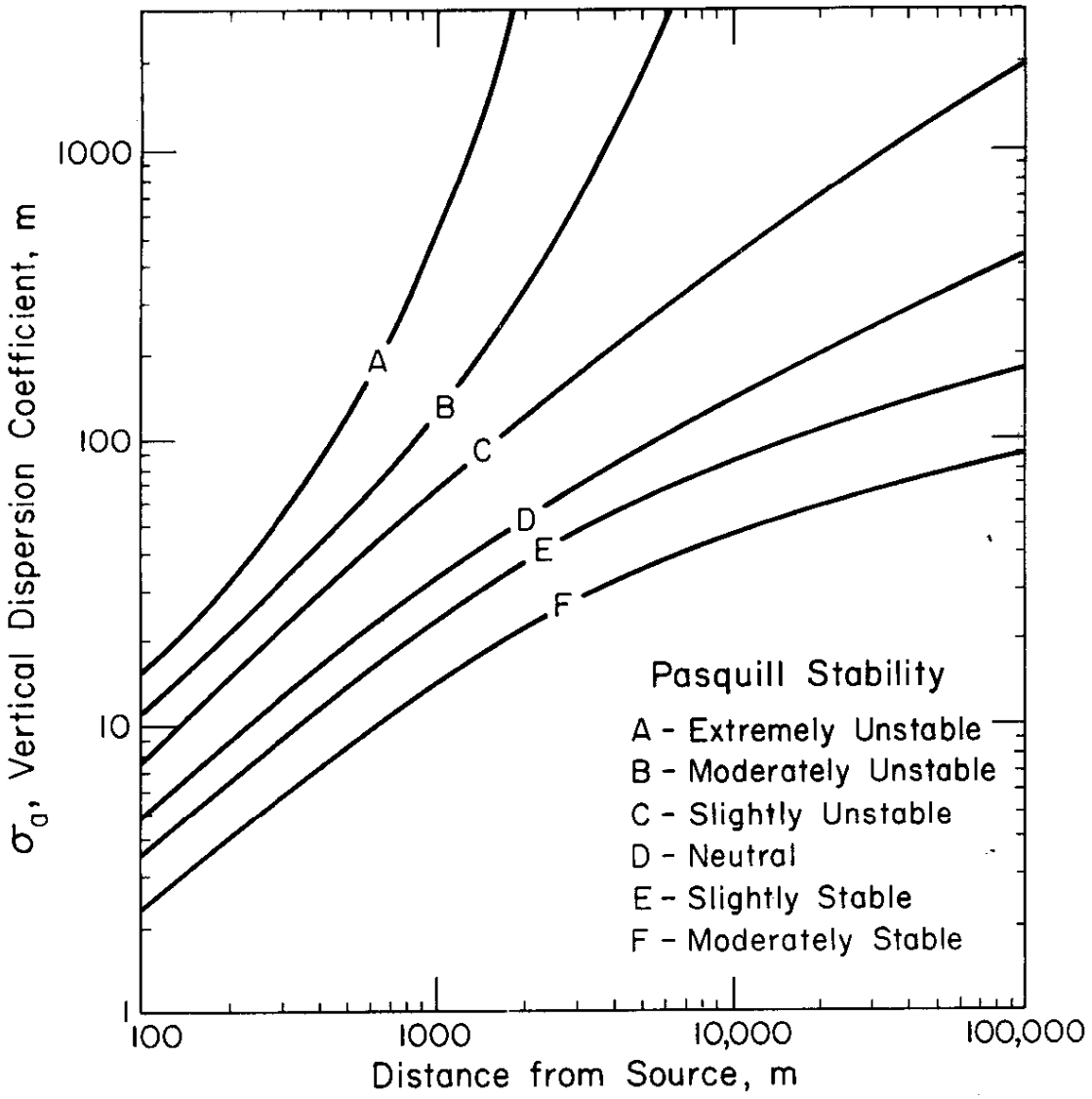

FIGURE 3. Vertical Diffusion (σ_z) vs Downwind Distance from Source

The analytical approximation for the horizontal dispersion function (σ_y) is made by using an empirical power law in the same form as listed above, except substituting σ_y for σ_z. The parameters a and b for various stabilities and for all distances are given in Table 2.

TABLE 2

Parametric Values for σ_y (meters)

Stability Class (σ_a)	a	b
A (25°)	200	0.9006
B (20°)	150	0.9006
C (15°)	105	0.9006
D (10°)	68	0.9006
E (5°)	51	0.9006
F (2.5°)	33.7	0.9006

For σ_a or σ_e, which are different than those that equal the values coinciding with the Pasquill categories A through F, logarithmic interpolation is made producing curves parallel to those listed in Figures 2 and 3 for those different angles. Thus, for any σ_a or σ_e in the range of 25° to 2.5°, a particular value of σ_y or σ_z is obtained analytically for any distance from the source. For stability greater than 25° or less than 2.5°, the Pasquill Category A or Pasquill Category F curves are used.

For straightline plumes or nearly straightline plumes, off-centerline calculations are made. The plume centerline is established within one of the 33 x 33 grids. Than calculations for points not falling on the plume centerline are made according to the Gaussian plume equation, where the y distance is the distance from a grid point to the closest approach of the centerline of the plume, and the x distance is the distance along the plume centerline to the location of the closest approach to the plume centerline.

RESULTS

Figures 4 and 5 show the concentration at one meter above ground level along the centerline of the plume shown in Figure 1. Figure 4 shows the same information calculated by the BNL Method,[5] and Figure 5, the same information as calculated by the Slade Method.[3] The release height is at 61 m, and the source term is

set equal to a hypothetical value of 2.0×10^9 pCi/sec for ^{41}Ar with a half life of 1.83 hours.

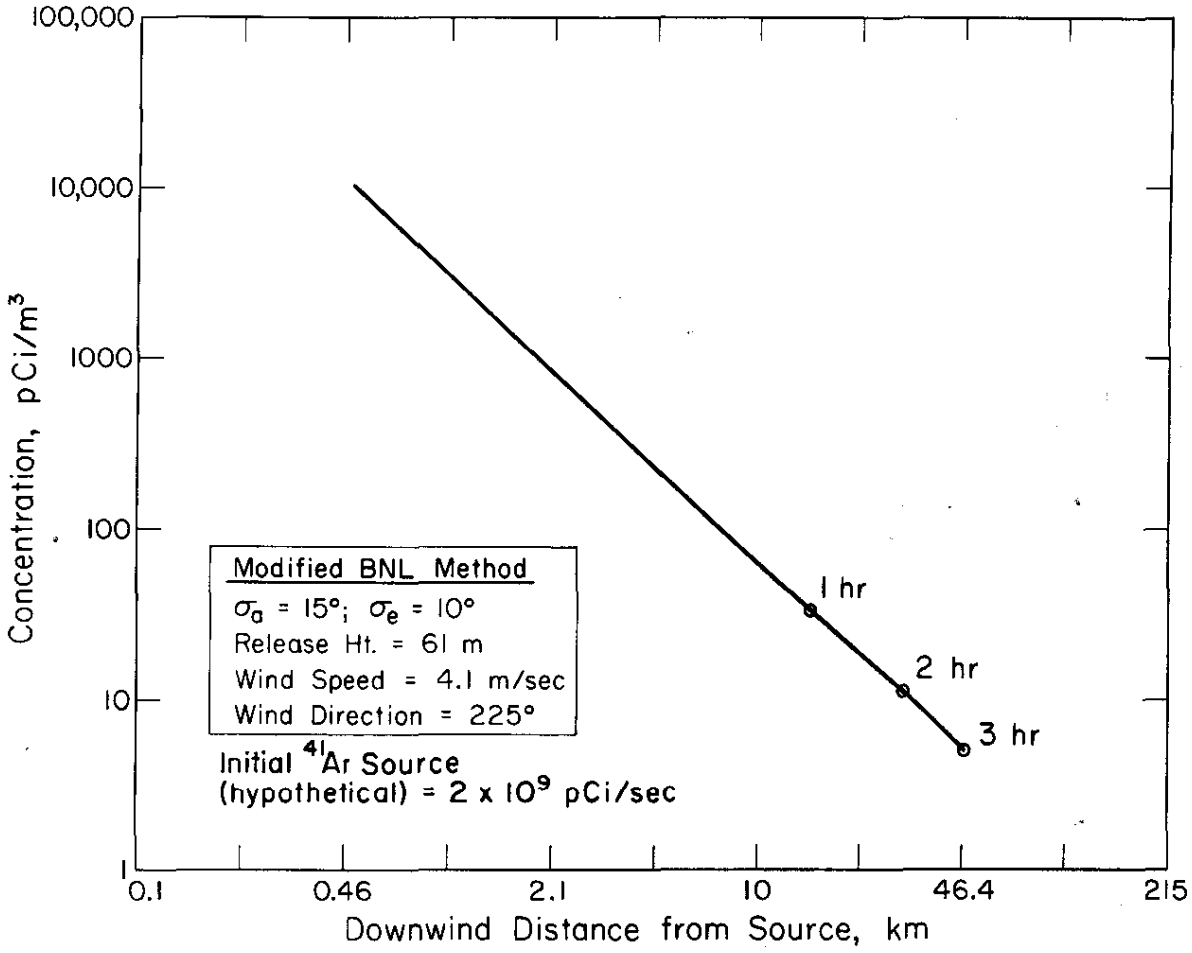

FIGURE 4. Centerline Concentration (1 m above ground) for Trajectory Shown in Figure 1 (modified BNL method)

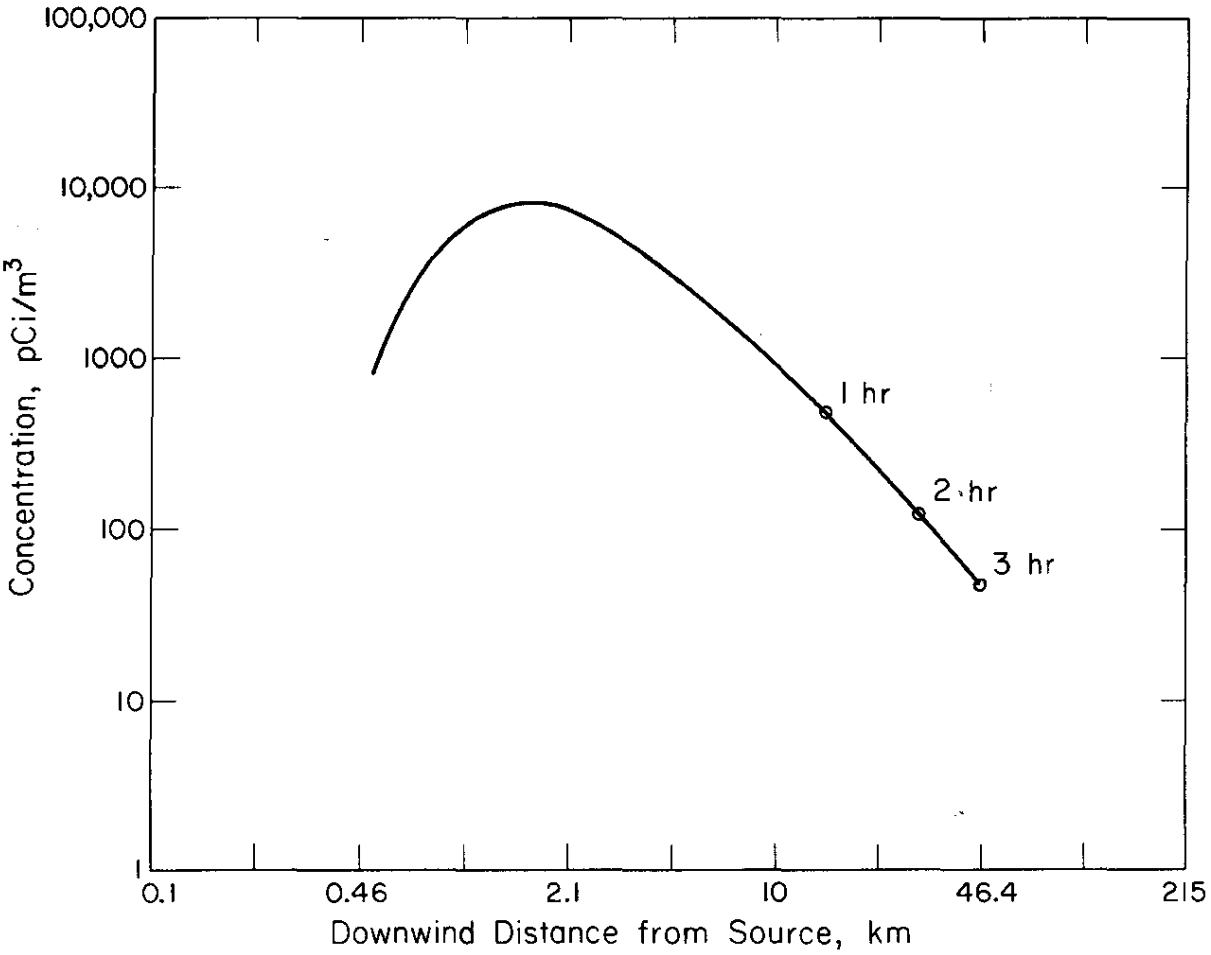

FIGURE 5. Centerline Concentration (1 m above ground) for Trajectory Shown in Figure 1 (Slade method)

CONCLUSIONS

Two-dimensional trajectories from either analyzed or forecast wind fields have been adequately generated. Concentration values along these trajectories were made from the two methods described; i.e., the BNL method[5] or the Slade method.[3] Contours from these trajectories were also made over gridded analysis networks. One method is expected to be shown to be better for our use than the other. Future models can be expected to be able to generate three-dimensional trajectories, and also will generate air-borne pollutant concentrations determined by solving a) the diffusion equation for areas distant from point sources and b), the plume equation for areas near the point sources of pollution. Both methods are being tested by analyzing routine releases from SRP.

The modified BNL method gives much lower centerline values for concentrations and wider down-wind plumes than the Slade method, which yields correspondingly much higher centerline values but has much narrower plumes.

REFERENCES

1. C. D. Kern. "A Computer Program for Objective Analysis and Display of Meteorological Fields." Paper No. 8 of this report.

2. C. D. Kern. "Preliminary Mesoscale Calculations for the Southeastern United States Using the Two and One-Half Dimensional Lavoie Model." Paper No. 9 of this report.

3. D. H. Slade. *Meteorology and Atomic Energy*. USAEC Division of Technical Information Report TID-24190, p. 407, Oak Ridge, Tenn. (1968).

4. R. E. Cooper and B. C. Rusche. *The SRL Meteorological Program and Off-Site Dose Calculations*. USAEC Report DP-1163, E. I. du Pont de Nemours and Company, Savannah River Laboratory, Aiken, S. C. (1968).

5. I. A. Singer, J. A. Frizzola, and M. E. Smith. "A Simplified Method of Estimating Atmospheric Diffusion Parameters." *J. Air Pollution Control Assoc. 16*, 594 (1966).

11. REAL TIME PREDICTION AND VERIFICATION OF ARGON-41 CONCENTRATIONS - A JOINT EFFORT WITH THE LAWRENCE LIVERMORE LABORATORY †

INTRODUCTION

To test some of the concepts of the Atmospheric Release Advisory Capability (ARAC), developed by the Lawrence Livermore Laboratory (LLL), feasibility tests were run at the Savannah River Plant (SRP) with joint participation by members of the Savannah River Laboratory (SRL) and LLL. The purpose of these tests was to demonstrate the feasibility of the ARAC concept to predict location, time, and concentration of releases to the atmosphere. Computer models, utilizing data gathered from meteorological sensors located on towers on and near the SRP plus data from National Weather Service Stations near the SRP, were developed both at LLL and SRL. These models provided forecasts of the location and concentration of ^{41}Ar from routine releases at three nuclear reactors at the SRP. Knowing the source strength, the source geometry, and the meteorological conditions in and about the plant, forecasting downwind concentrations is theoretically possible. Testing these models is required to determine their validity in predicting downwind concentrations. To provide data to validate these models, SRL cars (equipped with ^{41}Ar gamma detectors) and a USAF UH-1N helicopter (equipped with EG&G designed and operated gamma detectors) were given routes to follow and assigned locations to take measurements. The model forecasts are in the process of being validated against these observations.

METEOROLOGICAL DATA ACQUISITION AND UTILIZATION

Argon Tracking Tests

Tests were run during five days of May and June of 1974. The initial two tests on May 21 and 29 were preliminary ("shakedown") tests of the system using car observations but not helicopter support. These tests demonstrated the feasibility of linking the various systems at LLL and SRL and the test procedures. Actual full-scale tests were made on June 11, 18, and 20. On these three days, all elements of the ARAC group participated. Ground observations of ^{41}Ar were made by the two SRL cars and airborne observations were made from the helicopter. The general test plan was for SRL to alert participants the previous afternoon when the meteorological conditions were expected to be satisfactory.

---

† Work done by C. D. Kern.

During the period where the helicopter was available for such use, ideal plume tracking weather conditions were not available. The three days on which observations were taken were barely satisfactory for such purposes. The tests were conducted according to a fairly fixed test schedule. Figure 1 shows the actual test schedule used for the June 20 mission. The helicopter data on June 18 were not usable due to equipment malfunction; however, the data collected on June 11 and 20 demonstrated the feasibility of the argon tracking test.

Data from Stationary Towers and Upper Air Sensing Devices

The facilities for atmospheric sciences research were reported previously.[1] For the second part of the ARAC tests, data from the TV tower and from the seven 62-meter towers around the plant were fed into the Weather Center-Analysis Laboratory. These data were placed on a magnetic tape compatible with the SRL IBM S/360-195 computer. A Dataphone was linked to the magnetic tape reading system to allow the data acquisition and processing center at LLL to acquire these tower data in real time. The National Weather Service (NWS) data are available for first order weather stations in the southeastern United States on a teletype machine within the Weather Center-Analysis Laboratory. Hourly data were transmitted to LLL by means of a telephone facsimile machine. Upper air observations available on a separate teletype circuit were also transmitted to LLL by means of the telephone facsimile circuit. All of these data were used to develop the initial concentration-forecast models at LLL and SRL.

Day	Time, CUT[a]	Activity
June 19	1930	SRL alert for next day. Telephone list alerted.
June 20	1030	SFC data sent to LLL.
	1100	OOCUT SE US UA data to LLL.
	1115	SFC data sent to LLL.
	1200	Initial briefing with EG&G at Bush Field.
	1210	LLL/SRL discussion of general wind flow.
	1215	SE sfc data fax to LLL.
	1220	SRL run forecast trajectories.
	1250	First output from ADPIC fax to SRL, valid 1300 Z, all levels, 60M, also valid 1400 Z.
	1315	SE sfc data fax to LLL.
	1315	EG&G briefed at Bush Field.
	1330	SRL cars briefed and dispatched.
	1345	Day briefing map fax to LLL.
	1350	ADPIC fax to SRL, valid 1400 Z, and 1500 Z (60M).
	1400	DATA-COM tape to 703-A.
	1400 to 1700	SRL run programs.
	1400	Test officially starts.
	1400	Helicopter leave Bush Field to be over plume spiral Area and Metro. Data at this (1400 Z) time, then conduct plume recce.
	1415	SE United States sfc data fax to LLL.
	1445	SE United States UA collectives fax to LLL.
	1450	ADPIC fax to SRL, valid 1500 Z and 1600 Z (60M).
	1500	Helicopter RTB for refuel.
	1515	SE United States sfc data fax to LLL.
	1550	ADPIC fax to SRL, valid 1600 Z and 1700 Z (60M).
	1600	Helicopter back on plant site for plume recce.
	1615	SE United States sfc data fax to LLL.
	1650	ADPIC fax to SRL, valid 1700 Z and 1800 Z (60M).
	1715	SE United States sfc data fax to LLL.
	1800	Test over.
	1730	Helicopter RTB when fuel dictates.
	1800	SRL cars return to 735-A.

a. Note Eastern Daylight Time is CUT minus 4 hours, CUT is Coordinated Universal Time (formerly Greenwich Mean Time).

Figure 1. Schedule for ARAC Feasibility Test - June 20, 1974

MODELS

LLL Models

At LLL, data obtained from the Dataphone connection and by telephone facsimile machine were fitted to horizontal grid points spaced approximately 1 km apart over a 40-km square grid and spaced vertically every 25 m to the top of the 367-m WJBF-TV tower. From this analysis, a more complex analysis program was developed, called MATTHEW, a mass-consistent wind field analysis scheme.[2] This field was then used as input to a code called ADPIC (Atmospheric Diffusion by Particle in Cell).[3] The concentrations from the meteorological parameters supplied by the analysis scheme were calculated by ADPIC; persistence of the wind fields was assumed, and concentrations at the grid points of the models were determined by keeping track of the transport and diffusion of individual "markers". Isopleth analysis of ADPIC grid point data provided forecast concentrations over the area of interest at specified heights above the ground. Maps of these isopleth analyses were transmitted (via the telephone facsimile circuit) to SRL, and were then used to position the helicopter and cars. Figures 2 through 6 show concentrations at 2 m above the ground from ADPIC for the June 20 case. The calculations were started at 1200 CUT (Coordinated Universal Time) so the plumes were not fully developed initially (Figures 2 and 3).

SRL Models

The concentration calculational techniques described in the previous paper[4] supported the ARAC tests. Also, mesoscale forecasts were made using the Lavoie model.[5] Planetary boundary layer model output was obtained from the NWS. Output from this model will be used to generate meteorological fields in order to forecast concentrations in the future. These fields will be evaluated for the tests run on June 18 and 20. Figures 7 and 8 show concentration forecasts as derived from trajectories from the three reactors using the same wind data (persistent wind field) as for Figure 4. Concentrations were calculated by adding the concentrations of all three plumes and using the Brookhaven National Laboratory (BNL) or Slade methods.[4] Figure 9 shows comparable data from ADPIC.

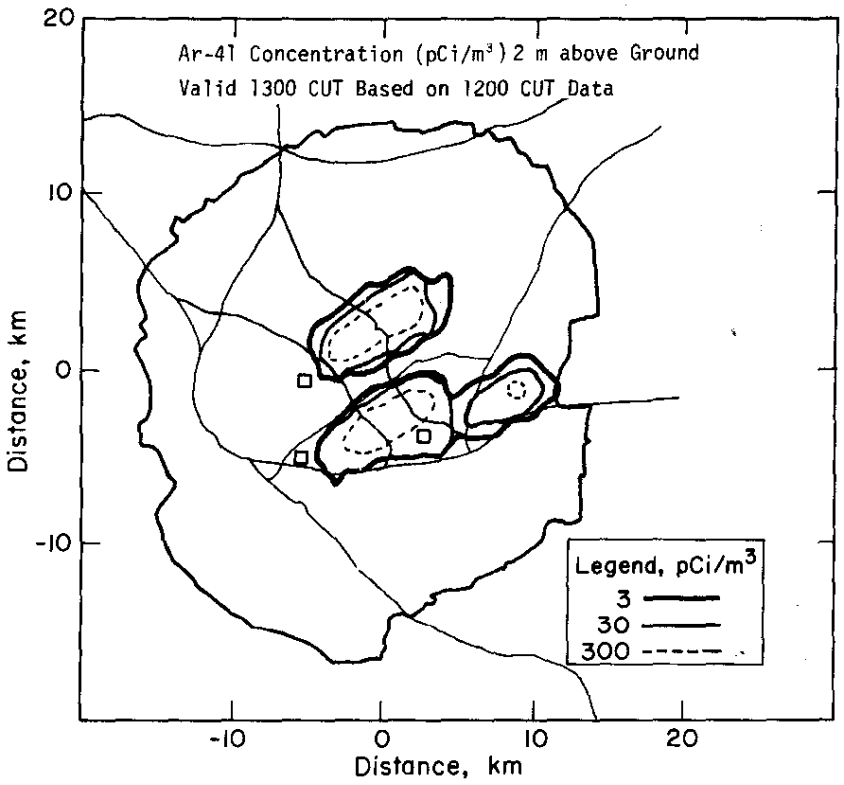

FIGURE 2. ADPIC Argon-41 Concentration Forecasts - June 20, 1974

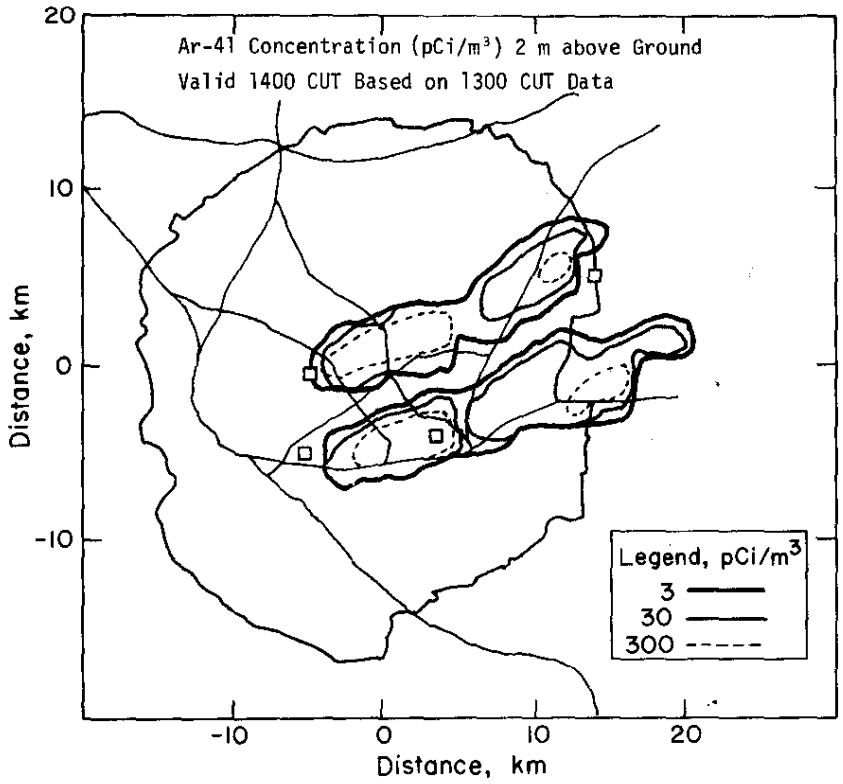

FIGURE 3. ADPIC Argon-41 Concentration Forecasts - June 20, 1974

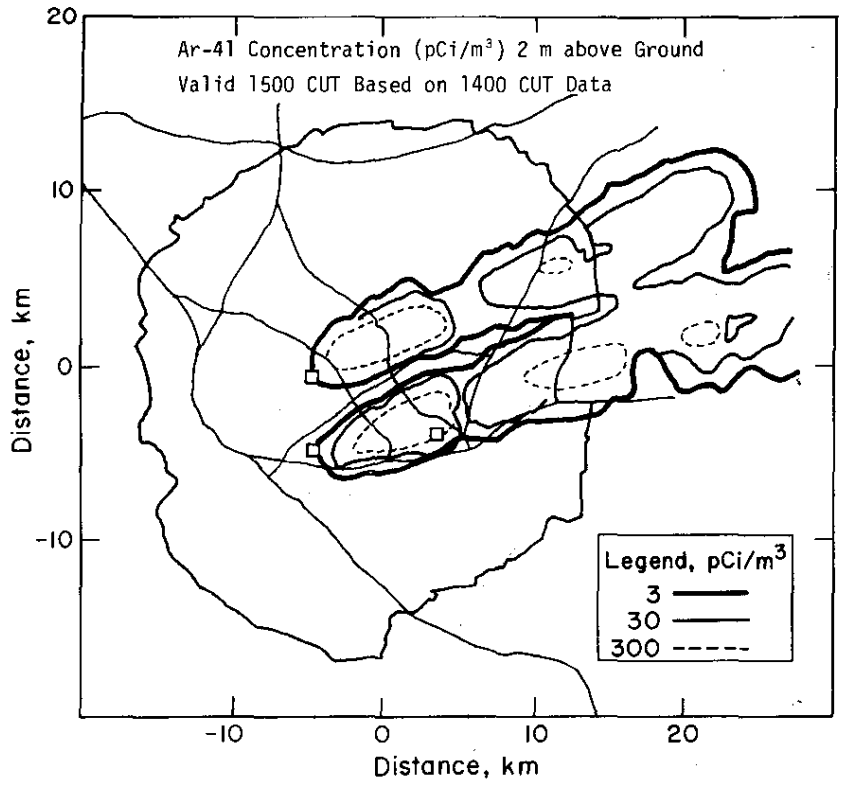

FIGURE 4. ADPIC Argon-41 Concentration Forecasts - June 20, 1974

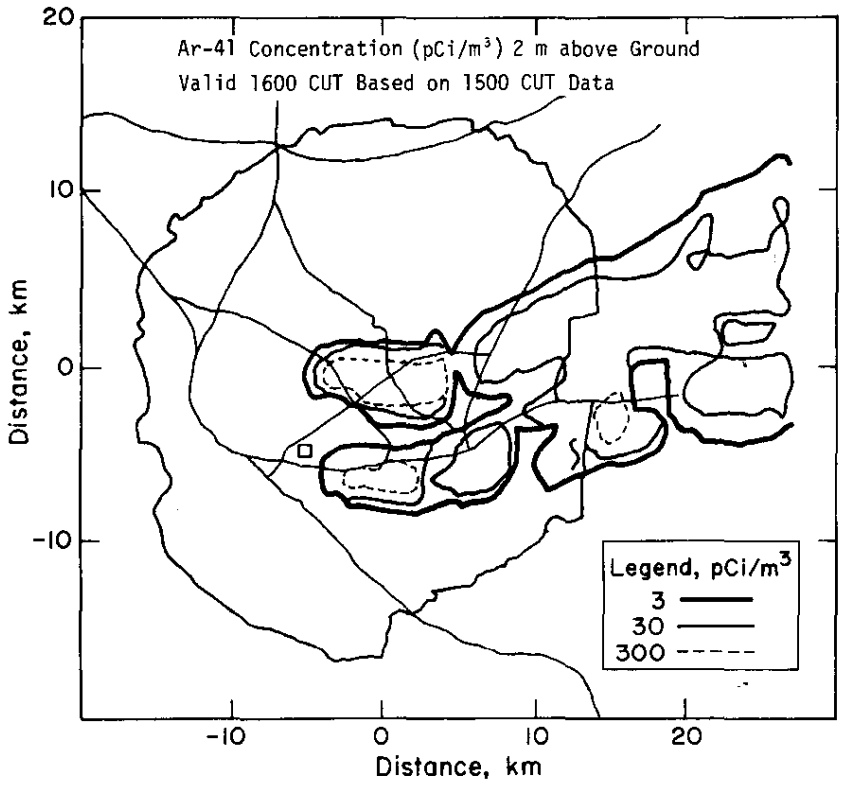

FIGURE 5. ADPIC Argon-41 Concentration Forecasts - June 20, 1974

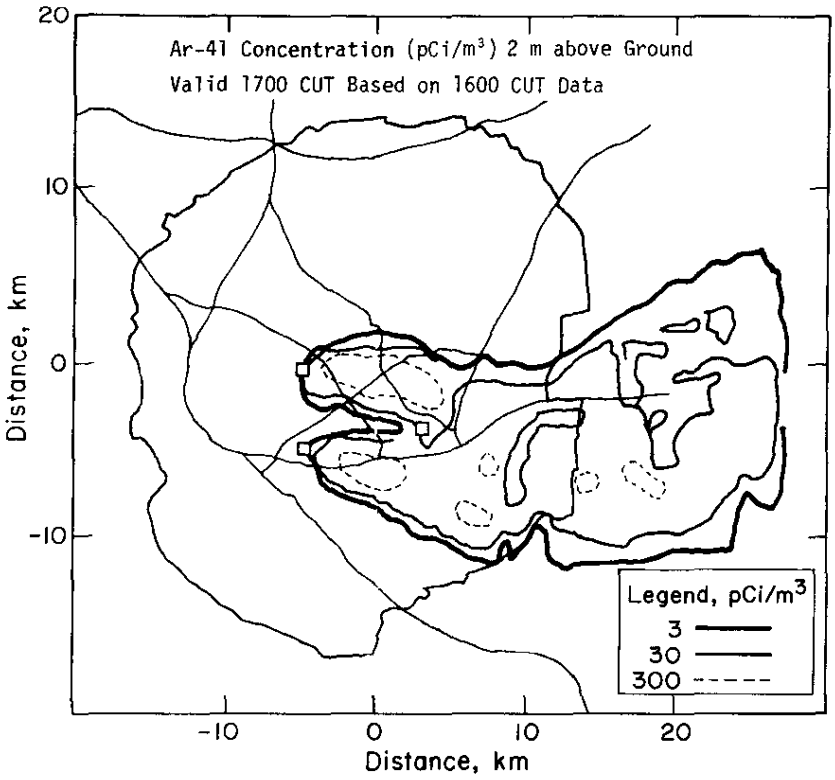

FIGURE 6. ADPIC Argon-41 Concentration Forecasts - June 20, 1974

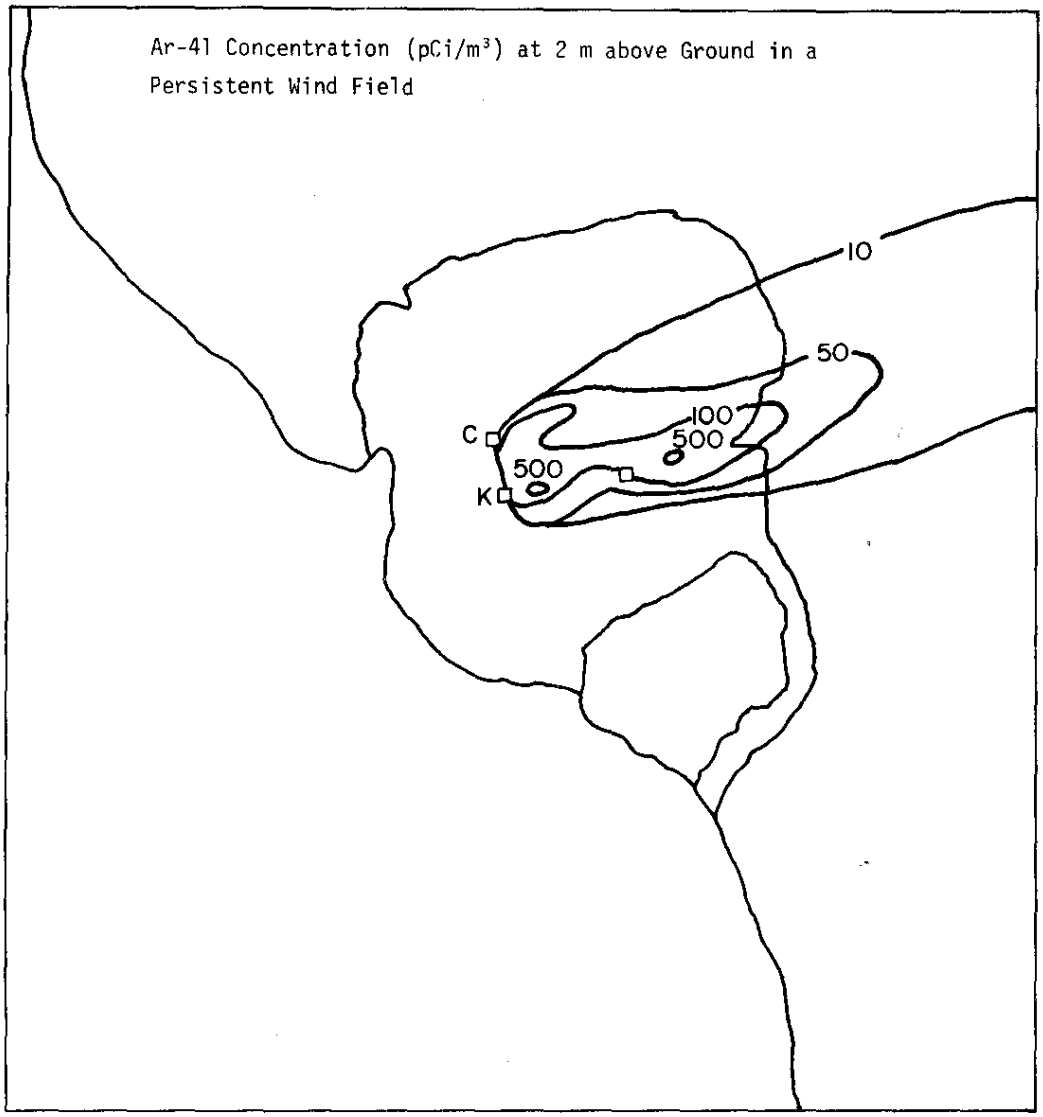

FIGURE 7. BNL Argon-41 Concentration over SRP at 1400 CUT - June 20, 1974

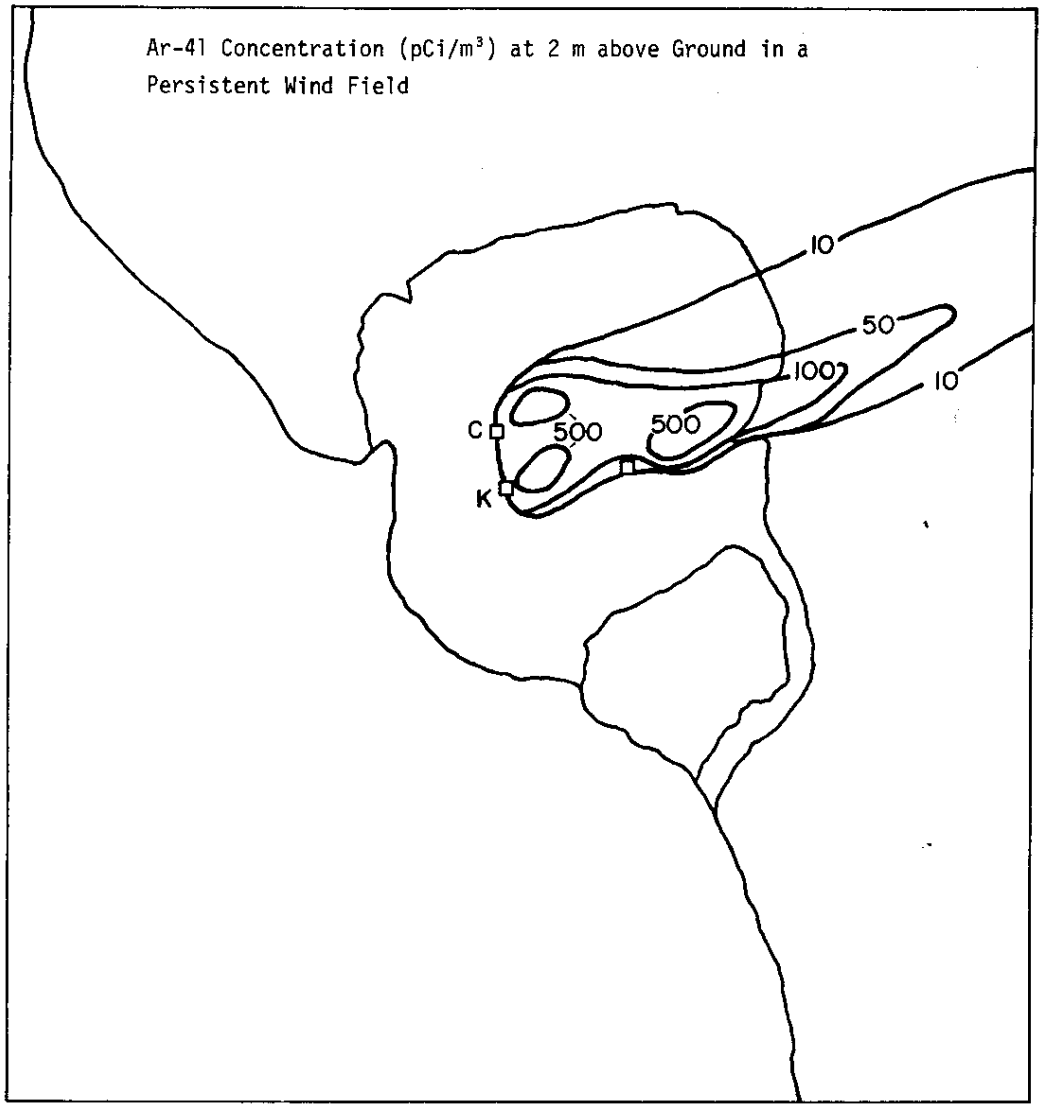

FIGURE 8. SLADE Argon-41 Concentration over SRP at 1400 CUT - June 20, 1974

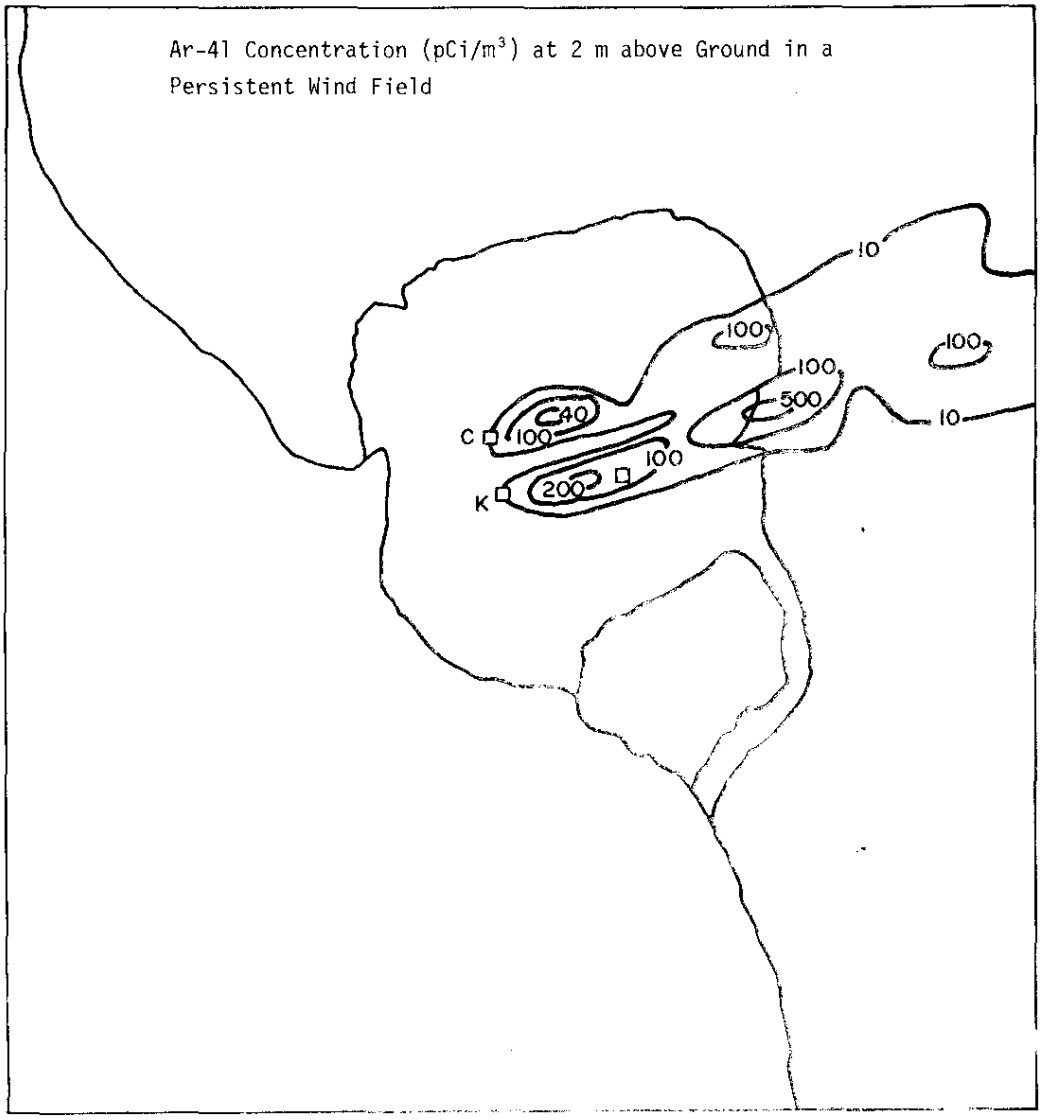

FIGURE 9. ADPIC Argon-41 Concentrations over SRP at 1400 CUT - June 20, 1974

MEASUREMENTS

SRL Instrumented Cars

Two portable battery-powered sodium-iodide (NaI) detector systems were mounted in radio-equipped SRL cars. The cars provided mobile platforms for monitoring ^{41}Ar plumes from the SRP reactors. Each of the two systems consisted of a shock-mounted 4 in. x 4 in. NaI detector with associated electronics. Knowing the efficiency and the detector surface area, and neglecting differences in angular response from incident gamma rays, the detector count rate can be converted into gamma flux rate and then related to predicted flux from a given geometry (usually a semi-infinite cloud). The cars were dispatched by radio to appropriate monitoring locations based on the ARAC predictions of plume movement. After calibrating the system with a ^{22}Na source, a 10-minute count was taken at a given location, then a second calibration check was made to ensure no drift had occurred during the count. At a later time, when no ^{41}Ar was expected to be in the area, background measurements were made at each of the locations where these measurements were taken. The difference between these two measurements then constituted the argon activity at the location during the test. The minimum ^{41}Ar detection limit for the systems based on typical field backgrounds and 10-minute counting periods was approximately 30 pCi/m^3 assuming a semi-infinite cloud geometry. Figure 10 gives the locations, time, and concentrations as derived from the data from the SRL cars on the June 20th tests.

EG&G Sensors

During three weeks in June, EG&G sensors were mounted on a USAF UH-1N helicopter flown to and operated from Bush Field, Augusta, Georgia. The aircraft belonged to the First Helicopter Squadron based at Andrews Air Force Base in Maryland. The aircraft was at SRP to perform a ground survey of the entire plant. The feasibility tests were run during this period to take advantage of this airborne measurement platform. The EG&G detection equipment was mounted in rocket pods on the helicopter together with onboard recording and readout information systems. The EG&G system was designed to detect low-activity natural and man-made gamma radiation. The gamma ray detectors were enclosed in two rocket pods containing an array of 20 5 in. x 2 in. NaI crystals. The detectors were operated in parallel allowing any or all signals to be summed into one output, thus providing the large amount of detector surface needed for taking spectra of low level activity in short periods of time. In flight, the energy spectrum from the detectors was accumulated in a 30-channel pulse height analyzer and automatically placed onto magnetic tape every

three seconds. Precise information on speed, altitude, and location from onboard navigational equipment were also placed onto magnetic tape at each of these times. Five single-channel analyzers allowed real time monitoring of selected regions of interest. Afterwards, the spectra on magnetic tape were analyzed by various computer codes to smooth the data, locate and integrate peaks, strip background, and print or plot the data in any number of desired formats. The EG&G system had an ^{41}Ar detection limit of approximately 10 pCi/m^3. Figures 11 and 12 show a flight path of one of the missions flown and the ^{41}Ar measurements made during this particular mission.

DISCUSSION

The validation of the models vs. actual observations is not yet completed. There will be essentially three types of validation.

A. Validation of predicted concentration from the meteorological data available at the start of each test will be made, such that SRL output may be compared with actual data. LLL models will also be compared with data, such that the actual real time outputs made available during the test can be compared with observations. Additional programs will be run with different averaging times of the tower meteorological data, a smaller grid during the second test, and with different diffusion parameters in the last test.

B. Data from forecast models of the Lavoie type and of data obtained from NWS Planetary Boundary Layer forecast model output will also be validated.

C. There will be a diagnostic validation of predicted concentrations using all possible after-the-fact data, both by SRL and by LLL.

CONCLUSIONS

For the few cases examined so far, tentative general conclusions can be drawn. For the general pattern of surface concentration, the simple models do well. The more complex ones (e.g., ADPIC) do, perhaps, a little better. All of the models used here did reasonably well in predicting the general pattern and concentration observed by the cars and the helicopter. In changing light wind patterns (as is normal during most of the time over the SRP), concentrations forecasts based on persistent wind fields are not good after a period of several hours. The

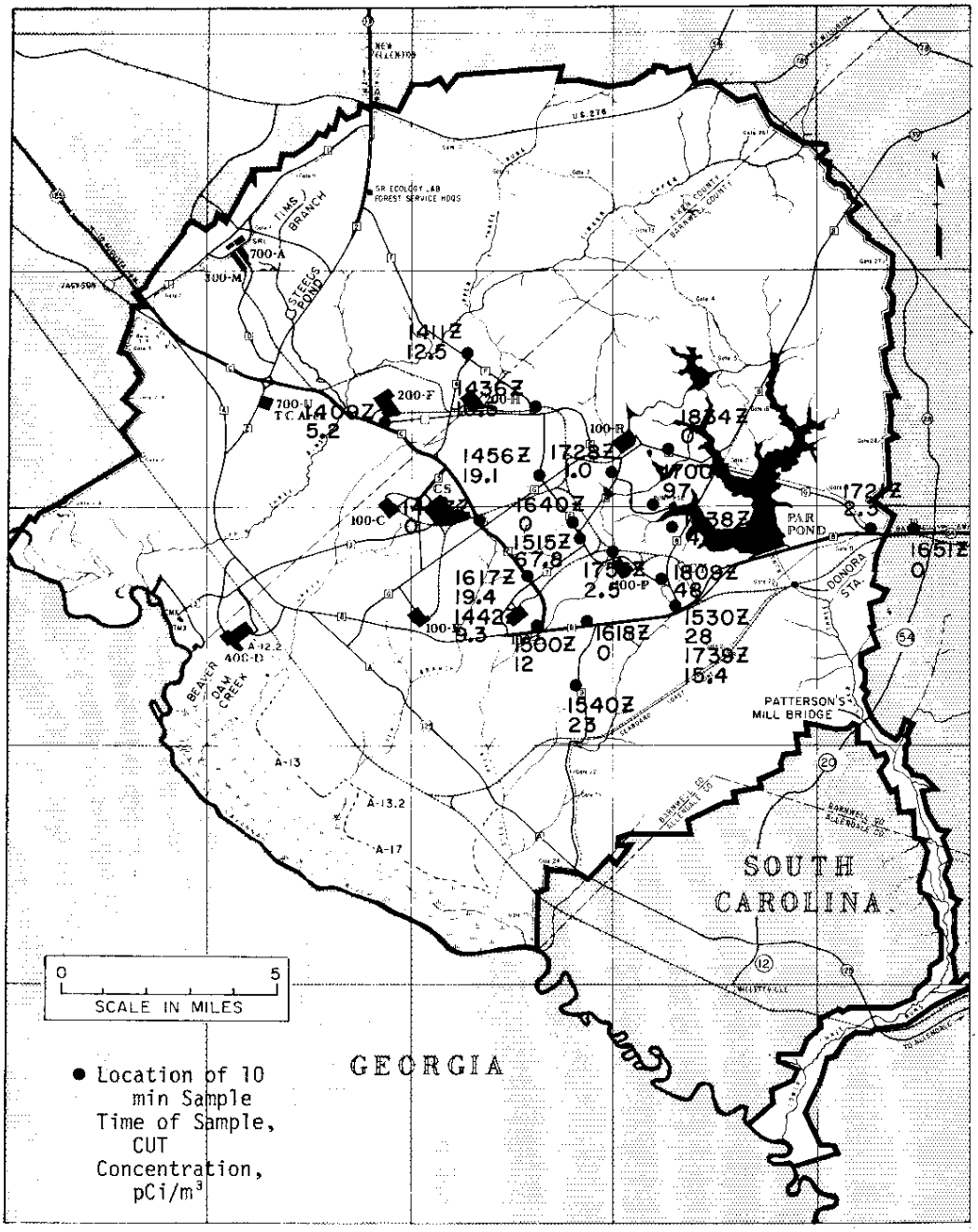

FIGURE 10. Argon 41 Concentrations as Measured from Parked Car Positions - June 20, 1974

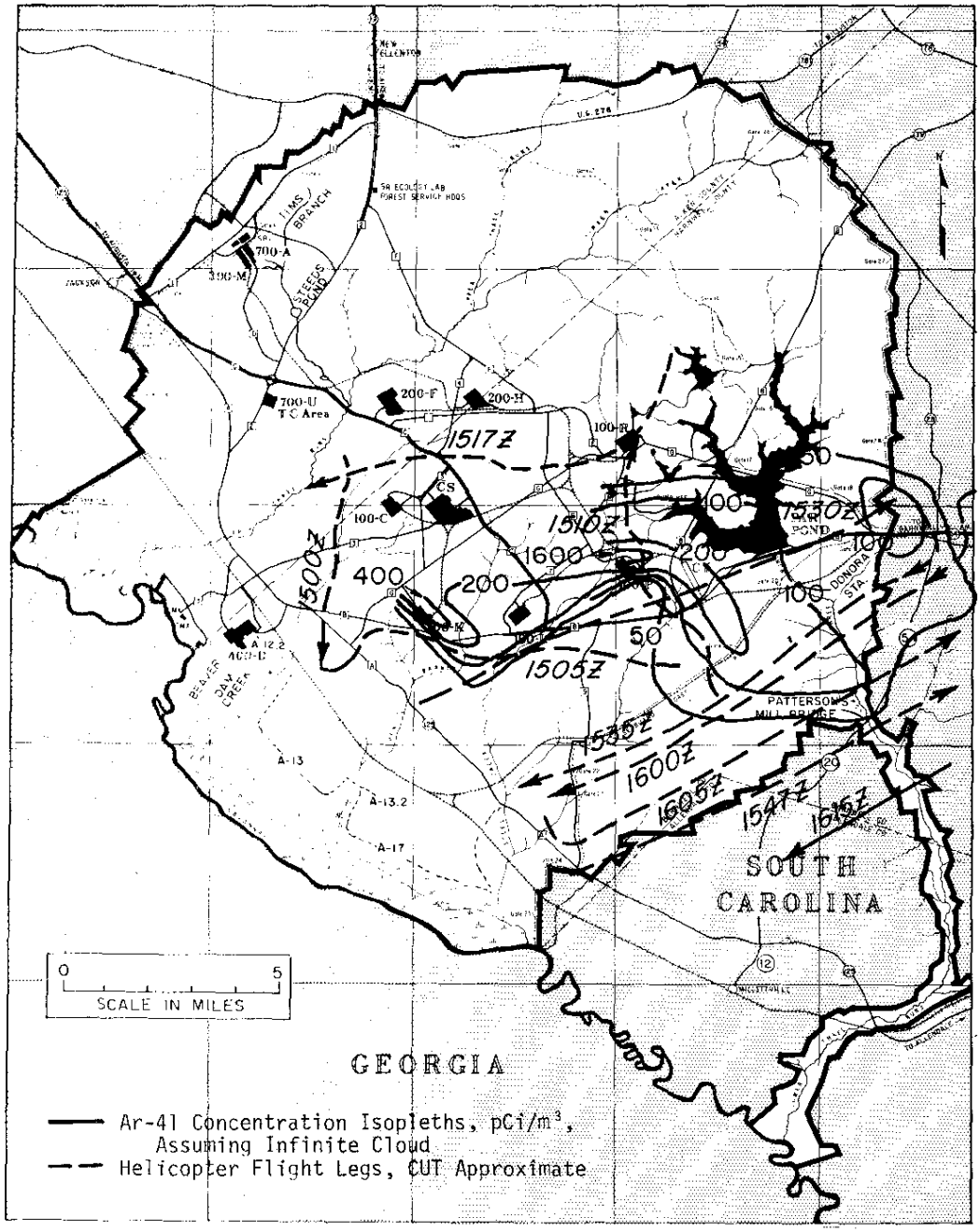

FIGURE 11. First Helicopter Mission of ARAC Test on June 20, 1974

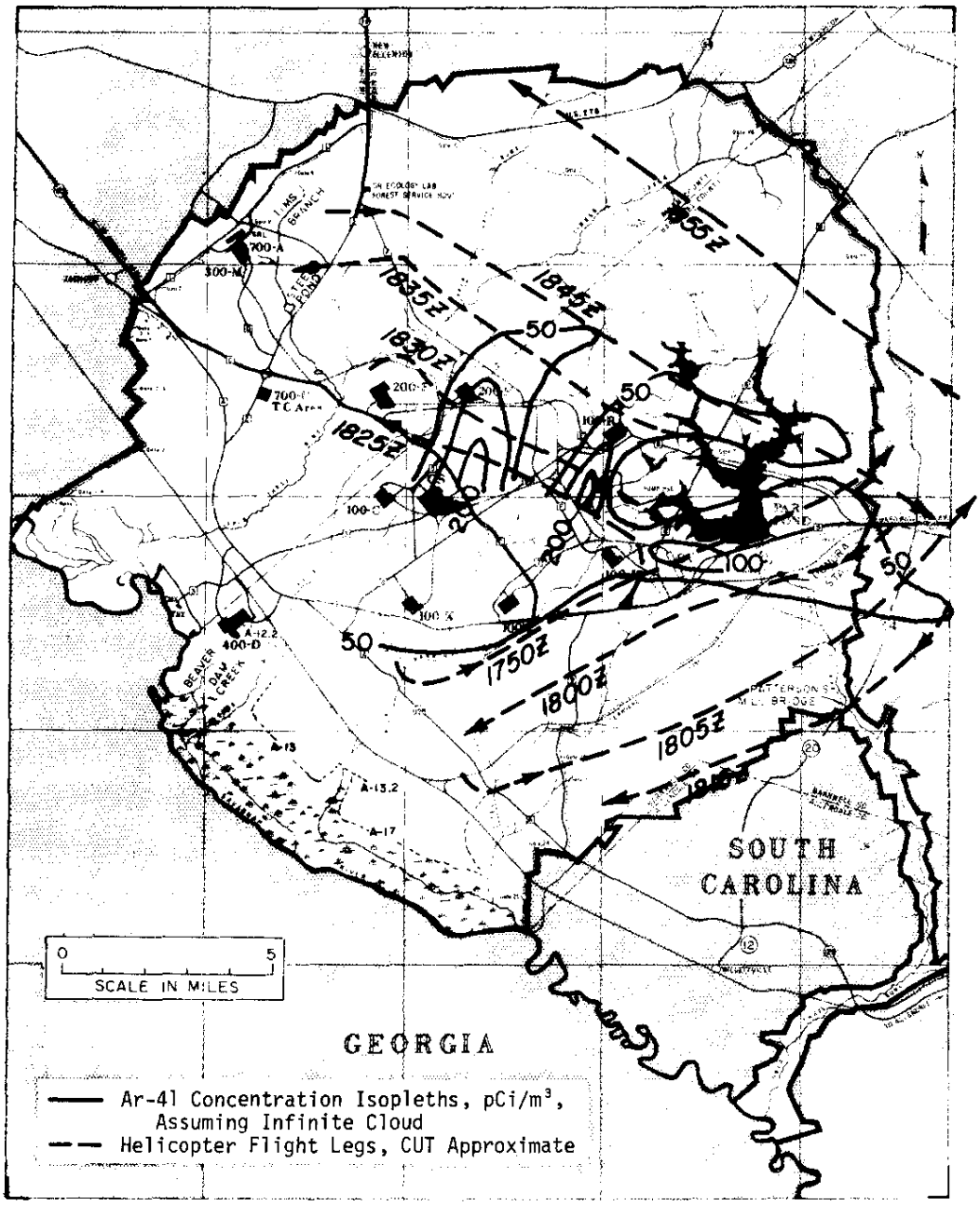

FIGURE 12. Second Helicopter Mission of June 20, 1974

worth of the meteorological forecast models studied during the feasibility tests can not now be given; however a good planetary boundary layer forecast model is probably needed in order to better support emergency release prediction. For quick-running and close-in distances (less than 40 km from source) the Gaussian plume model, either straight-line-to-infinity or puff calculations on curved trajectories provide useful estimates of downwind concentrations.

The joint tests between SRL and LLL have demonstrated that the ARAC concept is feasible. The models have not been totally validated, so the question cannot now be answered as to how good the models are. Support to emergency operations by such a system is a possibility and would work. The post-release analysis data are not yet available, but it can be tentatively concluded that ARAC can help in post-release analysis.

REFERENCES

1. T. V. Crawford. "Facilities for Atmospheric Sciences Research." *Progress Report, Dose-To-Man Program, FY-1973.* USAEC Report DP-1341, Savannah River Laboratory, E. I. du Pont de Nemours and Company, Aiken, S. C. (1973) pp. 13-20.
2. M. H. Dickerson. *A Mass-Consistent Wind Field Model for the San Francisco Bay Area.* USAEC Report UCRL-74265, Lawrence Livermore Laboratory, University of California, Livermore, Calif. (1973).
3. R. Lange. *ADPIC - A Three Dimensional Computer Code for the Study of Pollution Dispersal and Deposition under Complex Conditions.* USAEC Report UCRL-51462, Lawrence Livermore Laboratory, University of California, Livermore, Calif. (1973).
4. C. D. Kern. "A Trajectory and Dispersion Computer Program which Uses Objectively Analyzed Observed or Forecast Meteorological Fields." Paper No. 10 of this report.
5. C. D. Kern. "Preliminary Mesoscale Calculations for the Southeastern United States Using the Two and One-half Dimensional Lavoie Model." Paper No. 9 of this report.

II. SURFACE AND GROUND WATER TRANSPORT AND DISPERSION

The overall goal of the water transport and dispersion studies is to define travel time and downstream concentrations of various pollutants following a release to the soil surface or a flowing stream. To achieve this goal, active modeling programs are underway in both the stream-river region and the ground water region. A versatile water sampler was designed, constructed, and utilized to obtain experimental information for use in developing the stream models. The following articles summarize the progress in these areas.

12. COMPUTER MODELING OF STREAM AND RIVER SYSTEMS †

INTRODUCTION

Computer models of stream and river systems are being developed to predict the possible consequences of releases to SRP streams and to the Savannah River. The models predict travel times, maximum concentrations, and duration of concentration above a designated value (e.g., drinking water standard) at selected downstream locations. The general models will be capable of handling both conservative (tritium, chloride, etc.) and nonconservative (cesium, iodide, acid, etc.) constituents, if appropriate input coefficients are available. The models for conservative materials include bulk dispersion and dead-zone options. The models for nonconservative materials will also include sorption, ion exchange, and particle deposition options. This paper summarizes the equations used and the computer models developed, and an actual example of the river transport model calculations.

MODEL EQUATIONS

Transport of pollutants or tracers in streams and rivers is usually considered to follow the one dimensional dispersion model represented by Equation 1.

$$\frac{\partial C(x,t)}{\partial t} = \frac{\partial}{\partial x} D(x) \frac{\partial}{\partial x} C(x,t) - \frac{\partial}{\partial x} U(x)\, C(x,t) + \sum_{j=1}^{J} S_j \qquad (1)$$

(a) (b) (c) (d)

Boundary conditions: (1) $C(o,t) = r(t)$

(2) $C(x_\infty,t) = C_\infty$

or $\left.\frac{\partial C(x,t)}{\partial x}\right|_{x=x_\infty} = 0$

Initial conditions: $C(x,o) = 0$

†Work done by D. W. Hayes and M. R. Buckner. A paper, *Pollutant Transport in Natural Streams*, by M. R. Buckner and D. W. Hayes was accepted for presentation at the American Nuclear Society M & C Topical Meeting on Computational Methods in Nuclear Engineering in Charleston, South Carolina, on April 15-17, 1975.

where: $C(x,t)$ = radionuclide concentration at point x and time t.

$D(x)$ = dispersion coefficient at a point x.

$U(x)$ = longitudinal transport velocity at a point x.

S_j = uptake or release of particles by either a dead zone (j=1) or one of the interactive processes (j>1).

$r(t)$ = an analytic function describing pollutant concentration at the point of release.

x_∞ = point far downstream.

C_∞ = specified concentration.

J = number of source-sink effects.

The terms in Equation 1 represent, respectively:

(a) the temporal change in concentration,

(b) dispersion,

(c) longitudinal convective mass transfer, and

(d) source and sink effects within the stream.

The fourth term (d) has the general form:

$$S_j = T_{sj} [W_j(x,t) - C(x,t)] \qquad (2)$$

where $W_j(x,t)$ = concentration in the dead zone or interactive phase.

T_{sj} = transfer coefficient between stream and dead zone, or stream and interactive phase, or between stream and deposition area.

If the pollutant is transferred back into the stream from the interactive zone, then a coupled equation (Equation 3) is required to describe the zone's effect.

$$\frac{\partial W_j(x,t)}{\partial t} = T_{pj}[C(x,t) - W_j(x,t)] \qquad (3)$$

where T_{pj} = transfer coefficient between dead zone or interactive phase and stream.

A module for the SRL JOSHUA computer system called LODIPS (Longitudinal Dispersion of a Pollutant in a Natural Stream) has been written to solve these equations for selected pollutant release situations. The differential equations are represented by space-time difference equations, which are solved at each time step by the forward elimination-backward substitution method. Transport coefficients for the dispersion model are determined by an analysis code called TETRAD. This code uses the analytical solution to the dispersion equation (terms a, b, and c of Equation 1) to route a release from one measurement station to another. Nonlinear least-squares fitting predicts the dispersion coefficients and mean travel times that give the best agreement between the model and measured response at each station. Module LODIPS presently predicts dilution rates for streams and the Savannah River by using transport coefficients derived from experiments and the use of TETRAD. It is planned, however, to implement a parameter identification algorithm in the LODIPS module similar to that used in TETRAD to estimate transport coefficients and interactive zone coefficients for the full river model (Equations 1 and 2).

IMPLEMENTATION OF A CALCULATION

First estimates of dispersion coefficients and mean velocities are now in the JOSHUA data bank for all plant streams and the Savannah River. Appropriate distances from probable release points to plant boundary and from stream-river intersections to Highway 301, Beaufort-Jasper water supply, and Port Wentworth water supply are also in the data bank. Other downstream distances can be quickly entered via a JOSHUA terminal. LODIPS is capable of handling any release situation either using a specified analytic function or a tabulated time-concentration profile to represent the release. All that is necessary to predict downstream concentrations from a release is to select the stream casename, estimate initial time-concentration profile, add downstream location distances of interest if other than the ones shown above, and execute. Output is currently in tabular form.

EXAMPLE

A convenient example illustrating the use of LODIPS and TETRAD is a study of a tritium release from the SRP Heavy Water Plant to the Savannah River. TETRAD was used to estimate transport coefficients between Highway 301 and Purysburg, 84 miles downstream. Samples were collected by an SRL water sampler designed specifically for dispersion studies. LODIPS was used to estimate downstream tritium concentrations from Highway 301 to Purysburg using previously determined transport coefficients (TETRAD) from

a USGS Savannah River dye study on a 7-mile reach about 25 miles upstream from Highway 301. The release input is the tritium profile measured at Highway 301. The results are shown in Figure 1. Two LODIPS predictions with the bulk dispersion equation model were made using dye study coefficients and a new set of coefficients determined from the tritium release. A correction for the 18% increase in river volume between the two points was made. The new coefficients resulted in a more nearly accurate prediction because the coefficients were actually determined from the data set.

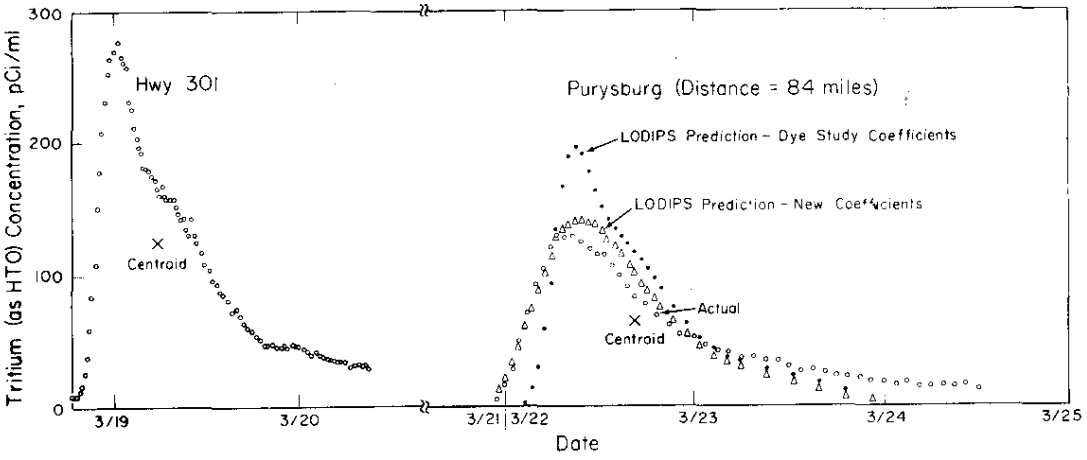

FIGURE 1. Profile of Tritium Release to Savannah River (Guideline for Safe Drinking Water is 3000 pCi/ml)

13. A UNIVERSAL ENVIRONMENTAL WATER SAMPLER (UEWS) †

INTRODUCTION

A versatile water sampler was needed to support programs to develop models for dilution, dispersion, travel time, and water transport of pollutants in streams, rivers, estuaries, and coastal regions. Existing water samplers, while having various desirable or specific features, did not offer the required versatility. A water sampler was built with the flexibility to composite water samples over a wide variety of sample volumes and sample times. The sampler has a capacity for 28 half-liter bottles and an automatic adjustment for sample tubing length.

DESCRIPTION

The water sampler consists of a controller and sampler combination (Figure 1) designed for low power consumption. The sampler consists of a peristaltic pump, water bottles, battery (12 V DC, 4.5 amp-hr to provide 1.5 A during pumping), water sensor, and relays. The controller, operating on less than 1 mA continuously, contains the time base (quartz crystal) and associated complimentary metal oxide semi-conductor (CMOS) digital logic and sampler control switches. The features of the controller are given in Table 1, and virtually any sampling situation can be accommodated. The "Hours Delay Before Sample" switch turns on the UEWS after the dialed-in hours have elapsed. This feature permits the sampling sequence of dispersion-travel time experiments to be arranged in advance, thereby optimizing sampling periods and personnel use, and also permits a specified period for the sampling. Automatic adjustment for sample tubing length, back flushing of sample tube, and volume determination are made by the peristaltic pump up-down counter and water sensor.

The sampler case and sample advancer is part of a stripped commercial water sampler. The sampler contains connections for a solar cell panel for extended operation periods. A connector permits other samplers to be connected in series, so that when one sampler cycle is completed, the other sampler is started.

Battery drain is a function of sampling program, tubing length, and water height. In general, the capacity of a single 4.5 amp-hr battery is sufficient for the 28 bottles.

---

† Work done by J. W. McMahan and D. W. Hayes.

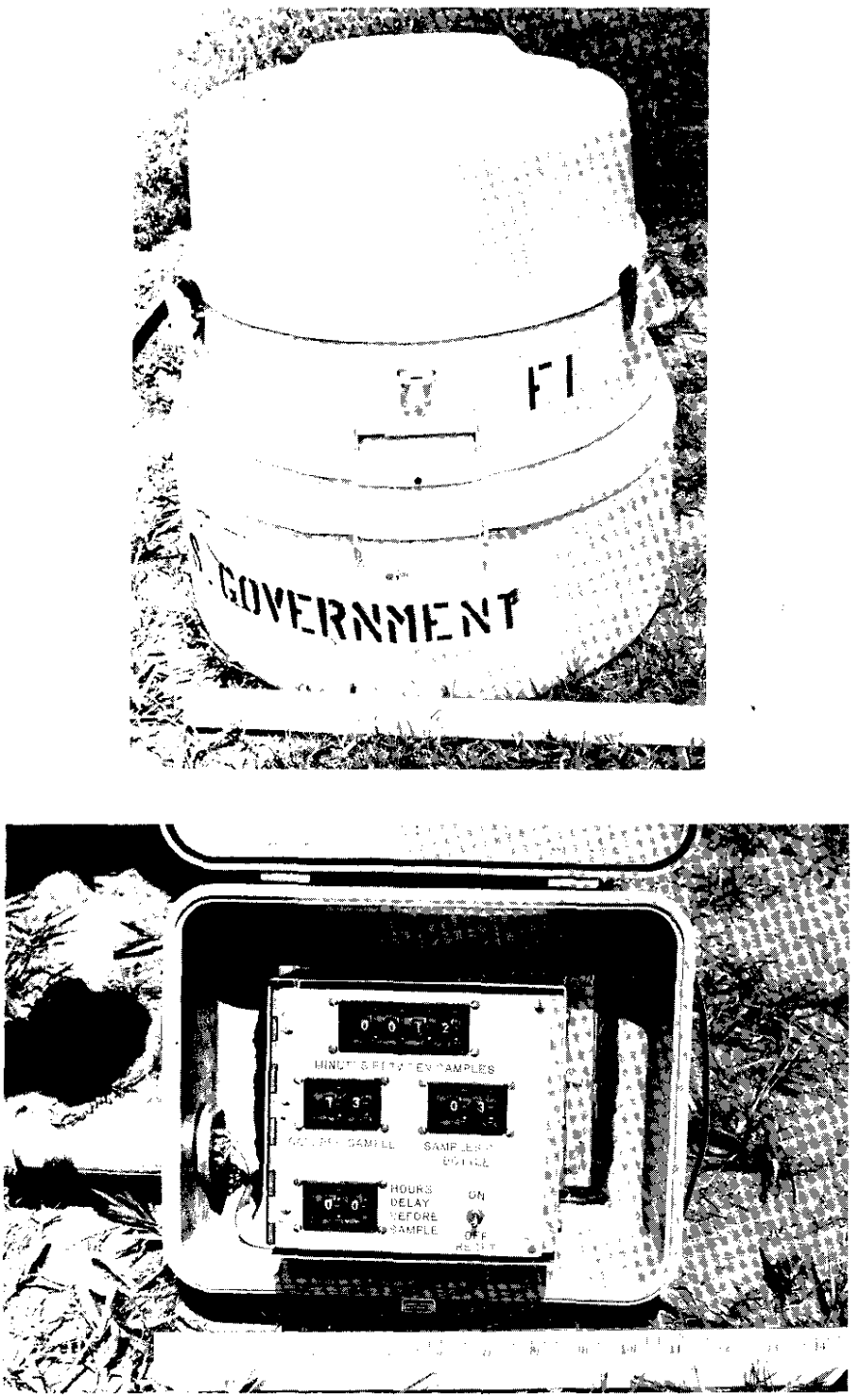

FIGURE 1. Controller Box Face and the Water Sampler

TABLE 1

UEWS Operating Features

Minutes between samples	2 to 9999 minutes
Samples per bottle[a]	Up to 99, but is limited by an incremental volume of 10 cc
Sample volume	10 to 990 cc[a]
Delay before sampling	Up to 99 hours[a]

---

a. Bottle volume determines limits for setting sample control switches.

14. A GROUND WATER MODEL OF THE TUSCALOOSA AQUIFER AT THE SAVANNAH RIVER PLANT†

INTRODUCTION

In areas of the South Carolina Coastal Plain within about 25 miles of the Fall Line, sand beds in the Tuscaloosa Formation form one of the major ground-water supplies. Industrial wells in this aquifer commonly yield more than 1000 gallons per minute of good quality water. This aquifer will be increasingly utilized for water supplies as the area becomes more industrialized. Due to several additional planned ground-water withdrawals from the Tuscaloosa Formation in the vicinity of SRP, a computer model of the Tuscaloosa aquifer was developed from existing information to obtain an estimate of the water flux through the system.

GEOLOGY AND HYDROLOGY OF THE TUSCALOOSA FORMATION

A cross section of the geology in the vicinity of SRP (Figure 1) shows that the Tuscaloosa Formation is the thickest (600 ft) of the Coastal Plain formations in this area. It is composed mostly of medium to coarse sand with several layers of clay. Near the center of the plant site the units of the Tuscaloosa Formation from top to bottom (Figure 2) are: (1) a unit of clay, sandy clay, or clayey sand about 60 ft thick; (2) an aquifer unit of well-sorted medium to coarse sand about 150 ft thick; (3) a unit, about 40 ft thick, in which one or more clay lenses occur; (4) an aquifer unit of well-sorted medium-to-coarse sand about 300 ft thick; and (5) a basal unit of sandy clay about 40 ft thick. The two aquifer units (2 and 4) combined are about 450 ft thick and are used singly and together to supply the water-production wells at SRP. For most purposes, including the present modeling effort, they are treated as one aquifer; however, they are hydraulically separated at SRP, except near wells that take water from both units.

The location of SRP and the outcrop area of the Tuscaloosa Formation are shown on Figure 3. Where the outcrop area is high in elevation, such as on the Aiken Plateau in the northeast sector (Figure 3), water recharged to the Tuscaloosa Formation exceeds the water discharged to local streams, and this excess water moves southeastward through the aquifer. Where the outcrop area is low in elevation, such as along the Savannah River Valley in

† Work done by I. W. Marine and K. R. Routt.

the northwest sector (Figure 3), water discharges from the formation. Thus the pattern of flow is an arcuate one (Figure 3).

In addition to showing more detailed geology at SRP, Figure 2 also shows that the water head in the Coastal Plain formations down to the Congaree Formation generally decreases with increasing depth, indicating some downward movement of water in addition to its horizontal movement. The Congaree Formation crops out in the more deeply incised stream valleys on the plant site, and the water head in this aquifer is controlled in part by the elevation of these onplant streams. The water head in the Tuscaloosa and Ellenton Formations is higher than that in the Congaree Formation (Figure 2), showing that the Tuscaloosa Formation at SRP is not part of the same hydrologic system as the formations above. Because the recharge and discharge controls on the water in the Tuscaloosa Formation are offsite, its water level on the plant is independent of water levels in the formations above it. Thus, the Tuscaloosa aquifer acts as a water conduit through which water passes beneath SRP in going from the high areas of the Aiken Plateau to the Savannah River Valley. Major amounts of water are probably neither added to this conduit nor removed from it through natural processes on the plant site. Of course, water is removed by pumpage.

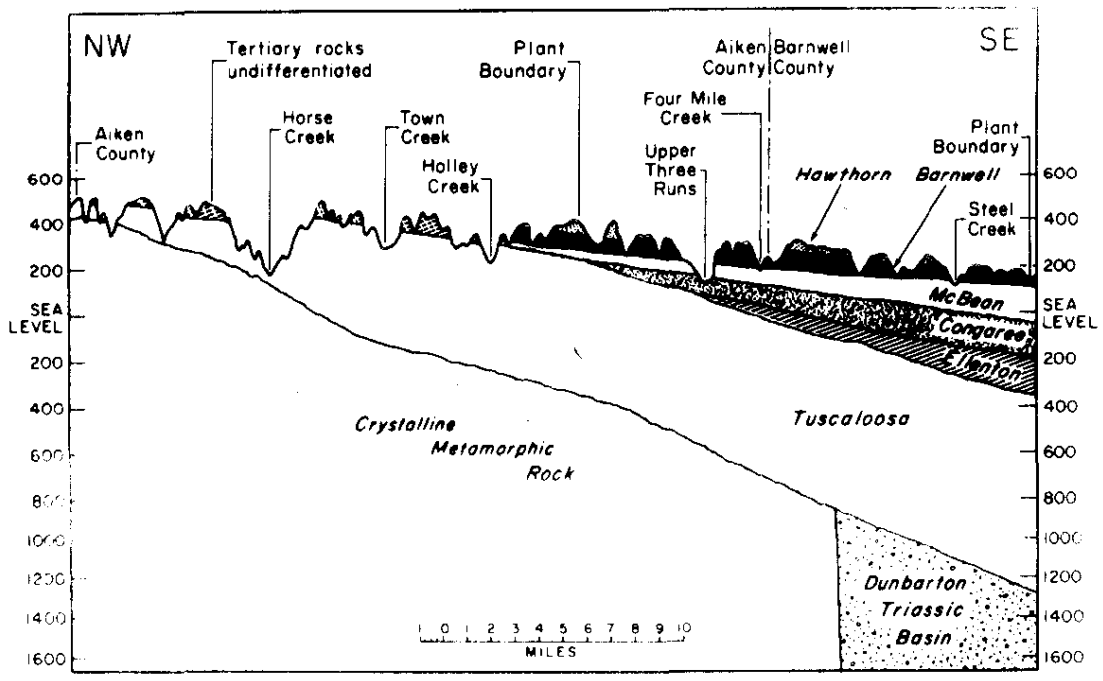

FIGURE 1. Generalized NW to SE Geologic Profile Across the Savannah River Plant

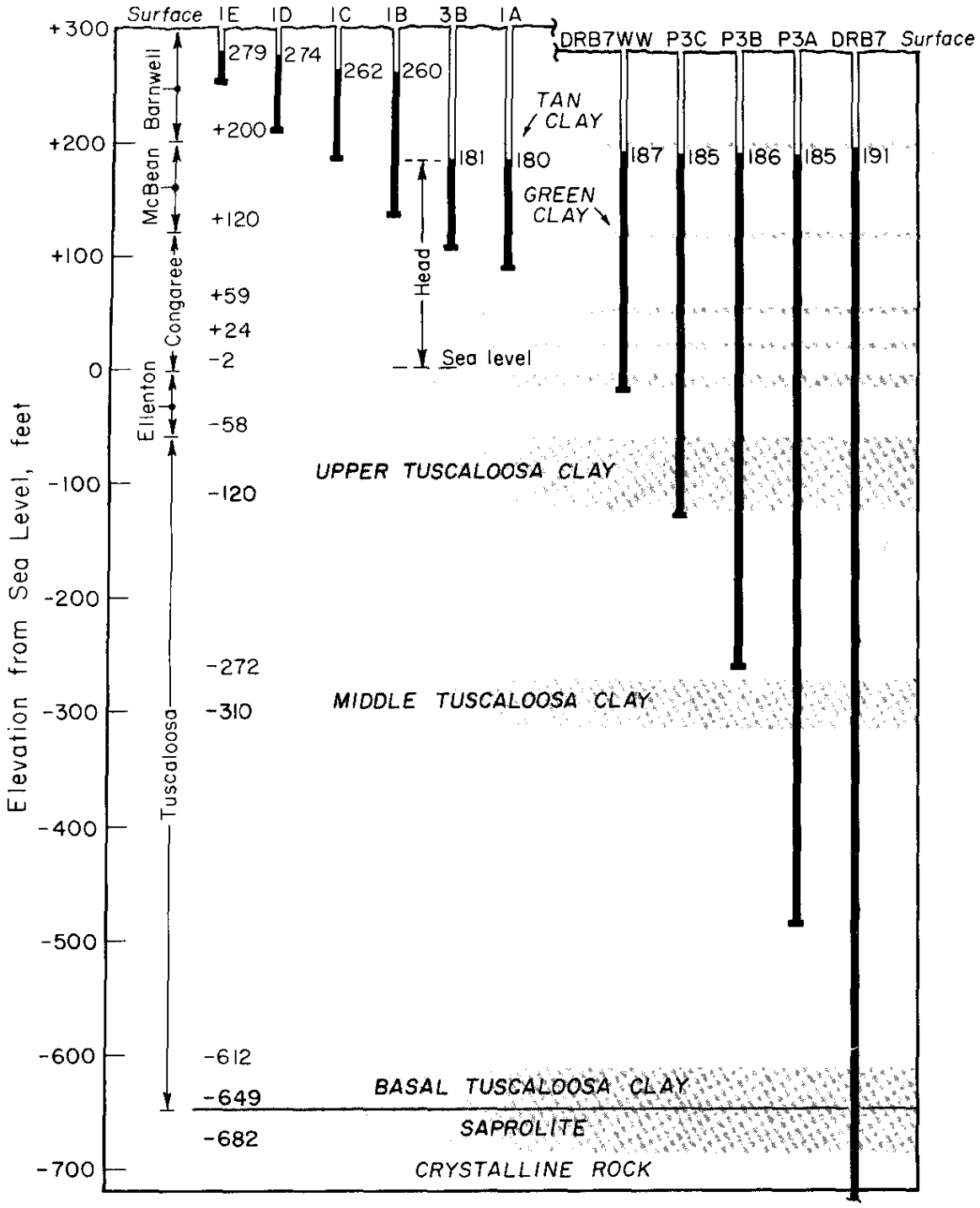

FIGURE 2. Geology and Hydrostatic Head in Ground Water near the Center of the Savannah River Plant

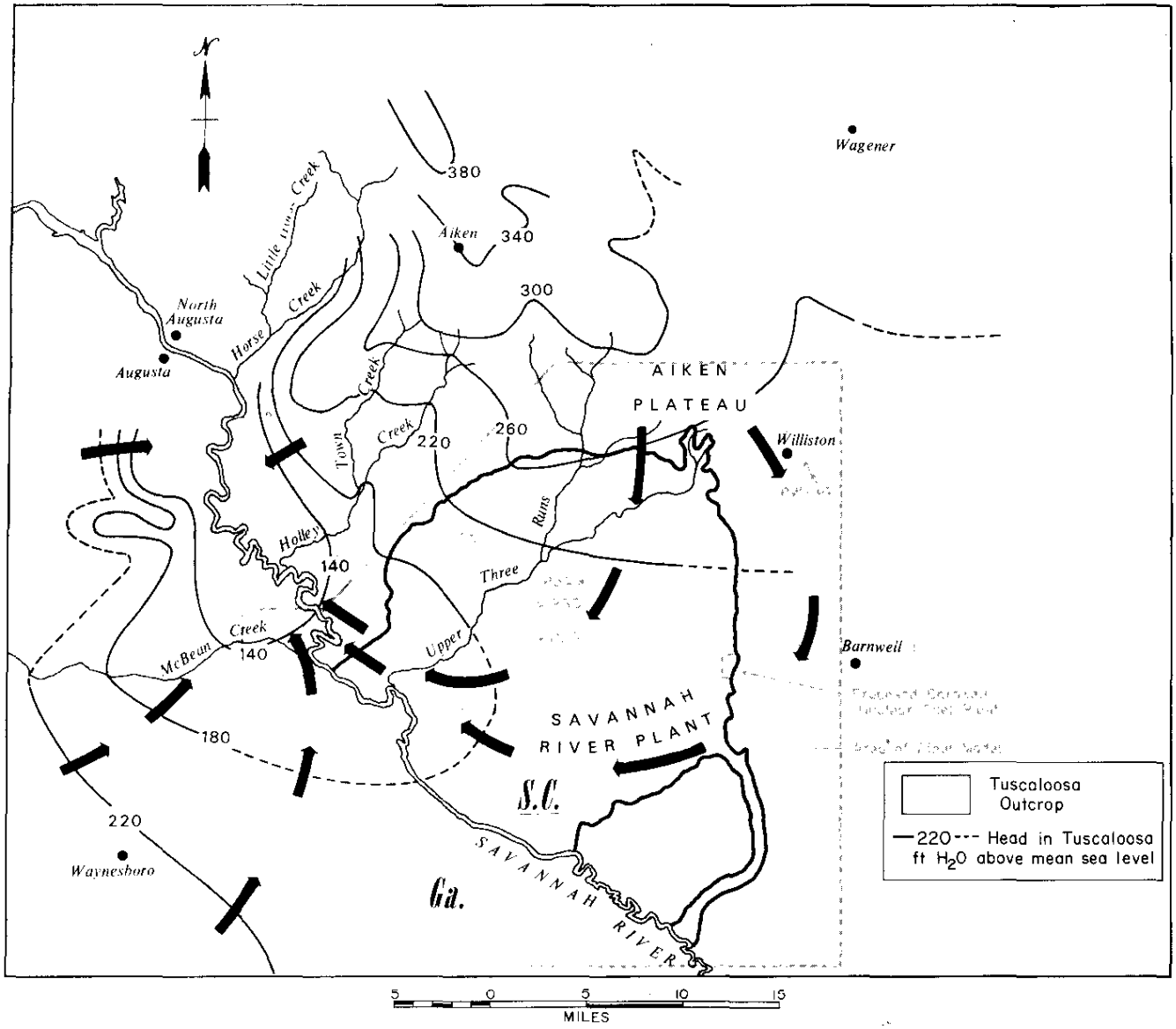

FIGURE 3. Flow in Tuscaloosa Aquifer

HYDRAULIC DATA ON THE TUSCALOOSA FORMATION

Field tests were made for transmissivity of the Tuscaloosa Formation when the original wells were drilled during the construction of SRP. The results of these tests and others were given by Siple.[1] In pumping tests, if the production well is in one unit of the Tuscaloosa aquifer, and the observation well is in the other unit, the results may indicate erroneously high values for transmissivity. Thus, some of the higher values reported are disregarded for use in the model. A representative transmissivity is given for each area on Table 1. The average of these 11 transmissivity values is 118,000 gallons per day

per foot; the median is 110,000 gpd/ft. For modeling purposes, a value of 120,000 gpd/ft was used.

Seven determined storage coefficients are also given by Siple,[1] and the average was 4.5×10^{-4}. The value used for the model is 5×10^{-4}.

Siple[1] also gives a "head map" of the Tuscaloosa Formation showing the hydrologic pressure in feet above sea level. Many of the water levels on which this head map was based were measured early in the plant's history, 1952-58; but continuous hydrographs on selected wells show that there has been no progressive decline in water level as a result of plant pumpage. These hydrographs are shown on Figure 4.

TABLE 1

Transmissivity Values for the Tuscaloosa Formation

Location	Transmissivity, gpd/ft
Savannah River Plant	
A Area	100,000
C	115,000
F	200,000
H	200,000
K	110,000
L	70,000
P	50,000
R	90,000
Aiken	100,000
Williston	120,000
Barnwell Nuclear Fuel Plant	143,000[a]
Average	118,000
Median	110,000
For Use in Model	120,000

a. Reference 2.

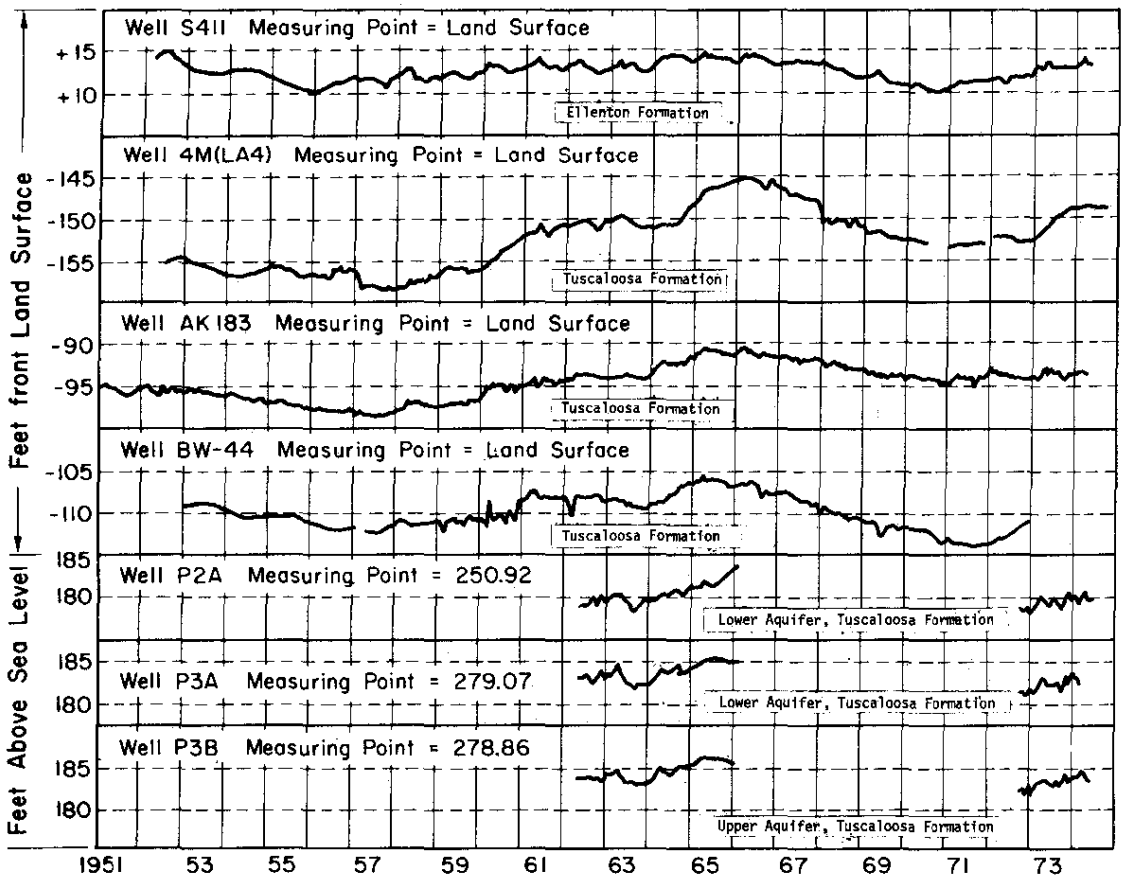

FIGURE 4. Long Term Hydrographs of Water Levels in the Tuscaloosa and Ellenton Formations

Plant pumpage is relatively constant although there are small temporal variations. Table 2 shows the average pumpage at each of the major areas for the last year or so. In addition, Table 2 shows the anticipated pumpage at the Barnwell Nuclear Fuel Plant and the Vogtle Power Plant.

TABLE 2

Average Continuous Pumping Rate in the Savannah River Plant Area

Location	Rate, cfs
Savannah River Plant	
A Area	2.90
F	3.33
H	3.55
Total Pumping Rate	9.78 ≅10
Planned	
Barnwell Nuclear Fuel Plant	4.45[a]
Vogtle Power Plant	4.45[b]
Total Future Pumping Rate	18.68 ≅19

---

a. Reference 2.

b. Reference 3.

COMPUTER MODEL

A digital computer model of transient ground-water flow in a confined aquifer (similar to that given by Pinder and Bredehoeft[4]) was used to simulate the effects of SRP pumpage over the past 22 years. The model is two-dimensional, providing the head (as a function of space and time) as output, and using the initial head, transmissivity, storage coefficient, and pumping rate as input. The model uses an alternating direction, implicit finite-difference method to solve the differential equation for non-steady flow of a compressible fluid in an elastic nonhomogeneous porous medium:

$$\frac{\partial}{\partial x_i}\left(T_{ij}\frac{\partial h}{\partial x_j}\right) = S\frac{\partial h}{\partial t} + W(x,y,t)$$

where:

T_{ij} is the transmissivity tensor (L^2/T)

h is the hydraulic head (L)

S is the storage coefficient (dimensionless)

t is time (T)

W is the volume flux per unit area (L/T)

In the first use of this model for the present purpose, it was assumed that there was no recharge to the Tuscaloosa aquifer and that all water pumped by the plant had been derived from storage. This model was 36 nodes by 36 nodes and represented a square area 160 miles on a side. The node spacing was dense at SRP and became progressively greater near the margins of the model. After 22 years of pumping about 10 cfs, the drawdown near F and H Areas would be 62 ft, and the drawdown at Columbia, South Carolina, 60 miles away, would be 47 ft. (For this model only, a transmissivity of 200,000 gpd/ft was used, but the conclusion would be similar if 120,000 gpd/ft had been used.) Obviously from this and the horizontal trend of the hydrographs shown on Figure 4, the water pumped by SRP has not been derived from storage but has come from water continually recharged to the aquifer. When SRP started to pump water from the aquifer either the volume of water entering the aquifer was increased by decreasing the rejected recharge in the outcrop area, or the natural discharge of water from the aquifer to the Savannah River Valley was decreased.

Although changes are made in the recharge-discharge regimen when new wells are added to a ground-water system, the natural water flux through the Tuscaloosa aquifer is of some interest to indicate whether there should be concern about depleting the aquifer.

To determine the ground-water flux through the Tuscaloosa Formation, the model was altered to permit recharge or discharge at every node in a quantity sufficient to maintain the steady state head. The hydrographs on Figure 4 indicate that the head map shown on Figure 3 is an approximation of a regional steady state. Because recharge and discharge were permitted, the size of this model did not have to be any larger than the area of interest. This model was 42 nodes by 42 nodes and represented the entire area covered by Siple's[1] head map, which is 47 miles on a side. This model included much of the outcrop area of the Tuscaloosa Formation around Horse Creek and Town Creek (Figure 3). The ground water flux through this model was about 1900 cfs. However, the ground-water gradients around Horse Creek are steep,

and much of this flux is local recharge and discharge and is not available to SRP wells. This number is also inaccurate because where the ground water gradients are steep, it is difficult to know the head value with the precision required at every node. Because of their steepness, 20-ft contours were used, and this contour interval is too large for accurate computation of recharge and discharge.

For these reasons, the size of the model was contracted again to omit the regions of steep ground water gradients. The resulting model was 25 nodes by 25 nodes and represented an area 31 miles on a side with a large corner segment omitted (Figure 3). Because this model only portrayed the region around SRP where ground water gradients are relatively flat, 5-ft contours could be interpolated on Siple's map.[1] In digitizing this refined head map, nodal values were estimated to the nearest foot, but are probably no more accurate than 3 ft. A 3-ft head difference between nodes in this model is equivalent to a ground water flux of about 1/2 cfs. Flux between nodes below 1/2 cfs was disregarded in summing the nodal flux values because it could be caused by inaccuracies in the head map. The total ground water flux thus summed through the area represented on Figure 3 is about 65 cfs. As would be expected, most of this recharge enters along the northeast boundary of the model, and discharges along the Savannah River Valley in the northwest part of the model. If, instead of neglecting all flux below 1/2 cfs (equivalent to a 3-ft accuracy in the head map), the nodal fluxes less than 0.9 cfs (equivalent to 5 ft of head difference) are neglected, the total flux would be 30 cfs. An error of 5 ft on the head map is not very probable.

CONCLUSIONS

Any determination of the flux through the aquifer depends on the accuracy with which the head, the transmissivity, and the storage coefficient are known. This model used a single average storage coefficient, a single average transmissivity, and the head map that was available; but from these, one concludes the flux is at least 30 cfs and more probably 65 cfs. These estimates could be refined with more accurate data. However, in view of the undiscernible effect of pumping 10 cfs for 22 years and in view of the presently anticipated pumpage of only 19 cfs in the foreseeable future, further refinement of the data and model do not appear justified. On the other hand, the ground water flux through the Tuscaloosa aquifer in this area is not infinite, and it will be worthwhile to continue monitoring water levels of the Tuscaloosa Formation for use in the future when refinement of the model may become necessary.

REFERENCES

1. G. E. Siple. *Geology and Ground Water of the Savannah River Plant and Vicinity, South Carolina.* U. S. Geol. Survey Water-Supply Paper 1841, 113 p. (1967).

2. P. G. Mayer. *The Impact of the Barnwell Nuclear Fuel Plant's Pumpage from the Tuscaloosa Aquifer.* Allied Gulf Nuclear Services Report No. EMP-104 (1972).

3. *Preliminary Safety Analysis Report V-1 - Vogtle Nuclear Power Plant.* Georgia Power Company, Atlanta, Ga.

4. G. F. Pinder and J. D. Bredehoeft. "Application of Digital Computer for Aquifer Evaluation". *Water Resources Research, 5,* 1069 (1968).

III. BIOTIC TRANSPORT AND EFFECTS

One of the objectives of the biotic studies is to evaluate the role of biota in ecosystem processes. Such evaluations include considerations of the role of biota as material vectors, as material sinks, or as the recipients of a man-induced stress. The following section emphasizes current efforts in the area of thermal effects on aquatic ecosystems, but also includes several items relating to the roles of biota as material sinks, as recycling agents, and as the recipient of a potential radioactive dose.

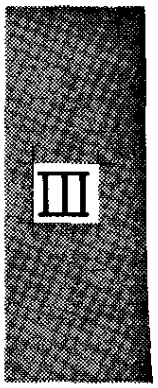

15. TRITIUM BEHAVIOR IN PINE TREES †

INTRODUCTION

On May 2, 1974, a process failure resulted in the release of about 500,000 curies of tritium; 1% as the oxide (HTO), and the rest as tritium gas (T_2). This release provided an opportunity to investigate the role of the pine tree as an initial sink and later, as a source of tritium oxide.

METHOD

The pine needles on trees in the region of elevated tritium levels were sampled at least weekly for 11 weeks after the release. Needle collection was from actively growing pine trees. The needles were placed in plastic bags following collection. Free water was obtained from the needles using a freeze-dry apparatus, and then the HTO content of the free water was measured using a liquid scintillation counting method.

Occasional measurements were obtained of the HTO content of air moisture, transpired water, and soil cores. Air moisture was collected using a cold trap. Transpired water samples were obtained by enclosing a pine branch with a polyethylene bag for approximately 20 hours. Soil cores were obtained by driving a 3.5 cm tube into the ground and then cutting the tube and contained core into desired lengths prior to freeze drying.

RESULTS

The puff containing tritium first contacted the trees about 16 kilometers from the point of release (Figure 1). Measurements of the tritium content of pine needles and soil in the vicinity of contact indicated rapid assimilation of HTO into the biosphere (Table 1). Comparison measurements revealed that lower elevation sample locations contained less tritium than adjacent locations at higher elevations. This observation indicated that the tritium release did not follow the stream valleys.

---

† Work done by J. R. Watts. A paper, "Absorption of Tritiated Water Vapor from the Atmosphere by Pine Trees," by C. E. Murphy and J. C. Corey has been accepted for presentation at the *Fourth National Symposium on Radioecology*, Corvallis, Oregon, May 12-15, 1975.

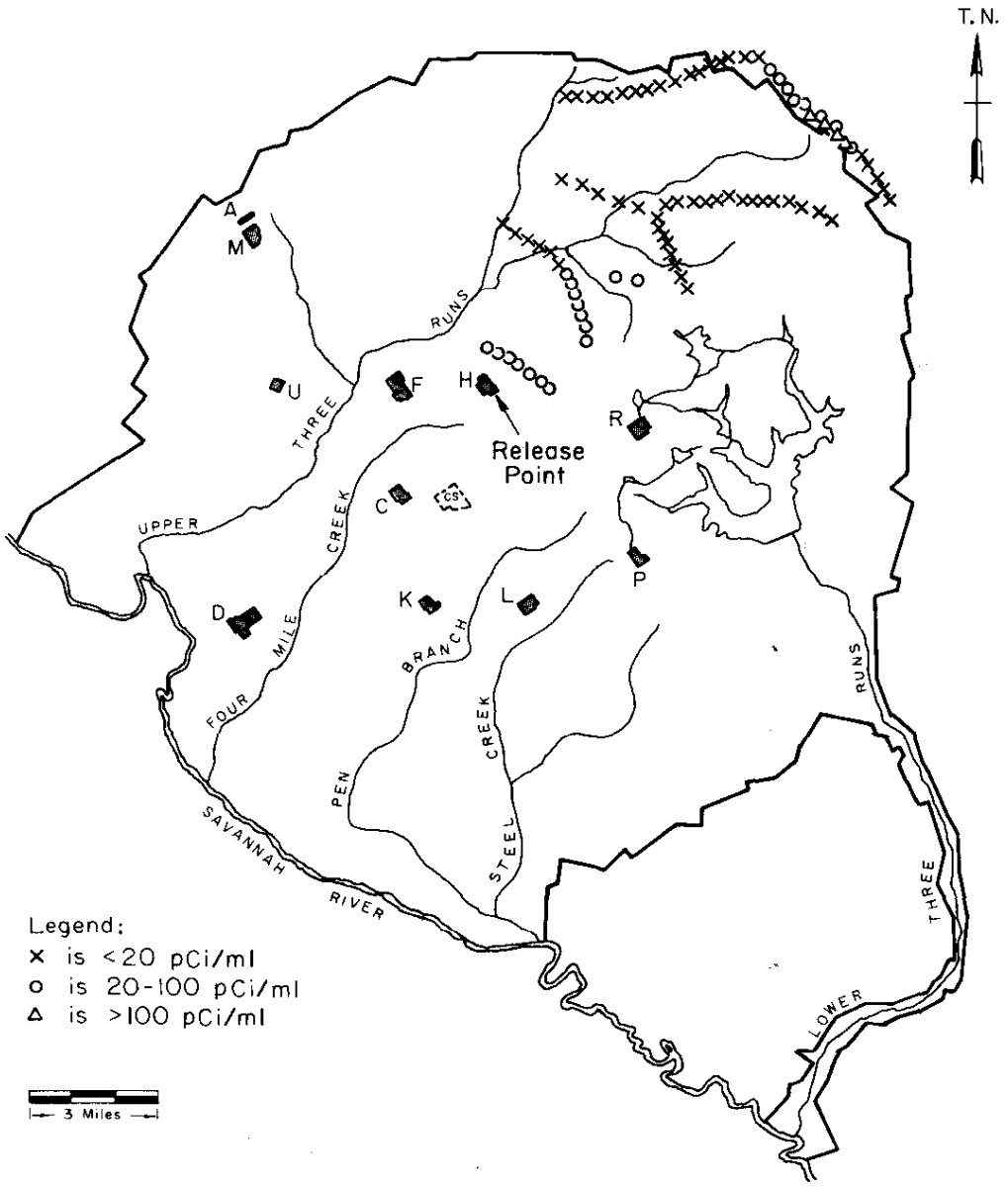

FIGURE 1. Tritium (HTO) Concentrations Measured in Vegetation at SRP Following a Stack Release of Tritium on May 2, 1974. Elevated Levels Adjacent to the Release Point are Attributed to Routine SRP Operations

15. TRITIUM BEHAVIOR IN PINE TREES †

INTRODUCTION

On May 2, 1974, a process failure resulted in the release of about 500,000 curies of tritium; 1% as the oxide (HTO), and the rest as tritium gas (T_2). This release provided an opportunity to investigate the role of the pine tree as an initial sink and later, as a source of tritium oxide.

METHOD

The pine needles on trees in the region of elevated tritium levels were sampled at least weekly for 11 weeks after the release. Needle collection was from actively growing pine trees. The needles were placed in plastic bags following collection. Free water was obtained from the needles using a freeze-dry apparatus, and then the HTO content of the free water was measured using a liquid scintillation counting method.

Occasional measurements were obtained of the HTO content of air moisture, transpired water, and soil cores. Air moisture was collected using a cold trap. Transpired water samples were obtained by enclosing a pine branch with a polyethylene bag for approximately 20 hours. Soil cores were obtained by driving a 3.5 cm tube into the ground and then cutting the tube and contained core into desired lengths prior to freeze drying.

RESULTS

The puff containing tritium first contacted the trees about 16 kilometers from the point of release (Figure 1). Measurements of the tritium content of pine needles and soil in the vicinity of contact indicated rapid assimilation of HTO into the biosphere (Table 1). Comparison measurements revealed that lower elevation sample locations contained less tritium than adjacent locations at higher elevations. This observation indicated that the tritium release did not follow the stream valleys.

---

† Work done by J. R. Watts. A paper, "Absorption of Tritiated Water Vapor from the Atmosphere by Pine Trees," by C. E. Murphy and J. C. Corey has been accepted for presentation at the *Fourth National Symposium on Radioecology*, Corvallis, Oregon, May 12-15, 1975.

TABLE 1

HTO Measurements 10 Hours after Release

Location	pCi/ml of water	
	Pine Needles	Soil
1	135	7240
2	22	926
3	22	113

Repeated measurements from pine trees at the same locations permitted retention information on atmospheric released HTO to be obtained. The tritium concentration with time for the location of highest uptake (Figure 2) was representative of the retention pattern for the affected area. The retention pattern can be described as the sum of two exponential curves. The shorter component had a half-life of about 4 days and the longer component had a half-life of about 100 days.

Soil samples up to 55 cm deep were collected during the latter portion of the needle sampling program. Two months after the release, the soil samples showed highest tritium concentrations at 35 to 40 cm below the surface (Figure 3). The maximum concentration (270 pCi/ml) in the soil water was about five times the concentration in the pine needles from the same location. All samples below 5 cm showed higher tritium concentrations than the pine needles at that location. The HTO content in the soil will not be removed readily* by evaporation and will either be displaced downward by infiltrating rainwater or lost by transpiration; hence, its residence time in the location of deposition will be very long.

---

* J. C. Corey. "Contribution of Tritiated Water at Various Depths in Soil to Evaporation at the Soil Surface." *Environmental Surveillance in the Vicinity of Nuclear Facilities*. Charles C. Thomas, Springfield, Illinois, pp 309-318 (1968).

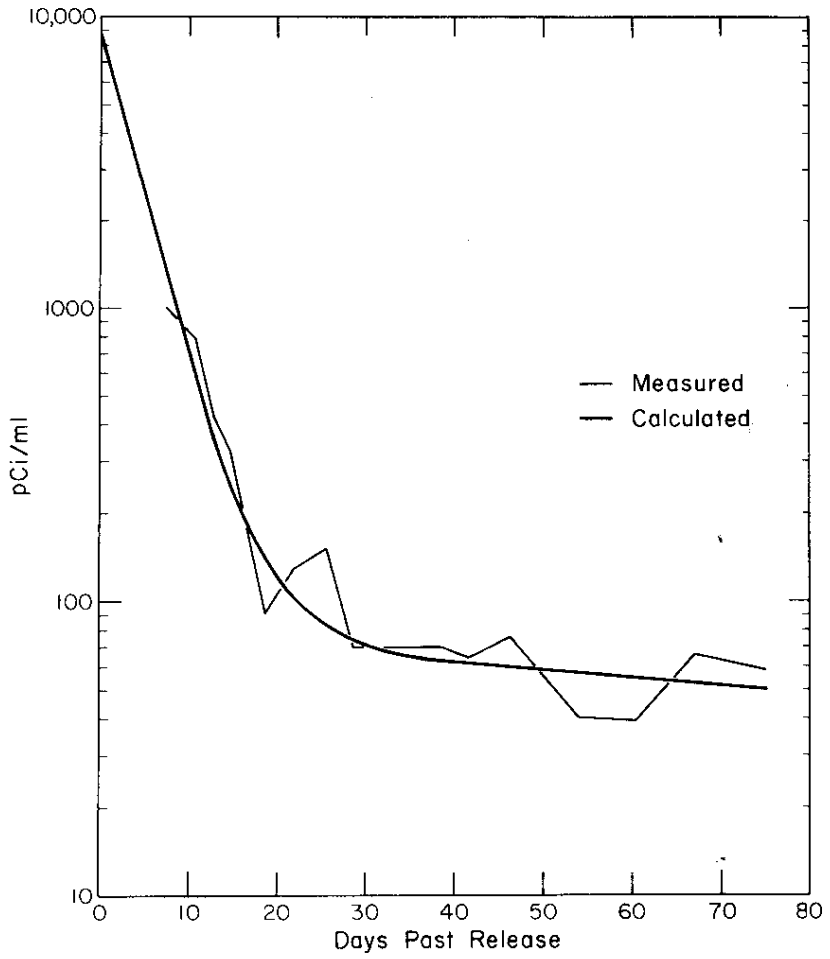

FIGURE 2. Retention Pattern of Tritium (HTO) in Free Water from Pine Needles from the Location of Maximum Uptake (Δ) in Figure 1.

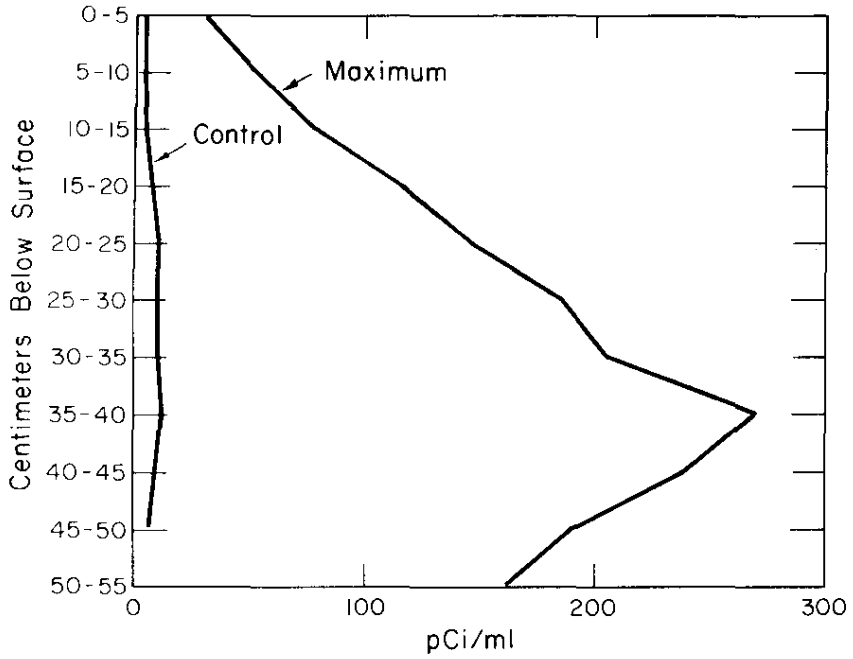

FIGURE 3. Tritiated Water Concentrations in Soil from a Control Area and from the Location of Maximum Uptake (Δ) in Figure 1.

Measurements of air moisture and free water in pine needles indicated (Table 2) that transpired water in the vicinity of the measurements was not affecting the HTO content of the air 29 days after the release, while on day of release, the tritium content of air moisture was higher than in free water from pine needles.

Comparison of the HTO content of transpired water (collected in plastic bags placed over the branches) with the free water obtained by freeze-drying indicated slightly higher tritium concentrations in the transpired water (Table 3).

TABLE 2

Comparison of HTO in Free Water with that in Air Moisture

		pCi/ml of Water	
Location	Date	Free Water	Air Moisture
1	5/2	22	91
2	5/2	6.4	24
3	5/31	67	8.2
4	5/31	56	6.9
5	5/31	12	13

TABLE 3

Comparison of HTO in Free Water with that in Transpired Water

		pCi/ml of Water	
Location	Date	Free Water	Transpired Water
1	5/2	22	18
2	5/2	6.4	8.7
3	5/31	67	125
4	5.31	56	81

16. STRONTIUM, CESIUM, AND PLUTONIUM IN VARIOUS SOILS AND PLANTS AT THE SAVANNAH RIVER PLANT †

INTRODUCTION

An extensive program is being prepared to determine the behavior of plutonium in the ecology of the southeastern United States. Some preliminary measurements were conducted to determine the sample size required for plutonium analysis of vegetation, to delineate the most appropriate areas on the Savannah River Plant to conduct such experiments, and to obtain approximate concentration factors for strontium, cesium, and plutonium for the vegetation in these areas to assist in sample sizing prior to analysis.

RESULTS AND DISCUSSION

Four locations were sampled for soil and vegetation (*Lespedezia*). Appropriate methods were used for strontium, cesium, and plutonium analyses. Concentration factors, pCi/g dry weight vegetation per pCi/g of soil, were approximately 0.5 (cesium), 0.15 (strontium) and 10^{-2} (plutonium). Plutonium analyses on vegetation grown on soils treated with plutonium (2 mCi/km^2) required approximately 200-g samples of dry vegetation and counting periods of several days using alpha detectors with virtually zero background (2 counts per day over 3 MeV range).

† Work done by J. C. Corey and P. J. Schneider (Undergraduate Research Trainee).

17. CONTAMINATED SOLVENT DEGRADATION †

INTRODUCTION

Approximately 170,000 gallons of organic solvent (tributylphosphate and kerosene) are stored in 20 underground storage tanks in the burial ground at the Savannah River Plant (SRP). Possible safe methods to remove radioactivity from this solvent and to dispose of the solvent include incineration, distillation, evaporation, ion exchange, bacterial degradation, high pressure aqueous combustion, radiation, and solvent recovery with sludge solidification. This report discusses results obtained using bacterial degradation in an aqueous phase and on soil.

Bacterial degradation of organics has received extensive attention in oil spill situations[1] and in laboratory studies.[2] Data indicate such methods are effective in converting the hydrocarbons to carbon dioxide, water, and to materials in bacterial cells. Appropriate parameters for engineering design were experimentally determined.

EXPERIMENTAL METHODS AND RESULTS USING AN AQUEOUS BIO SYSTEM

To determine if the radiation associated with the contaminated solvent was detrimental to bacterial growth, an immiscible mixture of solvent and water (40 mℓ solvent, 50 mℓ water, 1 g calcium nitrate, and 1 g bacterial mixture) was aerated for two weeks. Plating of a small amount of solution on a culture media indicated microflora were present.

Additional tests using simulated SRP organic waste (nonradioactive) were conducted with a Warburg respirometer to determine whether the waste was amenable to biological degradation. A Warburg respirometer is the standard manometric apparatus for measuring oxygen utilization. The pressure difference or oxygen utilization is measured by a change in manometric fluid levels and oxygen uptake is recorded as a function of time. The waste for this study was immiscible with water, so testing was performed on emulsified as well as nonemulsified samples. To study potential toxicity problems, oxygen uptake rates were recorded for tributylphosphate (TBP) and kerosene separately. The data indicated that oxygen uptake was more rapid on the emulsified solutions and on solutions containing kerosene, rather than TBP.

† Work done by J. C. Corey.

Because the Warburg tests indicated that bacteria can live in an aqueous system in contact with the waste, two batch units were fed synthetic waste at loadings of 0.05 and 0.1 pounds per day of waste per pound of sludge under aeration. A number of difficulties arose in these tests, such as:

- Organic carbon contents were consistently higher 20 hours after feeding than immediately after feeding. This observation is inconsistent with normal results in which organic carbon removal is measured for kinetic information.

- Dilutions were inaccurate because a portion of the waste was left in all glassware as a film, and the solvent was not water soluble.

- An oily film on the surface of the batch units trapped sludge and had to be removed periodically.

These difficulties in maintaining an active aqueous bio system with the organic feed available, implied that aqueous biological treatment should be avoided as an easy means of disposing of the stored solvent.

EXPERIMENTAL METHODS AND RESULTS USING A SOLID MATRIX SYSTEM

Published results[3] from degradation studies of waste petroleum products in soil suggested a similar approach be attempted for the waste solvent present at SRP. The oil degradation technique utilizes naturally occurring microbial processes in the soil to convert the oily wastes to innocuous products, principally carbon dioxide, water, and bacterial cells.

Laboratory tests are currently in progress to determine maximum degradation rates and conditions. Preliminary studies utilize a mixture containing 3 kg of washed sand, 10 g of agricultural fertilizer (10-10-10), 150 g of water, 50 g of sewage sludge, and 150 mℓ of solvent (with n-paraffin or 50 mℓ of TBP and 100 mℓ of n-paraffin). Materials were placed in large plastic containers and purged with 3 mℓ of oxygen per minute. A significant acclimatization period (5 days for n-paraffin and 30 days for the TBP — n-paraffin mixture) was required. Carbon dioxide evolution from a control specimen (no solvent addition) remained low (<0.05 g/day carbon dioxide) over this period, while carbon dioxide evolution increased to 7.7 g and 3.5 g, respectively, per day for the two treatments. Introduction of anaerobic conditions required a renewed acclimatization period (2 days) before carbon dioxide production commenced. These preliminary data suggest a degradation rate of approximately 1 ton per day of carbon per acre-foot of soil for n-paraffin, and 0.5 ton per day of carbon per acre-foot of soil for the mixture of n-paraffin and TBP.

The current program includes characterizing organisms causing degradation, delineating temperature and substrate effects to optimize degradation rates, and determining necessary parameters for engineering design.

REFERENCES

1. J. E. Zajic, B. Supplisson, and B. Volesky. "Bacterial Degradation and Emulsification of No. 6 Fuel Oil." *Envir. Sci. Technol. 8(7)*, 664 (1974).

2. R. W. Stone, M. R. Fenske, and A. G. C. White. "Bacteria Attacking Petroleum and Oil Fractions." *J. of Bacteriology 44*, 169 (1942).

3. R. Ellis, Jr. and R. S. Adams, Jr. "Contamination of Soils by Petroleum Hydrocarbons." *Advances in Agronomy 13*, 197 (1961).

18. CARBON-14 PRODUCTION BY THE NUCLEAR INDUSTRY AND ITS POTENTIAL EFFECTS †

INTRODUCTION

Carbon-14 is known to be produced by the nuclear industry,[1] but its anticipated release rate has not been published.[2] Carbon-14 is of interest because of the biological importance of carbon and the long half-life (5730 years) of this isotope. The Savannah River Plant (SRP) with both heavy-water-moderated reactors and a separations complex offered an opportunity to determine ^{14}C production. This information permitted predictive equations to be tested and used to estimate the ^{14}C inventory in the nuclear power industry and its relative magnitude compared with existing ^{14}C levels in the environment.

CARBON-14 PRODUCTION MECHANISMS, CALCULATIONS, AND MEASUREMENTS

Carbon-14 is produced in a reactor by various reactions in the fuel, moderator, and core construction materials. The production mechanisms include neutron-induced reactions [(n,p); (n,α); and (n,γ)] and ternary fission (Table 1). Calculations of ^{14}C production within the fuel and moderator were made for the heavy water production reactors of SRP. The rate of production from neutron-induced-reactions was calculated from

$$R = N \sigma_{eff} \phi_{th}$$

where N is the number of target atoms, σ_{eff} is the effective cross section in cm^2, and ϕ_{th} is the thermal neutron flux in neutrons/(cm^2-sec). Pertinent data for the thermal neutron flux, in-core moderator volume, fuel loading, and nitrogen impurity in the fuel were used to calculate production of ^{14}C.

---

† Work done by D. W. Hayes and K. W. MacMurdo; submitted in September, 1974, for publication in *Health Physics*.

TABLE 1

Carbon-14 Production Modes in a Nuclear Reactor and Pertinent Nuclear Data

Neutron-Induced Reactions	Cross Section, barns	Natural Isotopic Abundance of Target Element, %
$^{14}N(n,p)^{14}C$	1.8	99.6
$^{17}O(n,\alpha)^{14}C$	0.24	0.039
$^{13}C(n,\gamma)^{14}C$	0.001	1.11
Ternary Fission		
$^{235}U(n,f)^{14}C$	1.7×10^6 fissions[3]	
$^{239}Pu(n,f)^{14}C$	1.8×10^6 fissions[4]	

An alternate procedure based on SRP effluents was also developed to determine ^{14}C production at SRP. Carbon-14 produced in the SRP reactors may be released to the environment by several means. It may be exhausted to the atmosphere as ^{14}CO and $^{14}CO_2$ through the reactor and separations complex ventilation systems, to the aqueous environment by way of liquid waste in waste tanks, and to the burial ground on the ion exchange resin (demineralizers) used to maintain moderator purity.[5]

SRP produces ^{14}C at a rate of 392 $\pm$40 Ci/yr based on effluents, as compared to a calculated rate of 383 $\pm$75 Ci/yr.

POWER REACTOR CARBON-14 PRODUCTION

The calculational model successfully applied to SRP production reactors was extended to cover reactors typical of the nuclear power industry. Two actual operating power reactors, one a pressurized water reactor (PWR), and the other a boiling water reactor (BWR), were chosen as representative examples. Pertinent data from these reactors [1,6,7] were used to compare the absolute ^{14}C production by different reactor types (Table 2) relative to a power level of 1000 MW(t). The following simplifying assumptions were made: thermal neutron fluxes in the fuel and moderator are equal, production of ^{14}C by fast neutron reactions is negligible,

and the fuel nitrogen impurity is 10 ppm.*

TABLE 2

Calculated Reactor Production Rate of Carbon-14 in Ci/Year at 1000 MW(t)[a]

	BWR	PWR
$^{17}O(n,\alpha)^{14}C$		
Moderator (H_2O-D_2O)	3.8	1.1
Fuel (UO_2)	3.6	1.3
$^{14}N(n,p)^{14}C$		
Fuel	7.0	2.5
Moderator + Other Sources	-	0.1
Fission	0.2	0.2
Total	14.6	6.3

a. 1000 MW(t) - A reactor operating at a thermal power level of 1000 megawatts.

ENVIRONMENTAL CARBON-14 LEVELS

Figure 1 compares environmental levels with estimated ^{14}C production by the nuclear power industry between 1975 and the year 2000. The inventory of ^{14}C produced by the nuclear power industry will be 10% of that from weapons testing, and only 0.3% of the natural ^{14}C level. This conservative calculation assumed 1) all electric power will be generated by light water reactors (2/3 pressurized water reactors and 1/3 boiling water reactors in the U.S.; 1/2 pressurized water reactors and 1/2 boiling water reactors in the remainder of the world) operating at a capacity factor of 0.75; and 2) growth rates will follow published forecasts.[8]

DOSE

The dose commitment from ^{14}C released to the environs can be considered in two ways: the total dose commitment, and the fractional

* G. F. Molen, Manager, Nuclear Materials Safeguards, Allied General Nuclear Services, Barnwell, SC.

dose commitment delivered over various time periods. The total dose commitment ("legacy dose") is defined as the integral over infinite time of the average dose rate delivered to a hypothetical individual with an infinite life in the world's population as a result of a specific practice.[9,10] The fractional dose commitment is important because it includes the removal mechanisms of the dose delivered to present populations. The fractional dose was calculated in two ways: no removal from the atmosphere, and removal from the atmosphere by the oceans (2-reservoir model).

For dose calculation purposes, all ^{14}C produced by the nuclear power industry was assumed to be released directly to the atmosphere. ^{14}C concentrations were calculated with dose formulae from a U.N. Report,[9] except for the fractional dose calculation where a function to account for the varying product rate with time of ^{14}C was included. The results are shown in Table 3. The possible effects of reduction of ^{14}C specific activity in the global environment from combustion of fossil fuel was not considered, but would reduce the dose slightly.

ACKNOWLEDGMENT

The authors thank Dr. H. Lee Dodds, Savannah River Laboratory, for his valuable suggestions.

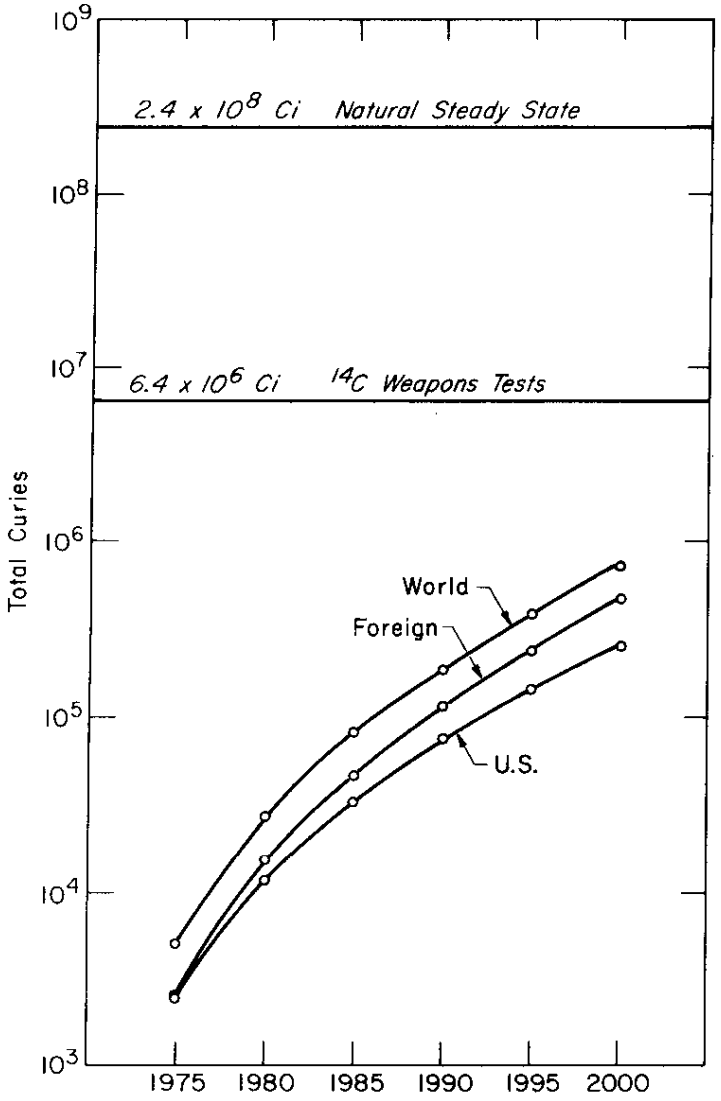

FIGURE 1. Carbon-14 Produced by the Nuclear Power Industry

TABLE 3

Calculated Dose to a Single Individual from Carbon-14 Contributions of the Nuclear Power Industry Natural Processes and Weapons Tests (mrems)

Mode of ^{14}C Production	Total Dose Commitment to a Hypothetical Individual Having an Infinite Life	Dose, 1975 to 2000		Dose, 1975 to 2025		Dose, 1975 to 2075	
		Nonremoval	Removal	Nonremoval	Removal	Nonremoval	Removal
Nuclear Power Industry	27.0	0.55	0.50	2.5	1.9	6.5	3.3
Natural Processes	NR	25.5	NR	51.0	NR	102.0	NR
Weapons Tests	255.0	19.3	15.0	38.6	24	77.2	34.0

NR = Not relevant because natural ^{14}C is at environmental steady state.

REFERENCES

1. B. Kahn, et al. *Radiological Surveillance Studies at a Boiling Water Nuclear Power Reactor.* USEPA Report BRH/DER 70-1, National Environmental Research Center, Cincinnati, Ohio (February, 1970).

2. G. H. Whipple. *Proceedings for the Symposium on Public Health Aspects of Peaceful Use of Nuclear Explosives, Las Vegas, 1969,* p 684. Clearinghouse of Federal Scientific and Technical Information, Springfield, Va. (1969).

3. V. M. Andreev, V. G. Neodopekin, and V. I. Rogov. *Sov. J. Nucl. Phys. 8* (1), 22 (1969).

4. V. M. Andreev, V. G. Neodopekin, and V. I. Rogov. *Sov. J. Nucl. Phys. 8* (1), 14 (1969).

5. R. I. Martens, W. L. Poe, and A. E. Wible. *Chem. Eng. Prog. Sym. Ser. 60* (51), 44 (1964).

6. B. Kahn, et al. *Radiological Surveillance Studies at a Pressurized Water Nuclear Power Reactor.* USEPA Report RD 71-1, National Environmental Research Center, Cincinnati, Ohio (August, 1971).

7. *Handbook of Nuclear Research and Technology.* McGraw-Hill, Inc., New York, N. Y. (1962).

8. *Nuclear Power 1973-2000.* USAEC Report WASH-1139 (72), Superintendent of Documents, U. S. Government Printing Office, Washington, DC 20402 (1972).

9. *Report of the United Nations Scientific Committee on the Effects of Atomic Radiation, New York, 1962.* Official Records of the General Assembly, Seventeenth Session, Supplement 16 (A/5216), United Nations, N. Y. (1962).

10. *Report of the United Nations Scientific Committee on the Effects of Atomic Radiation, New York, 1964.* Official Records of the General Assembly, Nineteenth Session, Supplement 14 (A/5814), United Nations, N. Y. (1964).

19. THE DIFFERING TEMPERATURE RESPONSES OF TWO SPECIES OF RAMSHORN SNAILS †

INTRODUCTION

This study was designed to investigate the adaptive significance of respiration in two species of freshwater pulmonate snails from different temperature environments in the field.

The ramshorn snail, *Helisoma*, is abundantly and widely distributed in Par Pond, a reactor cooling reservoir on the Savannah River Plant. *Helisoma trivolvis* occurs in regions near the thermal effluent as well as in unaffected areas. *Helisoma anceps* is very infrequently found in thermally affected waters but is common in the rest of the pond.

METHODS

At two week intervals between February 1973 and July 1974, adult *Helisoma* specimens from a "warm" and a "cold" station were subjected to respiration rate measurements at three temperatures--at field temperature immediately after collection and subsequently at 5°C and 10°C above field. The resulting data show two kinds of metabolism-temperature relations:

1. the dependence of respiration on field temperature for an annual cycle, and

2. the dependence of respiration on experimental temperature (field, field plus 5°C, and field plus 10°C) over a restricted time period.

The second relation may also be expressed as a Q_{10}, the ratio of respiration rates for a 10°C change in temperature.

Organisms used in routine respiration rate experiments had been experiencing the normal diurnal temperature fluctuations observed in the field. To examine the comparability of our results with those obtained from laboratory organisms held at constant temperature, an acclimation experiment was performed. *H. trivolvis* specimens were held at 20°C, a temperature within the range of diurnal fluctuation, and at 5°C and 10°C above that temperature for 48 hours before measuring respiration at those

† Work done by G. B. Johnson.

temperatures. The respiration of acclimated snails was compared to that of nonacclimated ones (control group).

TEMPERATURE RESPONSES

As evidenced by the slopes of the regression of the log of respiration on field temperature over the span of a year, *H. anceps* shows a significantly stronger response to temperature than *H. trivolvis* from either the "warm" or "cold" station (Figure 1).* The response of *H. trivolvis* from the "cold" station is intermediate between *H. anceps* -- also "cold"-adapted -- and *H. trivolvis* from the "warm" station; however, there is no significant difference between the regression slopes of the log of respiration on temperature for *H. trivolvis* from the two stations.

The more pronounced temperature response in *H. anceps* is clearly evident when the organisms are subjected to experimental temperature elevations (Figure 1). The positive correlation between respiration and temperature for this species persists through temperatures 10°C above field. At 5°C and 10°C above field, the slopes are significantly different from zero for *H. anceps*, whereas the slopes are not different from zero at above field temperatures for *H. trivolvis*.

Q_{10} values for both species from the two locations decrease with increasing field temperature (Figure 2). The slopes for the regression of Q_{10} on field temperature are significantly different from zero for *H. trivolvis* but not for *H. anceps*. No differences in the rates of decrease between stations or species is evident.

At most temperatures between 10°C and 35°C (normal range of field temperature) no significant differences in average rates of respiration due to station of origin or species could be demonstrated. Variability in respiration between individuals was considerable through the range of field temperatures.

Of the several factors experimentally examined as probable sources of variation, only body size and acclimation showed substantial effects. Dry weight of individuals and constant temperature acclimation appeared to affect respiration. Respiration generally decreased with increasing size in both *H. trivolvis* and *H. anceps*. This inverse relationship was especially evident in young organisms. At most temperatures the predictability of the relationship was poor as evidenced by low R^2 values. When respiration was graphed against temperature, the slopes were

---

* Test of differences between slopes and means based on t-test at the 0.05 probability level.

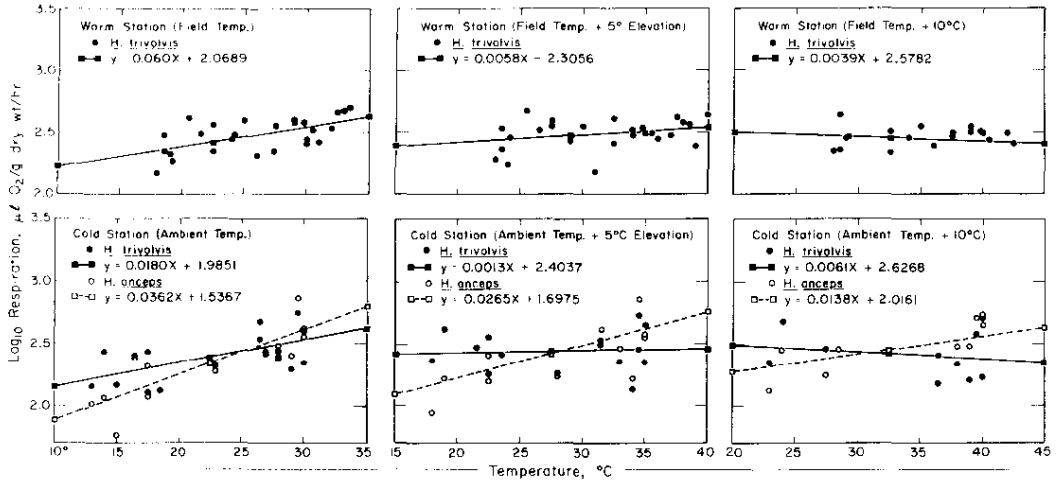

FIGURE 1 Relationship Between Respiration and Temperature for *Helisoma* at Field Temperature and Two Levels of Temperature Elevation. All Points are Averages for 2 to 10 Organisms

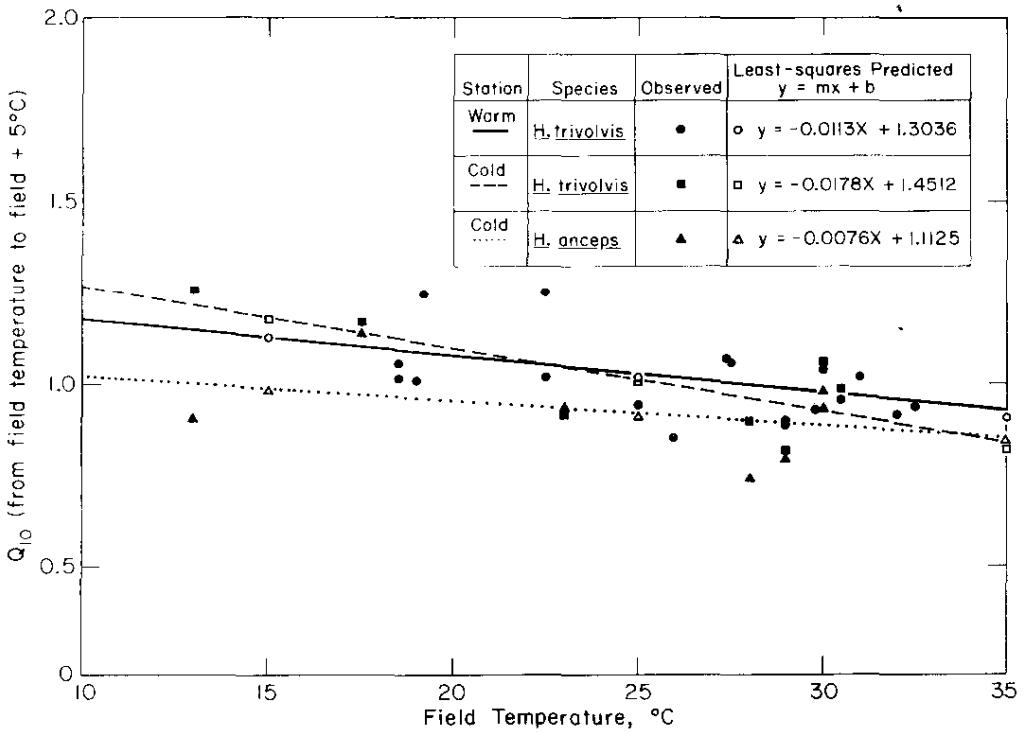

FIGURE 2 Change in Q_{10} for Respiration with Increasing Field Temperature

similar for *H. trivolvis* from the two stations under conditions of acclimation and nonacclimation (Figure 3). Acclimated snails from both stations showed a significant change in respiration between 20°C and 30°C while non-acclimated snails showed no change. The F-test showed no significant differences ($p = 0.05$) in the variances of acclimated and non-acclimated organisms except between the warm station samples at 25°C.

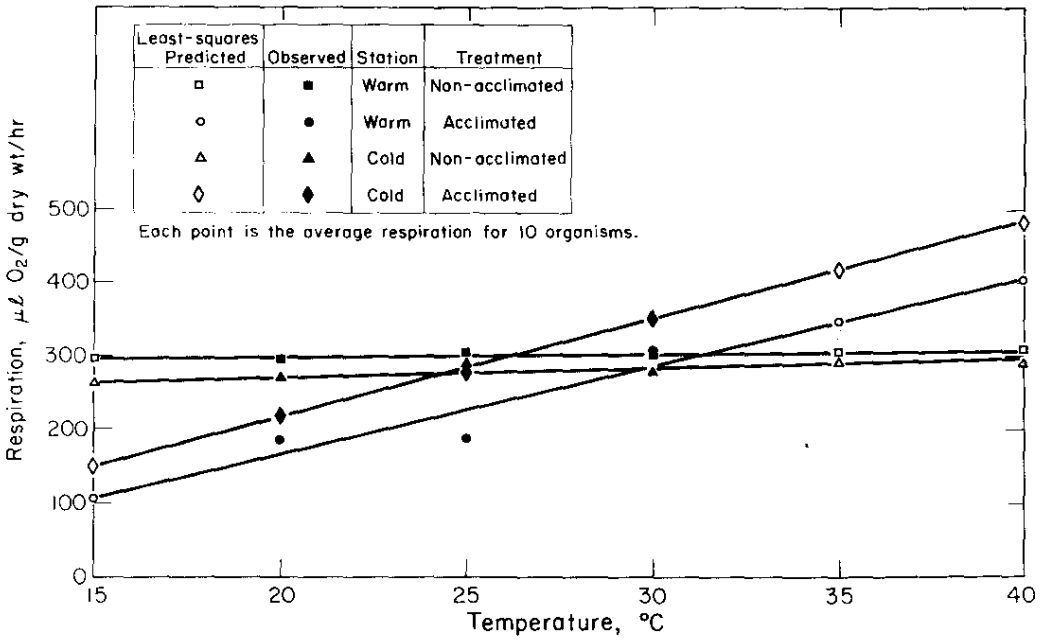

FIGURE 3 Effect of Acclimation on Temperature-Respiration Regression for *H. trivolvis*.

CONCLUSIONS

In view of the variability, these data are not sufficient to attribute the observed species differences in respiratory response to differences in thermal tolerance resulting in a differential distribution of *Helisoma*. Adults of both species show similar respiration rates over a wide range of temperatures and appear to be relatively insensistive to temperature. The effect of acclimation on respiration suggests that -- at least in *H. trivolvis* -- diurnal and temporal fluctuations of temperature in the field enables the organism to function metabolically at a fairly constant level over a wide range of temperatures. This finding makes questionable the applicability of constant temperature acclimation studies to real field situations.

20. THE CRITICAL THERMAL MAXIMA OF SNAILS RAISED IN WARM AND IN COLD WATER †

SUMMARY

Helisoma specimens from a "warm" and a "cold" station in a reactor cooling reservoir were subjected to critical thermal maximum (CTM) tests. The mean temperature at those two locations for the month prior to the beginning of the experiment (May) were chosen for acclimation of the specimens. Evaluation of the CTM results for three separate tests revealed no consistent differences between the CTM of the "warm" and "cold" station snails. The data for three separate determinations are combined in Figures 1 and 2.

The average CTM's after 24 hours acclimation are summarized by species in Table 1. Based on the results of the t-test, at 27.9° the differences between species are significant and at 33.2°C the differences between stations are significant at the 0.05 probability level.

TABLE 1

CTM[a] of *Helisoma* from Par Pond

	Warm Station (No. 2)		Cold Station (No. 6)	
Species	CTM, 27.9°C[b]	CTM, 33.2°C[c]	CTM, 27.9°C[b]	CTM, 33.2°C[c]
H. trivolvis	47.4 ± 0.1 N = 100	47.7 ± 0.1 N = 80	47.3 ± 0.1 N = 32	47.1 ± 0.2 N = 25
H. anceps	-	-	47.0 ± 0.1 N = 87	46.7 ± 0.2 N = 51

a. CTM is defined as the mean of the collective death point temperatures for a species of organisms under given conditions of temperature increase and temperature history.

b. Composite data from July, August, and November determinations.

c. Composite data from July and August.

† Work done by G. B. Johnson.

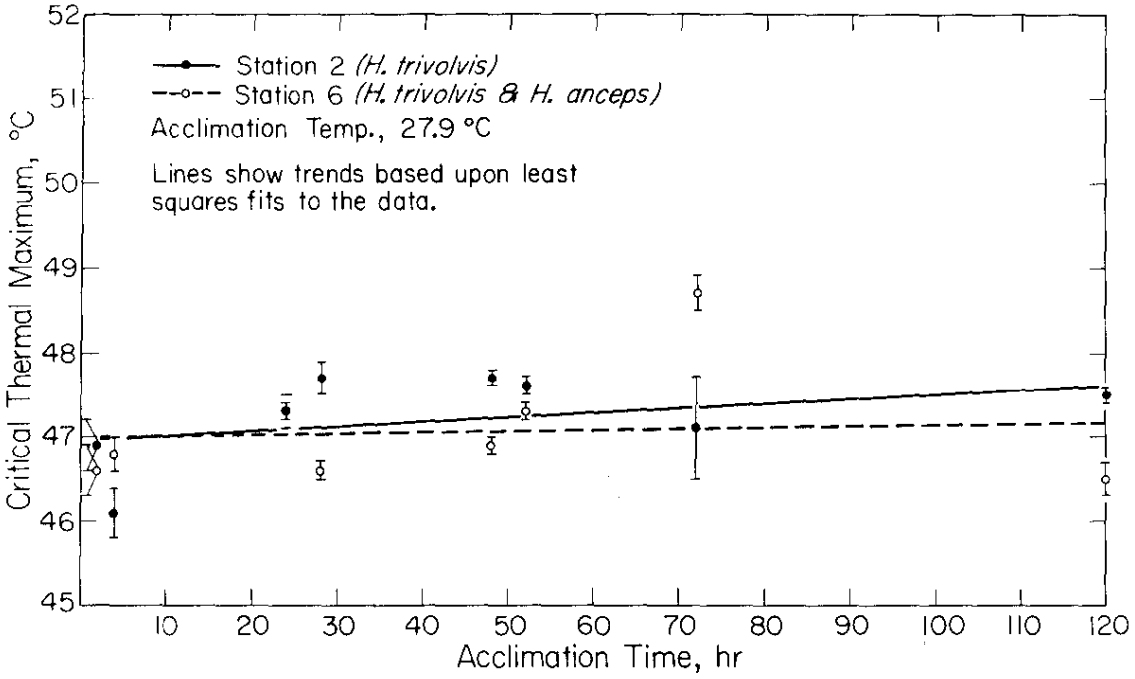

FIGURE 1 Acclimation Curves of Composited CTM Measurements at 27.9°C.

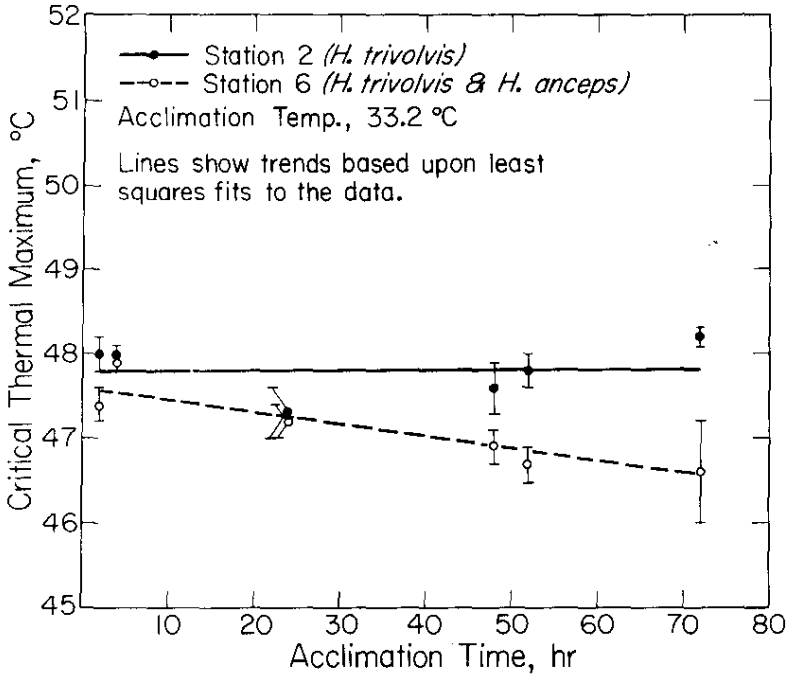

FIGURE 2 Acclimation Curves of Composited CTM Measurements at 33.2°C.

21. THE EFFECT OF DISTANCE FROM THERMAL EFFLUENT AND OF SPECIES ON REPRODUCTION IN HELISOMA SNAILS †

INTRODUCTION

H. trivolvis and *H. anceps* are resident at the "cold" station and only the former at the "warm" station. Samples were collected on May 21, 1974; the snails were marked, placed in "Plexiglas"* enclosures with standard food, and returned to their original stations on the same day.

Initially the rates of egg production (average number of eggs/snail/day) were essentially the same at the two stations (Figure 1). The frequency of egg-laying was initially greater for warm station snails than for "cold" station snails (both species), but the clutch size was smaller. The survivorship of the young that hatched during the first few weeks of the experiment was better for "warm" station organisms than for either of the "cold" station species. At the "cold" station, young *H. anceps* showed a higher survival rate than young *H. trivolvis*.

Reproduction was not quantitatively monitored during the preceding winter. However, based on data taken in conjunction with other experiments, *H. anceps* was less abundant than *H. trivolvis* during the cold months. Density samples taken in the spring also showed this discrepancy (Figure 2). The escalated reproduction in *H. anceps* during the experimental period has resulted in a change in the density ratios of the two species at the "cold" station.

Sixty days after the initiation of the present study, egg production at the "warm" station decreased quite sharply, but continued at a fairly constant rate at the "cold" station for both species. The period of depressed production at the "warm" station corresponds to the peak of summer temperatures in the pond.

In concert with the initial relative increase in the reproduction rate of *H. anceps*, dip net samples showed an increase in the relative density of *H. anceps* and a decrease in the average size of individuals.

---

† Work done by G. B. Johnson.

* Trademark of Rohm & Haas.

The reverse was observed among *H. trivolvis* taken from the "cold" station. During the spring, the relative density of *H. trivolvis* from the "warm" station was higher than the overall density at the "cold" station; but it has now been overwhelmed by the recent recruitment of young of both species at the "cold" station (Figure 2).

The nonsynchronous fluctuations in the populations of *Helisoma* at the two locations suggested that some external factors peculiar to the stations were influencing the population dynamics. Our lab studies have shown a depression of reproduction in winter *H. trivolvis* at 30°C and cessation at 35°C. In the field a similar decrease occurred when "cold" station *H. trivolvis* were enclosed at the "warm" station where temperatures reached that range. The translocated snails ceased ovipositing while "cold" snails enclosed concurrently at the "cold" station exhibited unchanged rates.

Temperature and possibly some secondary factor appears to influence reproduction in *Helisoma* under field conditions. Extensions of the swap design are planned and should reveal with more certainty the effect of temperature on population growth in the field.

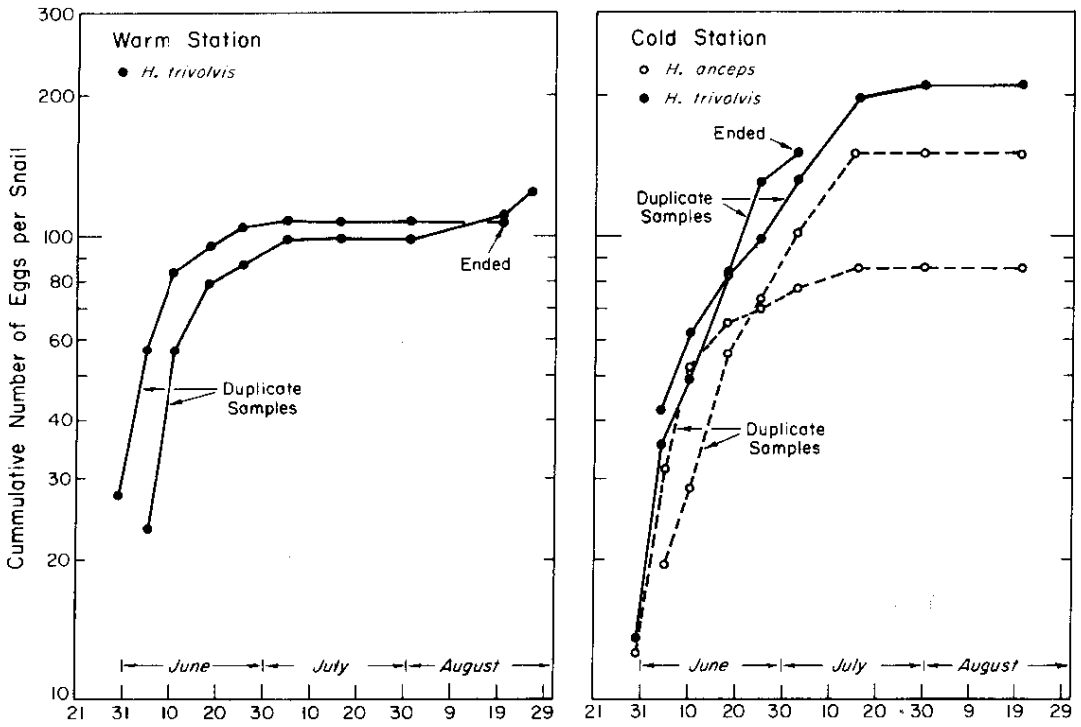

FIGURE 1 Reproduction Curves of *Helisoma* Snails in Par Pond.

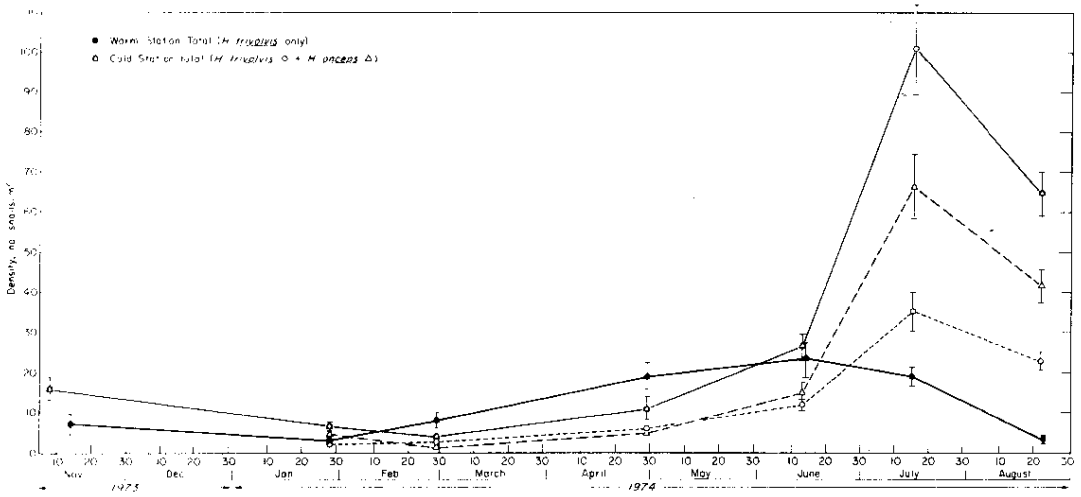

FIGURE 2 Population Density of *Helisoma* Snails in Par Pond.

22. PLANKTON PRODUCTIVITY AS A FUNCTION OF NUTRIENT CONCENTRATION CHANGES OVER A DECADE OF TIME IN A REACTOR COOLING POND†

INTRODUCTION

Par Pond is a 10 km^2 reservoir impounding water from a tributary of the Savannah River, Lower Three Runs Creek, constructed in 1958 for use as a reactor cooling basin by the Savannah River Plant (SRP). A program of limnological research was begun in 1965. A recent examination of unpublished data from some of these studies indicated hitherto unsuspected changes in lake characteristics, including primary productivity and water chemistry, that appear to be related to reactor operations. Par Pond has a mean depth of 6.2 m, a maximum depth of 16 m, a volume of 6.2 x 10^7 m^3, and a shore-line of 57 km. Water color averages about 12.7 Pt-Co units, turbidity, about 1.0 JTU; Secchi transparency 2.5 m; surface temperature, about 22°C; and epilimnion oxygen about 8.6 mg/l^{-1} during a typical year in the main (unheated) body of the lake. Par Pond behaves as a warm monomictic lake, stratifying from April through October and, except in the arm receiving the thermal effluent, is nearly homothermous the remainder of the year. The littoral community of Par Pond is unusually well developed for lakes in this vicinity, probably because water levels remain relatively stable. Large drawdowns due to water consumption do not occur, and deficits are made up with water pumped from the Savannah River.

RESULTS AND DISCUSSIONS

The most striking change was the approximately sixfold increase and subsequent leveling in plankton primary productivity observed from 1965 through 1973 (Figure 1). As illustrated by Figure 2, ^{14}C productivity correlated very highly with conductivity ($r = 0.976$; $p < 0.001$; 6 df). As could be expected, good correlations were also found with total dissolved solids and salinity; however, these were not as strong as for conductivity.

---

† Work done by L. J. Tilly; presented at the *Symposium on Mineral Cycling in Southeastern Ecosystems* in Augusta, Georgia, May 1-3, 1974.

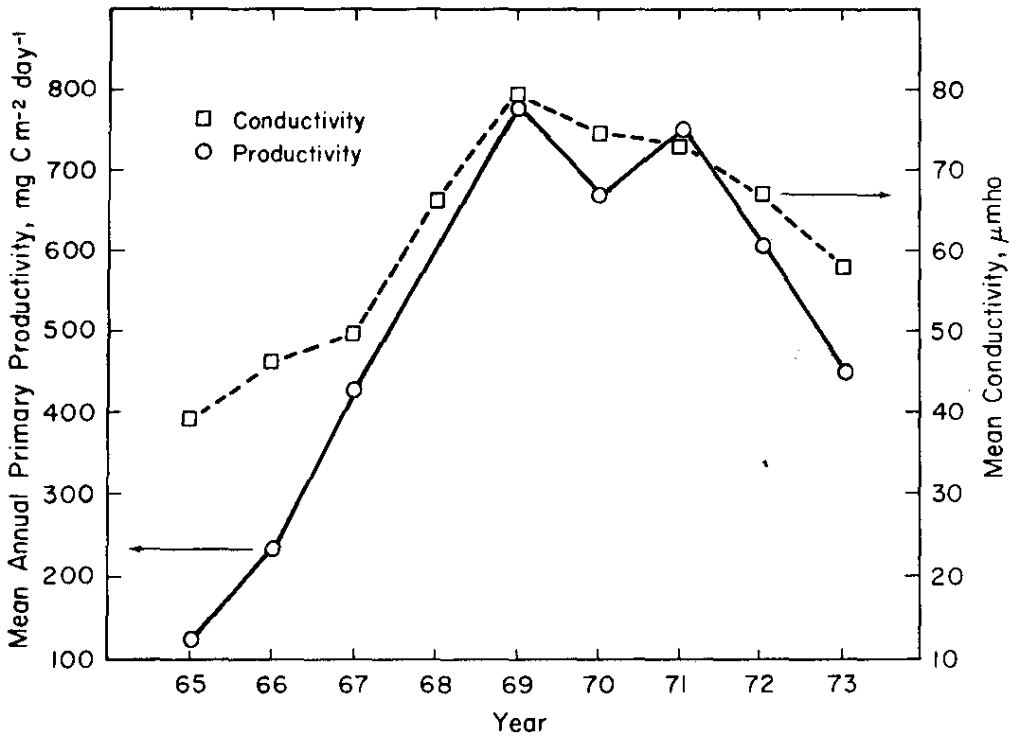

FIGURE 1. Conductivity and Annual Plankton Productivity in Par Pond (1965-1973)

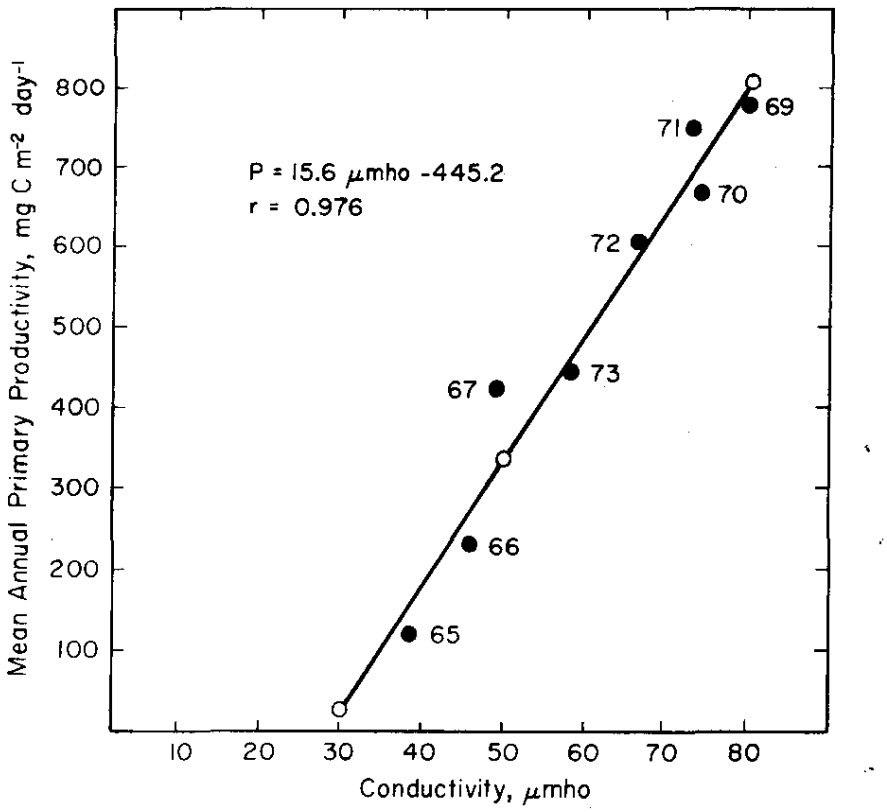

FIGURE 2. Plankton Productivity vs Conductivity of Par Pond

Productivity correlated significantly with all major cations and anions except chloride and magnesium. A negative correlation was found between productivity and silica. Data were inadequate for computing correlations with phosphorus or nitrogen.

The productivity increase clearly appears to be a function of a general increase in nutrients. Two closely-related aspects of reactor operation appear to be involved: use of Savannah River water in makeup additions, and progressive evaporative concentration of recycled cooling water.

Savannah River water is continuously added at the reactor to recirculated Par Pond water before passing through the heat exchangers. Relative volumes added per year from 1966-1973 are included in Table 1. River water added annually has ranged from volumes equivalent to 0.36 to 1.25 times the average annual rainfall to the (93×10^6 m^2) Par Pond drainage basin and from 3 to 10 times the volume of direct rainfall into the lake. Considering the magnitude of makeup additions, it is not surprising that Par Pond water resembles Savannah River water in composition and ionic concentrations. Except for Cl^- and HCO_3^- ions, concentrations of major ions in Par Pond correlated significantly with those from the Savannah River. Conductivities of the two systems correlated significantly. The upward trend in Par Pond concentrations is in response to a similar steady increase in Savannah River concentrations.

The changes in Savannah River water are probably associated with changes in the industrial and municipal pollution of the river upstream of the Savannah River Plant (SRP). Degradative alterations in the condition of the river upstream of the SRP noted circa 1969 are documented in a series of reports by the Institute of Paper Chemistry (1960 through 1973)[1] and by The Academy of Natural Sciences of Philadelphia (1952 et seq.).[2] The recent period of leveling and decline of nutrient concentrations and productivity in Par Pond is coincident with the establishment of several primary and secondary waste treatment facilities along the Savannah River above SRP.

Although it is clear from the foregoing information that makeup additions are a dominant source of nutrients to the reservoir, there is some evidence that more than just nutrient import is involved in the observed eutrophication. Productivity : concentration correlations are weaker when computed in relation to Savannah River water than in relation to Par Pond. Stronger evidence comes from ratios of Par Pond concentrations/Savannah River concentrations. Ratios calculated for the 1965-1970 interval show a general increase with average values exceeding 1.0 during the period of highest productivity (and conductivity) and lowest makeup water additions.

TABLE 1

Par Pond Annual Averages of Monthly Means of Epilimnion 0-7 Means or Composites

Inorganic Ion Concentrations:	Year 1965	1966	1967	1968	1969	1970	1971	1972	1973
Ca, mg ℓ^{-1}	2.07±0.12	1.95±0.14	2.11±0.10	2.68±0.30	3.18±0.32	3.74±0.27	3.37±0.22	3.28±0.16	3.28±0.22
Mg, mg ℓ^{-1}	1.20±0.14	1.24±0.04	1.24±0.02	1.23±0.03	1.67±0.13	1.38±0.02	1.19±0.04	1.13±0.03	0.96±0.03
Na, mg ℓ^{-1}	3.77±0.14	5.33±0.24	6.40±0.09	6.51±0.11	7.75±0.22	7.63±0.09	6.73±0.23	6.29±0.14	5.29±0.24
K, mg ℓ^{-1}	1.10±0.03	1.17±0.06	1.35±0.03	1.32±0.03	1.50±0.04	1.56±0.04	1.30±0.04	1.34±0.08	1.14±0.11
Cl, mg ℓ^{-1}	1.84[a]	3.9[b]	4.7±0.2	6.4±1.0	7.0±1.1	18.8±5.4	9.5±2.6	8.4±1.7	5.2±0.5
SO_4, mg ℓ^{-1}	1.73[a]	2.0[b]	4.1±0.5	3.4±0.5	5.3±1.4	5.1±0.7	3.4±0.5	4.3±1.1	3.6±0.3
HCO_3, mg ℓ^{-1}	17.5[a]	17.0	17.8±0.6	17.4±0.6	22.1	22.7	22.4±0.3	20.4±0.4	16.9±0.5
Si, mg ℓ^{-1}	-	2.87±0.24	2.99±0.16[c]	2.30±0.43	1.75±0.10	0.87±0.09	1.72±0.17	2.45±0.11	1.8±0.3
PO_4-P, µg ℓ^{-1}	-	-	-	-	11±2	6±2	6±2	12±2	10±3
NO_3-N, µg ℓ^{-1}	-	-	-	-	15±3	39±11	33±10	10±2	16±2
Physical Measurements:									
Salinity, mg ℓ^{-1}	29.2[a]	37.6	37.8	38.9	48.5	50.9	49.4	45.7	36.6
Conductivity, µmho cm^{-1}	56.5	45.7	49.2	66.0	79.2	74.4	73.0	66.5	57.6
TDS, mg ℓ^{-1}	31.5	36.7	37.1	42.7	47.4	51.7	46.5	44.5	35.6
NVDS, mg ℓ^{-1}	25.4	29.0	27.5	31.1	34.6	38.1	34.1	31.2	22.2
VS, mg ℓ^{-1}	13.7	11.7	9.6	10.4	12.8	13.6	12.4	13.3	13.4
Rainfall, in.	45.04	48.96	47.63	37.71	38.64	43.80	59.90	46.80	55.71
Relative makeup water		3.452	3.488	1.453	1.000	1.156	1.070	1.126	1.096
Relative water replacement		1.870	1.855	1.110	1.000	1.138	1.417	1.194	1.448
Biotic Measurements:									
Plankton Productivity, mg C (m^{-2} day^{-1})	318	229[d]	424		777	663	746	604	443
Centrifuge seston, (ash-free), mg ℓ^{-1}	0.78	1.02	0.90	0.71	0.75	0.76	0.50	0.74	0.73
Net seston (ash-free), mg ℓ^{-1}	0.22	0.34	0.12	0.30	0.23	0.15	0.11	0.04	0.07

a. Data from E. St. John, SRP; supplemented by information from routine monitoring.

b. April - August mean only.

c. Mean of 8 months; June - January.

d. Mean of three November experiments; combining the average rates (± 1σ) for 1968, 1969, and 1970.

REMARKS:

Except where noted, mean values are annual averages of epilimnion samples with monthly values equally weighted. Salinity is computed following Hutchinson (1957). Rainfall data are averages of data from measurements at two gages located within two miles of the lake at 100-P and Barricade 3.

Relative makeup water is the ratio of total makeup water added in any year to the amount added in 1969.

Relative water replacement is the total water calculated to be delivered to Par Pond from rainfall, runoff, and makeup additions divided by the lowest sum recorded. Blanks indicate missing data.

NVDS is nonvolatile dissolved solids; TDS is total dissolved solids; VS is volatile solids.

A few bioassay experiments were conducted in 1971 using 10X evaporative concentrates of Par Pond water. Additions of 100 ml of concentrate to bottles of Par Pond plankton from 2 m resulted in an average increase in ^{14}C uptake of 23% over controls. Together, these observations suggest that evaporative concentration of Par Pond water occurs during recirculatory cooling, and that resultant increases in nutrients are stimulatory to primary productivity.

REFERENCES

1. *A Biological Study of the Savannah River in the Vicinity of Augusta, Ga.* Reports Nos. 2 through 6, The Institute of Paper Chemistry, Appleton, Wis. (1960 through 1973).

2. *Savannah River Biological Survey, South Carolina and Georgia, for the E. I. du Pont de Nemours and Co. Savannah River Plant.* Academy of Natural Sciences of Philadelphia, Dept. of Limnology, Philadelphia, Pa. (1952 through 1973).

23. PERIPHYTON COLONIZATION AND PRODUCTIVITY AS A FUNCTION OF REACTOR EFFLUENT TEMPERATURES †

INTRODUCTION

Studies of the growth of periphyton on glass slides have been under way for more than a year at Par Pond, a 2500-acre cooling reservoir on the Savannah River Plantsite in South Carolina. Par Pond has been used since 1958 to dissipate thermal discharges from production reactors. Seven collection stations (Figure 1) have been sampled for periphyton at two-week intervals since March, 1972.

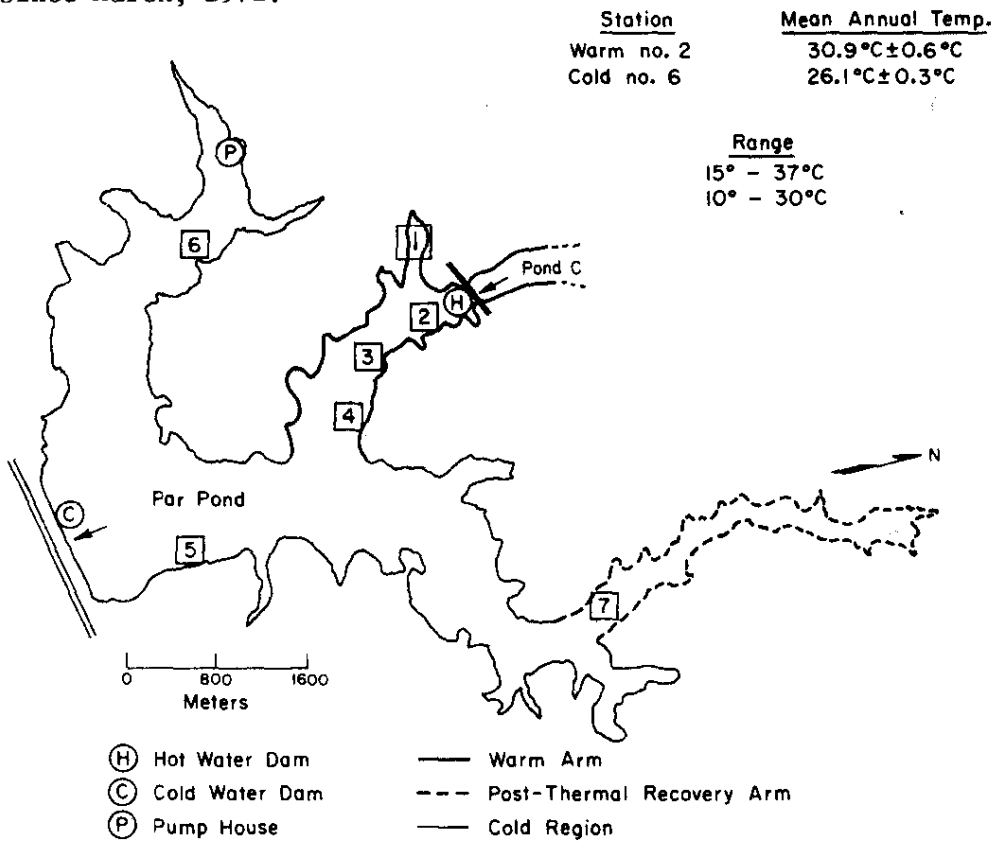

FIGURE 1. Par Pond, Showing Sampling Stations and the Mean Temperatures of a Warm and a Cold Station

†Work done by L. J. Tilly, presented at the *Thirty-fifth Annual Meeting of the Association of Southeastern Biologists* at the Desoto Hilton Hotel, Savannah, Georgia, on April 18-20, 1974.

RESULTS AND DISCUSSION

A summary of annual means for some of the biotic measurements is presented in Table 1. Results from three experiments (Figure 2) show the relation between (1) the average periphyton accumulated per square meter of artificial substratum (glass microscope slides) in a two-week interval ending on the date indicated, and (2) the average water temperature measured at each station during the growth interval. The lines in Figure 2 represent least-squares fits of the data with periphyton biomass plotted on a logarithmic scale. In 19 of 25 experiments analyzed for 1973, a significant or highly significant relationship was found between periphyton production and mean growing temperature. Figure 2 shows the slopes of regression lines roughly parallel, while intercepts differed greatly among experiments.

TABLE 1

Periphyton Annual Means

Collecting Station	1	2	3	4	5	6
Dry Weight, mg m^{-2}	2.32 ±0.30	4.45 ±0.91	2.69 ±0.32	1.93 ±0.24	0.62 ±0.12	0.53 ±0.09
Chlorophyll, mg m^{-2}	4.44 ±0.92	9.34 ±1.74	5.85 ±1.21	3.42 ±0.72	0.51 ±0.13	0.27 ±0.06
Diatom Density, cells mm^{-2}	518.8 ±98	1016.8 ±245.8	-	679.0 ±187.2	-	187.4 ±67.8
Number of Diatom Species Observed	54.8 ±5.1	57.2 ±5.6	-	54.4 ±4.4	-	48.3 ±4.2
Diatom Dominance, %	87.6 ±2.6	85.9 ±2.9	-	87.0 ±3.2	-	86.7 ±3.3
Growing Temperature, °C	25.59 ±1.31	26.78 ±1.30	25.17 ±1.31	25.18 ±1.33	23.24 ±1.36	22.89 ±1.36

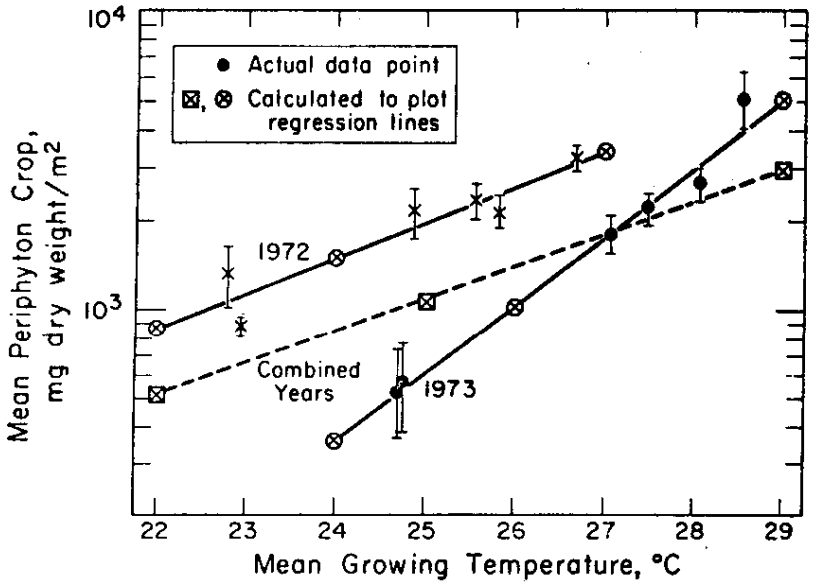

FIGURE 2. Periphyton Growth *vs* Water Temperature for March through December, 1972 and 1973

When data from all experiments were composited for regression and correlation analysis, the evidence for temperature dependence vanished. If all such data are reduced to means for temperatures and standing crop yields, and these are examined statistically, a highly significant relationship between average periphyton accumulation and growing temperatures is found (Figure 3). The correlation coefficient associated with these data is 0.995 (with 5 degrees of freedom; significant at the 0.001 level). The slope and intercept of the regression line are 0.528 and -13.69, respectively.

Is the regression relationship useful in prediction? Data from equivalent intervals in 1972 were compared with those from 1973 (Figure 3). Predictions for 1973 based on the 1972 regression relation averaged about 120% higher than the values actually observed.

The fact that consecutive experiments were often found to yield greatly different ranges of periphyton accumulations for little-different ranges of temperature reinforces the idea that factors other than temperature may be at work. The data are being examined for direct evidence that differences in light, assorted nutrients, and/or species composition, as well as temperature, account for the observed patterns of periphyton crop accumulation in Par Pond.

Whatever the causes, periphyton crops apparently accumulate more rapidly nearer the thermal effluent. This implies that a food-chain imbalance has occurred. Carbon-14 studies conducted concurrently, and to be reported elsewhere, show that the warm station periphyton is more productive per unit weight and per unit area of substratum covered than cold station periphyton.

Other observations suggest that during the summer, at least grazing intensity is lower at the warm station.

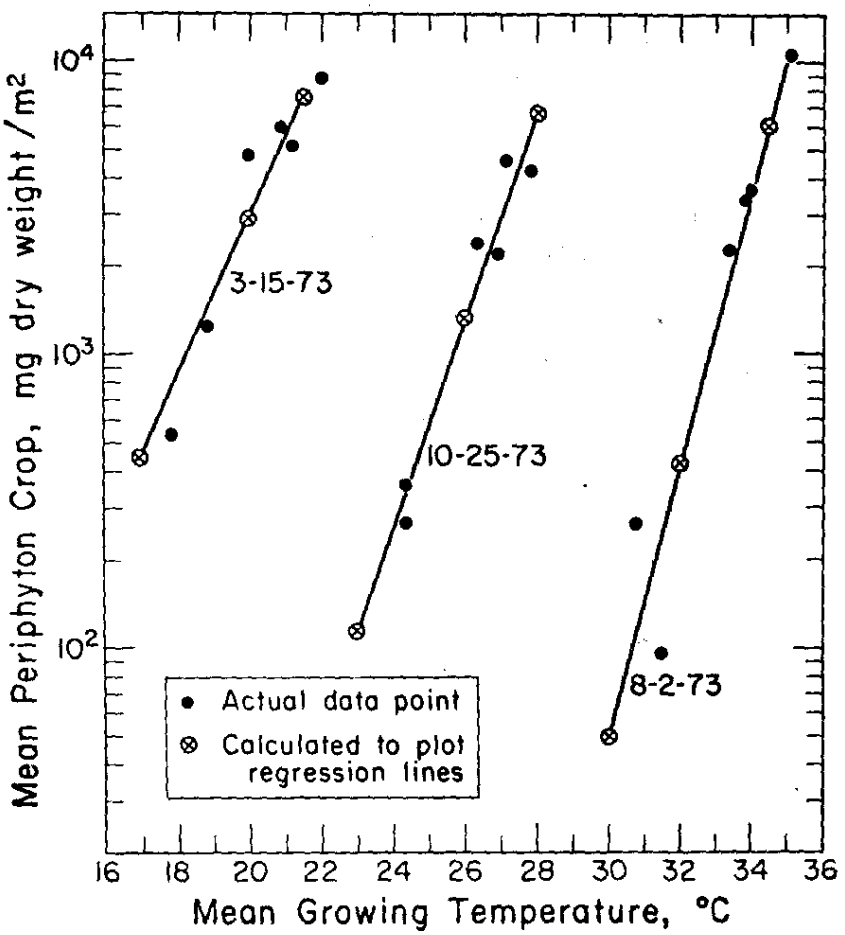

FIGURE 3. Periphyton Growth *vs* Water Temperature for Two-week Periods in March, August, and October, 1973

24. BASELINE STUDIES OF THE BIOTIC AND ABIOTIC FACTORS OF UPPER THREE RUNS CREEK AND SIX EXPERIMENTAL STREAMS IN THE THERMAL EFFECTS LABORATORY †

INTRODUCTION

The Thermal Effects Laboratory[1] on the banks of Upper Three Runs Creek on the Savannah River Plant, is an aquatic research facility with six experimental streams for studying the long-term effects of slight elevations in water temperature on the ecology of stream organisms. Although the facility was completed in October 1971,[2] the experimental streams will not be heated until early spring 1975. This allows time for the establishment of stable populations in the streams, testing of control systems, and determinations of seasonal variations in diversity, population density, and productivity of various species of algae and insects under natural conditions.

THE PARENT STREAM

Upper Three Runs Creek was selected as the source stream for water, substrates, and organisms because of its excellent water quality and wide diversity of plant and animal species. It is a soft black-water stream, typical of those found in the Atlantic Coastal Plain. The streambed is shaded by thick stands of alder, gum, hickory, and oak along the banks of the stream. Adjacent to the laboratory, the creek is approximately 50 feet wide. During low flow periods in the summer, the water is about 3 feet deep with a mean current velocity across the stream of 1.1 feet/second. Seasonal variations in the chemical and physical characteristics of the stream are shown in Table 1.

The biota of Upper Three Runs Creek were sampled intensively during the baseline studies to determine the structure and composition of the algae and aquatic insect communities. It was anticipated that algae and insect drift in the creek would colonize and continually reseed the experimental streams of the Thermal Effects Laboratory.

† Work done by R. S. Harvey.

TABLE 1

Mean Physical and Chemical Characteristics of
Upper Three Runs Creek

	JUNE 1973 - MAY 1974			
	Summer	Fall	Winter	Spring
Feet above sea level	125.0	124.5	124.9	124.5
Temperature, °C	21.7	17.8	12.5	17.1
Dissolved Oxygen, mg/ℓ	6.8	7.9	9.0	8.1
Bio. Oxygen Demand, mg/ℓ	1.1	1.2	1.9	1.2
pH	6.3	6.6	6.4	6.4
Alkalinity, mg/ℓ $CaCO_3$	2.5	4.4	3.2	3.2
Conductivity, µmho/cm	23.8	26.0	26.5	23.9
Turbidity, JTU	7.0	2.7	3.4	4.1
Calcium, mg/ℓ	0.93	0.87	1.20	1.37
Magnesium, mg/ℓ	0.30	0.31	0.24	0.27
Iron, mg/ℓ	0.33	0.25	0.22	0.71
Silica, mg/ℓ	5.2	2.7	3.4	3.0
Chlorides, mg/ℓ	2.0	2.0	2.1	2.2
Sulfates, mg/ℓ	1.1	1.7	2.0	1.6
Ammonia (N), mg/ℓ	0.02	0.01	0.02	0.02
Nitrate (N), mg/ℓ	0.34	0.10	0.11	0.14
Total Phosp (P) mg/ℓ	0.09	0.03	0.03	0.04

Attached algae were very common in open areas of the stream. Diatoms were most abundant with *Eunotia*, *Gomphonema*, and *Tabellaria* being dominant. The most common green algae were *Spirogyra*, *Oedogonium*, *Mougeotia*, *Draparnaldia*, and *Stigeoclonium*. The yellow-green alga *Vaucheria* was common on the sandy bottom. Three red algae *Tuomeya*, *Audouinella*, and *Batrachospermum* were present, but not in great abundance. The blue-green algae represented by *Oscillatoria*, *Schizothrix*, and *Microcoleus* were very scarce.

Aquatic insects were collected from as many different habitats as possible in Upper Three Runs Creek and from two of its main tributaries, Tinker Creek and Mill Creek. Both Upper Three Runs and Tinker Creeks had large areas of sand, soft silt, and occasional patches of rock substrate. Mill Creek was much smaller and rocky areas were not evident in the areas sampled. All streams contained logs, sticks, and limbs which were excellent substrates for many insects. The mayflies, represented by 27 species, were very common in all tributaries. *Hexagenia*, *Isonychia*, *Dolania*, and *Stenonema* were the most common genera in Upper Three Runs Creek. Caddis flies (27 species) were equally diverse; *Triaenodes*, *Molanna*, *Pycnopsyche*,

Hydropsyche, and *Phylocentropus* were well represented. The most common stoneflies were *Togoperla*, *Pteronarcys*, *Acroneuria*, and *Perlesta*. Twenty-six species of midges were found in Upper Three Runs. Dragonflies, damselflies, spongilla flies, and aquatic bugs were represented by fewer species.

THE EXPERIMENTAL STREAMS

The streams of the Thermal Effects Laboratory differ from other artificial stream systems in that: (1) the streams are inside a glasshouse so that they receive natural illumination with the same diurnal and seasonal patterns of sunlight as the parent stream (2) organisms are seeded naturally on substrates in the study channels by a once-through flow (50 gpm) of creek water through each stream, and (3) the influent water to four of the six streams can be heated to approximate the thermal discharges of nuclear power plants.

For the past two years, unheated creek water has flowed (50 gpm) once-through each experimental stream, transporting plants and animals into and out of the system. Throughout this period, various physical and chemical parameters were measured, artificial substrates were tested, and the biota were sampled intensively to compare the six experimental streams. Physical and chemical data showed that the creek water was not changed significantly by its passage through the Thermal Effects Laboratory, and that the six streams were not significantly different from each other.

Glass slides in diatometers,[3] acrylic plates, PVC plates, and styrofoam blocks were tested to determine the best artificial substrate for collecting diatoms and other algae in the experimental streams. Styrofoam blocks showed most growth and diversity. However, styrofoam was not chosen as a long-term substratum because: (1) it is bulky and tends to restrict flow in the experimental streams, (2) it floats and is difficult to anchor securely in the current, and (3) its surface is very difficult to clean of total algae. Glass slides in diatometers were adopted as test substrates for comparing the dominance and relative abundance of diatoms in the six streams because their data can be more reliably treated statistically. None of the substrates tested indicated good predictability for algae other than diatoms.

Nylon bottle brushes and plate samplers, placed in the experimental streams, collected insufficient numbers of immature insects for interstream comparisons. Once each season, larvae and nymphs from various habitats and niches in the experimental streams were sampled intensively to compare species diversity under natural conditions. Sample numbers for individual species were too low to compare species diversity for a particular group of insects. However, pooled data for all of the insects collected

from a given stream were adequate to show that the six streams were not significantly different in total number of species of all represented orders present. Total numbers of species have also been used in stream drift studies to show that all six streams have equal opportunity to be colonized or reseeded with aquatic insects.

CONCLUSION

The six experimental streams of the Thermal Effects Laboratory have been naturally colonized with plants and animals native to Upper Three Runs Creek. Physical, chemical, and biological parameters have been tested statistically to determine their variability and measure the extent to which the six streams differ under natural conditions. A heat stress, causing mixed water temperatures of 0, 2.5, 5, 7.5 and 10°F above ambient creek water temperatures, will be placed on the system in early 1975 when temperature control equipment is installed.

REFERENCES

1. R. S. Harvey. "A Flowing Stream Laboratory for Studying the Effects of Water Temperature on the Ecology of Stream Organisms." *ASB Bulletin 20: No. 1* (1973).

2. R. S. Harvey and D. Randall. "Measuring the Environmental Effect of Thermal Discharges." *Du Pont Innovations, 6(4),* 1-6 (1974).

3. R. Patrick, M. H. Hohn, and J. H. Wallace. "A New Method for Determining the Pattern of the Diatom Flora." *Notulae Naturae: Acad. Nat. Sci. Phila. 259*, 1, (1954).

25. TEMPERATURE EFFECTS ON GROWTH AND RESPIRATION RATES OF *DOLANIA AMERICANA* (EPHEMEROPTERA)†

INTRODUCTION

The experimental streams of the Thermal Effects Laboratory (Figure 1) are being used to study the long-range effects of nonlethal elevations in water temperature (analogous to power plant discharges) on the ecology of stream organisms. Upper Three Runs Creek is the source of water, substrates, and organisms for the experimental streams. The effects of elevated water temperatures on apparent growth and respiration rates of the sand-burrowing Mayfly, *Dolania americana* (Ephemeroptera), are reported here.

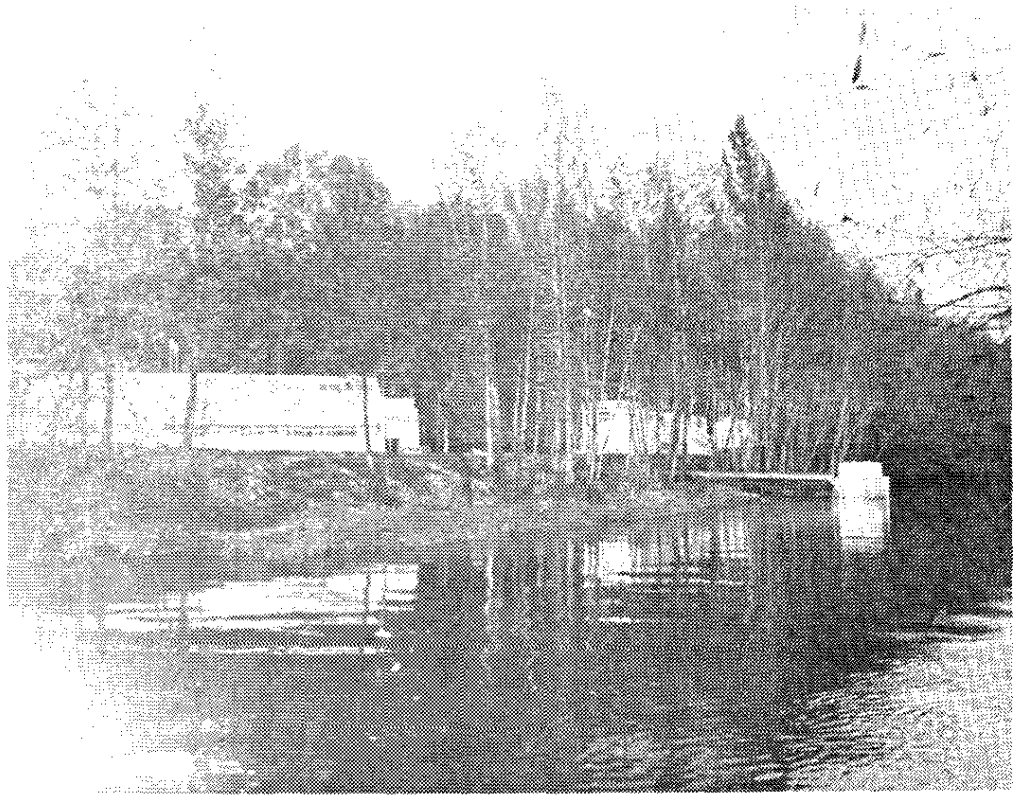

FIGURE 1. SRL Thermal Effects Laboratory

† Work done by R. S. Harvey.

Dolania, common in Upper Three Runs Creek, is apparently restricted to sandy substrates of black-water streams. In the United States, *Dolania* have been reported in only three other streams, all located in Florida. The nymphs are very hairy, and this supposedly keeps the sand away from their bodies. The gills, instead of being in the usual dorsal or lateral position, are ventral and boxed in on each side by the legs.[1] *Dolania* were selected for detailed preoperational studies because: (1) so much of the subtrate of Upper Three Runs Creek is sand, (2) *Dolania* are dominant sand-burrowing macroscopic animals, (3) information is needed on the effects of water temperature on the oxygen consumption rates of benthic species, and (4) information is needed on the biology of *Dolania americana*.

METHODS

A modified Needham scraper, covered with 14-mesh stainless steel screen wire, was used to collect *Dolania* from the stream. Smaller nymphs were generally found in fine sand near the edge of the stream, and larger specimens were collected from the coarser sand of the channel. The first 18 specimens collected each week were assumed to represent the mixed population.

Oxygen consumption measurements were made with a Gilson Medical Electronics - Submarine Respirometer, Model SGRP 20 (Figure 2). Prior to each test, 20 reaction vessels were one-third filled with washed creek sand and covered with filtered creek water. One milliliter of a 20% solution of potassium hydroxide (KOH) was placed in each reaction vessel side bulb to absorb the carbon dioxide (CO_2) given off during the experiment, and a single *Dolania* nymph was added to each of 18 vessels, leaving two vessels as blanks. After acclimation at ambient creek water temperature, oxygen consumption was measured for all specimens every half-hour over a three-hour period. Waterbath temperatures were gradually raised 5°C above ambient creek water temperature. Specimens were acclimated overnight at the higher temperatures before oxygen consumption measurements were repeated. Otherwise, procedures and calculations in this study followed those set forth by Umbreit, et al. (1972).[2]

RESULTS

Individual specimens were weighed to determine the apparent growth rate of the *Dolania* population collected adjacent to the laboratory. Nymphs were weighed immediately following the final respiration measurements, and again after drying for 24-hours at 100°C. Dry weights averaged 14.8% of the live weights for all specimens. Mean dry weights for both males and females increased steadily from September through May as second-year nymphs matured

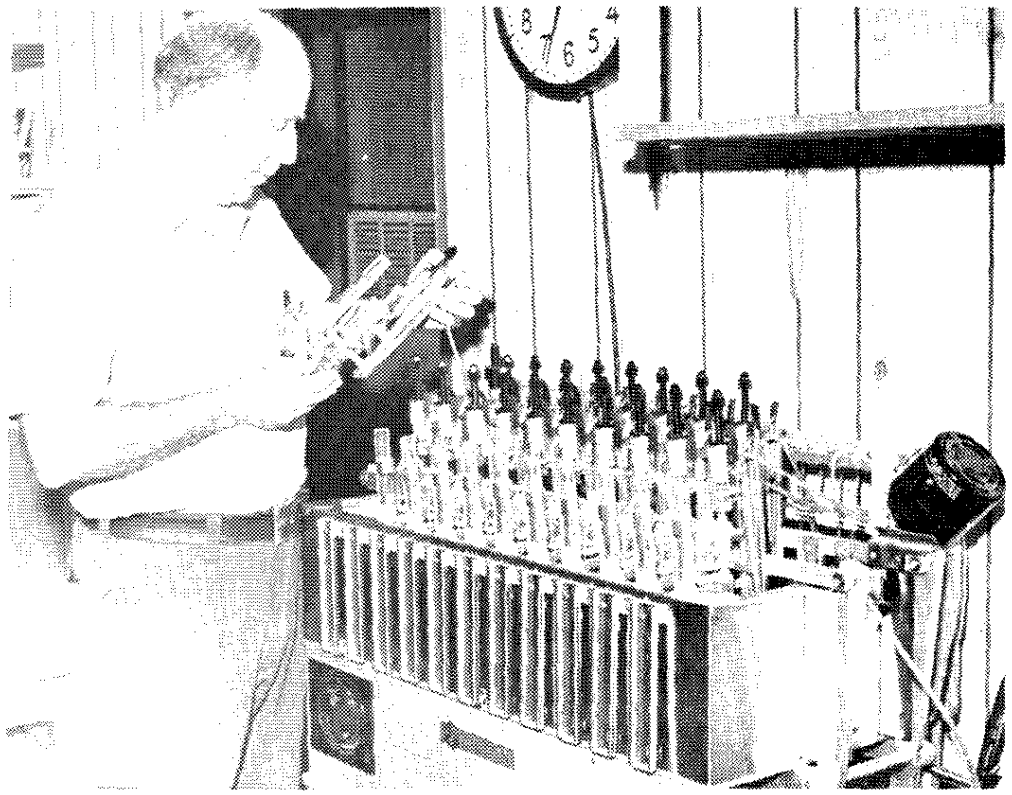

FIGURE 2. R. S. Harvey Inspecting Gilson Respirometer

and mean weights were reduced sharply in June and July as subimagoes emerged from the stream leaving only first-year nymphs behind (Figure 3).

The 389 specimens collected during the report period were arbitrarily placed into eight weight classes to determine the correlation between prothorax width and body weight. A linear correlation existed (Figure 4). Although not broken down by sex, the correlation coefficient was 0.9596 for males and 0.8775 for females. This relationship enabled respiration rates to be studied with cohort populations from early instars to subimagoes in the experimental streams of the Thermal Effects Laboratory without having to tissue-dry and weigh each specimen.

Oxygen consumption rates were directly proportional to water temperature for all weight classes (Figure 5). Smaller nymphs generally consumed oxygen at higher rates than larger specimens, and water temperatures 5°C above ambient caused slightly higher respiration rates for most *Dolania*. Edward,[3] in studies with *Chironomus* larvae, also found a progressive decrease in oxygen consumption per unit weight as the size of the animal increased.

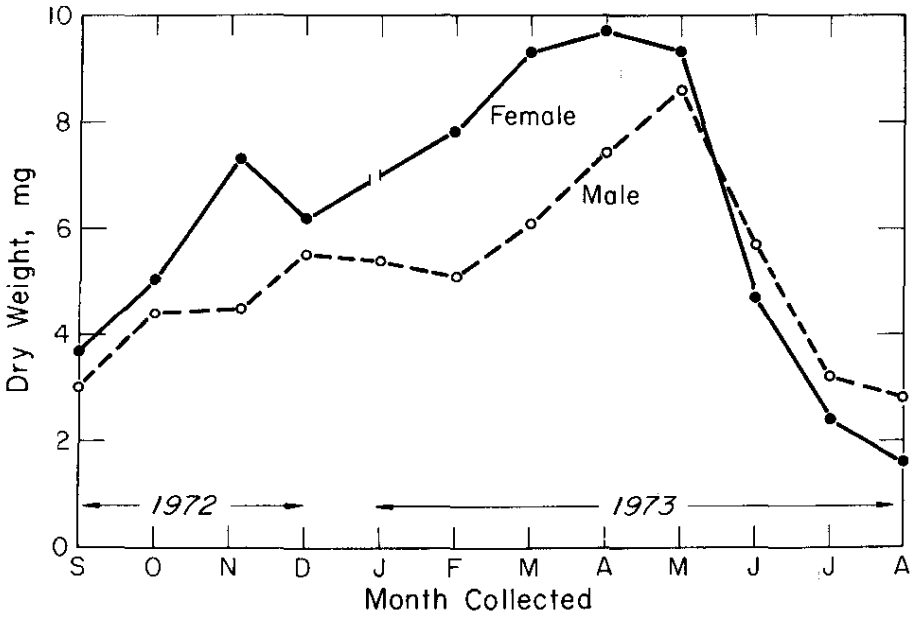

FIGURE 3. Growth of *Dolania* Nymphs

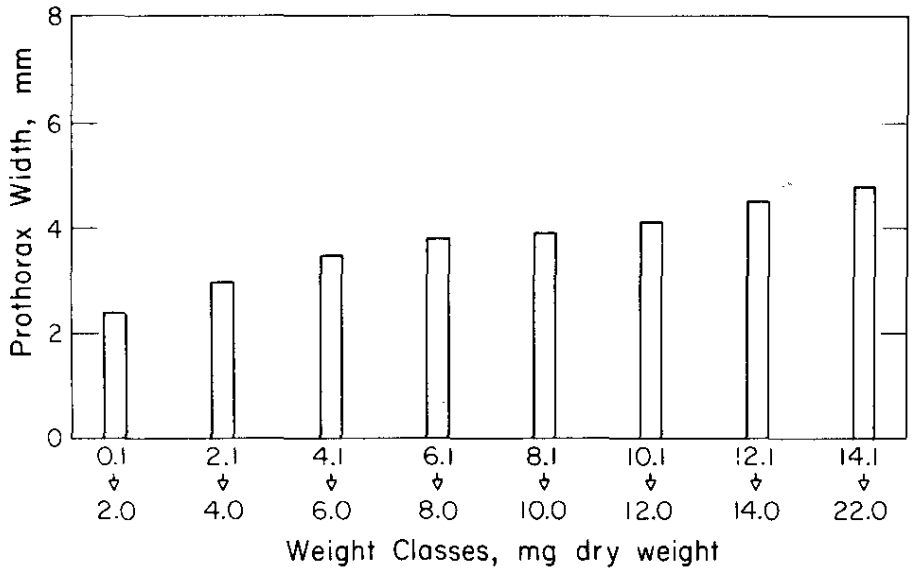

FIGURE 4. Correlation Between Prothorax Width and Body Weight of *Dolania* Nymphs

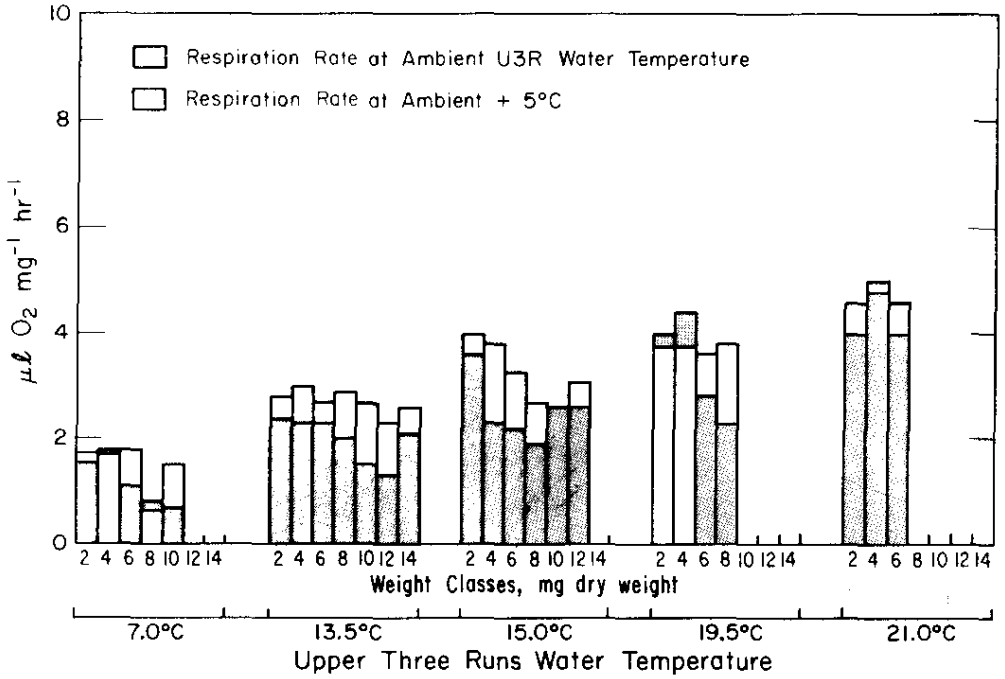

FIGURE 5. Correlation Between Oxygen Consumption, Water Temperature, and Body Weight of *Dolania* Nymphs

The effects of added heat stress on *Dolania* respiration are most apparent when examined for a single weight class. Oxygen consumption rates at 5°C above ambient water temperatures averaged about 15% higher than rates at ambient temperatures (Figure 6). However, seasonal patterns of respiration were not altered by the higher temperature. Respiration rates of the 4 to 6 mg weight class (Figure 7) increased steadily as the water temperature of Upper Three Runs creek increased.

REFERENCES

1. G. F. Edmunds and J. R. Traver. "The Classification of the Ephemeroptera I. Ephemeroidea: Behningiidae." *Ann. Ent. Soc. Amer. 52*: 43-51 (1959).

2. W. W. Umbreit, R. H. Burris, and J. F. Stauffer. *Manometric Biochemical Techniques*, 5th Ed., Burgess, Minneapolis, Minn. (1972).

3. R. W. Edwards. "The Relation of Oxygen Consumpton to Body Size and to Temperature in the Larvae of *Chironomus riparius* Meigen." *J. Exptl. Biol. 35*, 314-358 (1958).

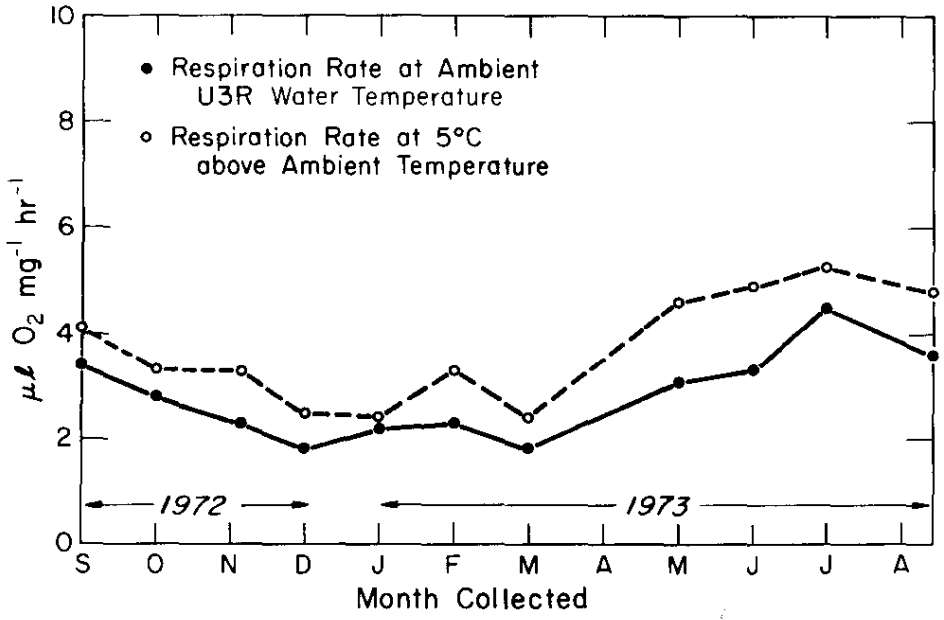

FIGURE 6. Seasonal Variation of Respiration Rates of *Dolania* Nymphs

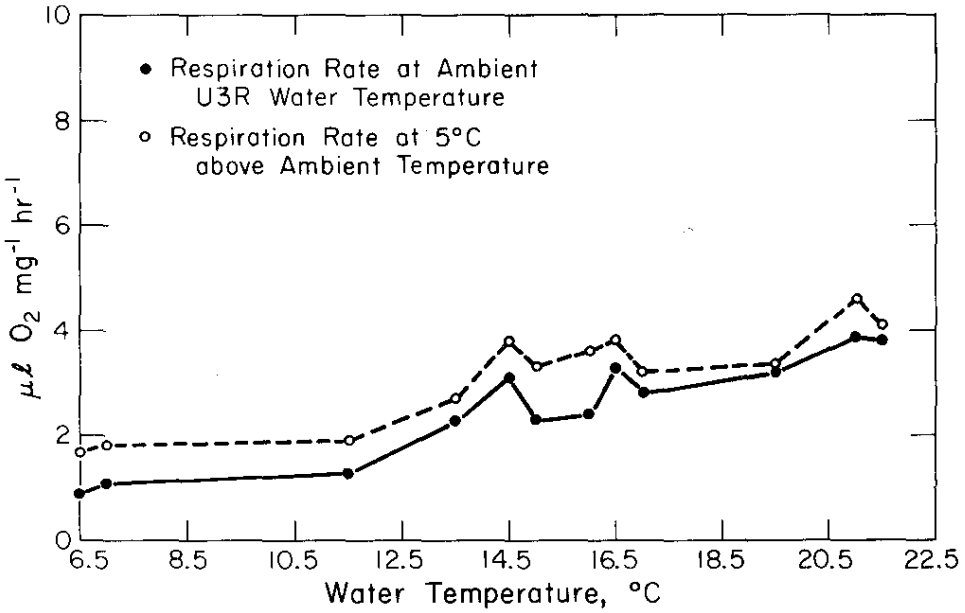

FIGURE 7. Correlation Between Water Temperature and Body Weight of *Dolania* Nymphs (4 to 6 mg class)

IV. SEISMIC EFFECTS

Seismic effects are being studied to develop an understanding of how earthquake shock waves are transmitted and attenuated through the solid earth characteristic of the southeastern United States. The studies are of an environmental and not an engineering nature. Current seismic literature, locally and nationally, was reviewed to determine the significance of recent advances in seismic research. This knowledge is necessary to develop a research program for determining the environmental effects of earthquakes in the southeastern United States.

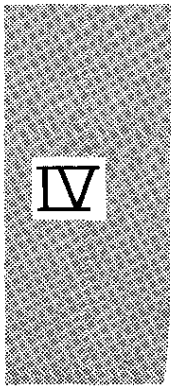

26. THE APPLICATION OF RECENT SEISMIC RESEARCH TO THE EVALUATION OF SEISMIC RISK IN THE SOUTHEASTERN UNITED STATES†

INTRODUCTION

In recent years, seismic research has increased greatly nationally and internationally, as well as in the southeastern United States. In addition, site reviews for power reactor locations as well as nuclear fuel reprocessing plants have brought a greater awareness of seismic risks. This paper reviews recent and on-going research relevant to evaluation of seismic risk in the southeastern United States.

USE OF HISTORICAL INFORMATION

Information about earthquakes for the southeastern region has, historically, come from scientific compilations of intensity (effects on people and structures), information from newspaper accounts, personal interviews, and inspection of structures. In the more recent past, information has come from observatory seismographs in Atlanta, Georgia; Blacksburg, Virginia; Washington, D. C.; and several other locations in the Southeast.

This historical information has been used by Bollinger[1] to develop recursion graphs for South Carolina as shown on Figure 1. Although the data are from South Carolina, they overwhelmingly reflect activity in the Charleston area (402 earthquakes as opposed to 36 elsewhere in South Carolina), and thus extrapolations are applicable primarily to that area. On the graph shown on Figure 1, the recursion interval for intensity X (that given the 1886 Charleston earthquake) is once in 330 years. The fact that the lone data point for this intensity is not on this line indicates that either it has not reached its recursion interval in historic time (which it hasn't) or that it is a unique event. Evidence for its uniqueness[1] is shown in Figure 2. The pattern shown on Figure 2 of the relatively abrupt occurrence of a great earthquake followed by diminishing seismic activity is characteristic of eastern United States earthquakes according to Howell.[2] He concludes that the basic cause for seismic unrest is the same throughout the eastern United States, and that areas where great

† Work done by I. W. Marine.

earthquakes have occurred and stress has been relieved (e.g., Charleston, South Carolina; New Madrid, Missouri; Cape Ann, Massachusetts; and eastern Newfoundland) are less subject to future earthquakes than areas where no great earthquake has occurred in historical time, such as Washington, D. C., and Pittsburgh, Pennsylvania.

SEISMIC INFORMATION

In 1971 and 1972, several small earthquakes (less than 4.5 on the Mercalli scale) occurred in the Orangeburg, South Carolina, area. This area was the subject of a Masters Dissertation at Georgia Institute of Technology[3], but no specific conclusion was reached as to the cause of these earthquakes. Seismographs show that earthquakes too small to be felt are still occurring in this area. A small felt earthquake also occurred near McCormick, South Carolina, on August 2, 1974, and was followed by numerous instrumentally detected aftershocks.

Because of the recent interest in seismicity in the eastern United States and the occurrence of the great Charleston earthquake, United States Geological Survey personnel installed 10 seismograph stations in 1973-74 on the Coastal Plain of South Carolina. The data from these stations are telemetered into the Geology Department at the University of South Carolina where they are displayed and recorded. This network[4] will, in the future, produce much valuable seismic data for this area. These data will be used to develop a crustal model for South Carolina and for analyzing fault motions. It is expected that the data will be used both by the United States Geological Survey and the University of South Carolina.

It has long been recognized that earthquake waves are more rapidly attenuated in the western United States than in the eastern portion, yet most of the earthquake studies and information are from the western area. As a result, until a few years ago, attenuation in the east was evaluated qualitatively by expert judgment. Nuttli[5,6] studied earthquake attenuation in the central United States and developed attenuation graphs for the three seismic quantities of engineering interest, namely, displacement, particle velocity, and acceleration. His graphs are shown in Figures 3, 4, and 5. Bollinger[7] showed that attenuation in the Southeast is similar to that in the central United States.

Some years ago, the Savannah River Plant had three of the very few strong motion recorders east of the Rocky Mountains. Recently, the United States Geological Survey has installed or is planning to install 12 strong motion accelerographs in South

Carolina and nearby Georgia. This will vastly improve the data coverage in the event of a strong earthquake, and may serve to validate or modify the conclusions based on Nuttli's curves for the attenuation of acceleration.

SUMMARY

The figures prepared by Nuttli[5] provide a basis for estimating the effects of large earthquakes (displacement, velocity, and acceleration) as a function of distance in the southeastern United States. The developing research and instrumentation programs in this part of the United States will provide a basis for improving these estimates of effects.

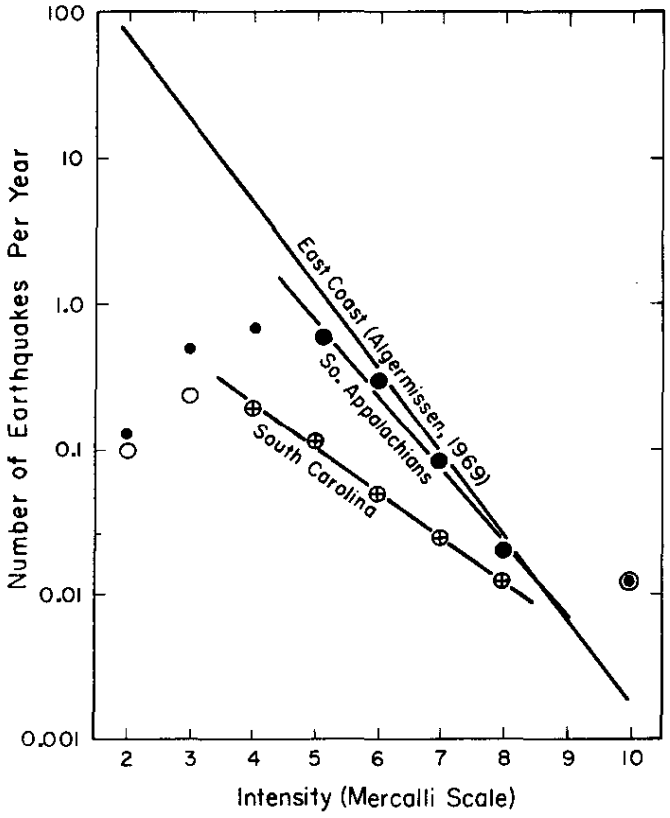

FIGURE 1. Frequency of Earthquake Occurrence in the Southeastern United States (Reference 1)

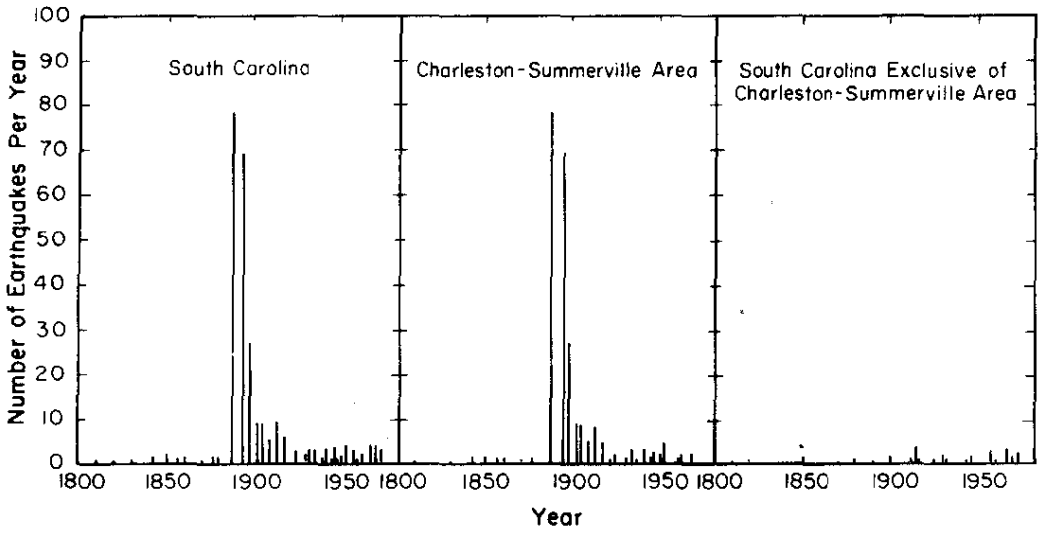

FIGURE 2. Earthquake Frequency in South Carolina for Three Different Regions, 1800-1971 (Reference 1)

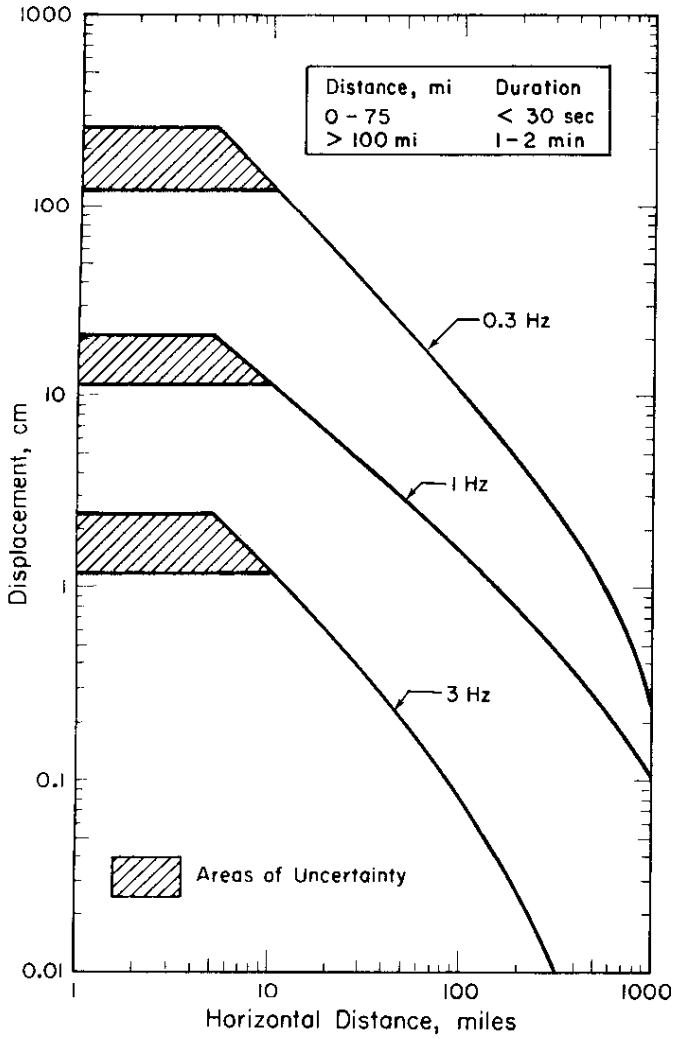

FIGURE 3. Attenuation of Ground Displacement with Distance on Hard Rock for Selected Wave Frequencies (References 5 and 6)

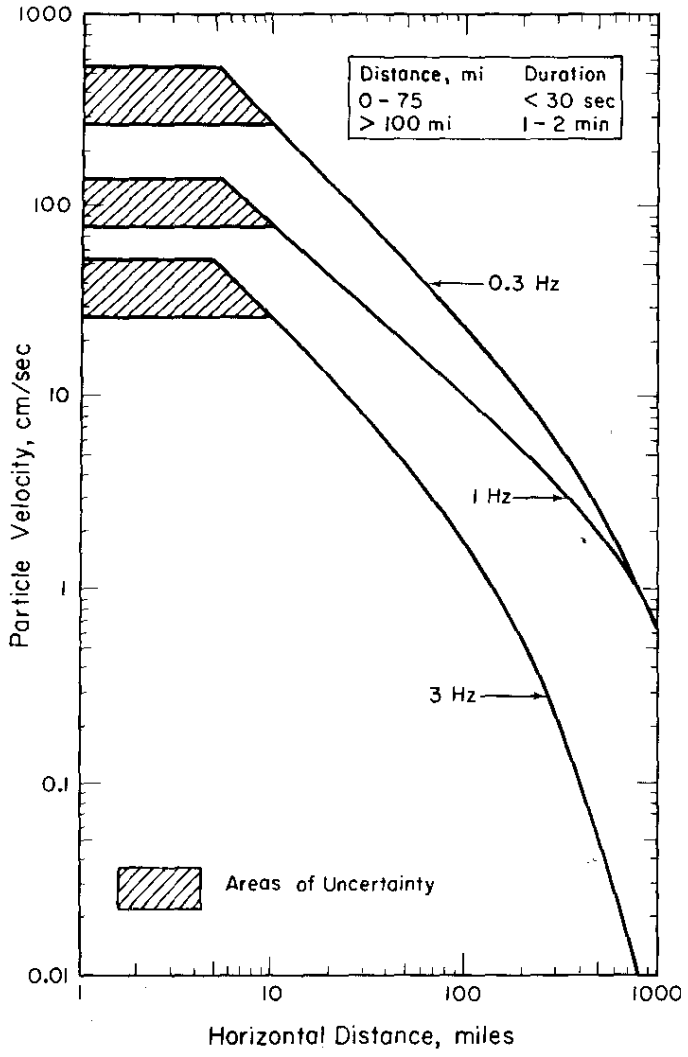

FIGURE 4. Attenuation of Ground Particle Velocities with Distance on Hard Rock for Selected Wave Frequencies (References 5 and 6)

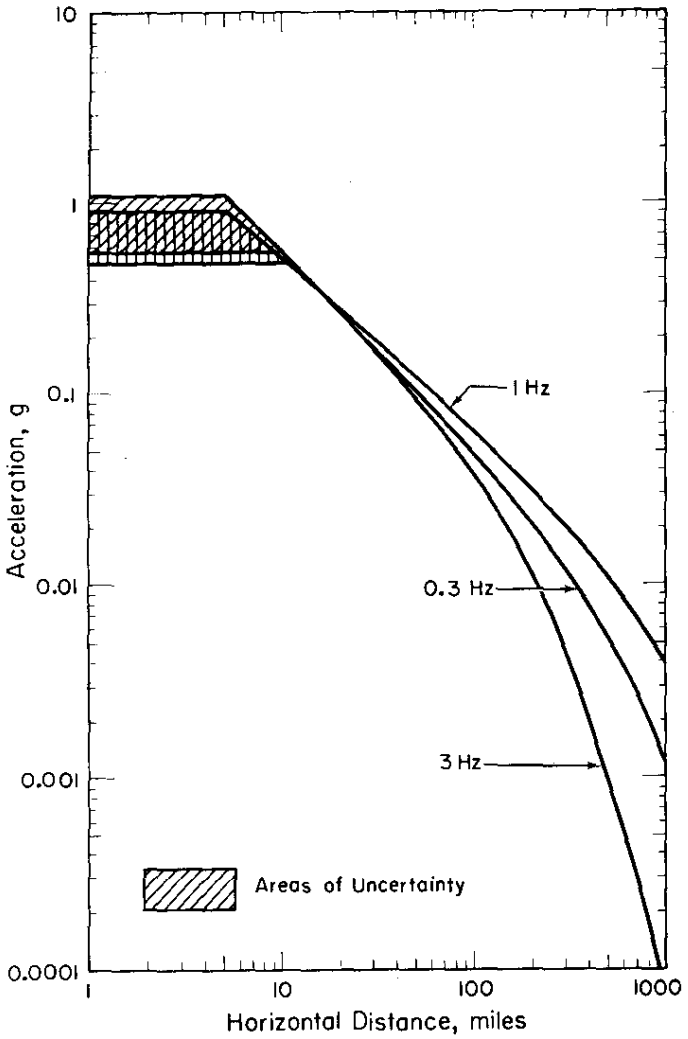

FIGURE 5. Attenuation of Ground Acceleration with Distance for Hard Rock Sites for Selected Wave Frequencies (References 5 and 6)

REFERENCES

1. G. A. Bollinger. "Historical and Recent Seismic Activity in South Carolina." *Bull. Seism. Soc. Amer. 62*, (3), 851-864 (1972).

2. B. F. Howell, Jr. "Earthquake Hazard in the Eastern United States." *Mineral Sciences 42*, No. 6, pp 41-45 (Pennsylvania State University, College Park, Pa. (1973).

3. J. H. McKee. *A Geophysical Study of Microearthquake Activity Near Bowman, S. C.* A thesis for the degree of Master of Science, Georgia Institute of Technology, Atlanta, Ga., 65 pp (1973).

4. A. C. Tarr and K. W. King. *South Carolina Seismic Program.* U. S. Geol. Survey Open-File Report, 74-58, 15 pp (1974).

5. O. W. Nuttli. "Design Earthquakes for the Central United States." U. S. Army Corps of Engineers, Waterway Experiment Station, Report 1, *State-of-the-Art for Assessing Earthquake Hazards in the United States*, Miscellaneous Paper S-73-1, 42 pp (1973a).

6. O. W. Nuttli. "Seismic Wave Attenuation and Magnitude Relations for Eastern North America." *J. Geophys. Res. 28* (5), 876-885 (1973b).

7. G. A. Bollinger, "Seismicity of the Southeastern United States." *Bull. Seism. Soc. Amer. 63*, (5), 1785-1808 (1973).